Physics Library
QC
1
.P5812
v.56
no.5

THE PHYSICAL REVIEW

VOLUME 56 | Second Series | NUMBER 5

SEPTEMBER 1, 1939

Published for the
AMERICAN PHYSICAL SOCIETY
by the
AMERICAN INSTITUTE OF PHYSICS
Incorporated
LANCASTER, PA., AND NEW YORK, N. Y.

UNIVERSITY OF MICHIGAN LIBRARIES

THE PHYSICAL REVIEW

A journal of experimental and theoretical physics established by E. L. Nichols in 1893

Published by the American Institute of Physics for the

American Physical Society

OFFICERS

President

JOHN T. TATE
University of Minnesota
Minneapolis, Minnesota

Vice President

JOHN ZELENY
Yale University
New Haven, Connecticut

Secretary

W. L. SEVERINGHAUS
Columbia University
New York, New York

Treasurer

G. B. PEGRAM
Columbia University
New York, New York

Local Secretary for the Pacific Coast

PAUL KIRKPATRICK
Stanford University
California

Editor

JOHN T. TATE
University of Minnesota
Minneapolis, Minnesota

BOARD OF EDITORS

JOHN T. TATE, *Editor* — J. W. BUCHTA, *Assistant Editor*

Associate Editors

K. T. BAINBRIDGE	A. L. HUGHES	W. BLEAKNEY
H. P. ROBERTSON	T. H. JOHNSON	G. BREIT
H. B. WAHLIN	F. A. JENKINS	D. M. DENNISON

Manuscripts for publication should be submitted to John T. Tate, University of Minnesota, Minneapolis, Minnesota.

Proof and all correspondence concerning papers in the process of publication, should be addressed to the Publications Manager, American Institute of Physics, 175 Fifth Avenue, New York, New York.

Subscription Price

United States and Possessions and Canada $15.00
Foreign $16.50

Back Numbers

Complete set: Series 2,[1] Vol. 1, 1913–Vol. 54, 1938—$390.00
Yearly rate: $16.50
Single copies: $1.50 each prior to July, 1929; $.75 each after July, 1929.

Subscriptions and orders for back numbers should be addressed to Prince and Lemon Streets, Lancaster, Pennsylvania, or to the American Institute of Physics, 175 Fifth Avenue, New York, New York.

Advertising is not accepted for the *Physical Review* but attention is called to the *Review of Scientific Instruments* and the *Journal of Applied Physics*, companion publications of the Institute, and media through which the field of physics can be reached most effectively. Rates and other information will be furnished on request.

Changes of address and complaints of failure to receive the *Physical Review* in the case of members of the American Physical Society, should be addressed to the Treasurer; in the case of other subscribers, to the Publications Manager. New copies can be sent free in response to complaints of non-delivery only if notice of non-delivery is received within three months of date of issue.

[1] For Series 1 inquire of Physics Department, Cornell University, Ithaca, N. Y.

The Physical Review is published semi-monthly at Prince and Lemon Streets, Lancaster, Pennsylvania.

Entered at the Post Office at Lancaster, Pennsylvania, as second class matter.

Acceptance for mailing at special rate of postage provided for in section 1103, Act of October 3, 1917, authorized September 6, 1926.

Physics
Physics-L.3A
Johnson
10-11-43
Replace

THE
PHYSICAL REVIEW

A Journal of Experimental and Theoretical Physics Established by E. L. Nichols in 1893

VOL. 56, NO. 5 SEPTEMBER 1, 1939 SECOND SERIES

The Intensities of the *K*-Series X-Ray Lines of Tungsten and Platinum

W. H. KLIEVER*
Ryerson Physical Laboratory, University of Chicago, Chicago, Illinois
(Received June 1, 1939)

Measurements of the relative intensities of the $K\alpha$ and $K\beta$ lines of $_{74}$ W and $_{78}$ Pt have been made with a double crystal spectrometer, high pressure argon ionization chamber, and FP-54 Pliotron amplifier by measuring with a planimeter the areas under the curves of the lines graphed against Bragg angle. The results in the $_{78}$ Pt spectrum, which are the more reliable, are: on the basis 100 for the intensity of $K\alpha_1$: $K\alpha_2=52$, $K\beta_3=10.2$. $K\beta_1=20.0$, $K\beta_5=0.38$, $K\beta_2=7.8$, $K\beta_4=0.8$,$(O_{II}O_{III}-K)=1.2$. Although the intensity of the quadrupole line $K\beta_5$ relative to $K\beta_1$ is in good agreement with the calculated value of Massey and Burhop, the predicted decrease in the relative intensity of this line at lower atomic numbers does not seem to be experimentally verified. The observed relative intensities of the stronger dipole lines seem to agree satisfactorily with the calculations of Pincherle and of Massey and Burhop.

MOST of the measurements of x-ray line shapes and intensities have been made only for elements of low atomic weights or were made photographically with x-ray spectrographs. This research was undertaken to study the *K*-series lines of heavy elements with a double-crystal spectrometer and ionization chamber, to look for anomalies and check against computed values for the intensities of regular and non-diagram lines.

I. THE TUBE AND SPECTROMETER

The x-ray tube, described previously,[1] was made at the Ryerson Laboratory, with metal ends, body of Pyrex piping, hot cathode and with target surrounded by metal shield with aluminum window. Electrodes were 48 mm apart. The measurements on the $K\alpha$ lines of tungsten were made with an earlier tube having similar electrodes spaced about 37 mm apart and a glass envelope of 3″ diameter throughout closed by large wax joints at the end. Tungsten target surfaces were tilted 30° with the perpendicular to the cathode beam; platinum, $22\frac{1}{2}$°.

Power for the tube was supplied by a synchronous motor and 540-cycle generator, a transformer, 2 kenotrons and two 0.050-mf filter condensers in the usual voltage doubling circuit. A calibrated electrostatic voltmeter was connected between the target and ground and a 2- and 4-ma calibrated meter mounted at the tube indicated electron current. The filament current required repeated adjustments and both the voltage and current across the tube were continuously observed and maintained constant by rheostats at the observer's position near the spectrometer.

The double crystal x-ray spectrometer designed by S. K. Allison[2] was used with calcite crystals in (1, 1) position. The entrance slit to the ionization

* With the Gaertner Scientific Corporation, Chicago, at time of this research. Now with U. S. Department of Agriculture, Leland, Mississippi.

[1] W. Kliever, Rev. Sci. Inst. **10**, 126 (1939).

[2] S. K. Allison, Phys. Rev. **41**, 1 (1932).

chamber was 5 cm from the crystal B axis. Lead shields were placed about 1 mm from and perpendicular to the crystal faces to eliminate diffuse scattered radiation, especially that from crystal A. Both crystals were rotated, and thus a constant spot on the target was used as a source. The spectrometer arm carrying crystal B is geared to rotate at double the speed of crystal A. The ionization chamber slit was sufficiently wide so that the chamber did not need to be moved during related measurements except when comparing $K\beta$ lines with $K\alpha_1$.

One slit only was used to limit the rays, the other being set slightly wider. Since the collimating property of the two crystals serves to select a parallel bundle of rays, *viz.*, all those rays which have an angle of incidence equal to one-half the angle between the crystal faces, it follows that, using two slits of equal width, the full aperture of the slits is used only when the rays selected by the crystal enter exactly parallel with the line of the slits. Otherwise the beam will be limited by one side of one slit and the opposite side of the other slit, and the horizontal aperture will be less than the slit widths and will vary if there is an error in crystal rotation. Under conditions of 0.3 mm slits 138 mm apart the width would be reduced about $\frac{1}{4}$ percent for an accumulated error of only 1 second in the motion of crystal A.

The vertical aperture was 2.2° except during the earlier determinations on the tungsten $K\alpha$ lines when it was 1.1°.

The crystals were split calcite one of which was etched 3 sec. in dilute HCl according to the method developed at Cornell University.[3] The full rocking curve width at half-maximum for parallel position is about $8\frac{1}{2}$ sec. of motion of crystal B only. A different pair of crystals used for the 74 W $K\alpha$ lines had similar resolving power for narrow slits but was found unsuited for use with the wide slits used on $K\beta$ lines.

II. Ionization Chamber and Amplifier

The ionization chamber was of steel of 25 mm diameter and 198 mm length internally, built for high pressure. The ends are bolted to flanges which are screwed to the cylindrical body. The inner electrode is a 1.6 mm rod off center by 3.2 mm and insulated by amber, with surrounding grounded guard ring. The entrance window is 3.2 mm off center opposite the rod, covered by Celluloid with rubber gasket. The chamber body is insulated from the spectrometer, shielded by a 3.2-mm grounded lead housing, and charged to 90 volts above ground by an Edison storage battery. The ionization current was found satisfactorily constant from 30 to over 200 volts. Stability was improved by connecting a 4-mf condenser between chamber and ground and a 1-megohm resistor between chamber and battery. The chamber was built by T. M. Hahn and is generally similar in design to the steel chamber described by Williams.[4]

An FP-54 Pliotron and L. and N. type R galvanometer were used in the well-known DuBridge and Brown circuit,[5] modified according to Fig. 1*f* of Penick[6] (modified Barth circuit). The tube was mounted in an evacuated, grounded metal case, with the additional precaution of a P_2O_5 drying tube. The ionization current conductor was supported only at the Pliotron grid cap and at the chamber electrode, and was entirely contained in the vacuum. A key operated through a sylphon permitted grounding the grid or applying known voltages. The wires to the tube base were soldered to the prongs of the tube, the latter passing out of the vacuum through rubber gaskets. The entire circuit including lead wires was carefully shielded, and all batteries were contained in a double wall, heat insulated steel box.

The sensitivity of the circuit was 2×10^{-16}A/mm with the 8×10^{10} ohm grid resistor used, and deviations from linearity were found negligible.

III. Corrections to Readings

1. *Zero drifts* were determined by periodically closing a lead shutter at the spectrometer slits and taking zero readings which thus take account of such factors as stray radiation, variations in batteries, amplifiers, etc. The zero readings were

[3] K. V. Manning, Rev. Sci. Inst. **5**, 316 (1934); F. K. Richtmyer, S. W. Barnes and K. V. Manning, Phys. Rev. **44**, 311 (1933).

[4] J. H. Williams, Rev. Sci. Inst. **3**, 586 (1932); T. M. Hahn, Phys. Rev. **46**, 149 (1934).

[5] L. A. DuBridge and H. Brown, Rev. Sci. Inst. **4**, 532 (1933).

[6] D. B. Penick, Rev. Sci. Inst. **6**, 116 (1935).

plotted against the number of readings, and the interpolated value subtracted from each reading before plotting.

2. The *sensitivity* of the amplifier, when less than its maximum was determined by comparing the reading at some point on the background spectrum with that at full sensitivity, other conditions remaining equal. All results have been computed for 100 percent sensitivity by dividing the measured values by the sensitivity. It should be mentioned here as a possible help to others that it would have been advantageous had the sensitivity of the amplifiers been adjustable in steps instead of continuously, so that settings could be repeated and more thoroughly calibrated.

3. *Absorption* by materials between the target and ionization chamber requires some correction which has been applied only to the computed ratios of more intense lines. If a material of thickness x and density ρ absorbs 2 rays of wavelengths λ_1 and λ_2 and intensities I_1 and I_2 before and I_1' and I_2' after absorption, if the respective mass absorption coefficients are μ_1 and μ_2, and if we let $I_1/I_2=R$ (the true ratio) and $I_1'/I_2'=R'$ (measured ratio), then

$$R=\frac{I_1}{I_2}=\frac{I_1'e^{\mu_1 x}}{I_2'e^{\mu_2 x}}=R'e^{(\mu_1-\mu_2)x}.$$

Only the absorption by the aluminum window and Pyrex wall of the tube was found appreciable. Absorption coefficients for aluminum were interpolated from curves plotted from data in the appendix of Compton and Allison's book on x-rays.[7] From the same data the mass absorption coefficients for Pyrex were computed from an analysis supplied through the courtesy of Corning Glass Works with the following results: W $K\alpha_1$, 0.241; W $K\alpha_2$, 0.247; W $K\beta_1$, 0.214; W $K\beta_2$, 0.209; Pt $K\alpha_1$, 0.215; Pt $K\alpha_2$, 0.220; Pt $K\beta_1$, 0.195; Pt $k\beta_2$, 0.193.

No attempt is made to correct for absorption of rays in the target.

4. *Ionization chamber corrections.* Correction has been made with the aforementioned coefficient data for the unabsorbed rays. The maximum photoelectron range has been estimated as 0.2 cm for Pt $K\beta_2$ and 45 atmospheres (hardest ray and lowest pressure used) from the formula[8] $x=v^2/b$ where v = photoelectron energy in electron kilovolts and $b=610\times45$. Thus the photoelectrons should be completely absorbed. Fluorescent radiation is assumed largely used in the Auger effect. Scattered radiation, modified and unmodified, has been neglected in its effect on line intensity ratios, because no convenient methods of correcting for it were found.

Considerable diffuse scattering by the calcite crystals was observed, which necessitated careful shielding. This may have affected the intensity ratios, but no corrections were attempted for this factor.

TABLE I. *Sample data taken in an experimental run. Voltage on x-ray tube, 108 kv. Current through x-ray tube, 0.77 ma. Slit width, 0.06 cm. Sensitivity of amplifier, 75 percent of maximum.*

X-Ray Line	Area (Arbitrary Units)	Area Ratio $K\alpha_2/K\alpha_1$	Atmospheres Pressure in Chamber	Absorption Correction in Percent			Final Intensity Ratio
				Al	Pyrex	Chamber	
Pt $K\alpha_1$	492.7						
$K\alpha_2$	247.3	0.507	83.1	—	0.4	−2.2	0.498
$K\alpha_1$	482.7						
$K\alpha_2$	275.6						
$K\alpha_2(M)$	261.4	0.542	83.1	—	0.4	−2.2	0.532

(M) indicates average of the two preceding determinations of area.

TABLE II. *Intensity of $K\alpha_2$ on the scale $K\alpha_1=100$.*

Element	Experiment	Theory Pincherle	Theory Massey and Burhop
74 W	47	52	—
78 Pt	52	—	—
79 Au	—	—	48

IV. Results

Table I shows a sample of the data taken in an experimental run. The intensities are taken (before correction) as proportional to the areas under the curves with Bragg angle as abscissae, as measured with an Ott planimeter.

The $K\alpha$ line intensities

Considerable interest is attached to measurements of the intensities in the K series of heavy elements, because of the chance to detect relativistic effects, if present. The nonrelativistic

[7] A. H. Compton and S. K. Allison, *X-Rays in Theory and Experiment* (Van Nostrand, 1935).

[8] Reference 7, page 494.

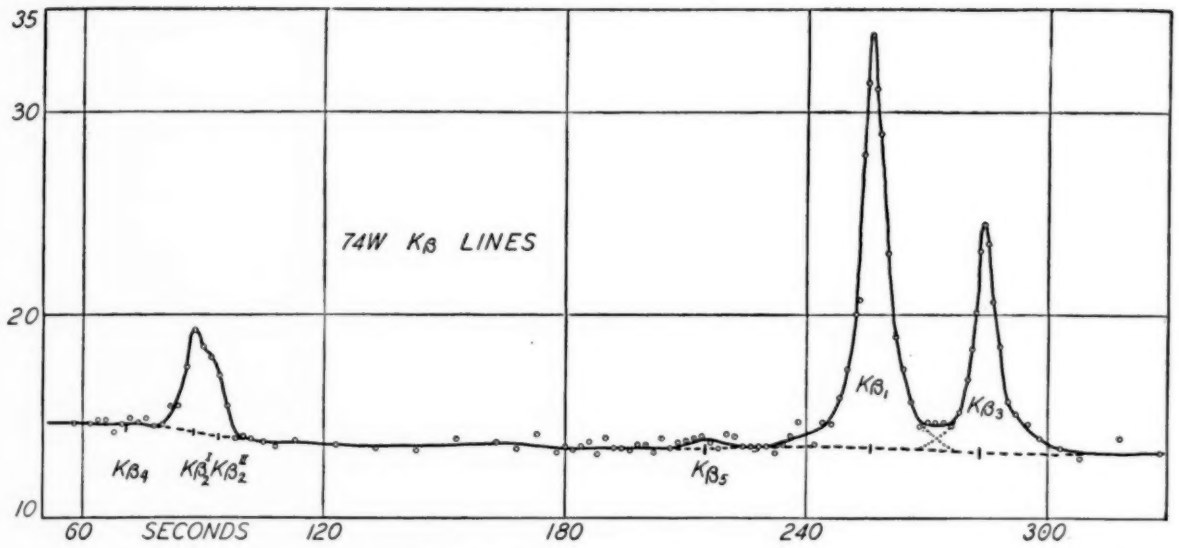

FIG. 1. Intensity curve of $_{74}$W $K\beta$ lines. The short cross lines on Figs. 1 and 2 give the positions of the x-ray lines according to Ingelstam, as measured from $K\beta_2^{I}$ and $K\beta_3$.

wave functions are certainly inadequate for the representation of these states in which the K electrons are bound with energies of approximately 70 kev. Massey and Burhop[9] have made calculations of x-ray intensities in which a rough approximation to a rigorous relativistic treatment has been introduced, and similar calculations have been made by L. Pincherle.[10] Massey and Burhop state that the relativistic treatment does not alter appreciably the nonrelativistic value of 0.500 for $K\alpha_2/K\alpha_1$, even in $_{92}$U. A previous experimental value of 0.500 was found by Duane and Stenström[11] in $_{74}$W. Table II summarizes the results on the $K\alpha$ lines.

No definite evidence of $K\alpha_3$ (L_I-K) was obtained, although some of the curves taken on tungsten showed slight irregularities in the expected region. According to Massey and Burhop, this line should be about as strong as $K\beta_5$ in $_{79}$Au.

The $K\beta$ line intensities

Since the advent of high resolving power spectrometers for x-rays, the β-group in the K series has been reexamined and several new, faint lines reported.[12] Since this work was begun, an excellent monograph by Ingelstam[13] has appeared, in which accurate measurements of the wave-lengths of the K lines of the heavy elements have been made with a high resolving power photographic spectrograph. Some visual estimates of intensities are made in this work.

Figures 1 and 2 show the present results on the $K\beta$ lines of $_{74}$W and $_{78}$Pt. Comparison of the curves shown on the $K\beta_2$ ($N_{II}N_{III}-K$) doublet with Fig. 23*a* of Ingelstam's monograph, and Fig. 4 of Richtmyer and Barnes[14] indicates that the resolving power was comparable to, but slightly lower than, that of the two other researches.

TABLE III. *Intensities of the $K\beta$ lines of* $_{74}$W *and* $_{78}$Pt, *based on the scale* $K\alpha_1=100$.

Symbol	Transition	$_{74}$W λ in X.U. Ingelstam	$_{74}$W Observed Intensity	$_{78}$Pt λ in X.U. Ingelstam	$_{78}$Pt Observed Intensity	Theoretical Intensity Pincherle $_{74}$W	Theoretical Intensity Massey Burhop $_{79}$Au
$K\beta_3$	$M_{II}-K$	184.795	9.6	164.157	10.2	11	13
$K\beta_1$	$M_{III}-K$	183.991	18.1	163.334	20.0	21	29
$K\beta_2^{II}$	$M_{IV}-K$	182.882	0.25	162.364	0.38	—	0.19
$K\beta_2^{I}$	M_V-K	182.711		162.203		—	0.41
$K\beta_2^{II}$	$N_{II}-K$	179.232	1.7	159.053	3.0	2.5	—
$K\beta_2^{I}$	$N_{III}-K$	179.049	3.1	158.863	4.8	4.5	—
$K\beta_4$	$N_{IV}N_V-K$	178.55	0.036	158.48	0.8	—	—
—	$O_{II}O_{III}-K$	178.073	0.04	157.922	1.2	1.5	—

[9] H. S. W. Massey and E. H. S. Burhop, Proc. Camb. Phil. Soc. **32**, part 3, p. 461 (1936).
[10] L. Pincherle, N. Cimento **10**, 344 (1933).
[11] W. Duane and W. Stenström, Proc. Nat. Acad. Sci. **6**, 477 (1920).
[12] A. H. Compton and S. K. Allison, *X-rays in Theory and Experiment* (Van Nostrand, 1935), pp. 632, 639.
[13] E. Ingelstam, Die K-Spektren der Schweren Elemente, Nova Acta Regiae Societatis Scientiarum Upsaliensis, Ser. IV, **10**, No. 5 (1937).
[14] F. K. Richtmyer and S. W. Barnes, Phys. Rev. **46**, 352 (1934).

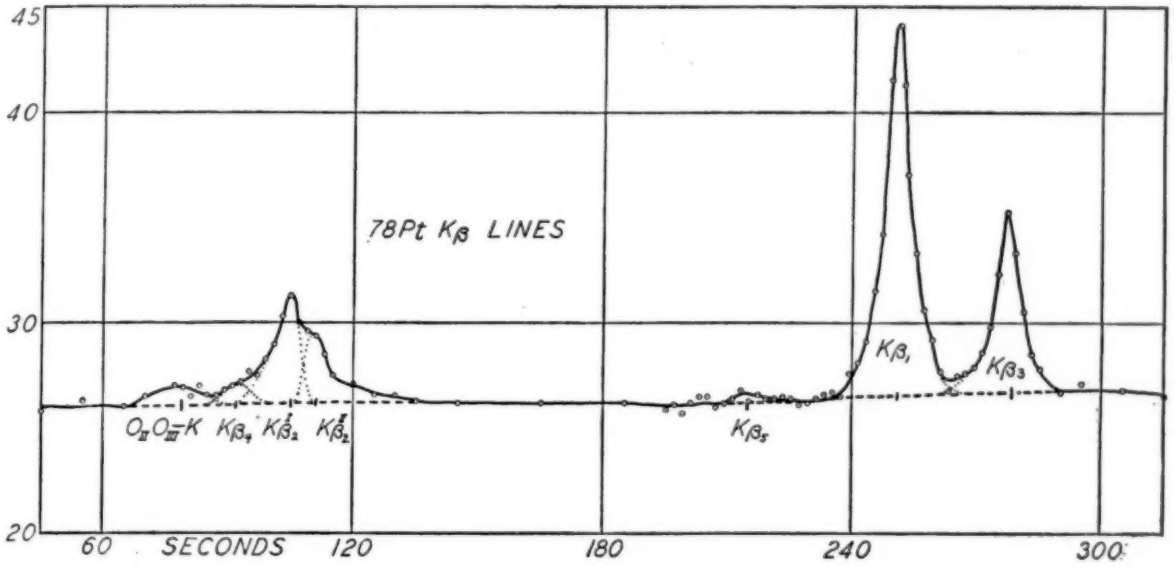

FIG. 2. Intensity curve of $_{78}$Pt $K\beta$ lines.

In addition to the diagram lines $K\beta_1$, $K\beta_3$ (M_{II}, $M_{III}-K$) and $K\beta_2^I$, $K\beta_2^{II}$ (N_{II}, $N_{III}-K$) which were known previous to Ingelstam's work, he reports evidence of $O_{II}O_{III}-K$, obtained first in $_{49}$In and observed in heavier elements also. In the $_{78}$Pt $K\beta$ spectrum given here, there is some evidence of a broad line in the required region. Ingelstam gives 157.922 x.u. as the wave-length; the maximum of the broad peak in the present work lies at 158.05 x.u. In the present work on tungsten, the corresponding line was not detected with certainty. Table III gives the results on the $K\beta$ lines.

The intensities given for the nondiagram lines $K\beta_5$ and $K\beta_4$ certainly have a large error, probably a factor of 2, because they lie so near the base-line. In the case of tungsten, the values seem less reliable than for platinum. The platinum curves were taken subsequent to the tungsten experiments, when the technique had been better developed.

If one takes the observed values of the intensity of Pt $K\beta_5$ with respect to Pt $K\beta_1$, namely 0.019, it agrees well with Massey and Burhop's value of 0.021 for this ratio. Although the intensity of this interesting quadrupole line agrees with Massey and Burhop's calculation at $_{78}$Pt, the meager experimental evidence available would seem to show that its intensity does not decrease with atomic number as they predict. At $_{44}$Ru, Wilhelmy[15] estimated $K\beta_5$ as 0.25 if $K\alpha_1$ is 100, whereas for $_{51}$ Sb according to Massey and Burhop's calculations, the line should have sunk to $\frac{1}{5}$ of its value at $_{78}$Pt, which means a value of 0.05–0.08 instead of Wilhelmy's 0.25.

The author wishes to express his thanks to Dr. S. K. Allison, under whose guidance the work was done, and to M. L. Dannis for assistance and for measuring the areas of the curves.

[15] E. Wilhelmy, Phys. Rev. **46**, 130 (1934).

The X-Ray K Absorption Edges of the Elements Fe (26) to Ge (32)

W. W. BEEMAN AND H. FRIEDMAN
Rowland Physical Laboratory, The Johns Hopkins University, Baltimore, Maryland

(Received July 5, 1939)

The structures of the x-ray K absorption edges of the elements Fe to Ge have been measured with a double crystal spectrometer. Measurements were extended about 20 volts beyond the main edge in each case. In the regions of secondary structure, new maxima and minima have been resolved, and their intensities compared with results obtained photographically. The two sets of measurements are found to disagree much more than could be expected from the estimated precisions. Wave-length positions of the first empty levels above the Fermi distribution have been assigned with a probable error of less than 0.1 X.U., and widths of K states have been determined to within half a volt by matching theoretical arctangent curves to the experimental edges. Previously measured $K\beta_{2,5}$ emission lines have been plotted with the corresponding absorption edges and the shapes of both lines and edges explained on the basis of distributions of states in the electronic energy bands of these metals. The $K\beta_5$ line is interpreted as a dipole transition arising from the mixture of p function in the $3d$ bands. Quantitative agreement is obtained in a correlation of the observed Cu emission and absorption structures with the recently calculated electronic bands of this metal.

INTRODUCTION

PREVIOUS experimental work[1] on the x-ray K absorption limits of Fe, Co, Ni, and Cu, has resolved considerable structure in the absorption edges themselves, but no satisfactory explanation of these structures of even a qualitative nature has been proposed, although it has been pointed out that the observed effects might be associated with the presence of an incomplete $3d$ shell.

For the very light elements, some success has been achieved by Mott, Jones, and Skinner and their co-workers[2–4] in interpreting observed shapes of soft x-ray emission lines and absorption jumps, through consideration of densities of states in filled and unfilled portions of the conduction bands. Since calculations have been carried out in recent years on the band structure of copper[5] with extrapolations to nickel,[6] we have attempted to correlate the results of these band calculations with experimental data on K absorption limits and $K\beta_{2,5}$ emission lines. The available emission data are very complete and reliable, but a lack of sufficiently complete and accurate data on the absorption limits has led us to repeat and extend older measurements, with greater resolving power, an improved technique for intensity measurement, and accurate wave-length determinations. The results of the present work on absorption limits from Fe (26) to Ge (32) differ considerably from those of past investigations. When taken together with the data on emission lines, the present measurements offer a semi-quantitative verification of the theoretical band calculations.

The material presented here may be divided into four sections, (1) a description of experimental technique, (2) intensities of secondary structures, (3) K and L level widths, and (4) a discussion of shapes of absorption limits and $K\beta_{2,5}$ emission lines in their relation to the electronic energy bands in the elements from Fe to Ge. The last-mentioned section constitutes the major portion of this paper. It offers an explanation of the large asymmetries of $K\beta_{2,5}$ emission lines and interprets their weak intensities as dipole transitions from bands of mixed states, rather than quadrupole transitions from discrete atomic levels, in Fe to Cu. In a similar manner, the shapes of the experimental absorption edges in these same elements are all qualitatively explained, as resulting from the variation in densities of unfilled states in the conduction and higher energy bands.

[1] A. H. Barnes, Phys. Rev. **44**, 141 (1933).
[2] H. M. O'Bryan and H. W. B. Skinner, Phys. Rev. **45**, 370 (1934).
[3] Jones, Mott and Skinner, Phys. Rev. **45**, 379 (1934).
[4] H. Jones and N. F. Mott, Proc. Roy. Soc. **162**, 49 (1937).
[5] H. Krutter, Phys. Rev. **48**, 664 (1935).
[6] J. C. Slater, Phys. Rev. **49**, 537 (1936).

Experimental

The high precision double crystal spectrometer and high voltage supply with which the data here presented have been obtained is described in detail in a paper by Bearden and Shaw.[7] To determine the diffraction angles, angular settings in the (1+1) and (1−1) positions were read by the four-microscope method. Since no calibration correction greater than 0.3 sec. is anywhere necessary,[7] no such corrections have been applied in these measurements. Angular settings were determined to the nearest second, one second of arc in the wave-length region between one and two angstroms, being always less than 0.02 X.U. Temperature corrections and wave-lengths have been calculated with values of calcite expansion coefficient and grating space as given in reference 7.

The calcite crystals used in this work had been previously selected and treated in the usual way by Dr. C. H. Shaw. Table I gives the (1−1) widths for various wave-lengths for the crystals, as measured by the authors in this work. These widths fall close to the theoretical widths of perfect crystals.[8] Most of the measurements have been carried out with a (1+1) width of 39.5 seconds for Cu K_{α_1}. The crystals compare favorably with any yet reported in double crystal work.

The gold-plated copper target was cut at an angle of 25 degrees with the horizontal, making the vertical projection of the focal spot 1.5 mm, which may be taken as the height of the first limiting slit for the spectrometer. The second slit, measuring 7 mm high, was separated by a distance of 55 cm from the first, giving a geometrical resolving power over 30,000.

All intensity measurements have been made with Geiger counters of the high pressure argon-alcohol type. The Getting type of multivibrator circuit[9] with a scale-of-sixteen Thyratron circuit[10] and a Cenco mechanical counter were used for recording pulses. In general, counts were taken over two-minute periods, alternately on incident and transmitted intensity at a given wave-length setting. Counting intervals were timed by a synchronous motor-driven switch. With an average counting rate of 2000 per minute in the Geiger counter, it was necessary to take a total of about twenty minutes of readings on incident intensity and an equivalent amount on transmitted intensity to obtain the desired precision per point. Aluminum foils were inserted for the measurement of incident intensity to bring the counting rate below the maximum of 8000 per minute. With this spectrometer it is possible to reset on any given point to 0.1 second, so that portions of curves can be repeated a number of times and corresponding points averaged. In most previous work of this type, such accurate resetting has not been possible, making it necessary to average a number of superposed curves, or publish only one of a set as a typical curve. The probable error per point in the curves shown here does not exceed one percent.

Absorbers were supported between the x-ray tube and the first crystal. To facilitate moving the foils in and out of the beam, they were mounted on a rotating sector, by means of which they could always be returned accurately to the same position in the beam. It was found unnecessary to oscillate the foils, direct tests showing that the curves obtained were independent of the position of the absorber. The x-ray beam was sufficiently wide, so that enough of the absorber was covered to average out small inhomogeneities.

Table I. (1−1) *widths of crystals.*

Wave-length in A	Exp. Width in sec.	Theoretical Widths* for Perfect Crystals
1.12	8.2	7.9
1.19	8.8	8.4
1.54	10.3	9.9
1.61	10.4	10.2
1.78	12.1	11.5

* R. K. Richtmyer and S. W. Barnes, Phys. Rev. **45**, 745(A) (1934)

In the region of secondary structure, occurring on the high frequency side of the edge, tests have been carried out with rolled, electroplated, and powder absorbers of the same element with no observable differences in the amount and position of such structure. Evidently, the effects of crystal orientation due to rolling, and energies involved in strains are very small. The electroplated foils, Fe, Co, Ni, and Cu were obtained by plating onto stainless steel from which the foils were after-

[7] J. A. Bearden and C. H. Shaw, Phys. Rev. **48**, 18 (1935).
[8] S. K. Allison, Phys. Rev. **41**, 1 (1932); L. G. Parratt, Phys. Rev. **41**, 561 (1932).
[9] I. A. Getting, Phys. Rev. **53**, 103 (1938).
[10] J. Giarratana, Rev. Sci. Inst. **8**, 390 (1937).

wards easily stripped. Zn and Pt foils were rolled. The foils ranged from 5μ to 10μ in thickness. Ge was used in powder form, and Ga was run at room temperature in the liquid state. Very homogeneous absorbing sheets of Ga were obtained by making an emulsion with castor oil on filter paper. Once melted, Ga remains supercooled to temperatures considerably below the melting point.

Since only the absorption coefficient has a physical meaning independent of the thickness of the absorber, all the curves given here are plotted with logarithmic ordinates. Most double crystal work on absorption limits has been published in the form of curves of I/I_0 or simply transmitted intensity against wave-length. It has been pointed out[11] that the appearance of such curves is determined largely by the thickness of the absorber. When $\log I/I_0$ rather than I/I_0 is plotted against wave-length the scattering of points on the high transmission side appears considerably reduced, while the contrast in the secondary structure is greatly enhanced relative to the total absorption jump. In double crystal measurements, where intensities of secondary structures have been reported from I/I_0 data, the values given ought not to be confused with the actual absorption coefficient variations.

In this investigation, much of the work has been done with second-order radiation being recorded. Second-order radiation reduces the top to bottom contrast in the absorption curves, affecting them mainly in the high absorption portion. Cobalt and gallium were run at voltages too low to excite second order. Other curves were checked for the effect of second-order radiation. For germanium and zinc, the effect was to reduce the top to bottom contrast by four percent and six percent, respectively. The effect on the intensity of secondary structure relative to the total jump is a much smaller percent. The curves for Ge, Zn, and Pt as presented here are uncorrected. Cu, Ni, and Fe have been rechecked and corrected for second-order radiation. In Fe, the largest correction was necessary, amounting to a 25-percent stretching of the entire curve and an increase in secondary structure intensity of 15 percent. Other corrections were all much smaller.

[11] R. K. Richtmyer and S. W. Barnes, Phys. Rev. **45**, 745(A) (1934).

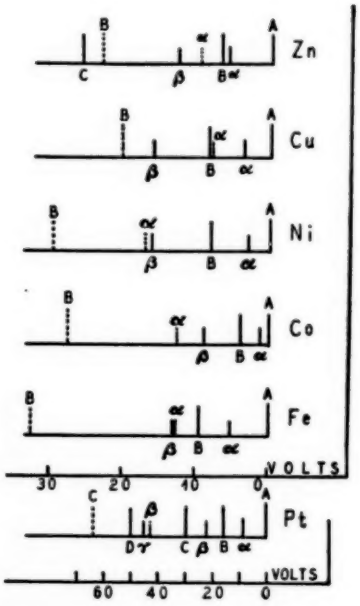

FIG. 1. Positions of secondary structures measured in volts from highest point in main absorption jump, A (See Figs. 3–10). Tall lines refer to maxima of absorption, short lines to minima. In each plot, results of the present work are drawn in solid lines, with letters below, while photographic results (reference 15, and Coster and Smoluchowski, Physica **2**, 1 (1935)) are plotted in dotted lines, lettered above. The platinum results are for the L_{III} edge. All others are K edges.

The smallness of these corrections is in part due to the weak absorption of the short wave-length second-order radiation in the argon counter.

SECONDARY STRUCTURES

That the double crystal spectrometer is well suited to measurements of secondary structure occurring on the high frequency side of an absorption limit has been demonstrated in a number of cases.[12–14] Extensive photographic work on all the metals worked with here, with the exception of germanium, may be used for comparison with our measurements, which have generally been carried out to 15 to 25 volts on the high frequency side. As is apparent from Fig. 1, the higher resolving power of the double crystal spectrometer has revealed, in each case, structure not detected photographically. In some cases, the first minimum in absorption, α, obtained photographically, may be fitted to our second minimum, β.

[12] P. A. Ross, Phys. Rev. **44**, 977 (1933).
[13] W. H. Zinn, Phys. Rev. **46**, 659 (1934).
[14] L. G. Parratt, Phys. Rev. **54**, 99 (1938).

In reports of secondary structure intensities from photographic measurements, two different definitions have been used for intensity. In some cases, the intensity of a given structure is defined as the ratio of the change in absorption coefficient from maximum to minimum in the structure, to the average absorption coefficient on the high frequency side of the limit. We shall call this definition (a). In other cases, the intensity of the structure is defined as the ratio of the change in absorption coefficient from maximum to minimum, to the total increase in absorption coefficient from the low to the high frequency side of the limit. We shall call this definition (b). Under "single crystal, photographic" in Table II are listed the results of measurements by Coster and Veldkamp,[15] and under "double crystal," the authors' results. The superscript (a) or (b), in each case, indicates the definition of intensity according to which the listed values have been calculated from the data. Structures referred to are indicated with the conventional letters used in labeling the curves in Figs. 2–10. Since the two sets of measurements do not refer to the same structures, no direct comparison of results can be made. However, it is apparent from the microphometer traces redrawn in Fig. 2, that we should expect the structures in Fe, Cu, and Pt, close to the edges, to be much weaker in intensity than the $D-\delta$ structures to which the photographic results in Table II refer. On the contrary, the present measurements show intensities close to the edges as great as or greater than that found far from the edges in single crystal work. For Zn and Pt, intensities measured with the double crystal spectrometer are considerably greater than anywhere in the photographically measured structures. Coster and Veldkamp's measured intensity for AuL_{III} was one-fifth that for Cu K, and only slightly less than for PtL_{III}. Our results on PtL_{III} would therefore lead us to expect intensities in AuL_{III} much closer to what we find in Cu K. All these discrepancies are far greater than one would be led to expect from the experimental errors, since both types of measurements claim precisions of much smaller order of magnitude than the differences observed. The inherently poor resolution in single crystal technique may be largely responsible for the lack of agreement between the two sets of observations. In PtL_{III} (see Figs. 1 and 2), the first clearly resolved photographic structure is β, which falls close to our γ. On the microphotometer trace, the structure A, α, B, is very uncertain and almost washed out, as would be expected in overlapping, poorly resolved absorption peaks. In Fig. 10, our A, α, B, β, C, and γ structures are easily resolved with consequently large intensities. From Fig. 1, and a comparison of the Fe curve in Fig. 2, with that in Fig. 3, it seems that our $A-\beta$ corresponds to photographic $A-\alpha$. Similarly, for Zn, our $A-\beta$ structure (Fig. 7) again must correspond to photographic $A-\alpha$, and for Cu (Fig. 6) our $\alpha-B$ structure is apparently unresolved and

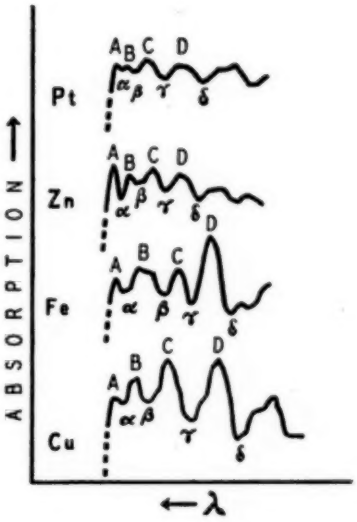

FIG. 2. Secondary structures for Fe, Cu, and Zn K edges, and for Pt L_{III}, copied from photographic microphotometer traces (reference 15). The $D-\delta$ intensities are much greater than the $A-\alpha$ in Fe, Cu, and Pt. The Zn structure is fairly uniform.

TABLE II. *Comparisons of secondary structure intensities.*

	Single Crystal Photographic		Double Crystal	
Edge	Intensity (percent)	Structure Referred to	Intensity (percent)	Structure Referred to
Fe K	19(a)	$D-\delta$	14(a)	$A-\alpha$
Cu K	13(a)	$D-\delta$	13(a)	$B-\beta$
Zn K	7(a)	$D-\delta$	17(a)	$A-\beta$
Co			5(a)	$B-\beta$
Ni			9(a)	$B-\beta$
Ga			11(a)	$A-\alpha$
Ge			19(a)	$A-\alpha$
Au L_{III}	2.8(b)	$D-\delta$		
Pt L_{III}	4.6(b)	$D-\delta$	14(b)	$A-\alpha$

[15] D. Coster and J. Veldkamp, Zeits. f. Physik **70**, 306 (1931); D. Coster and J. Veldkamp, Zeits. f. Physik **74**, 191 (1932).

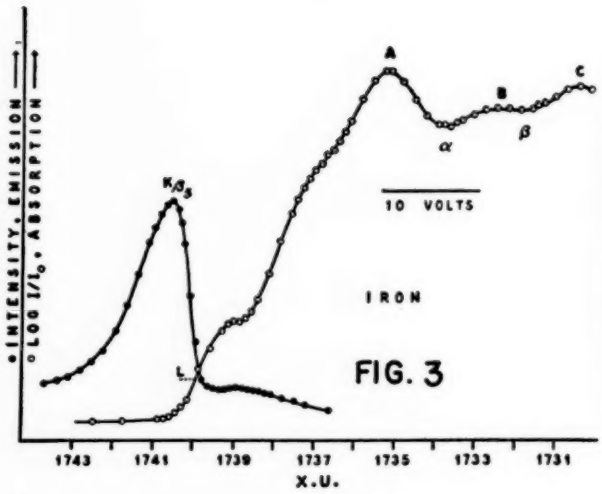

FIG. 3

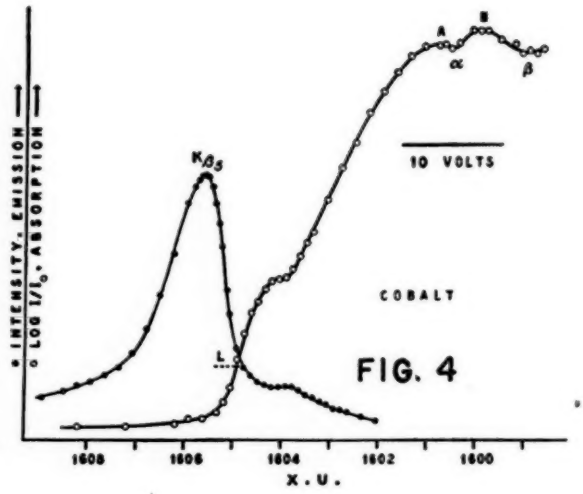

FIG. 4

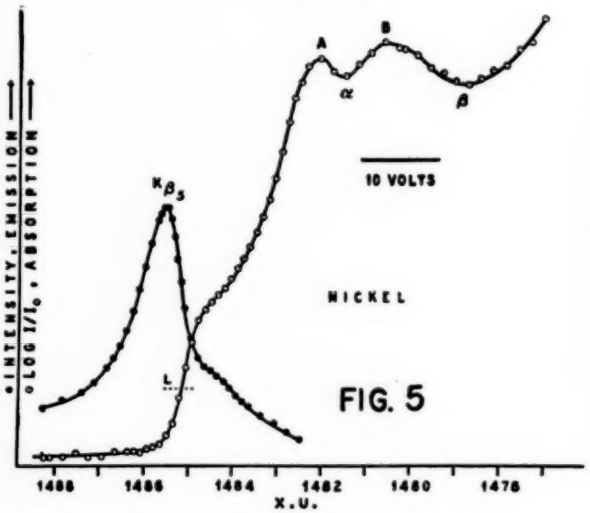

FIG. 5

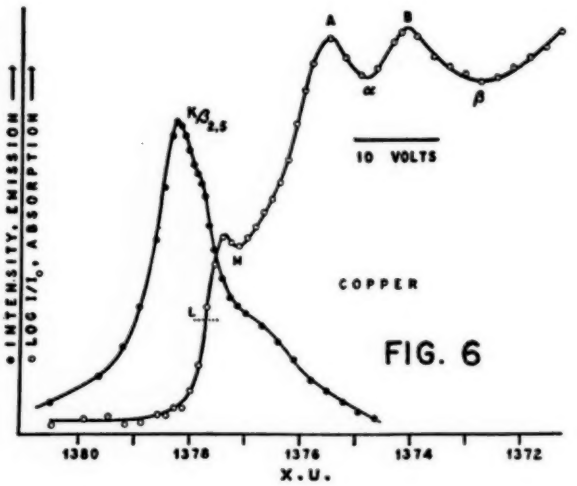

FIG. 6

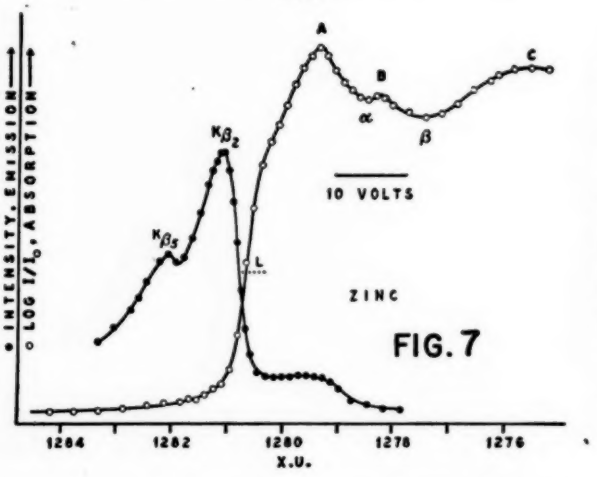

FIG. 7

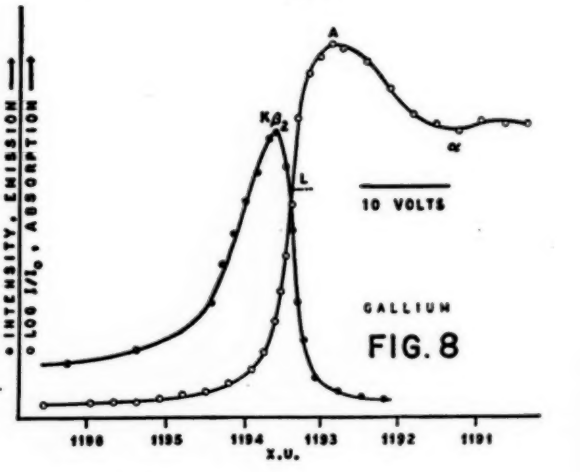

FIG. 8

FIG. 3. $K\beta_5$ line and K absorption limit of Fe. All emission lines in Figs. 3–10 are plotted to arbitrary intensity scales.

FIG. 4. $K\beta_5$ line and K absorption limit of Co.

FIG. 5. $K\beta_5$ line and K absorption limit of Ni.

FIG. 6. $K\beta_{2,5}$ line and K absorption limit of Cu.

FIG. 7. $K\beta_{2,5}$ line and K absorption limit of Zn.

FIG. 8. $K\beta_2$ line and K absorption limit of Ga.

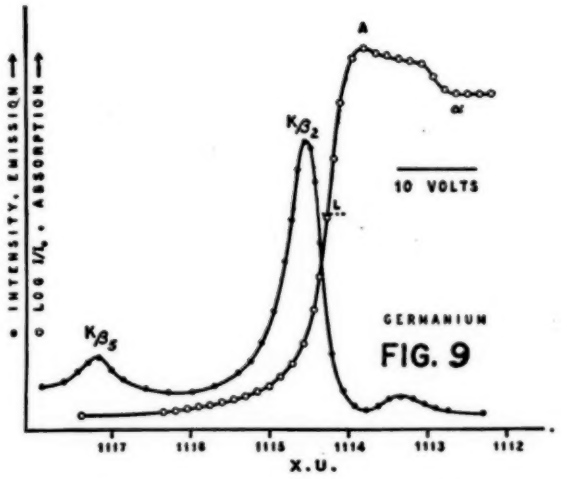

FIG. 9. $K\beta_2$ and $K\beta_5$ lines and K absorption limit of Ge.

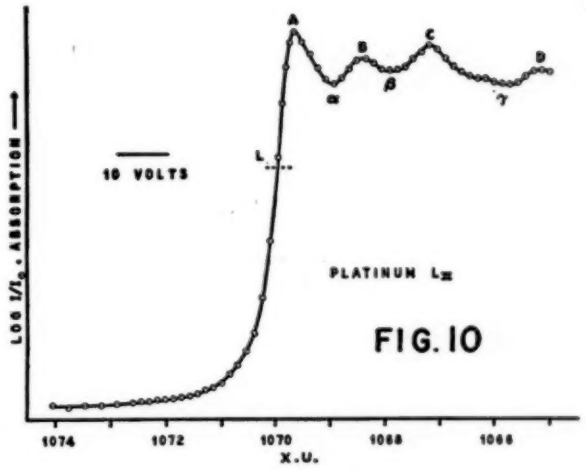

FIG. 10. L_{III} absorption limit of Pt.

lumped into photographic A. Whether poor single crystal resolution is entirely responsible for all the differences observed cannot be determined until the double crystal measurements are extended to the more widely spaced structures 50 to 100 volts from the edges.

The general rule proposed by Coster and Veldkamp,[15] from their results on Fe, Cu, and Zn, that intensities of structures in different elements vary approximately in the same way as the melting points, has not been borne out by more recent measurements on other elements,[13] nor by the results of the present investigation as far as it has gone.

Reference to Fig. 1 and to Figs. 5 and 6 shows that even near the edge, Cu and Ni, elements of adjacent atomic number, both with same lattice structure and only slightly different lattice spacings, have very similar structures, $A-\alpha -B-\beta$, as measured by the double crystal method. However, Co and Zn, Figs. 4 and 7, both with close-packed hexagonal crystal structures, are entirely different in absorption structure near the edge. The secondary absorption in Co resembles that in Ni, the element of adjacent atomic number but different lattice type, much more than the structure in Zn. It therefore seems that the atomic potential fields within 15 volts of the edges are still most important in determining observed absorption structures, and that the electrons cannot yet be considered entirely free.

Widths of Energy Levels

Richtmyer, Barnes and Ramberg[16] have applied the quantum-mechanical radiation theory of Weisskopf and Wigner[17] to the absorption process in such a way as to make possible a calculation of level widths from experimental data on absorption limits.

The quantum-mechanical derivation of the intensity distribution in a spectral line, according to Weisskopf and Wigner, yields the result,

$$I_{AB}(\nu)d\nu=\frac{\Gamma_A+\Gamma_B}{2\pi}\times\frac{d\nu}{(\nu_{AB}-\nu)^2+[(\Gamma_A+\Gamma_B)/2]^2}, \quad (1)$$

where Γ and Γ_B are the widths of the initial and final levels A and B between which the electronic transition takes place. The state A has a spectral distribution of the form,

$$I_A(\nu)d\nu=\frac{\Gamma_A}{2\pi}\frac{d\nu}{(\nu_A-\nu)^2+(\Gamma_A/2)^2} \quad (2)$$

and likewise for state B.

Equation (1), with $\Gamma=\Gamma_A+\Gamma_B$ and Eq. (2) are of the same form as the classical equation for the radiation from a damped harmonic oscillator,

[16] Richtmyer, Barnes and Ramberg, Phys. Rev. **46**, 843 (1934).
[17] V. Weisskopf and E. Wigner, Zeits. f. Physik **63**, 54 (1930); V. Weisskopf, Physik. Zeits. **34**, 1 (1933).

TABLE IIIa. *Widths in volts of K_{α_1} and K_{α_2} lines.*[7]

ELEMENT	$K\alpha_1, K \rightarrow L_{III}$	$K\alpha_2, K \rightarrow L_{II}$
Fe	3.0	3.5
Co	2.8	3.6
Ni	2.6	3.6
Cu	2.7	3.7
Zn	2.9	3.5
Ga	3.1	3.3
Ge	3.2	3.5

TABLE IIIb. *Widths of energy levels in volts.*

ELEMENT	K LEVEL	L_{II}	L_{III}
Fe	1.8±0.5	1.7	1.2
Co	1.5±0.5	2.1	1.3
Ni	1.9±0.5	1.7	0.7
Cu	1.3±0.5	2.4	1.4
Zn	1.5±0.5	2.0	1.4
Ga	1.9±0.5	1.4	1.2

where $2\pi\Gamma$ would be the damping factor, or the reciprocal mean life of the excited atom. Γ gives the half-maximum width of the radiated line. If one of the widths in Eq. (1), say Γ_A, is zero, the distribution in line intensity is of the same form as the energy distribution of the level B.

In the process of a K absorption, an electron from the K shell of an atom in state A, is raised to some level above the Fermi distribution leaving the system in one of a continuum of states of energy E, greater than E_0 (state with the electron from the K shell in the first level above the Fermi surface). Richtmyer, Barnes and Ramberg have shown that the absorption curve for the edge may be taken as the sum of successive absorption lines to the discrete states E, the shape of each absorption line being given by (1). The width of the absorption limit from $\frac{1}{4}$ to $\frac{3}{4}$ maximum of absorption coefficient, calculated with a distribution of excited levels uniform to higher energies, is then exactly equal to the width at half-maximum of one of the absorption lines. If Γ_A is zero, this is the width of the excited state, or K level.

In mathematical form[16] the partial absorption coefficient is given by

$$K(\nu) = C \sum_{\nu_{EA}=\nu_{E_0A}}^{\nu_{EA}=\infty} (E)\gamma_{EA} \times \left(\frac{\Gamma_E/2\pi}{(\nu_{EA}-\nu)^2+(\Gamma_E/2)^2} \right), \quad (3)$$

in which Γ_A, the width of the normal state, is neglected in comparison to Γ_E. C is a constant. $2\pi\gamma_{EA}$ is the transition probability from state E to the normal state A. By making a number of reasonable assumptions, the summation can be replaced by an integral, which yields the simple result,

$$K(\nu) = C' \left\{ \frac{1}{2} - \frac{1}{\pi} \arctan \left(\frac{\nu_{E_0A}-\nu}{\Gamma_E/2} \right) \right\}. \quad (4)$$

If instead of a uniform density of states E, assumed in deriving this expression, some more complicated distribution is chosen, the results on the low frequency side of the absorption limit are only slightly changed.[16]

By matching curves of the form (4), having different values of the parameters Γ_E and C', with the experimental curves, it is possible to find an arctangent curve, which up to the inflection point, closely fits the measured absorption curve. The value of Γ_E for the arctangent curve then, gives the width of the K energy level. The widths obtained by this method are listed in the first column of Table IIIb. The widths of the K levels within the probable errors indicated are about the same throughout the series measured. Table IIIa gives the widths of the K_{α_1} and K_{α_2} lines of the elements Fe to Ga,[7] from which the widths of the L_{II} and L_{III} levels can be obtained by means of the relation,

$$W_{\text{Line}} = \Gamma_A + \Gamma_B, \quad (5)$$

if the width of the K state is known. The widths calculated in this way are given in the last two columns of Table IIIb. The L_{II} level in each case is much wider than the L_{III}. The doublets $K_{\beta_{1,3}}$ in this series are not resolved, so that the M_{II} and M_{III} level widths cannot be calculated from the data.

The L_{III} edge for platinum gives a value of 4.1±0.5 volts, which is in good agreement with the value of 4.4 volts obtained for Au L_{III}.[16]

In the case of germanium, a powder absorber has been used and it has not been possible to fit the curve well with any arctangent curve. It is obvious that radiation transmitted through such an absorber does not all pass through a uniform thickness, and while it will show all the structure that would be found with a foil, the logarithmic

plot cannot be expected to vary in direct proportion to absorption coefficient. The arctangent curve which most nearly fits the germanium absorption curve would give a width for the edge almost as great as obtained for Pt L_{III}, but such a width for the Ge *K* state cannot be correct because it is greater than the width of several Ge lines in the *K* series. In contrast to Ge, the Pt curve fits almost perfectly with its arctangent curve.

To all these widths, corrections[18] for the (1−1) rocking curve widths have been applied. For the region covered the corrections run from 0.6 to 0.7 electron volt.

Wave-Lengths

With the poor resolution obtainable photographically, it has been customary to pick the midpoint of the apparently sharp increase in absorption as the wave-length position of the absorption edge. Since the double crystal spectrometer has revealed considerable width and structure in the edge itself, the question arises as to whether any meaning can be given a wave-length position for the edge. The inflection point of the arctangent curve fitted to an absorption edge gives the wave-length position of E_0, the energy of the first empty levels. It seems logical to pick this position then as the wave-length of the absorption edge. Table IV gives these positions as indicated by the letter *L* on each absorption curve, and for comparison, the wave-lengths given by other investigators. For the edges from Fe to Cu, as is apparent from Figs. (3–7), we should expect our values to be of shorter wave-length. For Zn, Ga, Ge, and Pt, our values should agree with the others to within at most 0.3 X.U. Since the measurements in the present work are good to 0.02 X.U., our uncertainties lie only in the assignment of the positions *L* by the arctangent fits. The results, therefore, indicate comparatively large errors in some of the previously reported wave-lengths.

Table IV. *Wave-lengths in X.U. of absorption limits.*

Edge	Authors' Measurements	Previous Measurements
Fe *K*	1739.9	1739.4[1]
Co *K*	1604.9	1604.0[1]
Ni *K*	1485.2	1483.9[1]
Cu *K*	1377.7	1377.4[1]
Zn *K*	1280.7	1280.5[1]
Ga *K*	1193.4	1190.2,[2] 1192.5[3] 1192.9[4]
Ge *K*	1114.3	1114.6[2]
Pt L_{III}	1070.0	1071.0[5]

[1] Ase, reported in Siegbahn, *Spektroskopie der Rontgenstrahlen* (1931).
[2] Duane, Blake and Hu, from W. Duane, Bull. Nat. Res. Counc. U. S. A. 1, 6 (1920).
[3] W. W. Mutch, Phys. Rev. **50**, 197 (1936).
[4] B. Kievit and G. A. Lindsay, Phys. Rev. **36**, 648 (1930).
[5] A. Sandström, Zeits. f. Physik **54**, 632 (1930).

[18] L. G. Parratt, Phys. Rev. **46**, 749 (1934).

Discussion

I. Calculation of band structure

The problem of calculating energy levels and wave functions for electrons in a metallic lattice has been approached from two different directions. If the electron is moving with an average kinetic energy large when compared with the maximum variation of potential energy in the lattice, one may say that its wave function will not be very different from that of a free electron. The actual problem can be approximately solved by starting with the solution of the constant potential case and calculating the effects of a perturbing periodic potential. It is found that the perturbation separates the allowed energy ranges into zones whose boundaries are determined by the possibility of reflection of the electron wave by the lattice. The propagation of an electron with such a direction and energy that the associated wave would suffer Bragg reflection from the lattice is not permitted.

Kronig,[19] using the free electron approximation, calculated the distribution of allowed levels and found some energy ranges where the level density was low and others where the levels tended to cluster. These regions agree well in position with the regions of low and high absorption coefficient, observed[15] on the high frequency sides of the *K* and *L* absorption edges of several metals.

The second method of calculating, instead of starting with free electron wave functions, uses atomic wave functions as the zero-order approximation. This approach is most applicable to the low-lying bands, where the overlapping of the electron clouds of adjacent atoms and therefore the splitting of the band is not too great. Except

[19] R. de L. Kronig, Zeits. f. Physik **70**, 317 (1931); **75**, 191 (1932).

for the work of Jones, Mott and Skinner[3] on the interpretation of shapes of emission lines in the very soft x-ray region, there has been no attempt to apply results of this second method to problems of x-ray spectroscopy.

The most careful calculations with the atomic approximation have been made by Krutter[5] and Slater[6, 20] following the general procedure developed by Wigner and Seitz[21] and Slater.[22] We will give a short description of these calculations since they furnish quite a convincing explanation of the observed shapes of the Cu K edge and $K\beta_{2,5}$ emission line. Calculations have been carried out only for Cu but all the plausible extrapolations made to nearby elements are borne out by the observations.

Bloch has shown that the wave functions of an electron in a periodic field must always be of the form

$$\psi_{\mathbf{k}}(\mathbf{r}) = u_{\mathbf{k}}(\mathbf{r}) \exp\left[2\pi i(\mathbf{k}\cdot\mathbf{r})\right],$$

where $\mathbf{k}$ is the wave vector and $u_{\mathbf{k}}(\mathbf{r})$ has the periodicity of the lattice. For electrons with large kinetic energies, $u_{\mathbf{k}}(\mathbf{r})$ is almost a constant and the wave function approximates that of a free electron. In the lower bands, $u_{\mathbf{k}}(\mathbf{r})$ may be a rapidly changing function of position and near the lattice points will behave much like an atomic wave function, as one would expect if an atomic approximation is to be valid.

From the form of the wave function it is seen to be determined everywhere if known in the neighborhood of one arbitrary lattice point. Its value around any other lattice point can be obtained by multiplying by $\exp\left[2\pi i(\mathbf{k}\cdot\mathbf{R}_0)\right]$ where $\mathbf{R}_0$ is the displacement vector from the first to the second nucleus. Krutter[5] chose as neighborhood a symmetrical twelve-sided polyhedral cell at whose center was a Cu nucleus. The cell was of such a size and shape that if one cell were placed about each point of the lattice, the set would pack together tightly and completely fill the space. It was assumed that within each cell the potential field is that of an isolated singly charged Cu ion and the radial part of Schrödinger's equation was solved for such a field. However, the boundary conditions are no longer the same as in the case of the isolated ion. Instead of the disappearance of the wave function at infinity, we now have the requirements that in going from one side of the polyhedral cell to the diametrically opposite side the wave function be multiplied by $\exp\left[2\pi i(\mathbf{k}\cdot\mathbf{R}_0)\right]$ where $\mathbf{R}_0$ is again the displacement vector involved. This is equivalent to requiring that the solution in one cell be joined onto the solution in an adjacent cell in such a way that when extended through the lattice the wave function is modulated as required by Bloch's theorem.

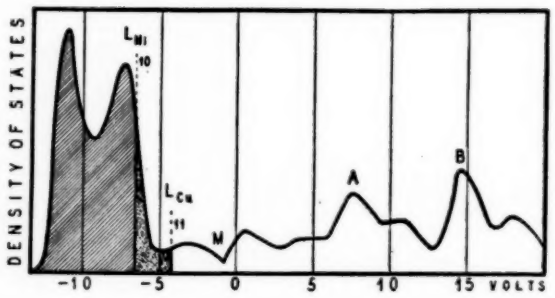

FIG. 11. Density of states as a function of energy in Cu (redrawn from a paper by Rudberg and Slater (reference 20), with some additional markings). Lines labeled L_{Ni} and L_{Cu} give the energies to which the bands are filled in Ni (assuming same energy levels as for copper) and in Cu by 10 and 11 band electrons per atom, respectively.

Krutter expresses the wave function in the cell as a linear combination of twelve independent functions whose angular parts are the twelve lowest spherical harmonics and whose radial parts are the above-mentioned solutions of Schrödinger's equation. The coefficients in the linear combination are determined by satisfying the boundary conditions at the midpoints of the twelve faces. The equations contain as supposedly known parameters, the energy entering through the Schrödinger equation and the direction of the wave vector $\mathbf{k}$ which enters through the boundary conditions. If values are assumed for these parameters, the magnitude of $\mathbf{k}$ can be calculated. It will sometimes be real, corresponding to an allowed choice of the energy for the assumed direction of propagation, and sometimes imaginary, corresponding to a forbidden energy.

Krutter was mainly interested in the splitting of the $3d$ band and actually solved his equations for only three directions in the lattice. The calculations were extended to higher bands by

[20] E. Rudberg and J. C. Slater, Phys. Rev. **50**, 150 (1936).
[21] E. Wigner and F. Seitz, Phys. Rev. **43**, 804 (1933).
[22] J. C. Slater, Phys. Rev. **45**, 794 (1934).

Slater[6, 20] and the results averaged over all directions of propagation. It was then possible to give a curve of density of allowed states against energy such as is here reproduced in Fig. 11 taken from reference 20.

The accuracy of this curve is difficult to estimate since there have previously been few comparisons with experiment and the calculations give little hint of their own reliability. There may be errors of volts in the position of the structure and possibly some change in the nature of band splitting, but our experimental results seem to indicate that the results of the calculations are better than one would generally expect from the approximations involved.

A knowledge of the density of states is not in itself sufficient to give a prediction of the shape of an emission line or of structure close to an absorption edge since the transition probability to those states will also be a function of energy. Jones and Mott[4] write the intensity of x-ray absorption or emission as $I(E)=N(E)\cdot p(E)$ where $N(E)$ is the density of states and $p(E)$ the transition probability. We are dealing with transitions to and from the K state, so $p(E)$ will be assumed directly proportional to the amount of p function used in the description of the band level. The variation of this quantity with energy is not made explicit in the calculations of Krutter and Slater, but enough can be determined about it to permit a comparison with experiment.

There is no great difference in the physical reasons for Kronig structure and structure in the absorption edge itself, inasmuch as the function $I(E)$ determines the intensity of absorption in both cases. Methods of calculating $I(E)$ will change depending upon the distance from the edge, which is equivalent to saying that the relative importance of the various factors, upon which $I(E)$ depends, will change. The crystal structure is decisive for the Kronig structure. Near the edge, the atomic field is more important. The energy regions in which the atomic and free electron approximations are useful do not quite overlap, and between about fifteen and forty volts beyond the main edge, no good calculations exist.

II. The $K\beta_{2,5}$ emission lines

We have plotted the $K\beta_{2,5}$ emission lines of the transition elements as measured by Bearden and Shaw[7] on the same wave-length scale as the K absorption edges. There are several reasons for believing that these lines should be interpreted in terms of transitions of electrons from the filled bands of the metal to the empty K state. In each case, the high frequency side of the line matches closely the beginning of absorption in the edge. While no other K series lines of these elements have half-widths in excess of four volts, these lines have half-widths of from five to ten volts. The latter widths are about what one would expect for filled bands. The band origin is also suggested by the asymmetries of the $K\beta_{2,5}$ lines. Bearden and Shaw[7] report values of indices of asymmetry between two and three for all the elements measured except Ni and Ge. Other K series lines of the same elements have asymmetries considerably less than two. The index of asymmetry is defined as the ratio of the part of the half-maximum width of the line on the low frequency side of the peak to the part on the high frequency side. A value greater than one indicates that the line falls off more steeply on the high frequency side of the maximum. This is just the behavior to be expected in lines arising from transitions from filled bands. The decrease in intensity on the high frequency side comes about because beyond a certain point the bands are no longer filled, and the sharpness of the decrease is limited only by the width of the K state. On the low frequency side, the falling off in intensity is determined by the function $I(E)$ and will generally be much more gradual.

It is not believed that reabsorption in the target of the high frequency side of the line, where the K absorption begins, had any part in producing the high asymmetries. The penetrating power of electrons is much less than that of the x-rays, so the x-rays are produced near enough to the surface of the target so that they will not be appreciably absorbed.

It is customary to classify $K\beta_5$ as a $K-M_{IV,\,V}$ transition, and $K\beta_2$ as a $K-N_{II,\,III}$ transition. This is undoubtedly correct for those elements of which these levels do not take part in band formation in the solid. In Zn, however, the lines are clearly separated, although there are still no electrons in the $N_{II,\,III}$ levels.

If one considers the ratio of the intensity of the line next to the edge (whether it be $K\beta_2$ or $K\beta_5$) to

K_{α_1}, as a function of atomic number, a further anomaly appears. It would be expected for the free atom that this intensity ratio should be very low for atomic numbers less than 31, since then, the outermost electrons are either $3d$ or $4s$ and the transition is from an even state to an even state which is not allowed as a dipole transition. At Ga the first $4p$ electron is added and the dipole transition becomes allowed. We would expect a sudden increase in the intensity ratio at Ga, but this is not found experimentally. H. T. Meyer[23] has made measurements extending from atomic number 23 to 49, and reports values of the relative intensity $\beta_{2,5}/\alpha_1$ of roughly 0.0020 for the elements Fe to Zn. Ga is not given but Ge is 0.0046 and As 0.0069. Williams[24] gives values of 0.0036 for Zn and 0.0132 for Ge. Beyond Ge both authors report a roughly linear increase of the ratio with atomic number, i.e., with added $4p$ electrons. Thus, in going from transitions which in the atomic picture are forbidden to those which are allowed, the probability increases by a factor of only three.

This behavior is understandable in transitions from filled bands. The radiation is probably always dipole, the necessary p function being furnished in the case of elements below Ga by the extensive mixing of states of different angular momentum which occurs when atoms are brought close together as in the metallic lattice. This constitutes a quantum-mechanical description of the breakdown of the conservation of angular momentum about an atomic center, which occurs when interaction with neighboring atoms becomes important.

That there is considerable mixing of p function in the $3d$ and $4s$ bands of Cu was shown by Krutter's calculations. The amount of this admixture will increase gradually as the $4p$ band is approached causing a gradual rather than a sudden increase in the intensity ratio. The magnitude of the initial K absorption jump as a function of atomic number in this series of elements varies in much the same manner.

III. Correlation of Cu and Ni data with the calculations

It is proposed to try to explain the shapes of the $K_{\beta_{2,5}}$ emission lines and the K absorption edges by comparison with the $I(E)$ function, but because of the width of the K state, the comparison is not direct in certain cases. If $I(E)$ has a high or low value for some range of levels in the band, its effect on the intensity of absorption is felt not just at the corresponding wave-length but over a range of about the half-width of the K state on each side. Conversely, the intensity of absorption or emission at a given wave-length is determined by an average of $I(E)$ over a range extending a volt or two to each side of the corresponding energy level. Most of the comparisons are concerned with the distances between maxima and minima of absorption, and these will not be greatly altered by the width of the K state provided that $I(E)$ varies approximately symmetrically on each side of the maximum or minimum.

As has been pointed out, the beginning of each absorption curve can be closely fitted to an arctangent and from this can be obtained the width of the K state and the height to which the levels in the band are filled. The latter position is particularly important in making comparisons with the theory.

The calculated density of states for Cu (Fig. 11) shows the $3d$ atomic wave functions drawn into a band with a high density of states (really five overlapping bands) extending from -13 to -5.5 volts. This high density of states is to be expected because the overlap of the $3d$ functions is relatively small. The $4s$ band extends from -13 to about -0.5 volt with a considerably lower density of states. At M the $4s$ and $4p$ bands barely overlap. Above this point, the density of states varies in a rather complicated manner. The intensity of absorption will be great in this region, since the band arises from the splitting of p atomic functions and will be largely described by such functions.

In the lower bands it is necessary to know something about $p(E)$. From Krutter's work, it can be found that of the five $3d$ bands which combine to give the double-peaked structure below -5 volts in Fig. 11, those which are split least contain no p function. It is these bands which give rise to the lower energy maximum in the density of states curve. The remaining bands do contain p function, and they combine to give

[23] Quoted in Compton and Allison, *X-rays in Theory and Experiment*, page 641.
[24] J. H. Williams, Phys. Rev. **44**, 146 (1933).

TABLE V. *Comparison of the calculated and observed structure of copper bands.*

STRUCTURE (FIG. 6)	THEORY (EV)	EXPERIMENT (EV)
$K\beta_5-L$	3.1	3.4
$L-M$	3.4	4.0
$M-A$	8.3	10.7
$A-B$	7.2	9.4

the higher energy maximum. $I(E)$ for the $3d$ band will then have a maximum at about the position of the higher energy maximum of $N(E)$. It will decrease gradually to zero at -13 volts and rapidly to zero at -5.5 volts.

In the $4s$ band, the admixture of p function is greater than in the $3d$, so much greater, in fact, that $I(E)$ assumes higher values there, in spite of the lower $N(E)$. Tibbs[25] has shown that for the (111) direction, the top and bottom state of the s band is a pure s function. In between, the admixture of p function has a maximum, and there seems to be no experimental evidence for more than a single maximum.

In the $4p$ band, nothing has been published about the variation of $p(E)$ except that the lowest state for the (111) direction is a pure p state.[25] For higher states the contribution of the p function will fall off, perhaps fast enough so that $I(E)$ will not exhibit the maximum at about one volt which $N(E)$ has and which fails to appear experimentally. Good agreement may be obtained between the higher calculated levels and experiment, by identifying the maxima of $N(E)$ labelled A and B in Fig. 11 with the absorption maxima A and B in the Cu K edge, Fig. 6.

According to the theory, the copper bands are filled to the point marked L_{Cu} in the curve (Fig. 11). With this information, a comparison with experiment can be made. The main peak in the emission line (Fig. 6) corresponds to the maximum of $I(E)$ in the $3d$ band. There is a further slight hump on the high frequency side of the line probably due to emission from the filled part of the $4s$ band beyond the high frequency limit of the $3d$ band.[26] Beyond the filled levels, the theoretical curve for $I(E)$ is to be correlated with the experimental absorption curve. In Fig. 6, there is an initial absorption into the $4s$ band and then a decrease in the absorption at M which is due to the small overlap between the $4s$ and $4p$ bands. Beyond M the absorption increases steadily to A with no suggestion of intermediate structure as has already been mentioned. The numerical comparison is given in Table V. The agreement is within the uncertainty to be expected from the calculations.

Nickel has the same crystal structure as Cu and not too close to the edge one would expect the same band structure. The experimental curves have very similar shapes in the region of high absorption. Near the filled levels the different atomic fields will alter the level distribution somewhat, but if we assume as a first approximation that the Cu levels apply also to Ni, as suggested by Slater,[6] then the ten band electrons of Ni will fill the levels to the height indicated L_{Ni} in Fig. 11. It would be expected from this that the structure on the high frequency side of the Cu $K\beta_5$ due to emission from the filled $4s$ levels would be missing in Ni. This is experimentally verified by the smooth emission curve in Fig. 5.

We do not obtain in Ni the absorption minimum M resulting from the small overlap of the $4s$ and $4p$ bands. This seems to indicate the inadequacy of the assumption that the Ni and Cu bands are identical. The failure is probably due to the smaller nuclear charge and slightly smaller lattice distance of Ni, both of which would cause a greater overlapping of the s and p bands in Ni.

If one identifies the absorption maxima A in Cu and Ni as arising from the same peak in $N(E)$, it is possible to measure the difference in the heights to which the bands are filled in the two metals. This is just the difference between the voltage separations of A and L in Cu and Ni, Figs. 5 and 6, which give an experimental 2.6 volts against the theoretical 2.4. At first sight, it would seem just as reasonable to match the peaks of the two K_{β_5} lines in emission. The distance from the peak of K_{β_5} to L is 3.4 volts in Cu and 2.0 volts in Ni, making an experimental 1.4 volts between the tops of the two Fermi distributions. This discrepancy comes about because in Ni the filled levels extend but a short distance beyond the position of maximum $I(E)$ in the $3d$ band. The width of the K state spreads

[25] S. R. Tibbs, Proc. Camb. Phil. Soc. **34**, 89 (1938).

[26] The small peak at the bottom of this line, on the high frequency side, is a satellite. Such satellites are also present in the $K\beta_{2,5}$ lines of the other elements.

the contribution of each level of the band over an energy range of about two volts, and there results a shift of the peak toward lower frequencies, essentially because at a frequency slightly less than that of $I(E)_{Max}$ contributions toward the measured intensity are received from states on both sides of the state for which the spectrometer is set, while at $I(E)_{Max}$ contributions are received only from the low frequency side.

TABLE VI. *Voltage separation $K\beta_5$ to A (from Figs. 2–9).*

ELEMENT	Fe	Co	Ni	Cu	Zn	Ge
$K\beta_5$ to A (ev)	22.2	23.6	19.3	18.1	21.0	33.5

An approximate calculation of the same type as that carried out to yield the arctangent curve for an absorption limit gives a shift of $\frac{3}{4}$ the width of the Ni K state, or 1.4 ev, if $I(E)$ is assumed to be a maximum at the high frequency limit of filled states, falling off to zero with lower frequencies in a distance of eight volts. This again gives agreement with the theoretical separation.

IV. Other elements

A. Identification of the 1st maximum of absorption.—For the other elements no quantitative comparison can be made with the present experimental results because changes in crystal structure make impossible even an approximate extrapolation of the theoretical results in Cu. However, certain general remarks may be made. The point A marking the first maximum of absorption beyond the edge itself is believed to be an absorption into the $4p$ band for each of the elements observed. This has already been shown for Cu and Ni and the extension to other elements can be seen by reference to Table VI where the voltage distance from K_{β_5} to A is given. It is seen that until one begins to add $4p$ electrons at Ge, the voltage separation remains about constant so that A must correspond to the same band in each element. It is known that K_{β_5} is the same emission line for each because the lines fall on the same Moseley diagram. At Ge, of course, the absorption is pushed to higher levels because of the filling of the $4p$ band. No comparison is possible with Ga since K_{β_5} could not be measured in the emission work, perhaps due to the fact that Ga was used on the target in the liquid state.

B. High density of states in 3d band.—All the theories of the transition elements agree in assigning a high density of states to the $3d$ band irrespective of the crystal structure and also agree that this band is in the process of being filled through Fe, Co, and Ni, and is full at Cu. One would expect that in the d band the addition of an extra electron would not raise the top of the filled levels nearly as much as the addition of an electron into the s or p band where the density of states is considerably lower.

Table VII gives the distances from L to A for each element.

Since A is an absorption into the same band for each, the differences in the above figures for the successive elements are a rough measure of how much the top of the Fermi distribution is raised by the addition of an electron. From Fe to Ni the levels are within three volts of each other indicating a high density of states. Co appears misplaced, but no better agreement can be expected when the crystal structure varies. The Cu electron completes the filling of the $3d$ band and overlaps partially into the $4s$ raising the filled levels 2.6 ev. However, at Zn and Ga, the electrons raise the top of the distribution 4.6 and 5.7 volts, respectively, giving direct evidence for the lesser density of states in the $4s$ and $4p$ bands. It is to be noted that this method of treating the data gives directly $N(E)$ and not $I(E)$. Ge and Pt are included in the table to indicate what edge widths are to be expected when there is strong absorption into the first empty levels.

C. Magnitude of initial absorption.—It is possible also to obtain approximately the ratio of $I(E)$ for the lowest empty levels to $I(E)$ for the $4p$ band at the point A. The point L (Figs. 3–10), marking the top of the filled levels, occurs just halfway up the absorption curve which would

TABLE VII. *Voltage distance from top of filled levels to first maximum absorption.*

ELEMENT	L TO A (EV) (FROM FIGS. (3–10))	ELEMENT	L TO A (EV) (FROM FIGS. (3–10))
Fe	19.8	Zn	10.1
Co	20.5	Ga	4.4
Ni	17.3	Ge	4.3
Cu	14.7	Pt	3.3

result if $I(E)$ were a constant for all the empty levels. Therefore, if double the ordinate of L is divided by the ordinate of A, the desired ratio is obtained. The results are given in Table VIII.

Table VIII indicates that $I(E)$ at the edge increases continuously from Fe to Ga as would be expected from the gradually increasing admixture of p function in going from the $3d$ and $4s$ to the $4p$ band. It is also clear that $I(E)$ is larger for the $4s$ than for the $3d$ band.

Checks have been made to determine how much the shape of the absorption curve up to the inflection point L was affected by absorption into levels some distance beyond the first empty ones. This was done by cutting off the summation at various distances past $\nu_{E_0 A}$ in Eq. (3) instead of continuing to infinity. The results indicate that levels removed from highest filled level by more than twice the width of the K state may be neglected. The magnitude of the initial absorption jump is determined then by an average value of $I(E)$ for the states within four volts of the edge, the states closest to the edge being the most heavily weighted in the average.

D. Platinum.—The Pt L_{III} edge, Fig. 10, is an interesting example of the influence of the selection rules on the shape of the edge. It has the same crystal structure and the same number of band electrons as Ni. Results[27] on the paramagnetic susceptibility of Pt alloys indicate that the d band lacks completion by about the same amount as in Ni. However, the shape of the edge is entirely different because in Ni the absorption process involves excitation of an s electron into the d and s band while in Pt a p electron is excited into the same bands. The fact that in Pt the inflection point L occurs more than halfway up the edge, indicates that $I(E)$ has its greatest value for the lowest empty levels, and for slightly higher levels, takes on considerably smaller values. This is to be expected since absorption into the p band will be weak.

E. Asymmetries of lines.—It is possible to understand the asymmetries of the $K_{\beta_{2,4}}$ lines in emission a little more completely by a more careful consideration of the band structure. It has been stated that the asymmetry of the line arises from the asymmetry of $I(E)$ where we assume while discussing emission lines that $I(E)=0$ for unfilled levels. Generally, the discontinuous drop to zero at the top of the filled levels is the decisive factor in giving the line its high asymmetry. If, however, the highest filled level is in a region of very small $I(E)$ then both sides of the line are determined by how $I(E)$ varies in the filled levels, and the line may or may not have high asymmetry. The best example of this is Ge which is a semi-conductor, so that there must be a gap between the top of the filled bands and the bottom of the first unfilled bands. Its K_{β_4} line (Fig. 9) is therefore not expected to be abnormally steepened on the high frequency side. Zinc, on the other hand, is a good conductor; there will be considerable overlap of the $4s$ and $4p$ bands and $I(E)$ at the top of the filled levels will be large. The $4p$ band of Ga is only half-full which again gives a large $I(E)$ at the cut-off. The indices of asymmetry for the K_{β_4} lines are Ge 1.21, Ga 2.93, and Zn 3.02, as reported by Bearden and Shaw.[7]

A somewhat similar situation occurs with the K_{β_4} lines of Ni, Co, and Fe, whose indices of asymmetry are 1.75, 2.06, and 2.44, respectively.[7] Calculations indicate that Ni is filled to slightly beyond the maximum density of states so that $I(E)$ has begun to drop at the top of the filled levels. Co and Fe with fewer electrons would have their highest filled levels in a region of maximum $I(E)$, and this probably explains their greater asymmetries.

TABLE VIII. *Percentage of the total absorption jump accounted for by absorption into the first empty levels.*

ELEMENTS	PERCENTAGE	ELEMENTS	PERCENTAGE
Fe	23.0	Zn	78
Co	29.0	Ga	100
Ni	37.0	Ge	100
Cu	53.0	Pt	100

We are indebted to Professor J. A. Bearden under whose direction this work was carried out; to Dr. C. H. Shaw for the Geiger counter technique used in recording the intensities; to Dr. M. Goeppert-Mayer for discussions on the theories involved; and to Dr. David R. Inglis for theoretical discussions and criticism of the manuscript. It is also a pleasure to acknowledge the financial assistance granted Professor J. A. Bearden from the Penrose Fund by the American Philosophical Society.

[27] N. F. Mott and H. Jones, *Properties of Metals and Alloys*, page 199.

X-Ray Dispersion and Atomic Electron Cloud Distortion in Zinc Crystals

E. M. McNatt
Wayman Crow Hall of Physics, Washington University, St. Louis, Missouri

(Received June 28, 1939)

Monochromatic x-rays of wave-lengths 1.54A (Cu $K\alpha$) and 1.433A (Zn $K\alpha$) were diffusely scattered at angles ϕ varying from 24° to 120° from single crystals of zinc ($\lambda_K = 1.28$A) whose orientation angles ψ were 0° and 90°. The intensity of the diffusely scattered rays was found to vary with $(\sin \frac{1}{2}\phi)/\lambda$ according to Jauncey's theoretical formula for the region of wave-lengths close to the K critical absorption wave-length of the scattering crystal. In the case of the scattering of Cu $K\alpha$ rays the decrement Δf in the atomic structure factor was 2.5 as compared with Hönl's value of 2.3. For the less intense Zn $K\alpha$ rays Δf was 3.65 as compared with Hönl's value of 2.8. The difference in the latter case is probably due to experimental error. More interesting was the "dip" or "valley" found in the diffuse scattering $S(\psi = 0°)$ values in the region of $(\sin \frac{1}{2}\phi)/\lambda = 0.3\text{A}^{-1}$. After considering various possible causes for this dip, it was finally decided that the cause of the dip is a corresponding dip in the atomic structure factor $f(\psi = 0°)$ values in this region. The maximum difference, $f(\psi = 90°) - f(\psi = 0°)$ is about 6 electrons. This is greater than the previous value of 2.4 electrons and indicates a larger and deeper distortion of the electron cloud of a zinc atom in the crystal than had previously been imagined.

I. Introduction

JAUNCEY[1] has recently extended the theory of diffuse scattering of x-rays by crystals to the case where the wave-length of the primary rays is longer than the K-critical absorption wave-length of the crystal. The extended theory shows that in the formula for S the change in the incoherent portion is negligible and that the atomic structure factor f in the coherent portion is replaced by $f - \Delta f$ where Δf is the decrement in f due to anomalous dispersion. Hence the theoretical value for S in the region of a K-absorption edge is

$$S = (f - \Delta f)^2(1 - e^{-2M})/Z + [1 - (1/Z)\Sigma E_r^2]/R, \quad (1)$$

where $R = (1 + h \text{ vers } \phi/mc)$[3]. For a hexagonal crystal like zinc, Zener[2] has shown that

$$M = (a \cos^2 \psi + b \sin^2 \psi) \cdot (\sin \tfrac{1}{2}\phi)^2/\lambda^2, \quad (2)$$

where ψ is the orientation angle.[3] For zinc[4] at room temperature, $a = 2.34\text{A}^2$ and $b = 0.68\text{A}^2$.

The original purpose of this investigation was to study the effect of anomalous dispersion on the diffuse scattering of x-rays and to measure the decrement Δf in the atomic structure factor, since Δf values had not been previously determined directly by diffuse scattering methods. Heretofore all experiments on the diffuse scattering of x-rays from zinc crystals had been done with general radiation of an average wave-length of about 0.44A which is much shorter than 1.28A, the K-critical absorption wave-length of zinc. In this investigation, monochromatic radiation of wave-length longer than that of 1.28A was used.

The use of general radiation has the advantage of high primary intensity, which is important because of the very low magnitude of the diffuse scattering coefficient. However, this method has the disadvantage of extreme analytical difficulty in calculating atomic structure values, involving the arithmetical solution of an integral equation.[4, 5] Furthermore there is always the possibility that fine structure effects will be so smeared out because of the range of wave-lengths used as to be indiscernible. Finally it is experimentally very difficult to make diffuse scattering measurements at small scattering angles, so that in order to study the interesting region of small values of $(\sin \frac{1}{2}\phi)/\lambda$ it is expedient to use comparatively soft x-rays, such as Cu $K\alpha$ ($\lambda = 1.54$A) or Zn $K\alpha$ ($\lambda = 1.433$A) radiation.

As the experiment proceeded it became evident that the distortion of the electron cloud in the

[1] G. E. M. Jauncey, paper to be published.
[2] C. Zener, Phys. Rev. **49**, 122 (1936).
[3] In diffuse scattering experiments the orientation angle ψ is the angle that the line bisecting the angle between the forward direction of the scattered rays and the backward direction of the primary rays makes with the c axis of the crystal.
[4] W. A. Bruce, Phys. Rev. **53**, 802 (1938).
[5] G. E. M. Jauncey and W. A. Bruce, Phys. Rev. **51**, 1068 (1937).

zinc atom was more important than had at first been realized[4, 5] and so this research became as much an investigation of the electron cloud distortion as of the anomalous dispersion effects on the long wave-length side of the K-absorption edge of zinc.

II. Apparatus

Since the coefficient of diffuse scattering is so exceedingly small it is necessary to have both a very intense incident beam of x-rays, and a sensitive method of measuring very weak ionization currents produced by the diffuse scattering. An all-metal continuous-pumping x-ray tube was the source of x-radiation. This tube followed in construction a design by Wollan[6] and was water-cooled in order to withstand the heating produced by large electron current-densities at voltages of the order of 25 kilovolts. The vacuum system for the x-ray tube was a two-stage oil-diffusion pump backed by a Cenco Hyvac mechanical pump. This diffusion pump, designed by Professor A. L. Hughes who combined the two-stage arrangement of Henderson[7] with Hickman's[8] refluxing device, performed excellently under adverse conditions. When a dry-ice trap was used pressures of the order of 10^{-6} mm of mercury were readily maintained.

Power to operate the tube was furnished by a conventional 60-cycle transformer-Kenetron high voltage full wave rectifier capable of producing continuously 100 milliamperes at 50 kilovolts. Targets used were of copper and zinc, the latter consisting of a zinc button fused to a copper backing.

Initially a rocksalt crystal was used as monochromatizer but this was soon abandoned in favor of a cleaved zinc crystal for two reasons. First, the deliquescent property of rocksalt caused it to be attacked by moisture in the air to such an extent that the reflected x-ray line became a jumble of lines after two or three weeks. Second, and more important, the absorption coefficients of zinc for Cu $K\alpha$ ($\lambda = 1.54$A) rays and for the rays of half wave-length ($\lambda = 0.77$A) are 58.6 and 64, respectively, because the two wave-lengths are on opposite sides of the K-absorption edge for zinc ($\lambda = 1.28$A). But with rocksalt the absorption coefficient for the Cu $K\alpha$ is roughly eight times that for the half wave-length. This means that the relative intensity of the half wave-length present in the reflected beam should be much less when zinc instead of rocksalt is the reflector. The importance of this effect will be shown later. With proper adjustment of the Seeman wedge, the $K\alpha$ and $K\beta$ lines could be seen easily on a fluorescent screen.

Measurement of the intensities of the primary and scattered x-ray beams was accomplished by means of a Cambridge type Compton electrometer in conjunction with a brass ionization chamber of 5 cm inside diameter and 8 cm length, filled with argon at atmospheric pressure. Although methyl bromide has a slightly greater absorption coefficient for the wave-lengths used, this advantage is not enough to compensate for its extremely corrosive properties. The chamber window was rectangular in shape, 2.12 cm by 0.52 cm, covered with Cellophane of thickness 2.78×10^{-3} g/cm^2, and was 11.5 cm from the spectrometer axis. This chamber is considerably smaller than those used recently in diffuse scattering work and although the background is still larger relative to the intensity of diffuse scattering than is desirable, it is an improvement in that respect over former apparatus.

Whenever the interior of the x-ray tube had been exposed to air, a process of "aging" the tube under increasingly high voltages was necessary for a period depending upon the length of time the tube had been exposed. During this process, a burst of gas occasionally caused a spark discharge within the tube and the resulting radio-frequency pulse picked up by the electrometer and ionization chamber circuit was strong enough to destroy the conducting film on the electrometer suspension. To avoid this minor catastrophe, the electrometer and its associated batteries were entirely isolated electrically by grounded metal shielding outside the electrometer casing, except for a slit through which light was focused on the electrometer mirror.

The electrometer was normally operated at a sensitivity of about 5000 mm per volt, which is a comparatively low voltage sensitivity, but, as

[6] E. O. Wollan, Rev. Sci. Inst. **9**, 3 (1938).
[7] J. E. Henderson, Rev. Sci. Inst. **6**, 66 (1935).
[8] K. C. D. Hickman, J. Frank. Inst. **221**, 215 and 383 (1936).

noted by Neher,[9] the current sensitivity is a maximum in this region. Since the primary intensity was of the order of 10^5 times the scattered intensity, it was necessary to use a shutter which would allow the primary beam to enter the ionization chamber for one-sixtieth of a second (one period of 60-cycle a.c.)

Some measurements were made using an evacuated crystal-holder with the aim of eliminating scattering from the air, but this was found to be not sufficiently important to justify the added complication.

Single crystals of zinc used in this experiment were prepared as described by Jauncey and Bruce[10] with the difference that the crystals were etched electrolytically following the method of Vernon and Stroud.[11]

III. Experimental Method

The experimental value of the diffuse scattering as given by Jauncey and Bruce[12] is

$$S=\frac{4R^2Wm^2c^4}{ANZe^4(1+\cos^2\chi\cos^2\phi)}\times\frac{D(\phi,\theta)}{D_0u(\phi,\theta)}\times\frac{\mu_1}{\rho}, \quad (3)$$

where $D(\phi, \theta)$ is the ionization current caused by the diffusely scattered rays when the ionization chamber is set at a scattering angle ϕ and the crystal face makes an angle θ with the incident rays, and where D_0 is the ionization current caused by the primary beam. It will be noted that the factor $(1+\cos^2\phi)$ as given by Jauncey and Bruce is replaced by $(1+\cos^2\chi\cos^2\phi)$. This change takes account of the polarization of the $K\alpha$ radiation reflected at a grazing angle $\chi/2$ from the monochromatizer. The remaining symbols in (1) are defined by Jauncey and Bruce.[12]

Because the output of characteristic x-radiation increases rapidly as the potential applied to the tube is raised above the excitation potential (8970 volts for Cu $K\alpha$ and 9750 volts for Zn $K\alpha$ rays), high primary intensity may be obtained by operating the tube at a relatively high voltage. However, the monochromatizer will reflect not only the $K\alpha$ radiation but also any submultiple of the $K\alpha$ wave-length. To excite wave-lengths of one-half the Cu $K\alpha$ and Zn $K\alpha$ wave-lengths in the general radiation requires peak potentials of 16,050 and 17,250 volts, respectively. Since in some cases a peak potential of 20,000 volts was used it was necessary to correct for the fluorescence radiation from the zinc crystal (critical K absorption wave-length = 1.28A).

Now the ionization current measured when x-rays are falling on the crystal of zinc is the sum of (1) background currents due to cosmic rays, alpha-particles, insulation leaks, and scattering from the air; (2) diffuse scattering of the half wave-length rays reflected from the monochromatizer; (3) fluorescent radiation from the zinc crystal excited by the half wave-length rays; and (4) diffuse scattering of the $K\alpha$ radiation. On account of the high fluorescence yield[13] it is very important to make the proper correction for the effects due to the half wave-length radiation. To illustrate, with a primary beam containing roughly one percent of half wave-length radiation, the fluorescent intensity was equal to that of the diffusely scattered $K\alpha$ radiation. To get the true $D(\phi, \theta)$, measurements were made as follows. Let B_1 be the background current for a given ϕ and θ, and let D' be the current due to the scattering of half wave-length rays and to the fluorescent radiation excited by it. Then the total current in the ionization chamber is

$$D_1=D(\phi,\theta)+D'+B_1. \quad (4)$$

Now insert a thickness t of aluminum into the primary beam and let the absorption coefficients of the $K\alpha$ rays and half wave-length rays in aluminum be μ_1 and μ_2, respectively. The ioniza-

[9] John Strong, *Procedures in Experimental Physics* (Prentice-Hall, New York, 1938), Chapter VI (H. V. Neher).

[10] G. E. M. Jauncey and W. A. Bruce, Phys. Rev. **51**, 1062 (1937).

[11] W. H. J. Vernon and E. G. Stroud, Nature **142**, 477 (1938).

[12] G. E. M. Jauncey and W. A. Bruce, Phys. Rev. **50**, 413 (1936).

[13] Compton and Allison, *X-Rays in Theory and Experiment* (D. Van Nostrand, 1935), pp. 477–492. The intensity of the fluorescent scattering is inversely proportional to the sum of the linear absorption coefficients for the fluorescent and exciting radiations, and directly proportional to the fluorescence yield. Since for the case at hand the linear absorption coefficients of zinc for $\lambda=0.77$A and for its own K radiation are relatively small, and since the fluorescence yield is about 0.5 we should expect a comparatively large amount of fluorescence radiation.

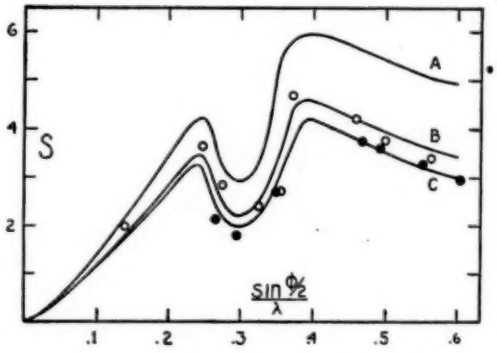

FIG. 1. S values for zinc, $\psi=0°$. Clear circles, Cu $K\alpha$ rays; black circles, Zn $K\alpha$ rays.

tion current is then[14]

$$D_2=\exp[-\mu_1 t]D(\phi,\theta)+\exp[-\mu_2 t]D'+B_2, \quad (5)$$

where B_2 is the background when the aluminum is inserted. Eliminating D' from (4) and (5), we obtain

$$D(\phi,\theta)=\{D_1-(D_2-B_2)\exp[\mu_2 t]-B_1\}/\{1-\exp[(\mu_2-\mu_1)t]\}. \quad (6)$$

The background currents B_1 and B_2 are measured by turning the crystal so that its face cannot be "seen" by the ionization chamber window. For the primary intensity D_0 we get similarly

$$D_0=\{I_1-(I_2-B)\exp[\mu_2 t]-B\}/\{1-\exp[(\mu_2-\mu_1)t]\}, \quad (7)$$

where I_1 and I_2 are the primary beam currents measured respectively without and with aluminum and B is the background.

This method was used for part of the Cu $K\alpha$ data, with the tube operated at 20 kilovolts peak and 50 ma. But with a zinc target it was not possible to use so much power because the zinc melted at the focal spot. Therefore all the Zn $K\alpha$ data (and part of the Cu $K\alpha$ data) were taken with the peak voltage ≤ 15 kilovolts, thus avoiding the necessity for correcting for the effect of the half wave-length radiation. As a matter of experience it was found to be more satisfactory to use the lower voltage than to correct for the fluorescence radiation, even though the primary beam was on this account decreased to about $\frac{1}{5}$ of that attained with the higher voltage. The reduced intensity and consequent increased length of time necessary for obtaining a single reading with the same probable error as with the higher intensity is compensated for by the fact that just two types of readings are necessary, whereas the correction method requires four. Furthermore, the correction for fluorescence introduces an additional possibility of systematic experimental error.

[14] H. Hönl, Ann. d. Physik **18**, 625 (1933). See also W. A. Bruce, reference 4.

IV. Experimental Results

The experimental S values as calculated by (3) are shown in Figs. 1 and 2, in which the white circles represent measurements made with Cu $K\alpha$ ($\lambda=1.54$A) rays and the black circles represent measurements made with Zn $K\alpha$ ($\lambda=1.434$A) rays. Fig. 1 is for zinc crystals with orientation angle $\psi=0°$, and Fig. 2 is for zinc crystals with $\psi=90$.

The writer wishes to point out that the "dip" or "valley" in the S curves jor $\psi=0°$ in the region $(\sin\frac{1}{2}\phi)/\lambda=0.3\text{A}^{-1}$ has not previously been found.

V. Effect of Anomalous Dispersion

The curves A, B, and C of Fig. 1 except in the region $0.25\text{A}^{-1}<(\sin\frac{1}{2}\phi)/\lambda<0.4\text{A}^{-1}$ were calculated from (1) on the basis of Bruce's[4] $f(\psi=0°)$ values with $\Delta f=0$, 2.5, and 3.3, respectively. The curves D, E, and F of Fig. 2 were calculated on the basis of Bruce's $f(\psi=90°)$ values over the whole region with $\Delta f=0$, 2.5, and 4.0. It will be seen that the experimental points fall reasonably well on the theoretical curves. The value 2.5 of Δf for Cu $K\alpha$ on zinc ($\lambda/\lambda_K=1.2$) is particularly gratifying in that it is reasonably close to Hönl's value[14] of 2.3. The average 3.65 of the two values 3.3 and 4.0 for Zn $K\alpha$ on zinc ($\lambda/\lambda_K=1.1$) is greater than Hönl's value of 2.8. The Zn $K\alpha$ rays

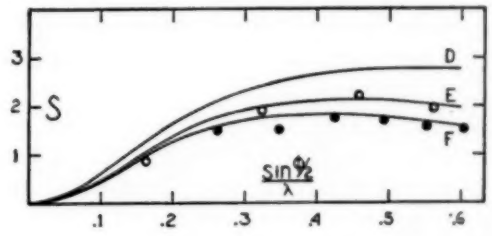

FIG. 2. S values for zinc, $\psi=90°$. Clear circles, Cu $K\alpha$ rays; black circles, Zn $K\alpha$ rays.

were much less intense than the Cu $K\alpha$ rays and the values 3.65 and 2.8 probably do not differ by more than the experimental error.

A collection of values for Δf obtained by different investigators is shown in Fig. 3. This diagram is taken from papers by Allison and Jesse[15, 16] with the points obtained by the writer added. It is seen that the experimental values form a kind of cloud about Hönl's theoretical curve. Perhaps the best that can be said in this connection is that the Δf values obtained by diffuse scattering like the values obtained by other methods show the necessity of taking account of anomalous dispersion in the region of λ/λ_K near unity.

The importance of taking account of Δf in diffuse scattering is shown by the curves A and D in Figs. 1 and 2, which were calculated on the basis of no dispersion ($\Delta f=0$). The departure of the experimental points from these curves is beyond doubt and the writer believes that the experimental evidence supports Jauncey's theoretical equation (1).

VI. Attempts at Explanation of Dip in the $S(\psi=0°)$ Curve

(a) Experimental error

At the close of Section IV the reader's attention was drawn to the existence of a "dip" in the experimental S ($\psi=0°$) curves. When Bruce's f values are used in (1) no such dip appears. At first it was thought that the low S values in the region of $(\sin\frac{1}{2}\phi)/\lambda=0.3\text{A}^{-1}$ might be due to experimental error and these S values have consequently been determined again and again with various crystals but they always exhibit the same behavior as shown in Fig. 1. The reality of the existence of the dip being established, the question arises as to its explanation.

The theory of diffuse scattering is well established only in those regions where the angle of scattering is not too close to the direction in which a Laue spot occurs. Therefore in making determinations of S values it is necessary to be far enough from the position of a Bragg reflection so that the readings are independent of θ when

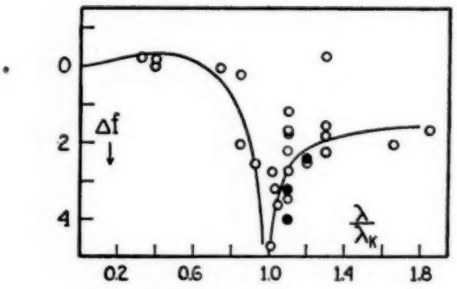

Fig. 3. Values of Δf. Clear circles, results from previous reflection measurements; black circles, results from diffuse scattering measurements; curve, Hönl's theory.

they are divided by

$$u(\phi,\theta)=\frac{2\sin(\phi-\theta)}{\sin(\phi-\theta)+\sin\theta}, \qquad (8)$$

where ϕ is the angle of scattering and θ is glancing angle of the x-rays on the surface of the crystal. Because of the width of the ionization chamber window and of the defining slits for the primary beam, it is a matter of experience that the scattering angle should differ from twice the Bragg angle for reflection by approximately four degrees or more. All observations made fulfilled this condition.

(b) Laval's discontinuities

In 1937 Laval[17] reported discontinuities in the diffuse scattering of Cu $K\alpha$ rays from powdered crystals in the region between a scattering angle of zero and a scattering angle less than twice the Bragg angle corresponding to the smallest angle of reflection. It was a disconcerting fact that one of the discontinuities found by Laval for powdered nickel occurred at $(\sin\frac{1}{2}\phi)/\lambda$ close to 0.3A^{-1}. Since, according to Laval, the $(\sin\frac{1}{2}\phi)/\lambda$ for a given discontinuity is a function of the atomic number, there should be a discontinuity for zinc in this region. However, Harvey[18] has shown that Laval's discontinuities for aluminum can all be explained on the basis of reflections of submultiples of the Cu $K\alpha$ rays from the powdered aluminum. In Table I are shown values of $\sin\frac{1}{2}\phi$ for Laval's reported discontinuities for aluminum. In the second row of the table are shown the values calculated according to Harvey's

[15] S. K. Allison and W. P. Jesse, Phys. Rev. **49**, 483 (1936).
[16] W. P. Jesse, Phys. Rev. **52**, 443 (1937).
[17] J. Laval, Comptes rendus **201**, 889 (1935).
[18] G. G. Harvey, Phys. Rev. **55**, 1147 (1939).

suggestion. In the third row are shown the respective reflections[19] of submultiples of the Cu $K\alpha$ wave-length. Thus (111)/3 means the (111) reflection of the wave-length (1.54/3)A from powdered aluminum. The figures in the second row of this table agree so well with those given by Laval (first row) that the writer feels with Harvey that the discontinuities claimed by Laval do not exist for pure Cu $K\alpha$ rays. Hence the writer has been forced to discard any explanation of the dip on the basis of Laval's discontinuities.

(c) Error in fluorescence correction

Since the unexpectedly low values of S occurred at approximately the value of ϕ for which a third-order Bragg reflection for the half-wave-length would occur, it was thought possible that there might be an error in the correction for the half-wave-length radiation present in the primary beam. For, if the correction factor for the half-wave-length radiation were too large, then a Bragg reflection of this radiation would result in a low S value because of over-correction. To remove this possibility the potential across the x-ray tube was reduced below the excitation potential for the half-wave-length. However, even with the lower operating voltage, when no correction for the half-wave-length rays was needed, the low S values persisted. The presence of uncorrected half-wave-length rays would of course result in a high S value. Consequently this explanation had to be discarded.

(d) Variation of electrometer sensitivity

When an electrometer set on the axis of a spectrometer is used, it is always possible that there is a variation of the sensitivity of the apparatus with different angular positions of the ionization chamber. This possibility was tested by placing a radon tube on the ionization chamber and checking the sensitivity at various values of ϕ. No such variation in sensitivity was found. Furthermore the $\psi=90°$ values of Fig. 2 show no dip comparable in magnitude with that shown by the $\psi=0°$ values.

TABLE I. *Laval's discontinuities for aluminum.*

Laval ($\sin\frac{1}{2}\phi$)	0.085	0.110	0.130	0.178	0.236	0.282
Harvey ($\sin\frac{1}{2}\phi$)	0.083	0.110	0.135	0.180	0.234	0.278
Reflection	(111)/4	(111)/3	(220)/4	(220)/3	(422)/4	(331)/3

(e) Extinction

In 1922 Jauncey[20] in the first experimental investigation on diffuse scattering looked for a change in the diffuse scattering of monochromatic x-rays in a direction ϕ when the glancing angle θ of the primary rays on the crystal was passed through a Bragg reflection value θ_B with $\phi \neq 2\theta_B$. It was felt that the apparent increase of absorption of the x-rays in the crystal (which is now known as extinction) might result in a decrease of the diffuse scattering. Jauncey was unable to find any such effect.

However, if such an effect exists, the low S values could be explained on such a basis. It was therefore thought worthwhile to test Jauncey's idea again. The Bragg angle of incidence for the (0002) reflection ($\psi=0°$) of Cu $K\alpha$ rays from zinc is 18° 15′. The ionization chamber was set at $\phi=60°$ and the crystal turned so that θ passed through 18° 15′. No decrease in the reading could be found for $\theta=18°\ 15'$. This same result was obtained with $\phi=100°$. It might be, however, that we were not obtaining the strongest possible reflection from the zinc crystal. In order to test this possibility the experiment of Bragg, James and Bosanquet[21] was repeated using the reflection rather than the transmission method. The ionization chamber was set at an angle ϕ equal to twice 18° 15′ and measurements were made with values of θ passing through 18° 15′. The results are shown in Fig. 4. The intensity of the incident beam was measured with the shutter mentioned before. The area under the curve represents what is known as the integrated intensity. This divided by the primary intensity gives $E\omega/P_0$ in the notation of Compton and Allison.[22] The ratio of the experimental to the theoretical value of

[19] The (h, k, l) reflection from a face-centered cubic crystal like aluminum is given by

$$(\sin\tfrac{1}{2}\phi)/\lambda=(h^2+k^2+l^2)^{\frac{1}{2}}/2a,$$

where h, k, l are all even or all odd integers. For aluminum $a=4.04$A.

[20] G. E. M. Jauncey, Phys. Rev. **20**, 405 (1922). Figs. 2 and 6 should be interchanged in this reference.

[21] W. L. Bragg, R. W. James, and C. H. Bosanquet, Phil. Mag. **42**, 1 (1921).

[22] A. H. Compton and S. K. Allison, *X-Rays in Theory and Experiment* (Van Nostrand, New York, 1935), p. 424 *et seq.*

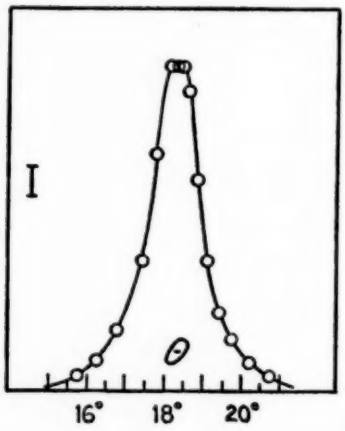

FIG. 4. Integrated intensity of (0002) reflection of Cu $K\alpha$ from a single crystal of zinc.

$E\omega/P_0$ is $\mu/(\mu+gQ)$, where μ is the absorption coefficient and gQ the extinction coefficient of the Cu $K\alpha$ rays in the zinc crystal. The ratio found was 1.59. This compares well with the value of 1.52 found by Bragg, James and Bosanquet[21] for Rh $K\alpha$ x-rays reflected in the first order from the (100) planes of rocksalt. This shows that the reflected intensity of Cu $K\alpha$ rays from the zinc crystal in this experiment was as strong as could be gotten.

The above test was necessary because of the possibility of passing unwittingly through a position for a Bragg reflection from planes other than the cleavage (0002) planes. Such a reflection would not necessarily be in the plane of scattering. To test this possibility measurements were made with the crystal face turned to different angles in its own plane; no change in the low S values was found.

VII. Distortion of Electron Cloud

The writer was finally forced to the conclusion that the low $S(\psi=0°)$ values are due to low atomic structure factor values in this region of $(\sin\frac{1}{2}\phi)/\lambda$. In Fig. 1 the curves in the region $0.25\text{A}^{-1}<(\sin\frac{1}{2}\phi)/\lambda<0.4\text{A}^{-1}$ have been plotted with the use of the f values shown in Table II and also shown in Fig. 5. It is seen that the experimental points now fall reasonably well on the theoretical curves, and that therefore the explanation of the dip in the $S(\psi=0°)$ curves is a corresponding dip on the $f(\psi=0°)$ curve. This latter dip is a result of a distortion of the electron cloud of the zinc atom. The greatest difference of the $f(\psi=0°)$ and the $f(\psi=90°)$ values is from Fig. 5 about six electrons. Although the writer does not maintain that this value is exact he does believe that the maximum difference in the two f values is considerably greater than 2.4, the greatest value previously reported by workers in this laboratory.[4, 5] This large difference implies that the forces holding a zinc crystal together in its hexagonal structure affect electrons which are lower down in the atomic structure than the valence electrons.

Although in Fig. 2 the experimental value for $S(\psi=90°)$ at $(\sin\frac{1}{2}\phi)/\lambda=0.35\text{A}^{-1}$ for Zn $K\alpha$ on zinc is slightly lower than the theoretical curve, and might possibly indicate a slight dip in the $f(\psi=90°)$ curve, the writer does not believe that the present experimental evidence warrants such a dip in the $f(\psi=90°)$ curve and no such dip is shown in Fig. 5.

Further evidence of a large value of the difference between $f(\psi=0°)$ and $f(\psi=90°)$ was reported at the Thanksgiving Meeting of the Physical Society in 1937 by Wollan.[23] According to Wollan a difference of about ten electrons was found for powdered crystals of a cadmium-silver alloy, which also has a hexagonal crystal structure. At the time of the meeting such a high difference was disturbing, but the writer feels that this large difference is probably due to a similar distortion of the electron clouds of the cadmium and silver atoms making up the crystalline alloy. Similar results were obtained by Howard[24] for powdered crystals of a copper-zinc alloy, although he does not attribute the large difference in f values entirely to electron cloud asymmetry.

In previous papers describing the work on zinc crystals in this laboratory the $\psi=0°$ curves were calculated for continuous general radiation and on the assumption of f values without the dip

TABLE II. *Structure factors for zinc.* $\lambda/\lambda_K\rightarrow 0$.

$(\sin\frac{1}{2}\phi)/\lambda$	0.250	0.275	0.300	0.325	0.350	0.375	0.400
f for $\psi=0°$	20.7	16.3	14.6	14.5	16.0	18.0	17.5

[23] E. O. Wollan, Phys. Rev. **53**, 203 (1938). This statement was made at the meeting, but is not reported in the abstract.

[24] R. A. Howard, Phys. Rev. **53**, 966 (1938). This paper also includes Wollan's f values mentioned above.

shown in Fig. 5. The effect of using the f values in Fig. 5 on the recalculated curves of the previous papers is negligible for scattering angles equal to or greater than 20°. For scattering angles less than 20° the new $f(\psi=0°)$ values do cause the theoretical $(S\rho/\mu_1)_{\text{avo}}$ curve to fall slightly below that shown, for instance, in Fig. 1 of Jauncey and McNatt's recent paper.[25] This illustrates the remark made in the introduction concerning the smearing-out of fine structure effects when general radiation is used. It is gratifying to note that the experimental point at $\phi=15°$ shown in the figure just mentioned is in somewhat better agreement with the new theoretical curve.

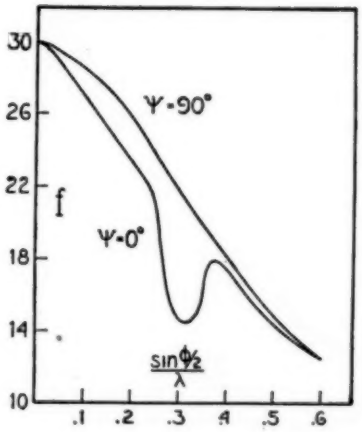

FIG. 5. Atomic structure factors for zinc ($\lambda/\lambda_K \to 0$).

VIII. CONCLUSION

The research reported in this paper is the first to show directly the effect of the anomalous dispersion of x-rays upon diffuse scattering and to measure the decrement in the atomic structure factor by this method. Jauncey's extension of the theory of diffuse scattering to include the effects of anomalous dispersion in the region $\lambda/\lambda_K \approx 1$ (Eq. (1)) has been shown to agree with experimental results for $\lambda/\lambda_K = 1.1$ and 1.2. Finally, and most important, the results indicate a much greater distortion of the electron atmospheres of the atoms in a zinc crystal than had previously been imagined. The dip in the $S(\psi=0°)$ values and the consequent dip in the atomic structure values for $\psi=0°$ are results which former diffuse scattering experiments on zinc could not have been expected to yield because of the use of general radiation. The writer also wishes to emphasize that these new results could not possibly have been obtained by crystal reflection methods because there is no $\psi=0°$ reflection for zinc between $(\sin\frac{1}{2}\phi)/\lambda = 0.203$ and 0.406A^{-1} (0002 and 0004 reflections, respectively), which values just bridge the region of low atomic structure factors. This illustrates the advantage of the diffuse scattering method, in which all values of the scattering angle except those corresponding to Bragg reflections may be investigated.

The writer is deeply indebted to Professor G. E. M. Jauncey, whose constant encouragement and unfailing advice aided greatly in the completion of the research reported here.

[25] G. E. M. Jauncey and E. M. McNatt, Phys. Rev. **55**, 498 (1939).

Proton Activation of Indium and Cadmium

S. W. BARNES
University of Rochester, Rochester, New York

(Received June 19, 1939)

Indium activated by 7.2-Mev protons exhibits two activities, one due to In^{115*} and one due to Sn^{113}. The other two activities previously reported have been shown to be due to impurities. Sn^{113} has a half-life of about 100 days and decays by K-electron capture emitting In K x-rays. An active In of 105 ± 10 min. half-life with a γ-ray of 0.39 Mev has been chemically separated from an aged Sn^{113} sample. An exactly similar In has been formed by proton bombardment of Cd which suggests the assignment of this activity to an excited state of stable In^{113}. The absence of Cd K x-rays indicates that In^{113*} decays to In^{113} with the emission of the 0.39-Mev γ-ray. In addition bombarded Cd shows the expected In isotopes In^{111} 20 min. (+), In^{114} 48 days (−) and In^{116} 54 min. (−). A positron emitter of 65 ± 5 min. half-life with a maximum positron energy of 1.6 ± 0.3 Mev is found and tentatively assigned to In^{110}. Activities of 72 sec. (−) and 2.7 ± 0.2 days (−) the latter accompanied by γ-rays of 170 and 250 kev are ascribed to isomeric states of In^{112}.

I. INTRODUCTION

THE various radioactive indium isotopes known at the present time have been formed in several ways, i.e., from the n-γ,[1] the n-$2n$,[2] the d-n,[2] the d-p[2] and the p-n[3] reactions. In addition one isotope In^{115*}[4] has been formed from stable In^{115} by nuclear excitation with neutrons,[5] protons,[6] x-rays,[7] and α-particles.[8]

A description of the known radioactive In isotopes which could be formed by proton bombardment of Cd is given in Table I. Of these radioactivities all but the 13 sec. have been found by proton activation of Cd. In addition activities ascribed to In^{110} and In^{113*} are found and described in the present report.* Proton bombardment of In gives a new period assigned to Sn^{113} which decays to In^{113*}.

II. APPARATUS

The Cd and In foils of 1 mil and 4 mils thickness, respectively, were bombarded within the cyclotron chamber with $\frac{1}{2}$ to 1μa beams of 7.2-Mev protons. In one instance a thick layer of indium was mounted on the probe for thirteen hours where it received a proton current of 20 to 30μa.

Activities were measured with an ionization chamber connected to a d.c. amplifier.[9] The chamber is closed with a window of Al of 3.4 mg/cm^2 thickness and 1″ diameter and is filled with Freon 12 to a pressure slightly more than one atmosphere. The system was calibrated with a standard source of U_3O_8 placed in a standard position above the window. With a grid resistance of 10^{11} ohms a deflection of 1 cm corresponds to a U_3O_8 source which emits 185 ± 10 β/sec. in all directions. When a floating grid is used, a rate of drift of 1 cm/sec. corresponds to a source emitting 110 ± 10 β/sec. in all directions. During the measurements on the long-lived decays the sensitivity was determined for each set of readings by means of a Ra E substandard. "Single sign" decay curves were obtained by mounting a small deflecting magnet over the window of the ionization chamber with the

TABLE I. *Some known radioactive isotopes of indium.*

Isotope	Half-life	Sign	ϵ_{MAX}	γ	Activity Ratio	Threshold
In^{111}	20 min.	+	1.75 Mev			
In^{112}	72 sec.	−				
In^{114}	50 days	−	2.15			
In^{115*}	4.1 hr.	γ		0.34		1.35 ±0.1 Mev
In^{116}	13 sec.	−	3.1			
	54 min.	−	1.4	1.4 Mev	1.12 ±06	

[1] Amaldi, D'Agostino, Fermi, Pontecorvo, Rosetti and Segrè, Proc. Roy. Soc. **149**, 522 (1935); A. C. G. Mitchell, Phys. Rev. **53**, 269 (1938).
[2] J. L. Lawson and J. M. Cork, Phys. Rev. **52**, 531 (1937); J. M. Cork and R. L. Thornton, Phys. Rev. **51**, 608 (1937).
[3] S. W. Barnes, Phys. Rev. **55**, 241 (1939).
[4] Szilard and Chalmers, Nature **135**, 98 (1935).
[5] Goldhaber, Hill and Szilard, Phys. Rev. **55**, 47 (1939).
[6] S. W. Barnes and P. W. Aradine, Phys. Rev. **55**, 50 (1939).
[7] Pontecorvo and Lazar, Comptes rendus **208**, 99 (1939); Collins, Waldman, Stubblefield and Goldhaber, Phys. Rev. **55**, 507 (1939).
[8] Lark-Horovitz, Risser and Smith, Phys. Rev. **55**, 878 (1939).
* These results supersede those of the preliminary report, reference 3.
[9] S. W. Barnes, Rev. Sci. Inst. **10**, 1 (1939).

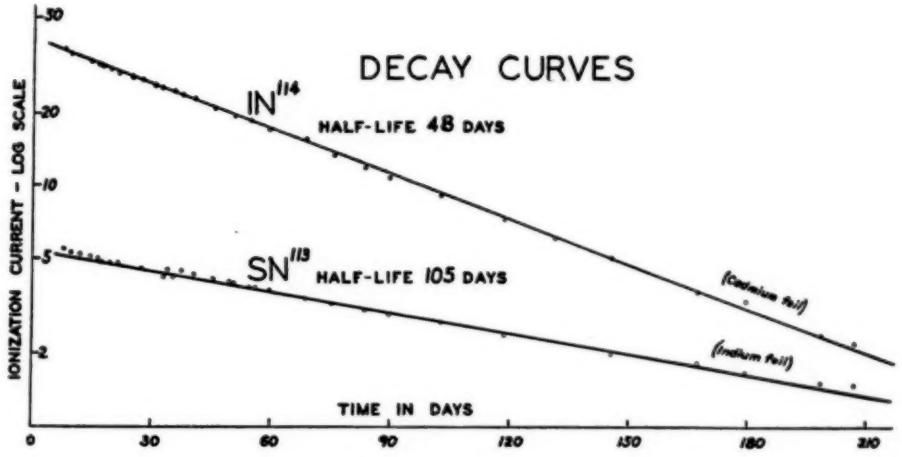

FIG. 1. Long-lived decay curves for Cd and In targets.

radioactive sample placed at the edge of the gap between the poles. For no magnetizing current the ionization current is produced by the γ-rays emitted by the source, though a contribution to this current of a few percent is made by β-particles scattered into the window from the air and from the cardboard covered poles of the magnet. About half of either the positive or negative electron distributions could be deflected into the window with the magnet used. The ordinates of the e^- and e^+ curves of Fig. 8 are the ionization currents observed with the magnetic field direct and then reversed, each reading then being reduced by the corresponding γ-ray ionization currents.

Measurements of β-ray and γ-ray energies were carried out with two β-ray spectrographs in one of which a photographic film and in the other a small ionization chamber was used as detector. These were of low resolving power because of the limited intensity of the thin Cd and In foils. The maximum and minimum radii of the spectrograph are 3.1 and 1.5 cm. The radius of the spectrometer is 7.8 ± 0.1 cm. The window of its small ionization chamber is 0.15 cm wide and the source widths were between 1 and 2 mm.

The magnetic field of the instruments was calibrated with a fixed 50-mh mutual inductance supposedly good to 0.1 percent and a 1″ diameter flip coil constructed with care. ThB deposited on a 5-mil (0.005″) wire was used as a source of known lines. The $H\rho$ values of the five lines found on the film agreed within the experimental error with Ellis'[10] $H\rho$ values for the lines J, I, F, B and A. The energy range covered by this group, from 0.025 to 0.234 Mev, was very convenient for the present work.

III. Activities Observed After Proton Bombardment of Indium

A. The long-lived activity

Preliminary work showed activated indium to have a long-lived decay.* Since the 50-day half-life value of In^{114} is known fairly accurately a sample of this activity was produced by the p-n reaction with Cd and its decay followed for seven months along with the decay of activated indium. The curves shown in Fig. 1 indicate a half-life of 105 days for the aged In. This period has been given as 70 days[11] by Livingood and Seaborg. A small amount of a longer-lived activity in the present sample would account for this difference. Therefore, the study of the decay of the sample will be continued for at least another year.

The results of a chemical separation are shown in Fig. 2. Since the long-lived activity appears in the Sn fraction it is assigned to Sn^{113} (Sn^{115} being stable), formed by a p-n reaction with In^{113}.

After a two-week aging period a portion of the indium used in the probe bombardment was separated into Sn and In fractions.† Both

[10] C. D. Ellis, Proc. Roy. Soc. **138**, 318 (1932).

* Given in reference 3 as 50 days.

[11] J. J. Livingood and G. T. Seaborg, Phys. Rev. **55**, 667 (1939).

† The indium was dissolved in concentrated HCl, a few milligrams of stannic chloride were added, and the solution

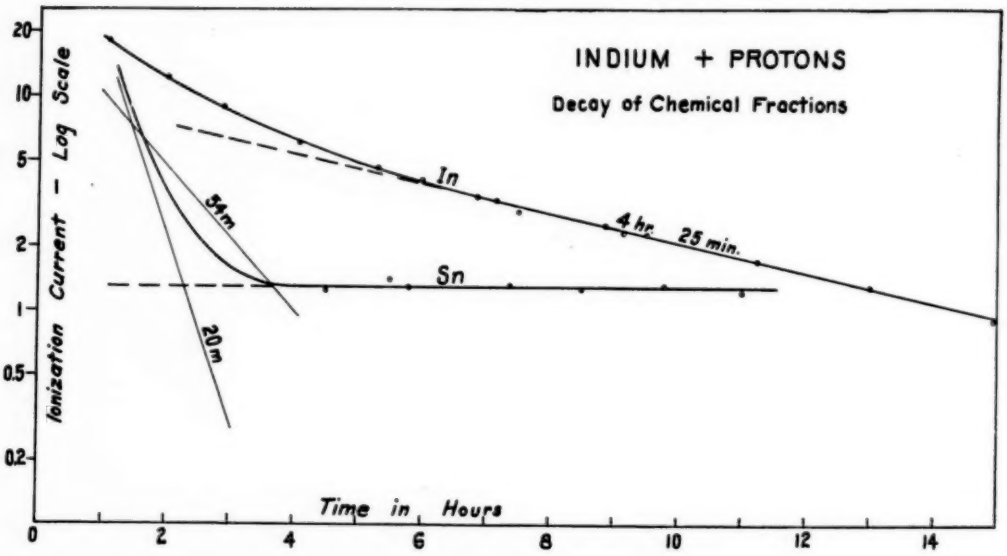

FIG. 2. Decay of In and Sn fractions from In target. (54-min. period is in In and 20-min. period in Sn.)

fractions showed activity, that of the indium decayed with a half-life of 105 minutes while that of the Sn grew with the same half-life. The data are plotted in Fig. 3. The broken line gives the intensity reached by the Sn fraction after two days. Time is reckoned from the moment of shaking the benzene water mixture.

Since Sn^{115} is stable and the In^{115*} 4-hr. activity is well known, the indium activity of 105 min. found in this experiment must be ascribed to In^{113*} formed by decay of Sn^{113} (105 days).

A well-aged proton-activated foil of indium was mounted close to the 1-mil Al window of a hydrogen filled cloud chamber. Some 400 negative electron tracks were measured and the histogram of Fig. 4 obtained. The absence of positron tracks indicates that Sn^{113} decays rarely if ever by positron emission. The shape of the distribution indicates that conversion electrons rather than negative β-particles are emitted, so that the decay is largely by K-electron capture.

A further investigation was made with a similarly aged but much stronger source in the β-ray spectrograph. Film 1 of Fig. 5 is a spectrogram obtained with an exposure of five days, beginning three weeks after bombardment. Electron lines corresponding to the K and L conversion electrons from a 0.39-Mev γ-ray are evident. In addition two weak lines are found on the original film which correspond to the K and L conversion of an 0.085-Mev γ-ray. There is no evidence either from the spectrograph or the cloud chamber of a continuous β-ray spectrum.

Sn^{113} must then decay entirely by K-electron capture and should emit In K x-rays. Evidence for these x-rays as well as for the γ-rays just

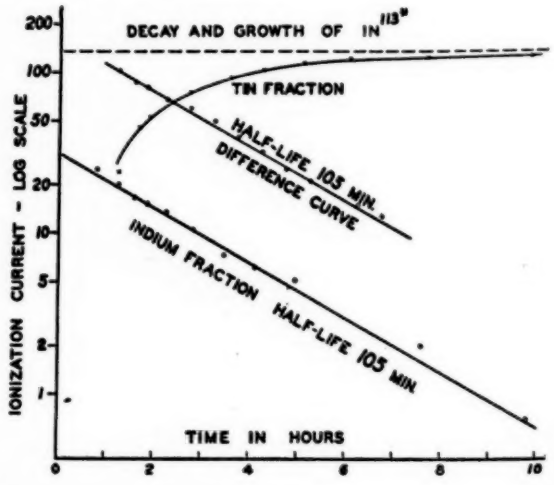

FIG. 3. Plots of the activity of Sn and In precipitates from an In target after three weeks' aging.

was diluted to about $\frac{1}{4}N$. Cupferron (ammonium nitrosophenylhydroxylamine) was then added to precipitate the tin, and the solution and precipitate were shaken up with benzene. The tin goes into the benzene layer, which was separated with a separatory funnel and evaporated to give the sample labeled Tin Fraction. The aqueous layer was neutralized, then made acid with acetic acid, and the indium was precipitated as the sulphide to give the sample labeled Indium Fraction.

mentioned is given by the absorption curve in Ag shown in Fig. 6. A 2-mm plate of beryllium placed between the source and the window stopped all electrons. The broken line is drawn through points corresponding to greater thicknesses of silver absorber than are shown on the plot. A comparison between the μ/ρ values obtained from the absorption curve and those calculated using the energy of the lines obtained from the spectrogram is given in Table II.

Although the agreement is only rough the difference in the absorption shown in Fig. 6 by the weighed Pd and Rh foils is satisfactory evidence for presence of In K x-rays. The nearly identical values of absorption shown by the Rh and Mo foils precludes the existence of Cd K x-rays, which could arise if In^{113*} decayed to Cd^{113} by positron emission or K-electron capture. This is confirmed by the absence of positrons in the cloud-chamber pictures.

Since (from Fig. 3) the activity to be ascribed to the Sn fraction at the instant of separation is very small the process must be the following. Sn^{113} captures a K electron, emits an In K x-ray quantum and becomes In^{113} in an excited state. It falls to the metastable state In^{113*} through the emission of the 0.085-Mev γ-ray. This metastable state has a half-life of 105 minutes and decays to the ground state of In^{113} with the emission of the 0.39-Mev γ-ray. From the ratio of intensity of the γ-ray ionization to that produced by the conversion electrons it is found that the coefficient of internal conversion for this 0.39-Mev line is about 70 ± 10 percent.

It may well be pointed out here that if this activity is correctly assigned to In^{113*} it should also be formed when Cd is bombarded by protons. This is found to be the case as will be shown in Section IV. Also it should be possible to raise In^{113} to the excited state In^{113*} with neutrons, protons, x-rays and α-particles as has been done for In^{115*}. The small relative abundance, five percent, may explain why In^{113*} has not been observed before.[12]

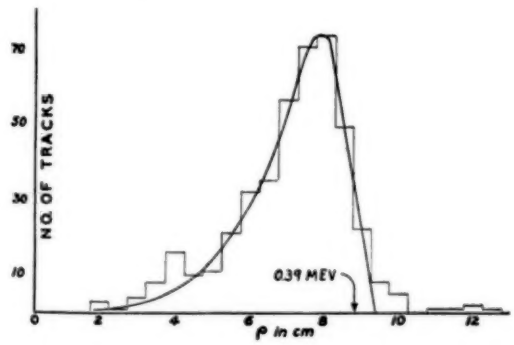

FIG. 4. Distribution of negative electron tracks in cloud chamber from In target one month after bombardment.

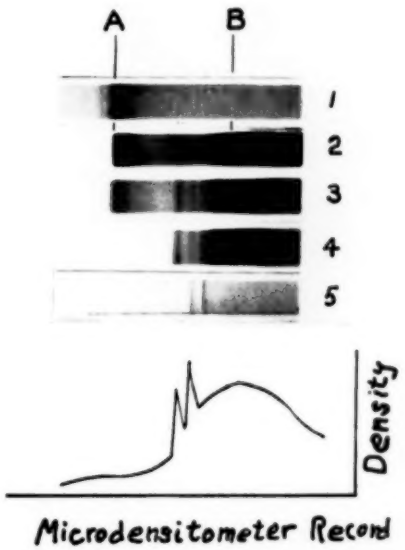

FIG. 5. β-ray spectrograms for Cd and In targets. Film 1 is for In target, 5-day exposure beginning 20 days after bombardment. Films 2–5 are for a Cd target the exposure intervals in terms of time after bombardment being as follows: film 2, 0 to 3.5 hr.; film 3, 3.5 to 15.5 hr.; film 4, 15.5 to 45 hr.; film 5, 30 to 34 days. The microdensitometer record below is for film 5, (not to same scale in the reproduction).

B. The short-lived activities

An early investigation showed a greater number of short-lived activities in proton activated indium than could easily be explained, unless some were assigned to impurities. The length of time required for good chemical separations together with the low initial activities made the solution of this problem by the ordinary chemical means difficult. Finally a sample of fairly pure indium* together with a quantitative statement of its impurities was acquired. The impurities consisted of 0.004 percent Cu and 0.005 percent Sn with negligible traces of a few

[12] G. T. Seaborg (private communication) has just reported finding a period of around 90 min. with a 0.4-Mev converted gamma-ray in fractions containing indium separated from old samples of Sn^{112} produced by the reaction Sn^{112} (d,p). This makes the assignment of this activity to In^{113*} almost certain.

* Indium Corporation of America, Utica, New York.

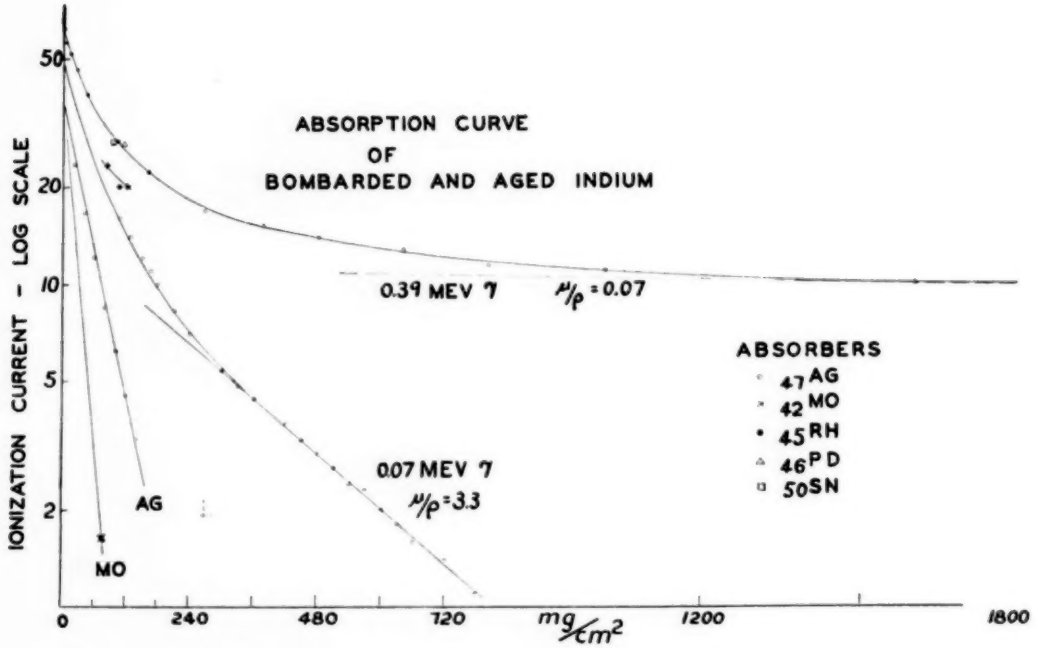

FIG. 6. Absorption curves for radiations from an aged In target. The β-rays were removed by a Be plate. The marked difference in absorption between the Pd and Rh foils shows the soft component to be In K x-rays.

other elements. The decay of two foils rolled from this indium is shown in Fig. 7. The curve In 1 is for a foil which faced the proton beam and received both protons and the neutrons present in the chamber. The In 2 curve is for a foil separated from foil 1 by a 10-mil sheet of lead and which therefore received only the neutrons.

The activity of foil 2 is seen to consist of the 54-min. period of In^{116} produced by In^{115} (n, γ) (the isomeric period of 13 sec. would not have been detected in this experiment) and the 4.1-hr. period of In^{115*} produced by neutron excitation. Presumably the same amounts of these two activities were produced by neutrons in foil 1. The excess 50-min. activity of foil 1 has been shown by single-sign decay curves to be a positron activity. The 0.005 percent of Cu present would give approximately this amount of 40-min. Zn^{63} activity through a p-n reaction with Cu^{63} so this period may be disregarded. Furthermore when the new and purer indium was substituted for the old—all other conditions of the experiment remaining the same, as indicated by the same initial activity of either the 4.1-hr. or 105-day activity—both the 18-min. and the 50-min. periods were found to have roughly one-tenth of their former activity. Thus the 18-min. activity which has previously been assigned[3] to an isomeric state of Sn^{113} is also due to an impurity (and is doubtless the 18-min. (e^+) activity of Sb^{120} formed[13] by a $(p$-$n)$ from Sn^{120}). Therefore the activities to be ascribed to indium following proton bombardment are In^{115*} formed by a p-p reaction with In^{115}, Sn^{113} formed by a p-n reaction with In^{113} and In^{113*} formed when Sn^{113} decays by K capture.

IV. Activities Resulting from Proton Bombardment of Cadmium

All the activities observed in a bombarded Cd foil have been found in the indium precipitate after a chemical separation.

TABLE II. *Absorption coefficients for x- and γ-rays.*

Source	Line Mev	Absorber	μ/ρ Observed	μ/ρ Calculated
In^{113*} γ-ray	0.39	Ag	0.07	0.07
Sn^{113} γ-ray	0.085	Ag	3.3	4.4
Indium K x-rays	0.024	Ag	17	10
	0.024	Mo	40	50

[13] G. T. Seaborg, private communication.

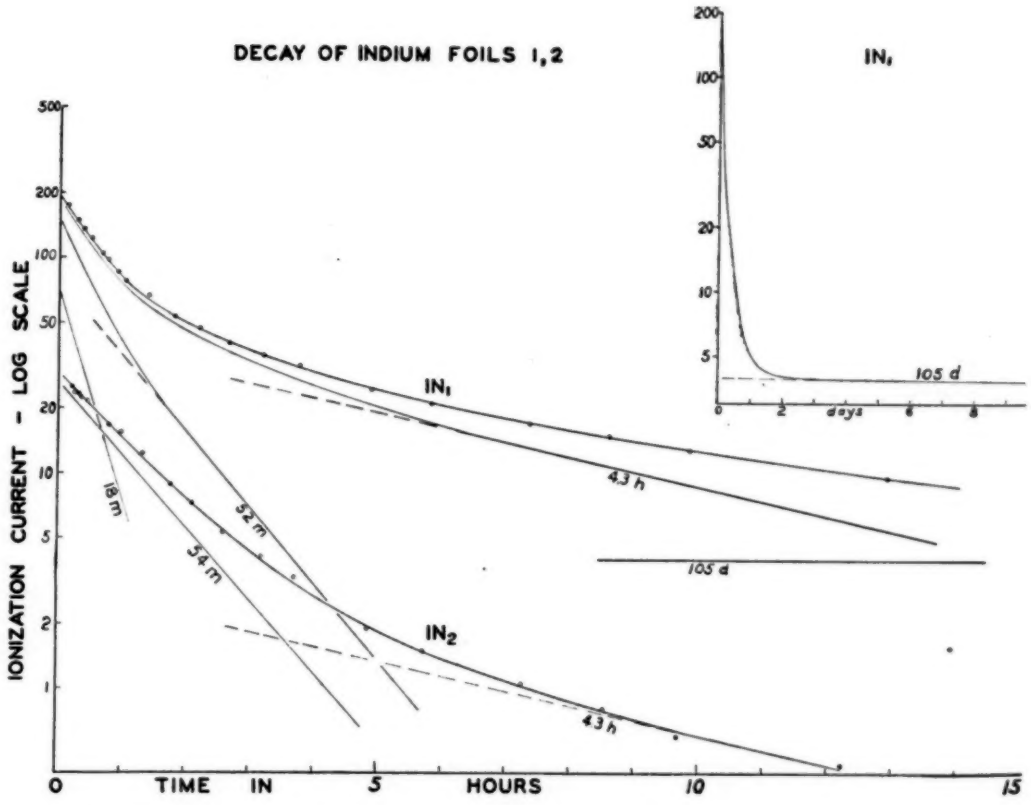

FIG. 7. Decay curves for bombarded In. In_1 is for a foil receiving both protons and neutrons; In_2 is for a foil receiving neutrons only.

In Fig. 8 are shown the single sign and γ-ray decay curves of the various activities observed in a proton-bombarded Cd foil. Fig. 5 shows spectrograms of the negative electrons obtained at the times indicated with the β-ray spectrograph. These are to be compared with the e^- decay curve of Fig. 8. The components of this e^- curve which may be immediately assigned are the 54-day activity which is due to In^{114} formed by Cd^{114} (p-n) and the 51-minute which is due to In^{116} formed by Cd^{116} (p-n). Film 5 of Fig. 5 and the microdensitometer record immediately below belong to In^{114} (50 day.) Two electron lines are evident which are assumed to be K and L conversion lines of a 0.195-Mev γ-ray although the L conversion is unusually strong.

The activity with the half-life of 105 ± 5 minutes seemed to be associated with the highly converted highest energy (0.39 Mev) γ-ray seen at A on films 2 and 3 of Fig. 5. This could not be proved, however, until the data of Fig. 9 were obtained, which represents three out of nine runs made at successive times with one sample on the spectrometer. Only two lines (marked A and B on Figs. 5 and 9) were intense enough to be measured. Line B which is plainly evident on the original film 2 unfortunately does not show on the print of Fig. 5. At the left of Fig. 9 are decay curves of these two lines, the ordinates represent line intensities, at the various times, obtained by subtracting from the peak of the line a reasonable base line. The value of the half-life of line A (115 ± 15 min.) definitely associates this conversion line with the 105-min. period of the e^- decay curve of Fig. 8. This activity is seen to be identical in its half-life and γ-ray* with the activity which grew from the Sn^{113} obtained from an indium target. It is ascribed therefore to In^{113*} formed by a p-n reaction with Cd^{113}.

The low energy (0.16 Mev) γ-ray of Fig. 9 with a half-life of 23 min. is undoubtedly to be

* On the basis of the assumed level scheme the 0.085 γ-ray should not be present here; however this could not be checked because of the presence of other strong lines in this region.

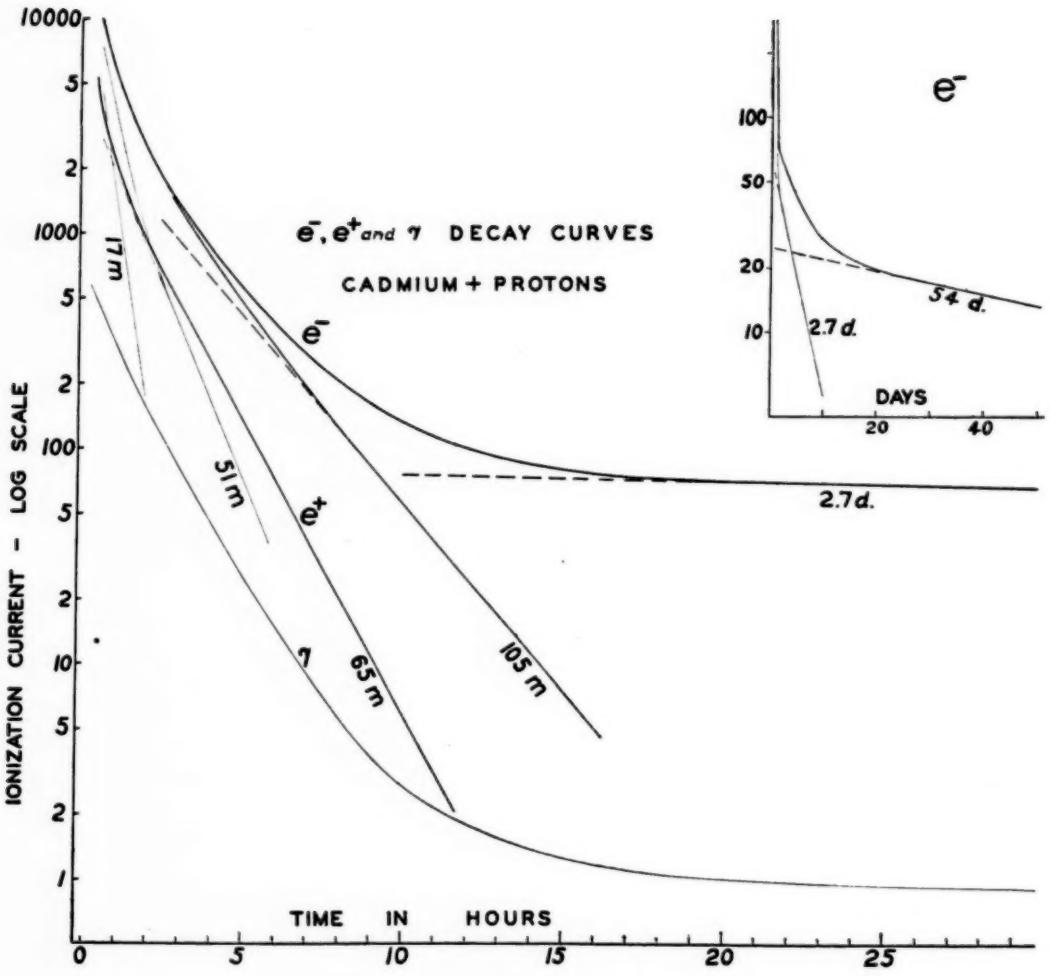

FIG. 8. Single sign and γ-ray decay curves for bombarded Cd.

associated with the 18- to 20-min. positron component always found in the e^+ decay curve. This component is not shown in Fig. 8 but arises when the 65-min. component is subtracted from the upper portion of the e^+ curve. This activity has been found by Cork[2] and assigned to In^{111}.

The 17-min. component of the e^- curve is thought to be due to the conversion electrons of In^{111} rather than to any new β-ray emitter. This is reasonable in view of the geometry of the apparatus even though the e^- 17-min. curve is more intense than the corresponding e^+.

The positron activity with half-life of 65 ± 5 min. has not been previously reported. A rough value of the maximum energy of the positrons has been determined by using both the spectrograph and spectrometer and is 1.6 ± 0.3 Mev. It has been found impossible to assign with certainty any of the conversion electron lines of Fig. 5 to this activity. In^{106}, In^{108} and In^{110} must be positron emitters, and since Cd^{110} is ten times as abundant as either Cd^{106} or Cd^{108} this activity is tentatively assigned to In^{110}. If this assignment is correct the activity should be produced by an α-n reaction with Ag.

The 2.7-day component of the e^- curve has two conversion electron lines (see film 4 of Fig. 5) corresponding to γ-rays of 0.253 and 0.168 Mev. Cork[14] has reported a similar activity after fast neutron bombardment of indium. If his activity is the same as the one found here it can be

[14] Cork and Lawson, Washington Meeting 1939. (Verbally reported; figures are not given in the abstract, Phys. Rev. **55**, 1136 (1939)).

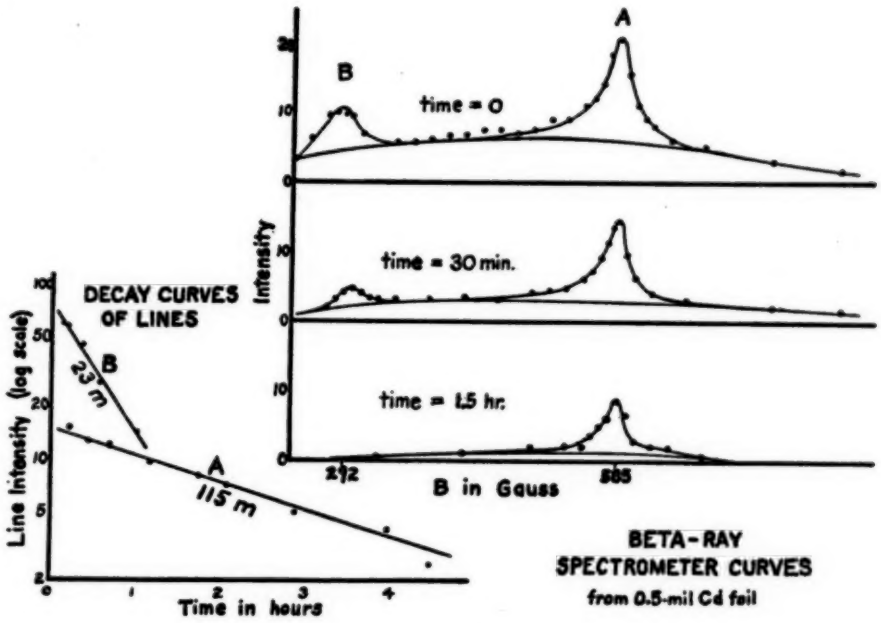

FIG. 9. Successive β-ray spectrometer curves for bombarded Cd, showing (lower left) decay curves for each line. Line A represents K and L conversion of a 0.39-Mev γ-ray (In^{113*}); line B for a 0.16-Mev γ-ray (In^{111}).

explained as an isomeric state of In^{112} (for which a period of 72 sec. has been reported)[2] formed in his case by an (n-$2n$) reaction and here by a (p-n) reaction. The 72-sec. activity has been found in the present work in total decay curves of cadmium targets.

TABLE III. *Summary of radioactive isotopes in* In *and* Cd *targets.***

Isotope	Half-life	Sign	ϵ_{MAX} in Mev	γ in Mev	Proton Cross Section for 6.9 Mev $cm^2 \times 10^{28}$
In^{110}	**66 ± 5 min.**	e^+	**1.6 ± 0.3**		**3***
In^{111}	**20 min.**	e^+	2.15	**0.16 ± 0.01**	**4**
In^{112}	**72 sec.**	e^-			**3***
	2.7 days	e^-?	1.73?	**0.253, 0.168**	**0.4**
In^{113*}	**105 ± 10 min.**	γ		**0.39 ± 0.02**	**2**
In^{114}	**48.5 ± 2 days**	e^-	1.75	**0.19 ± 0.01**	**3**
In^{115*}	**4.1 hr.**	γ		**0.34[19]**	**0.003**
In^{116}	**(13 sec.) 54 min.**	e^-			**3***
Sn^{113}	**105 ± 15 days**	**K capture**		**0.085 ± 0.01**	**3**

* These values are least certain.
** Figures in **bold face** are those reported for the first time in this paper. Others have been previously reported and are here confirmed.

V. SUMMARY

The results of this work are summarized in Table III, together with the data contained in Table I. The cross section values are not precise; however, they do indicate a striking constancy for the various p-n reactions. The small cross section found for the 2.7-day activity thus becomes a justification for the assignment of this activity to one of two isomeric states. The cross section for the one p-p reaction (In^{115*}) is seen to be about a thousand times smaller than that for the others which are all p-n reactions. Since the incident protons of 7.2 Mev lose about 0.6 Mev in a 1-mil foil of Cd or In these cross sections correspond to a mean energy of the protons of about 6.9 Mev.

It is a pleasure to give acknowledgment here for the valued suggestions of Dr. S. N. VanVoorhis, Professor L. A. DuBridge, and Dr. V. Weisskopf. The work was financed in part by a grant from the Research Corporation.

Coincidences Between Beta- and Gamma-Rays in Manganese*

LAWRENCE M. LANGER, ALLAN C. G. MITCHELL AND PAUL W. MCDANIEL
Department of Physics, Indiana University, Bloomington, Indiana

(Received July 3, 1939)

With two reliable high speed counters in a coincidence circuit of resolving time, $\tau = 3.4 \times 10^{-7}$ min., coincidences have been recorded between beta- and gamma-radiation from Mn^{56} (148 min.) formed by slow neutron capture. By interposing various thicknesses of aluminum between the source and the beta-ray counter, the ratio of beta-gamma coincidences to single beta-counts was observed as a function of the energy of the beta-rays. The number of coincidences per beta-ray was larger when electrons of all energies were striking the beta-ray counter than when only electrons of high energy were recorded. Coincidences were still recorded when only the high energy beta-rays were entering the counter. In addition gamma-gamma coincidences were found. From these experiments it is concluded that Fe^{56} is formed in two excited states from the disintegration of Mn^{56} and that one gamma-ray per disintegration is associated with the high energy group and about two gamma-rays per disintegration with the low energy group.

INTRODUCTION

A CERTAIN amount of work has been done on the beta- and gamma-rays associated with Mn^{56} of period 150 min. The beta-ray spectrum was investigated by Gaerttner, Turin and Crane[1] and Brown and Mitchell.[2] The two sets of observers agreed in fixing an extrapolated K-U end point of between 2.8 and 2.9 Mev. The latter group of observers, using thin emitters of MnO_2 deposited from irradiated $NaMnO_4$, found that the beta-ray spectrum was composite and consisted of two groups with end points at 1.2 and 2.9 Mev. They also pointed out that Gaerttner, Turin and Crane, who used thick emitters of metallic manganese, would probably not have found a composite spectrum because of distortion due to the thick source. Later, Bacon, Grisewood and van der Merwe[3] appear to have confirmed the existence of the two groups reported by Brown and Mitchell.

A measurement of the energy of the gamma-rays emitted by Mn^{56} was made by Mitchell and Langer[4] by recording the coincidences produced by Compton electrons ejected from an aluminum plate placed in front of two counters. Insertion of aluminum foils between the two counters causes a decrease in the number of coincidences and from these measurements the energy of the gamma-ray may be obtained. The value of the energy found by this method was 1.65 Mev. The close agreement between the energy of the gamma-ray and the difference between the energies of the two end points of the composite beta-ray spectrum led the authors to suppose that the two beta-ray transitions give rise to two different states of the product nucleus, Fe^{56}, and that the gamma-ray is emitted as a transition between these two states.

The present experiment was designed to test this hypothesis further and to give some information as to the number of gamma-rays per beta-ray transition.

EXPERIMENTAL ARRANGEMENT

The experimental arrangement is somewhat similar to that used by Norling[5] in his investigation of the beta-gamma coincidences in As^{76}. A concentrated solution of $NaMnO_4$ was irradiated with neutrons from a radium-beryllium neutron source containing 211 mg of radium salt. The MnO_2, containing most of the active material, was filtered and the filter paper mounted between two Geiger-Mueller tube counters arranged to count coincidences.

One of the counters was used as a gamma-ray counter and was separated from the source by 0.60 cm of Al, a thickness large enough to stop

* Reported at the Washington Meeting of the American Physical Society, April, 1939.

[1] E. R. Gaerttner, J. J. Turin and H. R. Crane, Phys. Rev. **49**, 793 (1936).

[2] M. V. Brown and A. C. G. Mitchell, Phys. Rev. **50**, 593 (1936).

[3] R. H. Bacon, E. N. Grisewood and C. W. van der Merwe, Phys. Rev. **52**, 668 (1937).

[4] A. C. G. Mitchell and L. M. Langer, Phys. Rev. **52**, 137 (1937).

[5] F. Norling, Zeits. f. Physik **111**, 158 (1938).

all beta-rays. The other counter, which we shall call the beta-ray counter, responded to both beta- and gamma-rays. The apparatus was so arranged that various thicknesses of aluminum could be placed between the source and the beta-ray counter. The aluminum served to define the energy of the beta-rays entering the beta-ray counter, since only electrons having an energy greater than a certain minimum could pass through the aluminum. By varying the thickness of the aluminum the coincidence rate could be measured as a function of the energy of the beta-rays.

Apparatus

The Geiger-Mueller counters used in this experiment are of the self-quenching type.[6] The negative electrode is a thin silver deposit on the inside surface of a glass tube 2.0 cm in diameter. The wall thickness of the glass is only 0.02 cm over the 5-cm length of the sensitive region. The central electrode is 0.010 cm tungsten. In order to insure a surface with a high work function, the counters were rinsed with a very dilute solution of lacquer in amyl acetate. After outgassing at high vacuum with a liquid-air trap, the counters were filled with 8 cm of pure argon and 1 cm vapor pressure of absolute alcohol. These counters have maintained, since their construction, a threshold voltage of about 1000 volts and an operating range of about 200 volts. They appear to be free from the spurious and multiple pulses sometimes encountered with counters and have the added advantage of operating at high counting rates with a simple low resistance-capacity input circuit.

The pulses from the counter are fed into a resistance-capacity coincidence amplifier similar to one previously described.[7] In the present case, the time constants have been further reduced to the minimum values that still give sufficient amplification and also maintain the desirable feature of having all the pulses reaching the mixer tube of the same size.

The output of the amplifier is connected to a hard vacuum tube scale of two, four, eight or sixteen recorder monitored by a cathode-ray oscillograph.

The over-all speed of counter, input circuit, amplifier and recorder is found to be limited by the mechanical counter. Tests in measuring the decay of the 54-minute period of In^{116} show counting losses of less than one percent at counting rates of 25,000 particles per minute.

The resolving time for coincidences was determined by recording the chance coincidences when an independent source of beta-rays was placed over each counter. From the relation

$$N_c = 2N_1N_2\tau,$$

the value of the resolving time, τ, was determined for widely different values of N_1 and N_2, and found to be 3.4×10^{-7} min.[8] independent of the rate of counting.

For coincidence measurements, the counters were mounted in a horizontal plane on a skeleton frame-work with their centers 4.0 cm apart. The source in the form of a thin filter paper about 4×7 cm was mounted midway between the

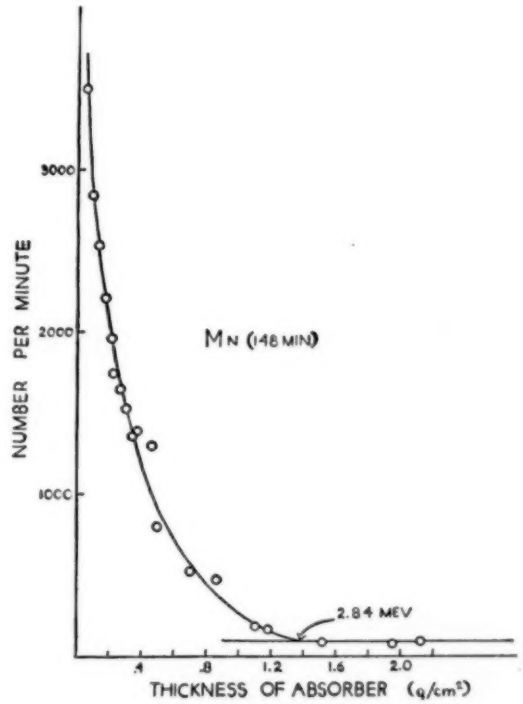

FIG. 1. Absorption of beta-rays from manganese.

[6] A. Trost, Zeits. f. Physik **105**, 399 (1937).
[7] L. M. Langer and M. D. Whitaker, Phys. Rev. **51**, 713 (1937).
[8] The resolving time has since been reduced to 0.56×10^{-7} min. which seems to be about the lower limit for this type of amplifier.

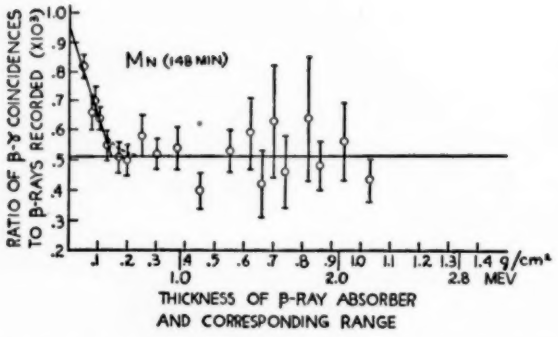

FIG. 2. Beta-gamma coincidences as a function of the beta-ray energy.

counters. For this geometry the coincidence background due to cosmic rays is 0.10 count per minute.

MEASUREMENTS

Measurement of the end point by absorption in aluminum

In order to determine, independently of other end-point measurements, the amount of aluminum necessary to absorb all the beta-rays from the source an absorption curve in aluminum was obtained using a single counter. The results are shown in Fig. 1, in which the number of counts per minute is plotted against the thickness of aluminum in g/cm². The point at which the absorption curve intersects the gamma-ray background is 1.38 g/cm². This range, according to the formula of Feather,[9] corresponds to an end point of 2.84 Mev, in good agreement with the cloud chamber measurements.

The half-life for the decay was measured carefully and found to be 148±5 min.

Gamma-gamma coincidences

In order to test for coincidences between time correlated gamma-rays, measurements were made in which 0.60 cm of aluminum was placed between the source and each counter. In order to calculate the number of chance coincidences the single counts in each counter were taken at the beginning and end of each run. The duration of each experiment was two hours. After subtracting the coincidences due to chance[10] and those due to cosmic rays there was a definite residual due to gamma-gamma coincidences of 0.21±0.10 per thousand gamma-rays.

Beta-gamma coincidences

The coincidences between beta- and gamma-rays were next investigated. This was accomplished by keeping 0.60 cm Al between the source and the gamma-ray counter and a thickness of aluminum, sufficient to stop all electrons of less than a given energy, between the source and the beta-ray counter. This thickness was varied in different experiments. The single counts in both the beta-ray counter and the gamma-ray counter were taken before and after each run. The beta-gamma coincidences were obtained from the total number of coincidences after subtracting the coincidences due to chance, cosmic rays, and gamma-gamma coincidences.

The number of beta-rays entering the beta-ray counter was also obtained from the above data and corrected for the relatively small number of counts due to gamma-rays. The number of beta-gamma coincidences per incident beta-ray is shown in Fig. 2 as a function of the energy of the beta-rays.

It will be seen that the errors at large thicknesses of absorber are greater than at the small thicknesses, since in the former case the total number of coincidences obtained is smaller and the gamma-gamma count is a larger fraction of the total. The data in Table I, selected from the results, will illustrate this.

DISCUSSION OF RESULTS

The fact that gamma-gamma coincidences are observed shows that in some cases there is more than one gamma-ray per disintegration. From Fig. 2 it will be seen that since there are beta-gamma coincidences associated with the high energy beta-rays right out to the beta-ray end point, it appears that the high energy part of the beta-ray spectrum leads to a transition to an

[9] N. Feather, Proc. Camb. Phil. Soc. **34**, 599 (1938).

[10] In calculating the chance rate for a source which is decaying with the time one proceeds as follows: Let $N_1(t)$ and $N_2(t)$ be the counting rate in each counter at time t and let ν be the natural background of each counter. The coincidence rate at time t is $2[N_1(t)+\nu][N_2(t)+\nu]\tau$, where τ is the resolving time of the apparatus. The average chance rate for a duration of the experiment of time T is therefore

$$\bar{N}_c=\frac{2\tau}{T}\int_0^T[N_1(t)+\nu][N_2(t)+\nu]dt.$$

Our values of the chance rate were calculated from this equation.

excited state of the product nucleus Fe^{56}. Furthermore, it will be seen from the curve that there are more beta-gamma coincidences per beta-ray when beta-rays of all energies are entering the counter than when the lower energy rays are excluded. This points to the existence of two groups of beta-rays with gamma-rays associated with each group.

One can calculate the average number of gamma-rays associated with each beta-ray transition by making certain plausible assumptions. Let N_{β_1} and N_{β_2} be the numbers of beta-rays emitted in the low and high energy groups, respectively; K_1 and K_2 the average number of gamma-rays per disintegration in each group; and S_β, S_γ the beta- and gamma-ray sensitivities of the counters (including solid angle). The number of beta-gamma coincidences per beta-ray detected is

$$\frac{N_{\beta\gamma}}{(N_{\beta_1}S_{\beta_1}+N_{\beta_2}S_{\beta_2})}=\frac{N_{\beta_1}S_{\beta_1}S_{\gamma_1}K_1+N_{\beta_2}S_{\beta_2}S_{\gamma_2}K_2}{N_{\beta_1}S_{\beta_1}+N_{\beta_2}S_{\beta_2})}. \quad (1)$$

If one assumes that $S_{\beta_1}=S_{\beta_2}=S_\beta$ and that $S_{\gamma_1}=S_{\gamma_2}=S_\gamma$, an average gamma-sensitivity for gamma-rays, then, for zero absorber, (1) becomes

$$\frac{N_{\beta\gamma}}{(N_{\beta_1}+N_{\beta_2})S_\beta}=(n_1K_1+n_2K_2)S_\gamma=0.95\times10^{-3} \quad (2)$$

and for large thicknesses of absorber, at which $N_{\beta_1}S_{\beta_1}=0$, (1) becomes

$$\frac{N_{\beta\gamma}}{N_{\beta_2}S_\beta}=S_\gamma K_2=0.5\times10^{-3}, \quad (3)$$

in which n_1 and n_2 are the fractions of electrons emitted in each group. The numerical values given in Eqs. (2) and (3) are taken from Fig. 2.

The number of gamma-gamma coincidences per gamma-ray, on the other hand, is given by

$$\frac{N_{\gamma\gamma}}{(N_{\gamma_1}+N_{\gamma_2})S_\gamma}=\frac{N_{\gamma_1}S_\gamma{}^2\dfrac{K_1(K_1-1)}{2}+N_{\gamma_2}S_\gamma{}^2\dfrac{K_2(K_2-1)}{2}}{(N_{\gamma_1}+N_{\gamma_2})S_\gamma}$$

$$=0.21\times10^{-3}. \quad (4)$$

Remembering that $N_{\gamma_1}=K_1N_{\beta_1}$ and $N_{\gamma_2}=K_2N_{\beta_2}$, one obtains from Eqs. (2), (3) and (4)

TABLE I. *Data on $\gamma-\gamma$ and $\beta-\gamma$ coincidences.*

G/CM²	TOTAL NO. COINCIDENCES (60 MIN.)	COINCIDENCE RATE MIN.⁻¹	CHANCE RATE MIN.⁻¹	$\gamma-\gamma$ RATE MIN.⁻¹	$\beta-\gamma$ RATE MIN.⁻¹
0.05	166	2.67	0.23	0.01	2.43
0.25	160	2.56	0.51	0.03	2.02
0.74	88	1.37	0.58	0.08	0.71

$$(n_1K_1{}^2/K_2{}^2)(K_1-1)+n_2(K_2-1)=1.6 \quad (5)$$

and $$K_1/K_2=(1.9-n_2)/n_1. \quad (6)$$

In addition $$n_1+n_2\equiv1. \quad (7)$$

Now, from the fact that the curve in Fig. 2 rises as it approaches the origin it follows that $K_1>K_2$. Furthermore, K_2 cannot be less than 1. It was found by trial that the only solution consistent with these conditions and satisfying (5), (6) and (7) is $K_2=1$. This gives as a result

$$K_1=2.2, \quad n_1=0.75 \quad \text{and} \quad n_2=0.25.$$

The values of n_1 and n_2 obtained from this analysis are consistent with values obtained by integrating under the beta-ray distribution curves given by Brown and Mitchell. The values obtained from their data give $n_1=0.70$ and $n_2=0.30$.

If one places the value $K_2=1$ in Eq. (3), one obtains for the sensitivity of the gamma-ray counter a value $S_\gamma=0.5\times10^{-3}$.

At present the energies and the intensities of the individual gamma-rays have not been measured. It should be pointed out that the method employed by Mitchell and Langer measures only the average energy of the gamma-rays and has no resolving power. It is to be hoped that good measurements on the energies of the individual gamma-rays will be made shortly so that an accurate energy level diagram may be obtained.

We may, however, conclude from the present experiment that there are two groups of beta-rays, both of which go to excited states of Fe^{56}. The high energy beta-ray group is followed by the emission of a single gamma-ray, while the low energy beta-ray group is, on the average, followed by two gamma-rays.

The authors wish to express their thanks to the Penrose Fund of the American Philosophical Society for a grant, and to Dr. E. J. Konopinski for many helpful suggestions.

The Mechanism of Nuclear Fission

NIELS BOHR
University of Copenhagen, Copenhagen, Denmark, and The Institute for Advanced Study, Princeton, New Jersey

AND

JOHN ARCHIBALD WHEELER
Princeton University, Princeton, New Jersey

(Received June 28, 1939)

On the basis of the liquid drop model of atomic nuclei, an account is given of the mechanism of nuclear fission. In particular, conclusions are drawn regarding the variation from nucleus to nucleus of the critical energy required for fission, and regarding the dependence of fission cross section for a given nucleus on energy of the exciting agency. A detailed discussion of the observations is presented on the basis of the theoretical considerations. Theory and experiment fit together in a reasonable way to give a satisfactory picture of nuclear fission.

INTRODUCTION

THE discovery by Fermi and his collaborators that neutrons can be captured by heavy nuclei to form new radioactive isotopes led especially in the case of uranium to the interesting finding of nuclei of higher mass and charge number than hitherto known. The pursuit of these investigations, particularly through the work of Meitner, Hahn, and Strassmann as well as Curie and Savitch, brought to light a number of unsuspected and startling results and finally led Hahn and Strassmann[1] to the discovery that from uranium elements of much smaller atomic weight and charge are also formed.

The new type of nuclear reaction thus discovered was given the name "fission" by Meitner and Frisch,[2] who on the basis of the liquid drop model of nuclei emphasized the analogy of the process concerned with the division of a fluid sphere into two smaller droplets as the result of a deformation caused by an external disturbance. In this connection they also drew attention to the fact that just for the heaviest nuclei the mutual repulsion of the electrical charges will to a large extent annul the effect of the short range nuclear forces, analogous to that of surface tension, in opposing a change of shape of the nucleus. To produce a critical deformation will therefore require only a comparatively small energy, and by the subsequent division of the nucleus a very large amount of energy will be set free.

Just the enormous energy release in the fission process has, as is well known, made it possible to observe these processes directly, partly by the great ionizing power of the nuclear fragments, first observed by Frisch[3] and shortly afterwards independently by a number of others, partly by the penetrating power of these fragments which allows in the most efficient way the separation from the uranium of the new nuclei formed by the fission.[4] These products are above all characterized by their specific beta-ray activities which allow their chemical and spectrographic identification. In addition, however, it has been found that the fission process is accompanied by an emission of neutrons, some of which seem to be directly associated with the fission, others associated with the subsequent beta-ray transformations of the nuclear fragments.

In accordance with the general picture of nuclear reactions developed in the course of the last few years, we must assume that any nuclear transformation initiated by collisions or irradiation takes place in two steps, of which the first is the formation of a highly excited compound nucleus with a comparatively long lifetime, while

[1] O. Hahn and F. Strassmann, Naturwiss. **27**, 11 (1939); see, also, P. Abelson, Phys. Rev. **55**, 418 (1939).

[2] L. Meitner and O. R. Frisch, Nature **143**, 239 (1939).

[3] O. R. Frisch, Nature **143**, 276 (1939); G. K. Green and Luis W. Alvarez, Phys. Rev. **55**, 417 (1939); R. D. Fowler and R. W. Dodson, Phys. Rev. **55**, 418 (1939); R. B. Roberts, R. C. Meyer and L. R. Hafstad, Phys. Rev. **55**, 417 (1939); W. Jentschke and F. Prankl, Naturwiss. **27**, 134 (1939); H. L. Anderson, E. T. Booth, J. R. Dunning, E. Fermi, G. N. Glasoe and F. G. Slack, Phys. Rev. **55**, 511 (1939).

[4] F. Joliot, Comptes rendus **208**, 341 (1939); L. Meitner and O. R. Frisch, Nature **143**, 471 (1939); H. L. Anderson, E. T. Booth, J. R. Dunning, E. Fermi, G. N. Glasoe and F. G. Slack, Phys. Rev. **55**, 511 (1939).

the second consists in the disintegration of this compound nucleus or its transition to a less excited state by the emission of radiation. For a heavy nucleus the disintegrative processes of the compound system which compete with the emission of radiation are the escape of a neutron and, according to the new discovery, the fission of the nucleus. While the first process demands the concentration on one particle at the nuclear surface of a large part of the excitation energy of the compound system which was initially distributed much as is thermal energy in a body of many degrees of freedom, the second process requires the transformation of a part of this energy into potential energy of a deformation of the nucleus sufficient to lead to division.[5]

Such a competition between the fission process and the neutron escape and capture processes seems in fact to be exhibited in a striking manner by the way in which the cross section for fission of thorium and uranium varies with the energy of the impinging neutrons. The remarkable difference observed by Meitner, Hahn, and Strassmann between the effects in these two elements seems also readily explained on such lines by the presence in uranium of several stable isotopes, a considerable part of the fission phenomena being reasonably attributable to the rare isotope U^{235} which, for a given neutron energy, will lead to a compound nucleus of higher excitation energy and smaller stability than that formed from the abundant uranium isotope.[6]

In the present article there is developed a more detailed treatment of the mechanism of the fission process and accompanying effects, based on the comparison between the nucleus and a liquid drop. The critical deformation energy is brought into connection with the potential energy of the drop in a state of unstable equilibrium, and is estimated in its dependence on nuclear charge and mass. Exactly how the excitation energy originally given to the nucleus is gradually exchanged among the various degrees of freedom and leads eventually to a critical deformation proves to be a question which needs not be discussed in order to determine the fission probability. In fact, simple statistical considerations lead to an approximate expression for the fission reaction rate which depends only on the critical energy of deformation and the properties of nuclear energy level distributions. The general theory presented appears to fit together well with the observations and to give a satisfactory description of the fission phenomenon.

For a first orientation as well as for the later considerations, we estimate quantitatively in Section I by means of the available evidence the energy which can be released by the division of a heavy nucleus in various ways, and in particular examine not only the energy released in the fission process itself, but also the energy required for subsequent neutron escape from the fragments and the energy available for beta-ray emission from these fragments.

In Section II the problem of the nuclear deformation is studied more closely from the point of view of the comparison between the nucleus and a liquid droplet in order to make an estimate of the energy required for different nuclei to realize the critical deformation necessary for fission.

In Section III the statistical mechanics of the fission process is considered in more detail, and an approximate estimate made of the fission probability. This is compared with the probability of radiation and of neutron escape. A discussion is then given on the basis of the theory for the variation with energy of the fission cross section.

In Section IV the preceding considerations are applied to an analysis of the observations of the cross sections for the fission of uranium and thorium by neutrons of various velocities. In particular it is shown how the comparison with the theory developed in Section III leads to values for the critical energies of fission for thorium and the various isotopes of uranium which are in good accord with the considerations of Section II.

In Section V the problem of the statistical distribution in size of the nuclear fragments arising from fission is considered, and also the questions of the excitation of these fragments and the origin of the secondary neutrons.

Finally, we consider in Section VI the fission effects to be expected for other elements than thorium and uranium at sufficiently high neutron velocities as well as the effect to be anticipated in

[5] N. Bohr, Nature **143**, 330 (1939).
[6] N. Bohr, Phys. Rev. **55**, 418 (1939).

thorium and uranium under deuteron and proton impact and radiative excitation.

I. Energy Released by Nuclear Division

The total energy released by the division of a nucleus into smaller parts is given by

$$\Delta E=(M_0-\Sigma M_i)c^2, \quad (1)$$

where M_0 and M_i are the masses of the original and product nuclei at rest and unexcited. We have available no observations on the masses of nuclei with the abnormal charge to mass ratio formed for example by the division of such a heavy nucleus as uranium into two nearly equal parts. The difference between the mass of such a fragment and the corresponding stable nucleus of the same mass number may, however, if we look apart for the moment from fluctuations in energy due to odd-even alternations and the finer details of nuclear binding, be reasonably assumed, according to an argument of Gamow, to be representable in the form

$$M(Z, A)-M(Z_A, A)=\tfrac{1}{2}B_A(Z-Z_A)^2, \quad (2)$$

where Z is the charge number of the fragment and Z_A is a quantity which in general will not be an integer. For the mass numbers $A=100$ to 140 this quantity Z_A is given by the dotted line in Fig. 8, and in a similar way it may be determined for lighter and heavier mass numbers.

B_A is a quantity which cannot as yet be determined directly from experiment but may be estimated in the following manner. Thus we may assume that the energies of nuclei with a given mass A will vary with the charge Z approximately according to the formula

$$M(Z, A)=C_A+\tfrac{1}{2}B_A'(Z-\tfrac{1}{2}A)^2 +(Z-\tfrac{1}{2}A)(M_p-M_n)+3Z^2e^2/5r_0A^{\frac{1}{3}}. \quad (3)$$

Here the second term gives the comparative masses of the various isobars neglecting the influence of the difference M_p-M_n of the proton and neutron mass included in the third term and of the pure electrostatic energy given by the fourth term. In the latter term the usual assumption is made that the effective radius of the nucleus is equal to $r_0A^{\frac{1}{3}}$, with r_0 estimated as 1.48×10^{-13} from the theory of alpha-ray disintegration. Identifying the relative mass values given by expressions (2) and (3), we find

$$B_A'=(M_p-M_n+6Z_Ae^2/5r_0A^{\frac{1}{3}})/(\tfrac{1}{2}A-Z_A) \quad (4)$$

and

$$B_A=B_A'+6e^2/5r_0A^{\frac{1}{3}} =(M_p-M_n+3A^{\frac{1}{3}}e^2/5r_0)/(\tfrac{1}{2}A-Z_A). \quad (5)$$

The values of B_A obtained for various nuclei from this last relation are listed in Table I.

On the basis just discussed, we shall be able to estimate the mass of the nucleus (Z, A) with the help of the packing fraction of the known nuclei. Thus we may write

$$M(Z, A)=A(1+f_A) +\tfrac{1}{2}B_A(Z-Z_A)^2-\tfrac{1}{2}\delta_A\begin{cases}+0 & A \text{ odd}\\ & A \text{ even, } Z \text{ even}\\ +\tfrac{1}{2}\delta_A & A \text{ even, } Z \text{ odd}\end{cases}, \quad (6)$$

where f_A is to be taken as the average value of the packing fraction over a small region of atomic weights and the last term allows for the typical differences in binding energy among nuclei according to the odd and even character of their neutron and proton numbers. In using Dempster's measurements of packing fractions we must recognize that the average value of the second term in (6) is included in such measurements.[7] This correction, however, is, as may be read from Fig. 8, practically compensated by the influence of the third term, owing to the fact that the great majority of nuclei studied in the mass spectrograph are of even-even character.

From (6) we find the energy release involved in electron emission or absorption by a nucleus unstable with respect to a beta-ray

Table I. *Values of the quantities which appear in Eqs.* (6) *and* (7), *estimated for various values of the nuclear mass number A. Both* B_A and δ_A *are in Mev.*

A	Z_A	B_A	δ_A	A	Z_A	B_A	δ_A
50	23.0	3.5	2.8	150	62.5	1.2	1.5
60	27.5	3.3	2.8	160	65.4	1.1	1.3
70	31.2	2.5	2.7	170	69.1	1.1	1.2
80	35.0	2.2	2.7	180	72.9	1.0	1.2
90	39.4	2.0	2.7	190	76.4	1.0	1.1
100	44.0	2.0	2.6	200	80.0	0.95	1.1
110	47.7	1.7	2.4	210	83.5	0.92	1.1
120	50.8	1.5	2.1	220	87.0	0.88	1.1
130	53.9	1.3	1.9	230	90.6	0.86	1.0
140	58.0	1.2	1.8	240	93.9	0.82	1.0

[7] A. J. Dempster, Phys. Rev. **53**, 869 (1938).

transformation:

$$E_\beta = B_A\{|Z_A - Z| - \tfrac{1}{2}\} - \delta_A \begin{cases} +0 & A \text{ odd} \\ & A \text{ even, } Z \text{ even} \\ +\delta_A & A \text{ even, } Z \text{ odd} \end{cases}. \quad (7)$$

This result gives us the possibility of estimating δ_A by an examination of the stability of isobars of even nuclei. In fact, if an even-even nucleus is stable or unstable, then δ_A is, respectively, greater or less than $B_A\{|Z_A - A| - \frac{1}{2}\}$. For nuclei of medium atomic weight this condition brackets δ_A very closely; for the region of very high mass numbers, on the other hand, we can estimate δ_A directly from the difference in energy release of the successive beta-ray transformations

$$UX_I \rightarrow (UX_{II}, UZ) \rightarrow U_{II},$$
$$MsTh_I \rightarrow MsTh_{II} \rightarrow RaTh,\ RaD \rightarrow RaE \rightarrow RaF.$$

The estimated values of δ_A are collected in Table I.

Applying the available measurements on nuclear masses supplemented by the above considerations, we obtain typical estimates as shown in Table II for the energy release on division of a nucleus into two approximately equal parts.[8]

Below mass number $A \sim 100$ nuclei are energetically stable with respect to division; above this limit energetic instability sets in with respect to division into two nearly equal fragments, essentially because the decrease in electrostatic energy associated with the separation overcompensates the desaturation of short range forces consequent on the greater exposed nuclear surface. The energy evolved on division of the nucleus U^{239} into two fragments of any given charge and mass numbers is shown in Fig. 1. It is seen that there is a large range of atomic masses for which the energy liberated reaches nearly the maximum attainable value 200 Mev; but that for a given size of one fragment there is only a small range of charge numbers which correspond to an energy release at all near the maximum value. Thus the fragments formed by division of uranium in the *energetically* most favorable way lie in a narrow band in Fig. 1, separated from the region of the stable nuclei by an amount which corresponds to the change in nuclear charge

TABLE II. *Estimates for the energy release on division of typical nuclei into two fragments are given in the third column. In the fourth is the estimated value of the total additional energy release associated with the subsequent beta-ray transformations. Energies are in Mev.*

ORIGINAL	TWO PRODUCTS	DIVISION	SUBSEQUENT
$_{28}Ni^{61}$	$_{14}Si^{30, 31}$	−11	2
$_{50}Sn^{117}$	$_{25}Mn^{58, 59}$	10	12
$_{68}Er^{167}$	$_{34}Se^{83, 84}$	94	13
$_{82}Pb^{206}$	$_{41}Nb^{103, 103}$	120	32
$_{92}U^{239}$	$_{46}Pd^{119, 120}$	200	31

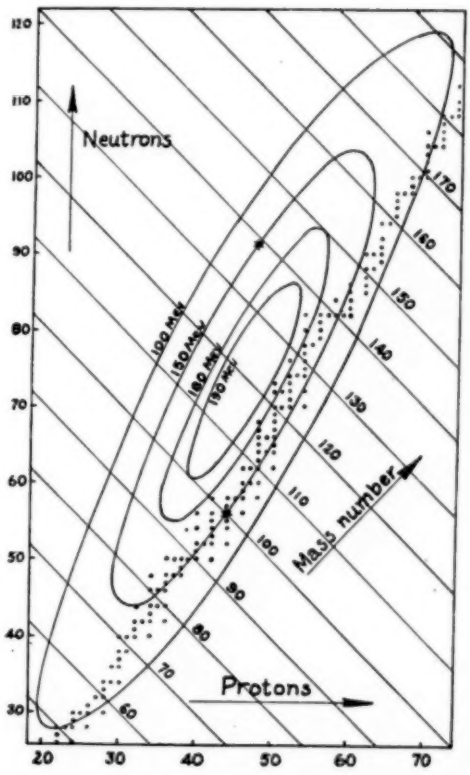

FIG. 1. The difference in energy between the nucleus $_{92}U^{239}$ in its normal state and the possible fragment nuclei $_{44}Ru^{100}$ and $_{48}Cd^{139}$ (indicated by the crosses in the figure) is estimated to be 150 Mev as shown by the corresponding contour line. In a similar way the estimated energy release for division of U^{239} into other possible fragments can be read from the figure. The region in the chart associated with the greatest energy release is seen to be at a distance from the region of the stable nuclei (dots in the figure) corresponding to the emission of from three to five beta-rays.

[8] Even if there is no question of actual fission processes by which nuclei break up into more than two comparable parts, it may be of interest to point out that such divisions in many cases would be accompanied by the release of energy. Thus nuclei of mass number greater than $A = 110$ are unstable with respect to division into three nearly equal parts. For uranium the corresponding total energy liberation will be ~210 Mev, and thus is even somewhat greater than the release on division into two parts. The energy evolution on division of U^{239} into four comparable parts will, however, be about 150 Mev, and already division into as many as 15 comparable parts will be endothermic.

associated with the emission of three to six beta-particles.

The amount of energy released in the beta-ray transformations following the creation of the fragment nuclei may be estimated from Eq. (7), using the constants in Table I. Approximate values obtained in this way for the energy liberation in typical chains of beta-disintegrations are shown on the arrows in Fig. 8.

The magnitude of the energy available for beta-ray emission from typical fragment nuclei does not stand in conflict with the stability of these nuclei with respect to spontaneous neutron emission, as one sees at once from the fact that the energy change associated with an increase of the nuclear charge by one unit is given by the *difference* between binding energy of a proton and of a neutron, plus the neutron-proton mass difference. A direct estimate from Eq. (6) of the binding energy of a neutron in typical nuclear fragments lying in the band of greatest energy release (Fig. 1) gives the results summarized in the last column of Table III. The comparison of the figures in this table shows that the neutron binding is in certain cases considerably smaller than the energy which can be released by beta-ray transformation. This fact offers a reasonable explanation as we shall see in Section V for the delayed neutron emission accompanying the fission process.

II. Nuclear Stability with Respect to Deformations

According to the liquid drop model of atomic nuclei, the excitation energy of a nucleus must be expected to give rise to modes of motion of the nuclear matter similar to the oscillations of a fluid sphere under the influence of surface tension.[9] For heavy nuclei the high nuclear charge will, however, give rise to an effect which will to a large extent counteract the restoring force due to the short range attractions responsible for the surface tension of nuclear matter. This effect, the importance of which for the fission phenomenon was stressed by Frisch and Meitner, will be more closely considered in this section, where we shall investigate the stability of a nucleus for small deformations of various types[10] as well as for such large deformations that division may actually be expected to occur.

Table III. *Estimated values of energy release in beta-ray transformations and energy of neutron binding in final nucleus, in typical cases; also estimates of the neutron binding in the dividing nucleus. Values in Mev.*

Beta-Transition		Release	Binding
$_{40}Zr^{99}$	$_{41}Nb^{99}$	6.3	8.2
$_{41}Nb^{100}$	$_{42}Mo^{100}$	7.8	8.6
$_{46}Pd^{125}$	$_{47}Ag^{125}$	7.8	6.7
$_{47}Ag^{125}$	$_{48}Cd^{125}$	6.5	5.0
$_{49}In^{130}$	$_{50}Sn^{130}$	7.6	7.1
$_{52}Te^{140}$	$_{53}I^{140}$	5.0	3.5
$_{53}I^{140}$	$_{54}Xe^{140}$	7.4	5.9
Compound Nucleus			
	$_{92}U^{235}$		5.4
	$_{92}U^{236}$		6.4
	$_{92}U^{239}$		5.2
	$_{90}Th^{233}$		5.2
	$_{91}Pa^{232}$		6.4

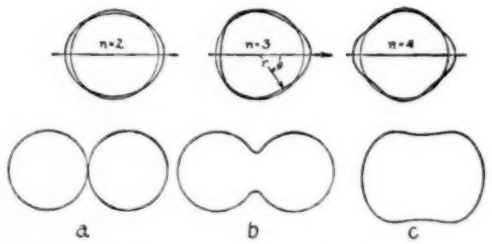

Fig. 2. Small deformations of a liquid drop of the type $\delta r(\theta)=\alpha_n P_n(\cos\theta)$ (upper portion of the figure) lead to characteristic oscillations of the fluid about the spherical form of stable equilibrium, even when the fluid has a uniform electrical charge. If the charge reaches the critical value $(10\times\text{surface tension}\times\text{volume})^{\frac{1}{2}}$, however, the spherical form becomes unstable with respect to even infinitesimal deformations of the type $n=2$. For a slightly smaller charge, on the other hand, a finite deformation (c) will be required to lead to a configuration of *unstable equilibrium*, and with smaller and smaller charge densities the critical form gradually goes over (c, b, a) into that of two uncharged spheres an infinitesimal distance from each other (a).

Consider a small arbitrary deformation of the liquid drop with which we compare the nucleus such that the distance from the center to an arbitrary point on the surface with colatitude θ is changed (see Fig. 2) from its original value R

[9] N. Bohr, Nature **137**, 344 and 351 (1936); N. Bohr and F. Kalckar, Kgl. Danske Vid. Selskab., Math. Phys. Medd. **14**, No. 10 (1937).

[10] After the formulae given below were derived, expressions for the potential energy associated with spheroidal deformations of nuclei were published by E. Feenberg (Phys. Rev. **55**, 504 (1939)) and F. Weizsäcker (Naturwiss. **27**, 133 (1939)). Further, Professor Frenkel in Leningrad has kindly sent us in manuscript a copy of a more comprehensive paper on various aspects of the fission problem, to appear in the U.S.S.R. "Annales Physicae," which contains a deduction of Eq. (9) below for nuclear stability against arbitrary small deformations, as well as some remarks, similar to those made below (Eq. (14)) about the shape of a drop corresponding to unstable equilibrium. A short abstract of this paper has since appeared in Phys. Rev. **55**, 987 (1939).

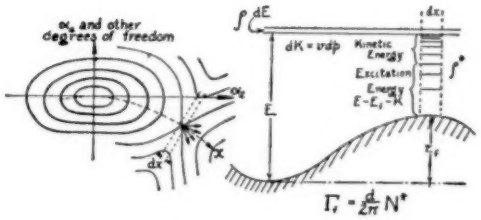

FIG. 3. The potential energy associated with any arbitrary deformation of the nuclear form may be plotted as a function of the parameters which specify the deformation, thus giving a contour surface which is represented schematically in the left-hand portion of the figure. The pass or saddle point corresponds to the critical deformation of unstable equilibrium. To the extent to which we may use classical terms, the course of the fission process may be symbolized by a ball lying in the hollow at the origin of coordinates (spherical form) which receives an impulse (neutron capture) which sets it to executing a complicated Lissajous figure of oscillation about equilibrium. If its energy is sufficient, it will in the course of time happen to move in the proper direction to pass over the saddle point (after which fission will occur), unless it loses its energy (radiation or neutron re-emission). At the right is a cross section taken through the fission barrier, illustrating the calculation in the text of the probability per unit time of fission occurring.

to the value

$$r(\theta)=R[1+\alpha_0+\alpha_2P_2(\cos\theta)+\alpha_3P_3(\cos\theta)+\cdots], \quad (8)$$

where the α_n are small quantities. Then a straightforward calculation shows that the surface energy plus the electrostatic energy of the comparison drop has increased to the value

$$E_{S+E}=4\pi(r_0A^{\frac{1}{3}})^2O[1+2\alpha_2^2/5+5\alpha_3^2/7+\cdots+(n-1)(n+2)\alpha_n^2/2(2n+1)+\cdots]+3(Ze)^2/5r_0A^{\frac{1}{3}}[1-\alpha_2^2/5-10\alpha_3^2/49-\cdots-5(n-1)\alpha_n^2/(2n+1)^2-\cdots], \quad (9)$$

where we have assumed that the drop is composed of an incompressible fluid of volume $(4\pi/3)R^3=(4\pi/3)r_0^3A$, uniformly electrified to a charge Ze, and possessing a surface tension O. Examination of the coefficient of α_2^2 in the above expression for the distortion energy, namely,

$$4\pi r_0^2OA^{\frac{2}{3}}(2/5)\{1-(Z^2/A)\times[e^2/10(4\pi/3)r_0^3O]\} \quad (10)$$

makes it clear that with increasing value of the ratio Z^2/A we come finally to a limiting value

$$(Z^2/A)_{\text{limiting}}=10(4\pi/3)r_0^3O/e^2, \quad (11)$$

beyond which the nucleus is no longer stable with respect to deformations of the simplest type. The actual value of the numerical factors can be calculated with the help of the semi-empirical formula given by Bethe for the respective contributions to nuclear binding energies due to electrostatic and long range forces, the influence of the latter being divided into volume and surface effects. A revision of the constants in Bethe's formula has been carried through by Feenberg[11] in such a way as to obtain the best agreement with the mass defects of Dempster; he finds

$$r_0\doteq 1.4\times10^{-13}\text{ cm}, \quad 4\pi r_0^2O\doteq 14\text{ Mev}. \quad (12)$$

From these values a limit for the ratio Z^2/A is obtained which is 17 percent greater than the ratio $(92)^2/238$ characterizing U^{238}. Thus we can conclude that nuclei such as those of uranium and thorium are indeed near the limit of stability set by the exact compensation of the effects of electrostatic and short range forces. On the other hand, we cannot rely on the precise value of the limit given by these semi-empirical and indirect determinations of the ratio of surface energy to electrostatic energy, and we shall investigate below a method of obtaining the ratio in question from a study of the fission phenomenon itself.

Although nuclei for which the quantity Z^2/A is slightly less than the limiting value (11) are stable with respect to small arbitrary deformations, a larger deformation will give the long range repulsions more advantage over the short range attractions responsible for the surface tension, and it will therefore be possible for the nucleus, when suitably deformed, to divide spontaneously. Particularly important will be that critical deformation for which the nucleus is just on the verge of division. The drop will then possess a shape corresponding to unstable equilibrium: the work required to produce any infinitesimal displacement from this equilibrium configuration vanishes in the first order. To examine this point in more detail, let us consider the surface obtained by plotting the potential energy of an arbitrary distortion as a function of the parameters which specify its form and magnitude. Then we have to recognize the fact that the

[11] E. Feenberg, Phys. Rev. **55**, 504 (1939).

potential barrier hindering division is to be compared with a pass or saddle point leading between two potential valleys on this surface. The energy relations are shown schematically in Fig. 3, where of course we are able to represent only two of the great number of parameters which are required to describe the shape of the system. The deformation parameters corresponding to the saddle point give us the critical form of the drop, and the potential energy required for this distortion we will term the critical energy for fission, E_f. If we consider a continuous change in the shape of the drop, leading from the original sphere to two spheres of half the size at infinite separation, then the critical energy in which we are interested is the lowest value which we can at all obtain, by suitable choice of this sequence of shapes, for the energy required to lead from the one configuration to the other.

Simple dimensional arguments show that the critical deformation energy for the droplet corresponding to a nucleus of given charge and mass number can be written as the product of the surface energy by a dimensionless function of the charge mass ratio:

$$E_f = 4\pi r_0^2 O A^{\frac{2}{3}} f\{(Z^2/A)/(Z^2/A)_{\text{limiting}}\}. \quad (13)$$

We can determine E_f if we know the shape of the nucleus in the critical state; this will be given by solution of the well-known equation for the form of a surface in equilibrium under the action of a surface tension O and volume forces described by a potential φ:

$$\kappa O + \varphi = \text{constant}, \quad (14)$$

where κ is the total normal curvature of the surface. Because of the great mathematical difficulties of treating large deformations, we are however able to calculate the critical surface and the dimensionless function f in (13) only for certain special values of the argument, as follows: (1) if the volume potential in (14) vanishes altogether, we see from (14) that the surface of unstable equilibrium has constant curvature; we have in fact to deal with a division of the fluid into spheres. Thus, when there are no electrostatic forces at all to aid the fission, the critical energy for division into two equal fragments will just equal the total work done against surface tension in the separation process, i.e., .

$$E_f = 2 \cdot 4\pi r_0^2 O (A/2)^{\frac{2}{3}} - 4\pi r_0^2 O A^{\frac{2}{3}}. \quad (15)$$

From this it follows that

$$f(0) = 2^{\frac{1}{3}} - 1 = 0.260. \quad (16)$$

(2) If the charge on the droplet is not zero, but is still very small, the critical shape will differ little from that of two spheres in contact. There will in fact exist only a narrow neck of fluid connecting the two portions of the figure, the radius of which, r_n, will be such as to bring about equilibrium; to a first approximation

$$2\pi r_n O = (Ze/2)^2/(2r_0(A/2)^{\frac{1}{3}})^2 \quad (17)$$

or

$$r_n/r_0 A^{\frac{1}{3}} = 0.66\left(\frac{Z^2}{A}\right)\Big/\left(\frac{Z^2}{A}\right)_{\text{limiting}}. \quad (18)$$

To calculate the critical energy to the first order in Z^2/A, we can omit the influence of the neck as producing only a second-order change in the energy. Thus we need only compare the sum of surface and electrostatic energy for the original nucleus with the corresponding energy for two spherical nuclei of half the size in contact with each other. We find

$$\begin{aligned} E_f = {} & 2 \cdot 4\pi r_0^2 O (A/2)^{\frac{2}{3}} - 4\pi r_0^2 O A^{\frac{2}{3}} \\ & + 2 \cdot 3(Ze/2)^2/5r_0(A/2)^{\frac{1}{3}} \\ & + (Ze/2)^2/2r_0(A/2)^{\frac{1}{3}} - 3(Ze)^2/5r_0 A^{\frac{1}{3}}, \end{aligned} \quad (19)$$

from which

$$E_f/4\pi r_0^2 O A^{\frac{2}{3}} \equiv f(x) = 0.260 - 0.215x, \quad (20)$$

provided

$$x = \left(\frac{Z^2}{A}\right)\Big/\left(\frac{Z^2}{A}\right)_{\text{limiting}} = (\text{charge})^2/\text{surface tension} \times \text{volume} \times 10 \quad (21)$$

is a small quantity. (3) In the case of greatest actual interest, when Z^2/A is very close to the critical value, only a small deformation from a spherical form will be required to reach the critical state. According to Eq. (9), the potential energy required for an infinitesimal distortion will increase as the square of the amplitude, and

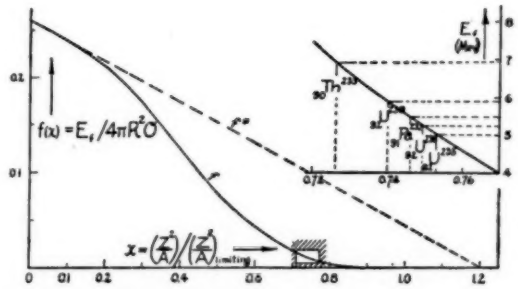

FIG. 4. The energy E_f required to produce a critical deformation leading to fission is divided by the surface energy $4\pi R^2O$ to obtain a dimensionless function of the quantity $x=(\text{charge})^2/(10\times\text{volume}\times\text{surface tension})$. The behavior of the function $f(x)$ is calculated in the text for $x=0$ and $x=1$, and a smooth curve is drawn here to connect these values. The curve $f^*(x)$ determines for comparison the energy required to deform the nucleus into two spheres in contact with each other. Over the cross-hatched region of the curve of interest for the heaviest nuclei the surface energy changes but little. Taking for it a value of 530 Mev, we obtain the energy scale in the upper part of the figure. In Section IV we estimate from the observations a value $E_f\sim 6$ Mev for U^{239}. Using the figure we thus find $(Z^2/A)_{\text{limiting}}=47.8$ and can estimate the fission barriers for other nuclei, as shown.

will moreover have the smallest possible value for a displacement of the form $P_2(\cos\theta)$. To find the deformation for which the potential energy has reached a maximum and is about to decrease, we have to carry out a more accurate calculation. We obtain for the distortion energy, accurate to the fourth order in α_2, the expression

$$\Delta E_{S+E}=4\pi r_0^2OA^{\frac{2}{3}}[2\alpha_2^2/5+116\alpha_2^3/105+101\alpha_2^4/35+2\alpha_2^2\alpha_4/35+\alpha_4^2]$$
$$-3(Ze)^2/5r_0A^{\frac{1}{3}}[\alpha_2^2/5+64\alpha_2^3/105+58\alpha_2^4/35+8\alpha_2^2\alpha_4/35+5\alpha_4^2/27], \quad (22)$$

in which it will be noted that we have had to include the terms in α_4^2 because of the coupling which sets in between the second and fourth modes of motion for appreciable amplitudes. Thus, on minimizing the potential energy with respect to α_4, we find

$$\alpha_4=-(243/595)\alpha_2^2 \quad (23)$$

in accordance with the fact that as the critical form becomes more elongated with decreasing Z^2/A, it must also develop a concavity about its equatorial belt such as to lead continuously with variation of the nuclear charge to the dumbbell shaped figure discussed in the preceding paragraph.

With the help of (23) we obtain the deformation energy as a function of α_2 alone. By a straightforward calculation we then find its maximum value as a function of α_2, thus determining the energy required to produce a distortion on the verge of leading to fission:

$$E_f/4\pi r_0^2OA^{\frac{2}{3}}=f(x)=98(1-x)^3/135-11368(1-x)^4/34425+\cdots \quad (24)$$

for values of Z^2/A near the instability limit.

Interpolating in a reasonable way between the two limiting values which we have obtained for the critical energy for fission, we obtain the curve of Fig. 4 for f as a function of the ratio of the square of the charge number of the nucleus to its mass number. The upper part of the figure shows the interesting portion of the curve in enlargement and with a scale of energy values at the right based on the surface tension estimate of Eq. (12) and a nuclear mass of $A=235$. The slight variation of the factor $4\pi r_0^2OA^{\frac{2}{3}}$ among the various thorium and uranium isotopes may be neglected in comparison with the changes of the factor $f(x)$.

In Section IV we estimate from the observations that the critical fission energy for U^{239} is not far from 6 Mev. According to Fig. 4, this corresponds to a value of $x=0.74$, from which we conclude that $(Z^2/A)_{\text{limiting}}=(92)^2/239\times 0.74=47.8$. This result enables us to estimate the critical energies for other isotopes, as indicated in the figure. It is seen that protactinium would be particularly interesting as a subject for fission experiments.

As a by product, we are also able from Eq. (12) to compute the nuclear radius in terms of the surface energy of the nucleus; assuming Feenberg's value of 14 Mev for $4\pi r_0^2O$, we obtain $r_0=1.47\times 10^{-13}$ cm, which gives a satisfactory and quite independent check on Feenberg's determination of the nuclear radius from the packing fraction curve.

So far the considerations are purely classical, and any actual state of motion must of course be described in terms of quantum-mechanical concepts. The possibility of applying classical pictures to a certain extent will depend on the smallness of the ratio between the zero point amplitudes for oscillations of the type discussed above and the nuclear radius. A simple calcu-

lation gives for the square of the ratio in question the result

$$\langle \alpha_n^2 \rangle_{Av;\ \text{zero point}} = A^{-7/6} \times \{(\hbar^2/12M_p r_0^2)/4\pi r_0^2 O\}^{\frac{1}{2}} n^{\frac{1}{2}}(2n+1)^{\frac{1}{2}} \times \{(n-1)(n+2)(2n+1) - 20(n-1)x\}^{-\frac{1}{2}}. \quad (25)$$

Since $\{(\hbar^2/12M_p r_0^2)/4\pi r_0^2 O\}^{\frac{1}{2}} \doteqdot \frac{1}{3}$, this ratio is indeed a small quantity, and it follows that deformations of magnitudes comparable with nuclear dimensions can be described approximately classically by suitable wave packets built up from quantum states. In particular we may describe the critical deformations which lead to fission in an approximately classical way. This follows from a comparison of the critical energy $E_f \sim 6$ Mev required, as we shall see in Section IV, to account for the observations on uranium, with the zero point energy

$$\tfrac{1}{2}\hbar\omega_2 = A^{-\frac{1}{2}}\{4\pi r_0^2 O \cdot 2(1-x)\hbar^2/3M_p r_0^2\}^{\frac{1}{2}} \sim 0.4 \text{ Mev} \quad (26)$$

of the simplest mode of capillary oscillation, from which it is apparent that the amplitude in question is considerably larger than the zero point disturbance:

$$\langle \alpha_2^2 \rangle_{Av} / \langle \alpha_2^2 \rangle_{Av;\ \text{zero point}} \approx E_f / \tfrac{1}{2}\hbar\omega_2 \sim 15. \quad (27)$$

The drop with which we compare the nucleus will also in the critical state be capable of executing small oscillations about the shape of unstable equilibrium. If we study the distribution in frequency of these characteristic oscillations, we must expect for high frequencies to find a spectrum qualitatively not very different from that of the normal modes of oscillation about the form of stable equilibrium. The oscillations in question will be represented symbolically in Fig. 3 by motion of the representative point of the system in configuration space normal to the direction leading to fission. The distribution of the available energy of the system between such modes of motion and the mode of motion leading to fission will be determining for the probability of fission if the system is near the critical state. The statistical mechanics of this problem is considered in Section III. Here we would only like to point out that the fission process is from a practical point of view a nearly irreversible process. In fact if we imagine the fragment nuclei resulting from a fission to be reflected without loss of energy and to run directly towards each other, the electrostatic repulsion between the two nuclei will ordinarily prevent them from coming into contact. Thus, relative to the original nucleus, the energy of two spherical nuclei of half the size is given by Eq. (19) and corresponds to the values $f^*(x)$ shown by the dashed line in Fig. 4. To compare this with the energy required for the original fission process (smooth curve for $f(x)$ in the figure), we note that the surface energy $4\pi r_0^2 O A^{\frac{2}{3}}$ is for the heaviest nuclei of the order of 500 Mev. We thus have to deal with a difference of $\sim 0.05 \times 500$ Mev $= 25$ Mev between the energy available when a heavy nucleus is just able to undergo fission, and the energy required to bring into contact two spherical fragments. There will of course be appreciable tidal forces exerted when the two fragments are brought together, and a simple estimate shows that this will lower the energy discrepancy just mentioned by something of the order of 10 Mev, which is not enough to alter our conclusions. That there is no paradox involved, however, follows from the fact that the fission process actually takes place for a configuration in which the sum of surface and electrostatic energy has a considerably smaller value than that corresponding to two rigid spheres in contact, or even two tidally distorted globes; namely, by arranging that in the division process the surface surrounding the original nucleus shall not tear until the mutual electrostatic energy of the two nascent nuclei has been brought down to a value essentially smaller than that corresponding to separated spheres, then there will be available enough electrostatic energy to provide the work required to tear the surface, which will of course have increased in total value to something more than that appropriate to two spheres. Thus it is clear that the two fragments formed by the division process will possess internal energy of excitation. Consequently, if we wish to reverse the fission process, we must take care that the fragments come together again sufficiently distorted, and indeed with the distortions so oriented, that contact can be made between projections on the two surfaces and the surface tension start drawing them together while the electrostatic repulsion between the effective electrical centers of gravity of the two parts is

still not excessive. The probability that two atomic nuclei in any actual encounter will be suitably excited and possess the proper phase relations so that union will be possible to form a compound system will be extremely small. Such union processes, converse to fission, can be expected to occur for unexcited nuclei only when we have available much more kinetic energy than is released in the fission processes with which we are concerned.

The above considerations on the fission process, based on a comparison between the properties of a nucleus and those of a liquid drop, should be supplemented by remarking that the distortion which leads to fission, although associated with a greater effective mass and lower quantum frequency, and hence more nearly approaching the possibilities of a classical description than any of the higher order oscillation frequencies of the nucleus, will still be characterized by certain specific quantum-mechanical properties. Thus there will be an essential ambiguity in the definition of the critical fission energy of the order of magnitude of the zero point energy, $\hbar\omega_2/2$, which however as we have seen above is only a relatively small quantity. More important from the point of view of nuclear stability will be the possibility of quantum-mechanical tunnel effects, which will make it possible for a nucleus to divide even in its ground state by passage through a portion of configuration space where classically the kinetic energy is negative.

An accurate estimate for the stability of a heavy nucleus against fission in its ground state will, of course, involve a very complicated mathematical problem. In natural extension of the well-known theory of α-decay, we should in principle determine the probability per unit time of a fission process, λ_f, by the formula

$$\lambda_f(=\Gamma_f/\hbar)=5(\omega_f/2\pi)$$
$$\times\exp -2\int_{P_1}^{P_2}\{2(V-E)\sum_i m_i(dx_i/d\alpha)^2\}^{\frac{1}{2}}d\alpha/\hbar. \quad (28)$$

The factor 5 represents the degree of degeneracy of the oscillation leading to instability. The quantum of energy characterizing this vibration is, according to (26), $\hbar\omega\sim 0.8$ Mev. The integral in the exponent leads in the case of a single particle to the Gamow penetration factor. Similarly, in the present problem, the integral is extended in configuration space from the point P_1 of stable equilibrium over the fission saddle point S (as indicated by the dotted line in Fig. 3) and down on a path of steepest descent to the point P_2 where the classical value of the kinetic energy, $E-V$, is again zero. Along this path we may write the coordinate x_i of each elementary particle m_i in terms of a certain parameter α. Since the integral is invariant with respect to how the parameter is chosen, we may for convenience take α to represent the distance between the centers of gravity of the nascent nuclei. To make an accurate calculation on the basis of the liquid-drop model for the integral in (28) would be quite complicated, and we shall therefore estimate the result by assuming each elementary particle to move a distance $\frac{1}{2}\alpha$ in a straight line either to the right or the left according as it is associated with the one or the other nascent nucleus. Moreover, we shall take $V-E$ to be of the order of the fission energy E_f. Thus we obtain for the exponent in (28) approximately

$$(2ME_f)^{\frac{1}{2}}\alpha/\hbar. \quad (29)$$

With $M=239\times 1.66\times 10^{-24}$, $E_f\sim 6$ Mev $=10^{-5}$ erg, and the distance of separation intermediate between the diameter of the nucleus and its radius, say of the order $\sim 1.3\times 10^{-13}$ cm, we thus find a mean lifetime against fission in the ground state equal to

$$1/\lambda_f\sim 10^{-21}\exp\left[(2\times 4\times 10^{-22}\times 10^{-5})^{\frac{1}{2}}1.3\right.$$
$$\left.\times 10^{-12}/10^{-27}\right]\sim 10^{30}\text{ sec.}\sim 10^{22}\text{ years.} \quad (30)$$

It will be seen that the lifetime thus estimated is not only enormously large compared with the time interval of the order 10^{-15} sec. involved in the actual fission processes initiated by neutron impacts, but that this is even large compared with the lifetime of uranium and thorium for α-ray decay. This remarkable stability of heavy nuclei against fission is as seen due to the large masses involved, a point which was already indicated in the cited article of Meitner and Frisch, where just the essential characteristics of the fission effect were stressed.

III. Break-up of the Compound System as a Monomolecular Reaction

To determine the fission probability, we consider a microcanonical ensemble of nuclei, all having excitation energies between E and $E+dE$. The number of nuclei will be chosen to be exactly equal to the number $\rho(E)dE$ of levels in this energy interval, so that there is one nucleus in each state. The number of nuclei which divide per unit time will then be $\rho(E)dE\Gamma_f/\hbar$, according to our definition of Γ_f. This number will be equal to the number of nuclei in the transition state which pass outward over the fission barrier per unit time.[11a] In a unit distance measured in the direction of fission there will be $(dp/h)\rho^*(E-E_f-K)dE$ quantum states of the microcanonical ensemble for which the momentum and kinetic energy associated with the fission distortion have values in the intervals dp and $dK=vdp$, respectively. Here ρ^* is the density of those levels of the compound nucleus in the transition state which arise from excitation of all degrees of freedom other than the fission itself. At the initial time we have one nucleus in each of the quantum states in question, and consequently the number of fissions per unit time will be

$$dE\int v(dp/h)\rho^*(E-E_f-K)=dEN^*/h, \quad (31)$$

where N^* is the number of levels in the transition state available with the given excitation. Comparing with our original expression for this number, we have

$$\Gamma_f=N^*/2\pi\rho(E)=(d/2\pi)N^* \quad (32)$$

for the fission width expressed in terms of the level density or the level spacing d of the compound nucleus.

The derivation just given for the level width will only be valid if N^* is sufficiently large compared to unity; that is, if the fission width is comparable with or greater than the level spacing. This corresponds to the conditions under which a correspondence principle treatment of the fission distortion becomes possible. On the other hand, when the excitation exceeds by only a little the critical energy, or falls below E_f, specific quantum-mechanical tunnel effects will begin to become of importance. The fission probability will of course fall off very rapidly with decreasing excitation energy at this point, the mathematical expression for the reaction rate eventually going over into the penetration formula of Eq. (28); this, as we have seen above, gives a negligible fission probability for uranium.

The probability of neutron re-emission, so important in limiting the fission yield for high excitation energies, has been estimated from statistical arguments by various authors, especially Weisskopf.[12] The result can be derived in a very simple form by considering the microcanonical ensemble introduced above. Only a few changes are necessary with respect to the reasoning used for the fission process. The transition state will be a spherical shell of unit thickness just outside the nuclear surface $4\pi R^2$; the critical energy is the neutron binding energy, E_n; and the density ρ^{**} of excitation levels in the transition state is given by the spectrum of the residual nucleus. The number of quantum states in the microcanonical ensemble which lie in the transition region and for which the neutron momentum lies in the range p to $p+dp$ and in the solid angle $d\Omega$ will be

$$(4\pi R^2\cdot p^2dpd\Omega/h^3)\rho^*(E-E_n-K)dE. \quad (33)$$

We multiply this by the normal velocity $v\cos\theta=(dK/dp)\cos\theta$ and integrate, obtaining

$$dE(4\pi R^2\cdot 2\pi m/h^3)\int\rho^*(E-E_n-K)KdK \quad (34)$$

for the number of neutron emission processes occurring per unit time. This is to be identified with $\rho(E)dE(\Gamma_n/\hbar)$. Therefore we have for the probability of neutron emission, expressed in energy units, the result

$$\Gamma_n=(1/2\pi\rho)(2mR^2/\hbar^2)\int\rho^{**}(E-E_n-K)KdK$$
$$=(d/2\pi)(A^{\frac{1}{3}}/K')\sum_i K_i \quad (35)$$

in complete analogy to the expression

$$\Gamma_f=(d/2\pi)\sum_i 1 \quad (36)$$

[11a] For a general discussion of the ideas involved in the concept of a transition state, reference is made to an article by E. Wigner, Trans. Faraday Soc. **34**, part 1, 29 (1938).

[12] V. Weisskopf, Phys. Rev. **52**, 295 (1937).

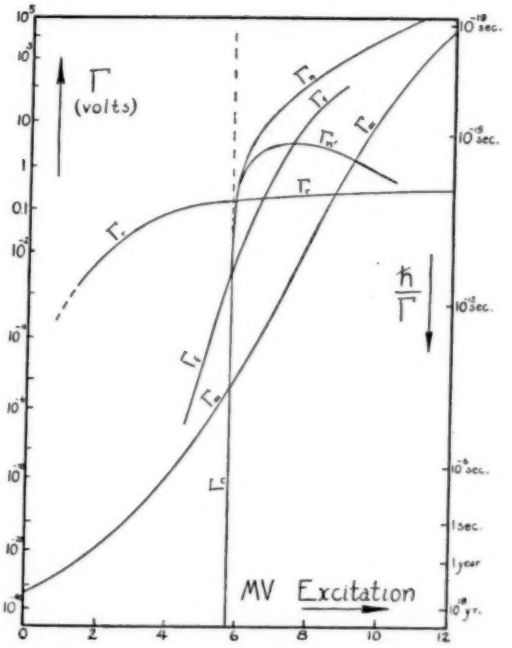

FIG. 5. Schematic diagram of the partial transition probabilities (multiplied by $\hbar$ and expressed in energy units) and their reciprocals (dimensions of a mean lifetime) for various excitation energies of a typical heavy nucleus. Γ_γ, Γ_f, and Γ_α refer to radiation, fission, and alpha-particle emission, while $\Gamma_{n'}$ and Γ_n determine, respectively, the probability of a neutron emission leaving the residual nucleus in its ground state or in any state. The latter quantities are of course zero if the excitation is less than the neutron binding, which is taken here to be about 6 Mev.

for the fission width. Just as the summation in the latter equation goes over all those levels of the nucleus in the transition state which are available with the given excitation, so the sum in the former is taken over all available states of the residual nucleus, K_i denoting the corresponding kinetic energy $E-E_n-E_i$ which will be left for the neutron. K' represents, except for a factor, the zero point kinetic energy of an elementary particle in the nucleus; it is given by $A^{\frac{1}{3}}\hbar^2/2mR^2$ and will be 9.3 Mev if the nuclear radius is $A^{\frac{1}{3}}1.48\times10^{-13}$ cm.

No specification was made as to the angular momentum of the nucleus in the derivation of (35) and (36). Thus the expressions in question give us averages of the level widths over states of the compound system corresponding to many different values of the rotational quantum number J, while actually capture of a neutron of one- or two-Mev energy by a normal nucleus will give rise only to a restricted range of values of J. This point is of little importance in general, as the widths will not depend much on J, and therefore in the following considerations we shall apply the above estimates of Γ_f and Γ_n as they stand. In particular, d will represent the average spacing of levels of a given angular momentum. If, however, we wish to determine the partial width $\Gamma_{n'}$ giving the probability that the compound nucleus will break up leaving the residual nucleus in its ground state and giving the neutron its full kinetic energy, we shall not be justified in simply selecting out the corresponding term in the sum in (35) and identifying it with $\Gamma_{n'}$. In fact, a more detailed calculation along the above lines, specifying the angular momentum of the microcanonical ensemble as well as its energy, leads to the expression

$$\Sigma(2J+1)\Gamma_{n'}{}^{J} = (2s+1)(2i+1)(d/2\pi)(R^2/\lambda^2) \quad (37)$$

for the partial neutron width, where the sum goes over those values of J which are realized when a nucleus of spin i is bombarded by a neutron of the given energy possessing spin $s=\frac{1}{2}$.

The smallness of the neutron mass in comparison with the reduced mass of two separating nascent nuclei will mean that we shall have in the former case to go to excitation energies much higher relative to the barrier than in the latter case before the condition is fulfilled for the application of the transition state method. In fact, only when the kinetic energy of the emerging particle is considerably greater than 1 Mev does the reduced wave-length $\lambda=\lambda/2\pi$ of the neutron become essentially smaller than the nuclear radius, allowing the use of the concepts of velocity and direction of the neutron emerging from the nuclear surface.

The absolute yield of the various processes initiated by neutron bombardment will depend upon the probability of absorption of the neutron to form a compound nucleus; this will be proportional to the converse probability $\Gamma_{n'}/\hbar$ of a neutron emission process which leaves the residual neutron emission process which leaves the residual nucleus in its ground state. $\Gamma_{n'}$ will vary as the neutron velocity itself for low neutron energies; according to the available information about nuclei of medium atomic weight, the width in volts is approximately 10^{-3} times the

square root of the neutron energy in volts.[13] As the neutron energy increases from thermal values to 100 kev, we have to expect then an increase of $\Gamma_{n'}$ from something of the order of 10^{-4} ev to 0.1 or 1 ev. For high neutron energies we can use Eq. (37), according to which $\Gamma_{n'}$ will increase as the neutron energy itself, except as compensated by the decrease in level spacing as higher excitations are attained. As an order of magnitude estimate, we can take the level spacing in U to decrease from 100 kev for the lowest levels to 20 ev at 6 Mev (capture of thermal neutrons) to $\frac{1}{5}$ ev for $2\frac{1}{2}$-Mev neutrons. With $d=\frac{1}{5}$ ev we obtain $\Gamma_{n'}=(1/2\pi\times 5)(239^{\frac{1}{3}}/10)2\frac{1}{2}\doteq\frac{1}{2}$ ev for neutrons from the D+D reaction. The partial neutron width will not exceed for any energy a value of this order of magnitude, since the decrease in level spacing will be the dominating factor at higher energies.

The compound nucleus once formed, the outcome of the competition between the possibilities of fission, neutron emission, and radiation, will be determined by the relative magnitudes of Γ_f, Γ_n, and the corresponding radiation width Γ_r. From our knowledge of nuclei comparable with thorium and uranium we can conclude that the radiation width Γ_r will not exceed something of the order of 1 ev, and moreover that it will be nearly constant for the range of excitation energies which results from neutron absorption (see Fig. 5). The fission width will be extremely small for excitation energies below the critical energy E_f, but above this point Γ_f will become appreciable, soon exceeding the radiation width and rising almost exponentially for higher energies. Therefore, if the critical energy E_f required for fission is comparable with or greater than the excitation consequent on neutron capture, we have to expect that radiation will be more likely than fission; but if the barrier height is somewhat lower than the value of the neutron binding, and in any case if we irradiate with sufficiently energetic neutrons, radiative capture will always be less probable than division. As the speed of the bombarding neutrons is increased, we shall not expect an indefinite rise in the fission yield, however, for the output will be governed by the competition in the compound system between the possibilities of fission and of neutron emission. The width Γ_n which gives the probability of the latter process will for energies less than something of the order of 100 kev be equal to $\Gamma_{n'}$, the partial width for emissions leaving the residual nucleus in the ground state, since excitation of the product nucleus will be energetically impossible. For higher neutron energies, however, the number of available levels in the residual nucleus will rise rapidly, and Γ_n will be much larger than $\Gamma_{n'}$, increasing almost exponentially with energy.

In the energy region where the levels of the compound nucleus are well separated, the cross sections governing the yield of the various processes considered above can be obtained by direct application of the dispersion theory of Breit and Wigner.[14] In the case of resonance, where the energy E of the incident neutron is close to a special value E_0 characterizing an isolated level of the compound system, we shall have

$$\sigma_f=\pi\lambda^2\frac{2J+1}{(2s+1)(2i+1)}\frac{\Gamma_{n'}\Gamma_f}{(E-E_0)^2+(\Gamma/2)^2} \tag{38}$$

and

$$\sigma_r=\pi\lambda^2\frac{2J+1}{(2s+1)(2i+1)}\frac{\Gamma_{n'}\Gamma_r}{(E-E_0)^2+(\Gamma/2)^2}. \tag{39}$$

for the fission and radiation cross sections. Here $\lambda=\hbar/p=\hbar/(2mE)^{\frac{1}{2}}$ is the neutron wave-length divided by 2π, i and J are the rotational quantum numbers of the original and the compound nucleus, $s=\frac{1}{2}$, and $\Gamma=\Gamma_n+\Gamma_r+\Gamma_f$ is the total width of the resonance level at half-maximum.

In the energy region where the compound nucleus has many levels whose spacing, d, is comparable with or smaller than the total width, the dispersion theory cannot be directly applied due to the phase relations between the contributions of the different levels. A closer discussion[15] shows, however, that in cases like fission and radiative capture, the cross section will be obtained by summing many terms of the form (38) or (39). If the neutron wave-length is large compared with nuclear dimensions, only those states of the compound nucleus will contribute to the

[13] H. A. Bethe, Rev. Mod. Phys. **9**, 150 (1937).

[14] G. Breit and E. Wigner, Phys. Rev. **49**, 519 (1936). Cf. also H. Bethe and G. Placzek, Phys. Rev. **51**, 450 (1937)

[15] N. Bohr, R. Peierls and G. Placzek, Nature (in press).

sum which can be realized by capture of a neutron of zero angular momentum, and we shall obtain

$$\sigma_f=\pi\lambda^2\Gamma_{n'}(\Gamma_f/\Gamma)(2\pi/d)\times\begin{cases}1 \text{ if } i=0\\ \frac{1}{2} \text{ if } i>0\end{cases}, \quad (40)$$

$$\sigma_r=\pi\lambda^2\Gamma_{n'}(\Gamma_r/\Gamma)(2\pi/d)\times\begin{cases}1 \text{ if } i=0\\ \frac{1}{2} \text{ if } i>0\end{cases}. \quad (41)$$

On the other hand, if λ becomes essentially smaller than R, the nuclear radius (case of neutron energy over a million volts), the summation will give

$$\sigma_f=\frac{\pi\lambda^2\sum(2J+1)\Gamma_{n'}}{(2s+1)(2i+1)}(\Gamma_f/\Gamma)(2\pi/d)$$

$$=\pi R^2\Gamma_f/\Gamma, \quad (42)$$

$$\sigma_r=\pi R^2\Gamma_r/\Gamma. \quad (43)$$

The simple form of the result, which follows by use of the equation (37) derived above for $\Gamma_{n'}$, is of course an immediate consequence of the fact that the cross section for any given process for fast neutrons is given by the projected area of the nucleus times the ratio of the probability per unit time that the compound system react in the given way to the total probability of all reactions. Of course for extremely high bombarding energies it will no longer be possible to draw any simple distinction between neutron emission and fission; evaporation will go on simultaneously with the division process itself; and in general we shall have to expect then the production of numerous fragments of widely assorted sizes as the final result of the reaction.

IV. Discussion of the Observations

A. The resonance capture process

Meitner, Hahn, and Strassmann[16] observed that neutrons of some volts energy produced in uranium a beta-ray activity of 23 min. half-life whose chemistry is that of uranium itself. Moreover, neutrons of such energy gave no noticeable yield of the complex of periods which is produced in uranium by irradiation with either thermal or fast neutrons, and which is now known to arise from the beta-instability of the fragments arising from fission processes. The origin of the activity in question therefore had to be attributed to the ordinary type of radiative capture observed in other nuclei; like such processes it has a resonance character. The effective energy E_0 of the resonance level or levels was determined by comparing the absorption in boron of the neutrons producing the activity and of neutrons of thermal energy:

$$E_0=(\pi kT/4)[\mu_{\text{thermal}}(B)/\mu_{\text{res}}(B)]^2$$

$$=25\pm10 \text{ ev}. \quad (44)$$

The absorption coefficient in uranium itself for the activating neutrons was found to be 3 cm²/g, corresponding to an effective cross section of $3 \text{ cm}^2/\text{g}\times238\times1.66\times10^{-24} \text{ g}=1.2\times10^{-21} \text{ cm}^2$. If we attribute the absorption to a single resonance level with no appreciable Doppler broadening, the cross section at exact resonance will be twice this amount, or 2.4×10^{-21} cm²; if on the other hand the true width Γ should be small compared with the Doppler broadening

$$\Delta=2(E_0kT/238)^{\frac{1}{2}}=0.12 \text{ ev},$$

we should have for the true cross section at exact resonance $2.7\times10^{-21}\Delta/\Gamma$, which would be even greater.[17] If the activity is actually due to several comparable resonance levels, we will clearly obtain the same result for the cross section of each at exact resonance.

According to Nier[18] the abundances of U^{235} and U^{234} relative to U^{238} are 1/139 and 1/17,000; therefore, if the resonance absorption is due to either of the latter, the cross section at resonance will have to be at least $139\times2.4\times10^{-21}$ cm² or 3.3×10^{-19} cm². However, as Meitner, Hahn and Strassmann pointed out, this is excluded (cf. Eq. (39)) because it would be greater in order of magnitude than the square of the neutron wavelength. In fact, $\pi\lambda^2$ is only 25×10^{-21} cm² for 25-volt neutrons. Therefore we have to attribute the capture to $U^{238}\rightarrow U^{239}$, a process in which the spin changes from $i=0$ to $J=\frac{1}{2}$. We apply the

[16] L. Meitner, O. Hahn and F. Strassmann, Zeits. f. Physik **106**, 249 (1937).

[17] We are using the treatment of Doppler broadening given by H. Bethe and G. Placzek, Phys. Rev. **51**, 450 (1937).

[18] A. O. Nier, Phys. Rev. **55**, 150 (1939).

resonance formula (39) and obtain

$$25\times10^{-21}\times4\Gamma_{n'}\Gamma_r/\Gamma^2 = 2.7\times10^{-21}(\Delta/\Gamma) \text{ or } 2.4\times10^{-21} \quad (45)$$

according as the level width $\Gamma=\Gamma_{n'}+\Gamma_r$ is or is not small compared with the Doppler broadening. In any case, we know[13] from experience with other nuclei for comparable neutron energies that $\Gamma_{n'}\ll\Gamma_r$; this condition makes the solution of (45) unique. We obtain $\Gamma_{n'}=\Gamma_r/40$ if the total width is greater than $\Delta=0.12$ ev; and if the total width is smaller than Δ we find $\Gamma_{n'}=0.003$ ev. Thus in neither case is the neutron width less than 0.003 ev. Comparison with observations on elements of medium atomic weight would lead us to expect a neutron width of $0.001\times(25)^{\frac{1}{2}}=0.005$ ev; and undoubtedly $\Gamma_{n'}$ can be no greater than this for uranium, in view of the small level spacing, or equivalently, in view of the small probability that enough energy be concentrated on a single particle in such a big nucleus to enable it to escape. We therefore conclude that $\Gamma_{n'}$ for 25-volt neutrons is approximately 0.003 ev.

Our result implies that the radiation width for the U^{239} resonance level cannot exceed ~0.12 ev; it may be less, but not much less, first, because values as great as a volt or more have been observed for Γ_r in nuclei of medium atomic weight, and second, because values of a millivolt or more are observed in the transitions between individual levels of the radioactive elements, and for the excitation with which we are concerned the number of available lower levels is great and the corresponding radiation frequencies are higher.[13] A reasonable estimate of Γ_r would be 0.1 ev; of course direct measurement of the activation yield due to neutrons continuously distributed in energy near the resonance level would give a definite value for the radiation width.

The above considerations on the capture of neutrons to form U^{239} are expressed for simplicity as if there were a single resonance level, but the results are altered only slightly if several levels give absorption. However, the contribution of the resonance effect to the radiative capture cross section for *thermal* neutrons does depend essentially on the number of levels as well as their strength. On this basis Anderson and Fermi have been able to show that the radiative capture of slow neutrons cannot be due to the tail at low energies of only a single level.[19] In fact, if it were, we should have for the cross section from (39)

$$\sigma_r(\text{thermal})=\pi\lambda\!\!\!^{-}_{th}{}^2\Gamma_{n'}(\text{thermal})\Gamma_r/E_0^2; \quad (46)$$

since $\Gamma_{n'}$ is proportional to neutron velocity, we should obtain at the effective thermal energy $\pi kT/4=0.028$ ev.

$$\sigma_r(\text{thermal})\sim23\times10^{-18}\times0.003(0.028/25)^{\frac{1}{2}}0.1/(25)^2 \sim0.4\times10^{-24}\text{ cm}^2. \quad (47)$$

Anderson and Fermi however obtain for this cross section by direct measurement 1.2×10^{-24} cm².

The conclusion that the resonance absorption at the effective energy of 25 ev is actually due to more than one level gives the possibility of an order of magnitude estimate of the spacing between energy levels in U^{239} if for simplicity we assume random phase relations between their individual contributions. Taking into consideration the factor between the observations and the result (47) of the one level formula, and recalling that levels below thermal energies as well as above contribute to the absorption, we arrive at a level spacing of the order of $d=20$ ev as a reasonable figure at the excitation in question.

B. Fission produced by thermal neutrons

According to Meitner, Hahn and Strassmann[20] and other observers, irradiation of uranium by thermal neutrons actually gives a large number of radioactive periods which arise from fission fragments. By direct measurement the fission cross section for thermal neutrons is found to be between 2 and 3×10^{-24} cm² (averaged over the actual mixture of isotopes), that is, about twice the cross section for radiative capture. No appreciable part of this effect can come from the isotope U^{239}, however, because the observations on the ~25-volt resonance capture of neutrons by this nucleus gave only the 23-minute activity; the inability of Meitner, Hahn, and Strassmann to find for neutrons of this energy any appreciable yield of the complex of periods

[19] H. L. Anderson and E. Fermi, Phys. Rev. **55**, 1106 (1939).

[20] L. Meitner, O. Hahn and F. Strassmann, Zeits. f. Physik **106**, 249 (1937).

now known to follow fission indicates that for slow neutrons in general the fission probability for this nucleus is certainly no greater than 1/10 of the radiation probability. Consequently, from comparison of (38) and (39), the fission cross section for this isotope cannot exceed something of the order $\sigma_f(\text{thermal})=(1/10)\sigma_\gamma(\text{thermal})=0.1\times10^{-24}$ cm². From reasoning of this nature, as was pointed out in an earlier paper by Bohr, we have to attribute practically all of the fission observed with thermal neutrons to one of the rarer isotopes of uranium.[21] If we assign it to the compound nucleus U^{235}, we shall have 17,000 $\times2.5\times10^{-24}$ or 4×10^{-20} cm² for σ_f(thermal); if we attribute the division to U^{236}, σ_f will be between 3 and 4×10^{-22} cm².

We have to expect that the radiation width and the neutron width for slow neutrons will differ in no essential way between the various uranium isotopes. Therefore we will assume $\Gamma_{n'}(\text{thermal})=0.003(0.028/25)^{\frac{1}{2}}=10^{-4}$ ev. The fission width, however, depends strongly on the barrier height; this is in turn a sensitive function of nuclear charge and mass numbers, as indicated in Fig. 4, and decreases strongly with decreasing isotopic weight. Thus it is reasonable that one of the lighter isotopes should be responsible for the fission.

Let us investigate first the possibility that the division produced by thermal neutrons is due to the compound nucleus U^{235}. If the level spacing d for this nucleus is essentially greater than the level width, the cross section will be due principally to one level ($J=\frac{1}{2}$ arising from $i=0$), and we shall have from

$$\sigma_f=\pi\lambda^2\frac{2J+1}{(2s+1)(2i+1)}\frac{\Gamma_{n'}\Gamma_f}{(E-E_0)^2+(\Gamma/2)^2} \quad (38)$$

the equation

$$\Gamma_f/[E_0^2+\Gamma^2/4]=4\times10^{-20}/23\times10^{-18}\times10^{-4}=17(\text{ev})^{-1}. \quad (48)$$

Since $\Gamma>\Gamma_f$, this condition can be put as an inequality,

$$E_0^2<(\Gamma/4)(4/17)-\Gamma) \quad (49)$$

from which it follows first, that $\Gamma\leq4/17$ ev, and second, that $|E_0|<2/17$ ev. Thus the level would have to be very narrow and very close to thermal energies. But in this case the fission cross section would have to fall off very rapidly with increasing neutron energy; since $\lambda\propto1/v$, $E\propto v^2$, $\Gamma_{n'}\propto v$, we should have according to (38) $\sigma_f\propto1/v^5$ for neutron energies greater than about half a volt. This behavior is quite inconsistent with the finding of the Columbia group that the fission cross section for cadmium resonance neutrons (~0.15 ev) and for the neutrons absorbed in boron (mean energy of several volts) stand to each other inversely in the ratio of the corresponding neutron velocities ($1/v$).[22] Therefore, if the fission is to be attributed to U^{235}, we must assume that the level width is greater than the level spacing (many levels effective); but as the level spacing itself will certainly exceed the radiative width, we will then have a situation in which the total width will be essentially equal to Γ_f. Consequently we can write the cross section (40) for overlapping levels in the form

$$\sigma_f=\pi\lambda^2\Gamma_{n'}2\pi/d. \quad (50)$$

From this we find a level spacing

$$d=23\times10^{-18}\times10^{-4}\times2\pi/4\times10^{-20}=0.4 \text{ ev}$$

which is unreasonably small: According to the estimates of Table III, the nuclear excitations consequent on the capture of slow neutrons to form U^{235} and U^{239} are approximately 5.4 Mev and 5.2 Mev, respectively; moreover, the two nuclei have the same odd-even properties and should therefore possess similar level distributions. From the difference ΔE between the excitation energies in the two cases we can therefore obtain the ratio of the corresponding level spacings from the expression $\exp(\Delta E/T)$. Here T is the nuclear temperature, a low estimate for which is 0.5 Mev, giving a factor of $\exp 0.6=2$. From our conclusion in IV-A that the order of magnitude of the level spacing in U^{239} is 20 ev, we would expect then in U^{235} a spacing of the order of 10 ev. Therefore the result of Eq. (51) makes it seem quite unlikely that the fission observed for the thermal neutrons can be due to the rarest uranium isotope; we consequently attribute it almost entirely to the reaction $U^{235}+n_{th}\rightarrow U^{236}\rightarrow$fission.

[21] N. Bohr, Phys. Rev. **55**, 418 (1939).

[22] Anderson, Booth, Dunning, Fermi, Glasoe and Slack, reference 4.

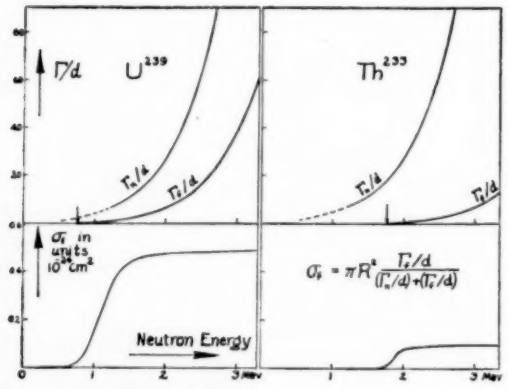

FIG. 6. Γ_n/d and Γ_f/d are the ratios of the neutron emission and fission probabilities (taken per unit of time and multiplied by $\hbar$) to the average level spacing in the compound nucleus at the given excitation. These ratios will vary with energy in nearly the same way for all heavy nuclei, except that the entire fission curve must be shifted to the left or right according as the critical fission energy E_f is less than or greater than the neutron binding E_n. The cross section for fission produced by fast neutrons depends on the ratio of the values in the two curves, and is given on the left for $E_f-E_n=(\frac{3}{4})$ Mev and on the right for $E_f-E_n=1\frac{3}{4}$ Mev, corresponding closely to the cases of U^{239} and Th^{233}, respectively.

We have two possibilities to account for the cross section $\sigma_f(\text{thermal})\sim 3.5\times 10^{-22}$ presented by the isotope U^{235} for formation of the compound nucleus U^{236}, according as the level width is smaller than or comparable with the level spacing. In the first case we shall have to attribute most of the fission to an isolated level, and by the reasoning which was employed previously, we conclude that for this level

$$\Gamma_f/[E_0^2+\Gamma^2/4] = [(2s+1)(2i+1)/(2J+1)]0.15(\text{ev})^{-1}=R. \quad (52)$$

If the spin of U^{235} is $\frac{3}{2}$ or greater, the right-hand side of (52) will be approximately 0.30 $(\text{ev})^{-1}$; but if i is as low as $\frac{1}{2}$, the right side will be either 0.6 or 0.2 $(\text{ev})^{-1}$. The resulting upper limits on the resonance energy and level width may be summarized as follows:

	$i\geq\frac{3}{2}$	$i=\frac{1}{2}$, $J=0$	$i=\frac{1}{2}$, $J=1$
$\Gamma<4/R=$	13	7	20 ev
$\lvert E_0\rvert<1/R=$	3	1.7	5 ev.

(53)

On the other hand, the indications[22] for low neutron energies of a $1/v$ variation of fission cross section with velocity lead us as in the discussion of the rarer uranium isotope to the conclusion that either E_0 or $\Gamma/2$ or both are greater than several electron volts. This allows us to obtain from (52) a lower limit also to Γ_f:

$$\Gamma_f=R[E_0^2+\Gamma^2/4]>10 \text{ to } 400 \text{ ev}. \quad (54)$$

In the present case, the various conditions are not inconsistent with each other, and it is therefore possible to attribute the fission to the effect of a single resonance level.

We can go further, however, by estimating the level spacing for the compound nucleus U^{236}. According to the values of Table III, the excitation following the neutron capture is considerably greater than in the case U^{239}, and we should therefore expect a rather smaller level spacing than the value $\sim$20 ev estimated in the latter case. On the other hand, it is known that for similar energies the level density is lower in even even than odd even nuclei. Thus the level spacing in U^{236} may still be as great as 20 ev, but it is undoubtedly no greater. From (54) we conclude then that we have probably to do with a case of overlapping resonance levels rather than a single absorption line, although the latter possibility is not entirely excluded by the observations available.

In the case of overlapping levels we shall have from Eq. (40)

$$\sigma_f=(\pi\lambda^2/2)\Gamma_{n'}(2\pi/d) \quad (55)$$

or consequently a level spacing

$$d=(23\times 10^{-18}/2)\times 10^{-4} \times 2\pi/3.5\times 10^{-22}=20 \text{ ev}; \quad (56)$$

and as we are attributing to the levels an unresolved structure, the fission width must be at least 10 ev. These values for level spacing and fission width give a reasonable account of the fission produced by slow neutrons.

C. Fission by fast neutrons

The discussion on the basis of theory of the fission produced by fast neutrons is simplified first by the fact that the probability of radiation can be neglected in comparison with the probabilities of fission and neutron escape and second by the circumstance that the neutron wavelength $/2\pi$ is small in comparison with the nuclear radius ($R\sim 9\times 10^{-13}$ cm) and we are in the region of continuous level distribution. Thus the fission cross section will be given by

$$\sigma_f=\pi R^2\Gamma_f/\Gamma\sim 2.4\times 10^{-24}\Gamma_f/(\Gamma_f+\Gamma_n), \quad (57)$$

or, in terms of the ratio of widths to level spacing,

$$\sigma_f \sim 2.4\times10^{-24}(\Gamma_f/d)/[(\Gamma_f/d)+(\Gamma_n/d)]. \quad (58)$$

According to the results of Section III,

$$\Gamma_n/d=(1/2\pi)(A^{\frac{2}{3}}/10\text{ Mev})\sum_i K_i \quad (59)$$

and

$$\Gamma_f/d=(1/2\pi)N^*. \quad (60)$$

In using Eq. (58) it is therefore seen that we do not have to know the level spacing d of the compound nucleus, but only that of the residual nucleus (Eq. (59)) and the number N^* of available levels of the dividing nucleus in the transition state (Eq. 60).

Considered as a function of energy, the ratio of fission width to level spacing will be extremely small for excitations less than the critical fission energy; with increase of the excitation above this value Eq. (60) will quickly become valid, and we shall have to anticipate a rapid rise in the ratio in question. If the spacing of levels in the transition state can be compared with that of the lower states of an ordinary heavy nucleus ($\sim$50 to 100 kev) we shall expect a value of $N^*=10$ to 20 for an energy 1 Mev above the fission barrier; but in any case the value of Γ_f/d will rise almost linearly with the available energy over a range of the order of a million volts, when the rise will become noticeably more rapid owing to the decrease to be expected at such excitations in the level spacing of the nucleus in the transition state. The associated behavior of Γ_f/d is illustrated in curves in Fig. 6. It should be remarked that the specific quantum-mechanical effects which set in at and below the critical fission energy may even show their influence to a certain extent above this energy and produce slight oscillations in the beginning of the Γ_f/d curve, allowing possibly a direct determination of N^*. How the ratio Γ_n/d will vary with energy is more accurately predictable than the ratio just considered. Denoting by K the neutron energy, we have for the number of levels which can be excited in the residual (=original) nucleus a figure of from $K/0.05$ Mev to $K/0.1$ Mev, and for the average kinetic energy of the inelastically scattered neutron $\sim K/2$, so that the sum K_i in (59) is easily evaluated, giving us, if we express K in Mev,

$$\Gamma_n/d \sim 3 \text{ to } 6 \text{ times } K^2. \quad (61)$$

This formula provides as a matter of fact however only a rough first orientation, since for energies below $K=1$ Mev it is not justified to apply the evaporation formula (a transition occurring until for slow neutrons Γ_n/d is proportional to velocity) and for energies above 1 Mev we have to take into account the gradual decrease which occurs in level spacing in the residual nucleus, and which has the effect of increasing the right-hand side of (61). An attempt has been made to estimate this increase in drawing Fig. 6.

The two ratios involved in the fast neutron fission cross section (58) will vary with energy in the same way for all the heaviest nuclei; the only difference from nucleus to nucleus will occur in the critical fission energy, which will have the effect of shifting one curve with respect to another as shown in the two portions of Fig. 6. Thus we can deduce the characteristic differences between nuclei to be expected in the variation with energy of the fast neutron cross section.

Meitner, Hahn, and Strassmann observed that fast neutrons as well as thermal ones produce in uranium the complex of activities which arise as a result of nuclear fission, and Ladenburg, Kanner, Barschall, and van Voorhis have made a direct measurement of the fission cross section for 2.5 Mev neutrons, obtaining 0.5×10^{-24} cm^2 ($\pm$25 percent).[23] Since the contribution to this cross section due to the U^{235} isotope cannot exceed $\pi R^2/139\sim0.02\times10^{-24}$ cm^2, the effect must be attributed to the compound nucleus U^{239}. For this nucleus however as we have seen from the slow neutron observations the fission probability is negligible at low energies. Therefore we have to conclude that the variation with energy of the corresponding cross section resembles in its general features Fig. 6a. In this connection we have the further observation of Ladenburg *et al.* that the cross section changes little between 2 Mev and 3 Mev.[23] This points to a value of the critical fission energy for U^{239} definitely less

[23] R. Ladenburg, M. H. Kanner, H. H. Barschall and C. C. van Voorhis, Phys. Rev. **56**, 168 (1939).

than 2 Mev in excess of the neutron binding. Unpublished results of the Washington group[24] give $\sigma_f = 0.003 \times 10^{-24}$ at 0.6 Mev and 0.012×10^{-24} cm² at 1 Mev. With the Princeton observations[23] we have enough information to say that the critical energy for U^{239} is not far from $\frac{3}{4}$ Mev in excess of the neutron binding (~ 5.2 Mev from Table III):

$$E_f(U^{239}) \sim 6 \text{ Mev}. \quad (62)$$

A second conclusion we can draw from the absolute cross section of Ladenburg *et al.* is that the ratio of (Γ_f/d) to (Γ_n/d) as indicated in the figure is substantially correct; this confirms our presumption that the energy level spacing in the transition state of the dividing nucleus is not different in order of magnitude from that of the low levels in the normal nucleus.

The fission cross section of Th^{232} for neutrons of 2 to 3 Mev energy has also been measured by the Princeton group; they find $\sigma_f = 0.1 \times 10^{-24}$ cm² in this energy range. On the basis of the considerations illustrated in Fig. 6 we are led in this case to a fission barrier $1\frac{3}{4}$ Mev greater than the neutron binding; hence, using Table III,

$$E_f(Th^{239}) \sim 7 \text{ Mev}. \quad (63)$$

A check on the consistency of the values obtained for the fission barriers is furnished by the possibility pointed out in Section II and Fig. 4 of obtaining the critical energy for all nuclei once we know it for one nucleus. Taking $E_f(U^{239}) = 6$ Mev as standard, we obtain $E_f(Th^{232}) = 7$ Mev, in good accord with (63).

As in the preceding paragraph we deduce from Fig. 4 $E_f(U^{236}) = 5\frac{1}{4}$ Mev, $E_f(U^{235}) = 5$ Mev. Both values are *less* than the corresponding neutron binding energies estimated in Table III, $E_n(U^{236}) = 6.4$ Mev, $E_n(U^{235}) = 5.4$ Mev. From the values of $E_n - E_d$ we conclude along the lines of Fig. 6 that for thermal neutrons Γ_f/d is, respectively, ~ 5 and ~ 1 for the two isotopes. Thus it appears that in both cases the level distribution will be continuous. We can estimate the as yet entirely unmeasured fission cross section of the lightest uranium isotope for the thermal neutrons from

$$\sigma_f = \pi \lambda^2 \Gamma_n' 2\pi/d. \quad (64)$$

[24] Reported by M. Tuve at the Princeton meeting of the American Physical Society, June 23, 1939.

d will not be much different from what it is for the similar compound nucleus U^{239}, say of the order of 20 ev. Thus

$$\sigma_f(\text{thermal}, U^{235}) \sim 23 \times 10^{-18} \times 10^{-4} \times 2\pi/20 \sim 500 \text{ to } 1000 \times 10^{-24} \text{ cm}^2, \quad (65)$$

which is of course practically the same figure which holds for the next heaviest compound nucleus.

The various values estimated for fission barriers and fission and neutron widths are summarized in Fig. 7. The level spacing f for past neutrons has been estimated from its value for slow neutrons and the fact that nuclear level densities appear to increase, according to Weisskopf, approximately exponentially as $2(E/a)^{\frac{1}{2}}$, where a is a quantity related to the spacing of the lowest nuclear levels and roughly 0.1 Mev in magnitude.[25] The relative values of Γ_n, Γ_f and d for fast neutrons in Fig. 7, being obtained less indirectly, will be more reliable than their absolute values.

V. Neutrons, Delayed and Otherwise

Roberts, Meyer and Wang[26] have reported the emission of neutrons following a few seconds after the end of neutron bombardment of a

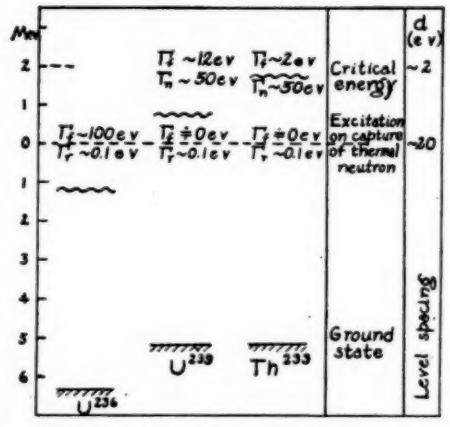

FIG. 7. Summary for comparative purposes of the estimated fission energies, neutron binding energies, level spacings, and neutron and fission widths for the three nuclei to which the observations refer. For fast neutrons the values of Γ_f, Γ_n, and d are less reliable than their ratios. The values in the top line refer to a neutron energy of 2 Mev in each case.

[25] V. Weisskopf, Phys. Rev. **52**, 295 (1937).

[26] R. B. Roberts, R. C. Meyer and P. Wang, Phys. Rev. **55**, 510 (1939).

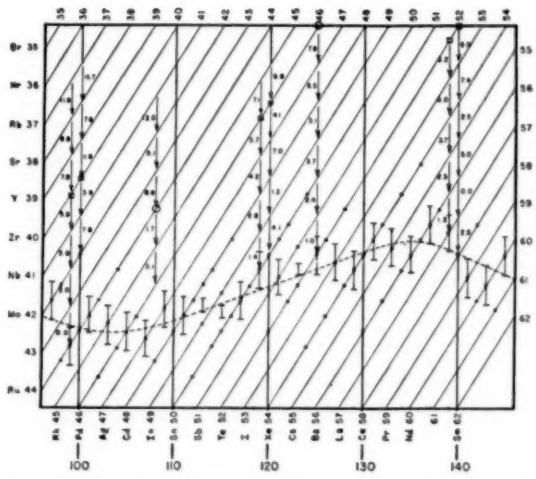

FIG. 8. Beta-decay of fission fragments leading to stable nuclei. Stable nuclei are represented by the small circles; thus the nucleus $_{50}Sn^{120}$ lies just under the arrow marked 4.1; the number indicates the estimated energy release in Mev (see Section I) in the beta-transformation of the preceding nucleus $_{49}In^{120}$. Characteristic differences are noted between nuclei of odd and even mass numbers in the energy of successive transformations, an aid in assigning activities to mass numbers. The dotted line has been drawn, as has been proposed by Gamow, in such a way as to lie within the indicated limits of nuclei of odd mass number; its use is described in Section I.

thorium or uranium target. Other observers have discovered the presence of additional neutrons following within an extremely short interval after the fission process.[27] We shall return later to the question as to the possible connection between the latter neutrons and the mechanism of the fission process. The delayed neutrons themselves are to be attributed however to a high nuclear excitation following beta-ray emission from a fission fragment, for the following reasons:

(1) The delayed neutrons are found only in association with nuclear fission, as is seen from the fact that the yields for both processes depend in the same way on the energy of the bombarding neutrons.

(2) They cannot, however, arise during the fission process itself, since the time required for the division is certainly less than 10^{-12} sec., according to the observations of Feather.[27a]

(3) Moreover, an excitation of a fission fragment in the course of the fission process to an energy sufficient for the subsequent evaporation of a neutron cannot be responsible for the *delayed* neutrons, since even by radiation alone such an excitation will disappear in a time of the order of 10^{-13} to 10^{-15} sec.

(4) The possibility that gamma-rays associated with the beta-ray transformations following fission might produce any appreciable number of photoneutrons in the source has been excluded by an experiment reported by Roberts, Hafstad, Meyer and Wang.[28]

(5) The energy release on beta-transformation is however in a number of cases sufficiently great to excite the product nucleus to a point where it can send out a neutron, as has been already pointed out in connection with the estimates in Table III. Typical values for the release are shown on the arrows in Fig. 8. The product nucleus will moreover have of the order of 10^4 to 10^5 levels to which beta-transformations can lead in this way, so that it will also be overwhelmingly probable that the product nucleus shall be highly excited.

We therefore conclude that the delayed emission of neutrons indeed arises as a result of nuclear excitation following the beta-decay of the nuclear fragments.

The actual probability of the occurrence of a nuclear excitation sufficient to make possible neutron emission will depend upon the comparative values of the matrix elements for the beta-ray transformation from the ground state of the original nucleus to the various excited states of the product nucleus. The simplest assumption we can make is that the matrix elements in question do not show any systematic variation with the energy of the final state. Then, according to the Fermi theory of beta-decay, the probability of a given beta-ray transition will be approximately proportional to the fifth power of the energy release.[29] If there are $\rho(E)dE$ excitation levels of the product nucleus in the range E to $E+dE$, it will follow from our assumptions that the probability of an excitation in the same energy interval will be given by

$$w(E)dE = \text{constant } (E_0-E)^5\rho(E)dE, \quad (66)$$

[27] H. L. Anderson, E. Fermi and H. B. Hanstein, Phys. Rev. **55**, 797 (1939); L. Szilard and W. H. Zinn, Phys. Rev. **55**, 799 (1939); H. von Halban, Jr., F. Joliot and L. Kowarski, Nature **143**, 680 (1939).

[27a] N. Feather, Nature **143**, 597 (1939).

[28] R. B. Roberts, L. R. Hafstad, R. C. Meyer and P. Wang, Phys. Rev. **55**, 664 (1939).

[29] L. W. Nordheim and F. L. Yost, Phys. Rev. **51**, 942 (1937).

where E_0 is the total available energy. According to (66) the probability $w(E)$ of a transition to the excited levels in a unit energy range at E reaches its maximum value for the energy $E=E_{\max}$ given by

$$E_{\max}=E_0-5/(d\ \ln\ \rho/dE)_{E_{\max}}=E_0-5T, \quad (67)$$

where T is the temperature (in energy units) to which the product nucleus must be heated to have on the average the excitation energy $E_{\max}$. Thus the most probable energy release on beta-transformation may be said to be five times the temperature of the product nucleus. According to our general information about the nuclei in question, an excitation of 4 Mev will correspond to a temperature of the order of 0.6 Mev. Therefore, on the basis of our assumptions, to realize an average excitation of 4 Mev by beta-transformation we shall require a total energy release of the order of $4+5\times0.6=7$ Mev.

The spacing of the lowest nuclear levels is of the order of 100 kev for elements of medium atomic weight, decreases to something of the order of 10 ev for excitations of the order of 8 Mev, and can, according to considerations of Weisskopf, be represented in terms of a nuclear level density varying approximately exponentially as the square root of the excitation energy.[23] Using such an expression for $\rho(E)$ in Eq. (66), we obtain the curve shown in Fig. 9 for the distribution function $w(E)$ giving the probability that an excitation E will result from the beta-decay of a typical fission fragment. It is seen that there will be appreciable probability for neutron emission if the neutron binding is somewhat less than the total energy available for the beta-ray transformation. We can of course draw only general conclusions because of the uncertainty in our original assumption that the matrix elements for the various possible transitions show no systematic trend with energy. Still, it is clear that the above considerations provide us with a reasonable qualitative account of the observation of Booth, Dunning and Slack that there is a chance of the order of 1 in 60 that a nuclear fission will result in the delayed emission of a neutron.[30]

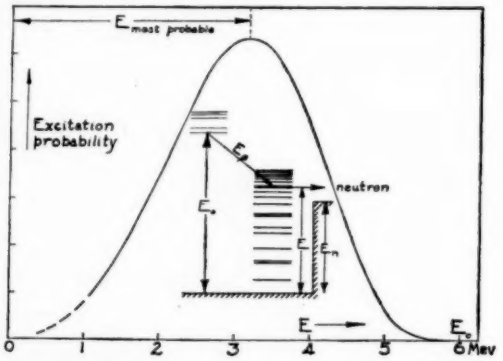

FIG. 9. The distribution in excitation of the product nuclei following beta-decay of fission fragments is estimated on the assumption of comparable matrix elements for the transformations to all excited levels. With sufficient available energy E_0 and a small enough neutron binding E_n it is seen that there will be an appreciable number of delayed neutrons. The quantity plotted is probability per unit range of excitation energy.

Another consequence of the high probability of transitions to excited levels will be to give a beta-ray spectrum which is the superposition of a very large number of elementary spectra. According to Bethe, Hoyle and Peierls, the observations on the beta-ray spectra of light elements point to the Fermi distribution in energy in the elementary spectra.[31] Adopting this result, and using the assumption of equal matrix elements discussed above, we obtain the curve of Fig. 10 for the qualitative type of intensity distribution to be expected for the electrons emitted in the beta-decay of a typical fission fragment. As is seen from the curve, we have to expect that the great majority of electrons will have energies much smaller in value than the actual transformation energy which is available. This is in accord with the failure of various observers to find any appreciable number of very high energy electrons following fission.[32]

The half-life for emission of a beta-ray of 8 Mev energy in an elementary transition will be something of the order of 1 to 1/10 sec., according to the empirical relation between lifetime and energy given by the first Sargent curve. Since we have to deal in the case of the nuclear fragments with transitions to 10^4 or 10^5 excited levels, we should therefore at first sight expect an extremely short lifetime with respect to electron emission. However, the existence of a

[30] E. T. Booth, J. R. Dunning and F. G. Slack, Phys. Rev. **55**, 876 (1939).

[31] H. A. Bethe, F. Hoyle and R. Peierls, Nature **143**, 200 (1939).

[32] H. H. Barschall, W. T. Harris, M. H. Kanner and L. A. Turner, Phys. Rev. **55**, 989 (1939).

sum rule for the matrix elements of the transitions in question has as a consequence that the individual matrix elements will actually be very much smaller than those involved in beta-ray transitions from which the Sargent curve is deduced. Consequently, there seems to be no difficulty in principle in understanding lifetimes of the order of seconds such as have been reported for typical beta-decay processes of the fission fragments.

In addition to the delayed neutrons discussed above there have been observed neutrons following within a very short time (within a time of the order of at most a second) after fission.[27] The corresponding yield has been reported as from two to three neutrons per fission.[33] To account for so many neutrons by the above considered mechanism of nuclear excitation following beta-ray transitions would require us to revise drastically the comparative estimates of beta-transformation energies and neutron binding made in Section I. As the estimates in question were based on indirect though simple arguments, it is in fact possible that they give misleading results. If however they are reasonably correct, we shall have to conclude that the neutrons arise either from the compound nucleus at the moment of fission or by evaporation from the fragments as a result of excitation imparted to them as they separate. In the latter case the time required for neutron emission will be 10^{-13} sec. or less (see Fig. 5). The time required to bring to rest a fragment with 100 Mev kinetic energy, on the other hand, will be at least the time required for a particle with average velocity 10^9 cm/sec. to traverse a distance of the order of 10^{-3} cm. Therefore the neutron will be evaporated before the fragment has lost much of its translational energy. The kinetic energy per particle in the fragment being about 1 Mev, a neutron evaporated in nearly the forward direction will thus have an energy which is certainly greater than 1 Mev, as has been emphasized by Szilard.[34] The observations so far published neither prove nor disprove the possibility of such an evaporation following fission.

[33] Anderson, Fermi and Hanstein, reference 27. Szilard and Zinn, reference 27. H. von Halban, Jr., F. Joliot and L. Kowarski, Nature **143** 680 (1939).

[34] Discussions, Washington meeting of American Physical Society, April 28, 1939.

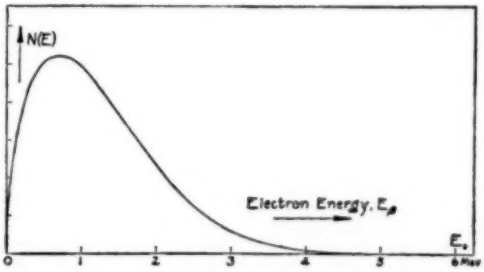

FIG. 10. The superposition of the beta-ray spectra corresponding to all the elementary transformations indicated in Fig. 9 gives a composite spectrum of a general type similar to that shown here, which is based on the assumption of comparable matrix elements and simple Fermi distributions for all transitions. The dependent variable is number of electrons per unit energy range.

We consider briefly the third possibility that the neutrons in question are produced during the fission process itself. In this connection attention may be called to observations on the manner in which a fluid mass of unstable form divides into two smaller masses of greater stability; it is found that tiny droplets are generally formed in the space where the original enveloping surface was torn apart. Although a detailed dynamical account of the division process will be even more complicated for a nucleus than for a fluid mass, the liquid drop model of the nucleus suggests that it is not unreasonable to expect at the moment of fission a production of neutrons from the nucleus analogous to the creation of the droplets from the fluid.

The statistical distribution in size of the fission fragments, like the possible production of neutrons at the moment of division, is essentially a problem of the dynamics of the fission process, rather than of the statistical mechanics of the critical state considered in Section II. Only after the deformation of the nucleus has exceeded the critical value, in fact, will there occur that rapid conversion of potential energy of distortion into energy of internal excitation and kinetic energy of separation which leads to the actual process of division.

For a classical liquid drop the course of the reaction in question will be completely determined by specifying the position and velocity in configuration space of the representative point of the system at the instant when it passes over the potential barrier in the direction of fission. If the energy of the original system is only

infinitesimally greater than the critical energy, the representative point of the system must cross the barrier very near the saddle point and with a very small velocity. Still, the wide range of directions available for the velocity vector in this multidimensional space, as suggested schematically in Fig. 3, indicates that production of a considerable variety of fragment sizes may be expected even at energies very close to the threshold for the division process. When the excitation energy increases above the critical fission energy, however, it follows from the statistical arguments in Section III that the representative point of the system will in general pass over the fission barrier at some distance from the saddle point. With general displacements of the representative point along the ridge of the barrier away from the saddle point there are associated asymmetrical deformations from the critical form, and we therefore have to anticipate a somewhat larger difference in size of the fission fragments as more energy is made available to the nucleus in the transition state. Moreover, as an influence of the finer details of nuclear binding, it will also be expected that the relative probability of observing fission fragments of odd mass number will be less when we have to do with the division of a compound nucleus of even charge and mass than one with even charge and odd mass.[35]

VI. Fission Produced by Deuterons and Protons and by Irradiation

Regardless of what excitation process is used, it is clear that an appreciable yield of nuclear fissions will be obtained provided that the excitation energy is well above the critical energy for fission and that the probability of division of the compound nucleus is comparable with the probability of other processes leading to the break up of the system. Neutron escape being the most important process competing with fission, the latter condition will be satisfied if the fission energy does not much exceed the neutron binding, which is in fact the case, as we have seen, for the heaviest nuclei. Thus we have to expect for these nuclei that not only neutrons but also sufficiently energetic deuterons, protons, and gamma-rays will give rise to observable fission.

A. Fission produced by deuteron and proton bombardment

Oppenheimer and Phillips have pointed out that nuclei of high charge react with deuterons of not too great energy by a mechanism of polarization and dissociation of the neutron-proton binding in the field of the nucleus, the neutron being absorbed and the proton repulsed.[36] The excitation energy E of the newly formed nucleus is given by the kinetic energy E_d of the deuteron diminished by its dissociation energy I and the kinetic energy K of the lost proton, all increased by the binding energy E_n of the neutron in the product nucleus:

$$E=E_d-I-K+E_n. \tag{68}$$

The kinetic energy of the proton cannot exceed E_d+E_n-I, nor on the other hand will it fall below the potential energy which the proton will have in the Coulomb field at the greatest possible distance from the nucleus consistent with the deuteron reaction taking place with appreciable probability. This distance and the corresponding kinetic energy $K_{\min}$ have been calculated by Bethe.[37] For very low values of the bombarding energy E_D, he finds $K_{\min}\sim 1$ Mev; when E_d rises to equality with the dissociation energy $I=2.2$ Mev he obtains $K_{\min}\sim E_d$; and even when the bombarding potential reaches a value corresponding to the height of the electrostatic barrier, $K_{\min}$ still continues to be of order E_d, although beyond this point increase of E_d produces no further rise in $K_{\min}$. Since the barrier height for single charged particles will be of the order of 10 Mev for the heaviest nuclei, we can therefore assume $K_{\min}\sim E_d$ for the ordinarily employed values of the deuteron bombarding energy. We conclude that the excitation energy of the product nucleus will have only a very small probability of exceeding the value

$$E_{\max}\sim E_n-I. \tag{69}$$

Since this figure is considerably less than the

[35] S. Flugge and G. v. Droste also have raised the question of the possible influence of finer details of nuclear binding on the statistical distribution in size of the fission fragments, Zeits. f. physik. Chemie **B42** 274 (1939).

[36] R. Oppenheimer and M. Phillips, Phys. Rev. **48**, 500 (1935).

[37] H. A. Bethe, Phys. Rev. **53**, 39 (1938).

estimated values of the fission barriers in thorium and uranium, we have to expect that Oppenheimer-Phillips processes of the type discussed will be followed in general by radiation rather than fission, unless the kinetic energy of the deuteron is greater than 10 Mev.

We must still consider, particularly when the energy of the deuteron approaches 10 Mev, the possibility of processes in which the deuteron as a whole is captured, leading to the formation of a compound nucleus with excitation of the order of

$$E_d+2E_n-I\sim E_d+10 \text{ Mev}. \quad (70)$$

There will then ensue a competition between the possibilities of fission and neutron emission, the outcome of which will be determined by the comparative values of Γ_f and Γ_n (proton emission being negligible because of the height of the electrostatic barrier). The increase of charge associated with the deuteron capture will of course lower the critical energy of fission and increase the probability of fission relative to neutron evaporation compared to what its value would be for the original nucleus at the same excitation. If after the deuteron capture the evaporation of a neutron actually takes place, the fission barrier will again be decreased relative to the binding energy of a neutron. Since the kinetic energy of the evaporated neutron will be only of the order of thermal energies (≈ 1 Mev), the product nucleus has still an excitation of the order of E_d+3 Mev. Thus, if we are dealing with the capture of 6-Mev deuterons by uranium, we have a good possibility of obtaining fission at either one of two distinct stages of the ensuing nuclear reaction.

The cross section for fission in the double reaction just considered can be estimated by multiplying the corresponding fission cross section (42) for neutrons by a factor allowing for the effect of the electrostatic repulsion of the nucleus in hindering the capture of a deuteron:

$$\sigma_f\sim\pi R^2 e^{-P}\{\Gamma_f(E')/\Gamma(E') +[\Gamma_n(E')/\Gamma(E')][\Gamma_f(E'')/\Gamma(E'')]\}. \quad (71)$$

Here P is the new Gamow penetration exponent for a deuteron of energy E and velocity v:[38]

$$P=(4Ze^2/\hbar v)\{\arccos x^{\frac{1}{2}}-x^{\frac{1}{2}}(1-x)^{\frac{1}{2}}\}, \quad (72)$$

with $x=(ER/Ze^2)$. πR^2 is the projected area of the nucleus. E' is the excitation of the compound nucleus, and E'' the average excitation of the residual nucleus formed by neutron emission. For deuteron bombardment of U^{238} at 6 Mev we estimate a fission cross section of the order of

$$\pi(9\times10^{-13})^2\exp(-12.9)\sim10^{-29}\text{ cm}^2 \quad (73)$$

if we make the reasonable assumption that the probability of fission following capture is of the order of magnitude unity. Observations are not yet available for comparison with our estimate.

Protons will be more efficient than deuterons for the same bombarding energy, since from (72) P will be smaller by the factor $2^{\frac{1}{2}}$ for the lighter particles. Thus for 6-Mev protons we estimate a cross section for production of fission in uranium of the order

$$\pi(9\times10^{-13})^2\exp(-12.9/2^{\frac{1}{2}})(\Gamma_f/\Gamma)\sim10^{-28}\text{ cm}^2,$$

which should be observable.

B. Photo-fission

According to the dispersion theory of nuclear reactions, the cross section presented by a nucleus for fission by a gamma-ray of wavelength $2\pi\lambda$ and energy $E=\hbar\omega$ will be given by

$$\sigma_f=\pi\lambda^2(2J+1)/2(2i+1)\frac{\Gamma_{r'}\Gamma_f}{(E-E_0)^2+(\Gamma/2)^2} \quad (74)$$

if we have to do with an isolated absorption line of natural frequency E_0/h. Here $\Gamma_{r'}/\hbar$ is the probability per unit time that the nucleus in the excited state will lose its entire excitation by emission of a single gamma-ray.

The situation of most interest, however, is that in which the excitation provided by the incident radiation is sufficient to carry the nucleus into the region of overlapping levels. On summing (74) over many levels, with average level spacing d, we obtain

$$\sigma_f=\pi\lambda^2[(2J_{hv}+1)/2(2i+1)](2\pi/d)\Gamma_{r'}\Gamma_f/\Gamma. \quad (75)$$

Without entering into a detailed discussion of the orders of magnitude of the various quantities involved in (75), we can form an estimate of the cross section for photo-fission by comparison with the yields of photoneutrons reported by various observers. The ratio of the cross sections

[38] H. A. Bethe, Rev. Mod. Phys. **9**, 163 (1937).

in question will be just Γ_f/Γ_n, so that

$$\sigma_f=(\Gamma_f/\Gamma_n)\sigma_n. \quad (76)$$

The observed values of σ_n for 12 to 17 Mev gamma-rays are $\sim 10^{-26}$ cm^2 for heavy elements.[39] In view of the comparative values of Γ_f and Γ_n arrived at in Section IV, it will therefore be reasonable to expect values of the order of 10^{-27} cm^2 for photo-fission of U^{238}, and 10^{-28} cm^2 for division of Th^{233}. Actually no radiative fission was found by Roberts, Meyer and Hafstad using the gamma-rays from 3 microamperes of 1-Mev protons bombarding either lithium or fluorine.[40] The former target gives the greater yield, about 7 quanta per 10^{10} protons, or 8×10^5 quanta/min. altogether. Under the most favorable circumstances, all these gamma-rays would have passed through that thickness, ~ 6 mg/cm^2, of a sheet of uranium from which the fission particles are able to emerge. Even then, adopting the cross section we have estimated, we should expect an effect of

$$8\times10^5\times10^{-27}\times6\times10^{-3}\times6.06\times10^{23}/238\sim 1 \text{ count/80 min}; \quad (77)$$

which is too small to have been observed. Consequently, we have as yet no test of the estimated theoretical cross section.

[39] W. Bothe and W. Gentner, Zeits. f. Physik **112**, 45 (1939).
[40] R. B. Roberts, R. C. Meyer and L. R. Hafstad, Phys. Rev. **55**, 417 (1939).

Conclusion

The detailed account which we can give on the basis of the liquid drop model of the nucleus, not only for the possibility of fission, but also for the dependence of fission cross section on energy and the variation of the critical energy from nucleus to nucleus, appears to be verified in its major features by the comparison carried out above between the predictions and observations. In the present stage of nuclear theory we are not able to predict accurately such detailed quantities as the nuclear level density and the ratio in the nucleus between surface energy and electrostatic energy; but if one is content to make approximate estimates for them on the basis of the observations, as we have done above, then the other details fit together in a reasonable way to give a satisfactory picture of the mechanism of nuclear fission.

SEPTEMBER 1, 1939 PHYSICAL REVIEW VOLUME 56

On the Behavior of Matter at Extremely High Temperatures and Pressures

FÉLIX CERNUSCHI*
Princeton University Observatory, Princeton, New Jersey
(Received July 3, 1939)

After some critical remarks on the current notions of stellar neutron cores the suggestion is set forth that an assembly of neutrons can form, under specified circumstances, two different phases by reason of the attracting forces between neutrons. The hypothetical transition from the dilute to the condensed neutron phase affords a concrete physical basis for the idea advocated by Zwicky that the supernovae originate from the sudden transition of an ordinary star into a centrally condensed one.

HUND[1] has analyzed in some detail the general behavior of matter at very high temperatures and pressures. This is a new field of theoretical speculation, and at present it appears impossible to arrive at definite conclusions on this subject, especially because of the extremely poor knowledge that we have today regarding the real nature of internuclear forces and the mechanism of the nuclear chain reactions.

We begin by making a few critical remarks on Hund's theory which is based on the assumption that the nuclear reactions satisfy the following

* On a fellowship from the Argentine Association for the Progress of Science.
[1] F. Hund, Ergebn. d. exakt. Naturwiss. **15**, 189 (1936).

equations:

$$\text{nucleus} \rightleftarrows z \text{ neutrons} + z \text{ protons}, \quad (1)$$

$$\text{proton} + \text{electron} \rightleftarrows \text{neutron}, \quad (2)$$

$$\text{nucleus} \rightleftarrows 2z \text{ protons} + z \text{ electrons}, \quad (3)$$

$$\text{nucleus} + z \text{ electrons} \rightleftarrows 2z \text{ neutrons}, \quad (4)$$

where z is the number of protons which also is equal to the number of neutrons.

In view of our present knowledge of nuclear physics, there is no reason to suppose that it is impossible to make an alternative assumption. For instance, Eq. (2) might be replaced by[2]

$$\text{neutron} + \text{positron} \rightleftarrows \text{proton}. \quad (2')$$

If we accept the existence of the neutrino to explain the β-disintegration, we must consider a nucleus in thermodynamical equilibrium with neutrons, electrons and neutrinos. In this case the Eqs. (2), (3) and (4) would be replaced by

$$\text{proton} + \text{electron} + \text{neutrino} \rightleftarrows \text{neutron}, \quad (2'')$$

$$\text{nucleus} \rightleftarrows 2z \text{ protons} + z \text{ electrons} + z \text{ neutrinos}, \quad (3'')$$

$$\text{nucleus} + z \text{ electrons} + z \text{ neutrinos} \rightleftarrows 2z \text{ neutrons}, \quad (4'')$$

and the set corresponding to (2') would be:

$$\text{neutron} + \text{pair (electron} + \text{positron)} \rightleftarrows \text{proton} + \text{electron} + \text{neutrino}, \quad (2''')$$

$$\text{nucleus} \rightleftarrows 2z \text{ protons} - z \text{ positrons} + z \text{ neutrinos}, \quad (3''')$$

$$\text{nucleus} - z \text{ pairs} + z \text{ electrons} + z \text{ neutrinos} \rightleftarrows 2z \text{ neutrons}. \quad (4''')$$

These simple considerations show that for the moment it is very difficult to draw definite conclusions as regards the behavior of matter in equilibrium at very high temperatures and pressures.

Kothari[3] was the first to introduce the neutron into the theory of the interior of white dwarf stars. He has studied the equilibrium of a gas consisting of protons, neutrons and electrons by using Eq. (2) and the experimental fact that the mass of the neutron is, in atomic units, 0.0009 $\pm$0.0001 greater than the mass of the hydrogen atom. It follows from his theory that wherever an electron of an energy of the order of, or greater than, 1 million electron volt collides with a proton, this will be transformed into a neutron. He applies Fermi-Dirac statistics and investigates the conditions under which the formation of neutrons from protons will be important. This is not the only possible mechanism, e.g., one might suppose that according to Eq. (2') on collision of a neutron with a photon of energy greater than 1 million electron volt (energy of pair formation) a pair of positive and negative electrons is formed, the former being absorbed thereafter by the neutron, producing a proton. In this case one ought to consider the equilibrium between radiation, pair production, neutrons and protons. On the other hand, Kothari does not give any regard to the hypothetical existence of the neutrino. In order to do so, one would have to substitute the reactions (2'') or (2''') for (2).

If the neutrino is produced in course of the β-disintegration according to Fermi's theory, the neutrino must be included into the thermodynamical treatment of the nuclear chain reactions. The existence of the neutrino does not constitute a physical fact for the moment; rather it is a hypothesis which serves to explain certain features of nuclear physics, but there may be advanced some day another hypothesis equally suited to the same end. However, if the neutrino does exist, it will be of great importance in the internal constitution of the stars, due to the fact that this particle should have an extremely high penetrability and, therefore, under certain conditions the transport of heat resulting from the neutrinos might not be negligible beside the flow of radiation. As the latter is held to be the only important mechanism of heat transport in normal stars (the white dwarfs excluded), the possible existence of the neutrino could make the current models of these stars, under certain circumstances, be far from a true representation of the actual stars.

Finally, another difficulty may be mentioned here. In quantum mechanics there exists—we believe—an implicit hypothesis which is important and not easy to understand, namely, the elementary particles have invariant properties. Every one of them has a finite rest energy, and

[2] F. Cernuschi, J. de phys. et rad. **8**, 273 (1937).
[3] D. S. Kothari, Proc. Roy. Soc. **A162**, 521 (1937).

it is a bold hypothesis to assume that this rest energy is invariant under all conditions. In a lecture delivered recently at Princeton, Professor Ellis has pointed out that the electron has a structure which allows internal changes. This assumption appears necessary to explain certain experimental facts in connection with the scattering of electrons by nuclei. The writer has considered the possibility of excited states of the electron.[4] If one admits that not only the electrons, but also the neutrons and protons possess excited states, the problem of the equilibrium of matter at very high temperatures and pressures becomes far more complicated, and the predictions of the current theory may become unacceptable.

In the preceding paragraphs we have reviewed some possible new cases which might occur in the equilibrium between matter of all kinds and radiation under the extreme conditions of the stellar interior. We shall now analyze some properties of a stellar neutron core, such as has been assumed to exist by several writers e.g. Zwicky, Landau, Oppenheimer and others.

If we apply the usual formulae of a perfect gas to the neutron gas, we shall have:

$$p=nkT \quad \text{and} \quad \rho=nm, \tag{5}$$

where p is the pressure, ρ the density, n the number of neutrons per cc and m the mass of the neutron. As it is well known, the partition function of a perfect gas of n particles per cc is given by

$$\psi=\left[\frac{(2\pi mkT)^{\frac{3}{2}}}{h^3}V\right]^{nV}=\left[\left(\frac{2\pi m}{h^2}\right)^{\frac{3}{2}}\frac{(kT)^{5/2}}{p}\right]^{nV}, \tag{6}$$

where V is the actual volume and $nV=N=\text{const.}$ The free energy F and the partition function are related by

$$F=-kT\log\psi$$
$$=-3NkT\log\frac{(2\pi mkT)^{\frac{1}{2}}}{h}-NkT\log V, \tag{7}$$

and the pressure is given by

$$p=-(\partial F/\partial V)_T=NkT/V=nkT. \tag{8}$$

Let us suppose for the moment that the perfect gas law is still valid for extremely high temperatures and pressures and calculate the pressure corresponding to a temperature of 20 million degrees, when the number of neutrons is of the order of 10^{39} per cc, i.e., when the mean distance between a pair of nearest neutrons is of the order of 10^{-13} cm. Substituting numerical values for the general constants in (5), we obtain a pressure of the order of 10^{24} atmospheres.

Hund[1] applied to the neutron gas the expression for p pertaining to Fermi-Dirac statistics, namely

$$p=\frac{3^{\frac{2}{3}}\pi^{-\frac{1}{3}}h^2n^{5/3}}{20m}. \tag{9}$$

If we equate (5) and (9), we should find the limiting value of n up to which the perfect gas law is valid. The result is

$$\frac{3^{\frac{2}{3}}\pi^{-\frac{1}{3}}h^2n^{\frac{2}{3}}}{20m}=kT. \tag{10}$$

This expression, for $T\approx 2\times 10^7$, gives $n\approx 10^{31}$, which means that the perfect gas law should only be applicable provided that the average distance between nearest neighbors is of the order of, or greater than, 10^{-10} cm. According to Fermi-Dirac statistics the value of the pressure for $n=10^{39}$ (density $\approx 10^{14}$ g/cm^3) is of the order of 10^{28} atmospheres, instead of 10^{24} which we have calculated on the perfect gas law. The greater value following from Fermi-Dirac statistics is due to the fact that this statistics implicitly assumes a repulsive interaction among the particles. Such is obviously the case in dealing with electrons, but between neutrons at distances of the order of 10^{-13} cm (order of nuclear diameters) one would expect strong attractive forces of the order of magnitude of the forces acting between a pair of particles inside the nucleus. Hence, for neutrons with $n=10^{39}$ the actual pressure should be even smaller than that derived from Eq. (5). Consequently, we believe that in dealing with a gas of neutrons the perfect gas law is a better approximation than the Fermi-Dirac statistics.

Landau[5] has studied the equilibrium of a neutron core in the interior of a star under the

[4] F. Cernuschi, Comptes rendus **203**, 777 (1936).

[5] L. Landau, Nature **141**, 333 (1938).

assumption that the density is uniform and of the order of magnitude 10^{14} g/cm^3. The energy necessary to transform matter into neutrons is supposed to be of the order of 7×10^{18} ergs/g. At equilibrium, the decrease of gravitational energy per gram when matter is transferred to the neutron core must be equal to the energy needed to transform one gram of matter into neutrons. If the first quantity is greater than the second, the energy equivalent of the difference should be released as radiation. In this way Landau tries to explain the energy liberation in stars. Yet Landau's theory neglects the interaction which must exist between nearest neighbors in the neutron core, and the value of the transformation energy from matter into neutrons is taken from mass defect of the oxygen atom. This would imply that the energy required to form a single neutron is of the order of 7.5 million electron volts. However, there may exist in direct contact with the neutron core an atmosphere of protons, and in this case one ought to consider the transformation from protons to neutrons which requires an energy of the order of 1 million electron volt per particle. For a neutron core at equilibrium with an atmosphere of protons, we calculate, using Landau's assumptions, that the mass of the core is of the order of 0.008 solar mass instead of 0.05 (Landau). If we would take into account the existence of attractive forces between nearest neighbors in the neutron core, the value of its mass would be decreased even further. On this assumption the star would be a compact sphere of neutrons at the end of its evolution, and in the case of the sun, taking the density of the neutron core to be 10^{14} g/cm^3, we find the final diameter would be of the order of 10 km. But another important phenomenon may arise as the density increases beyond a certain limit, namely the neutron core may become unstable.

From nuclear physics we know that when a nucleus has an excess of neutrons these are transformed into protons by emission of β-radiation till the excess has been removed. This fact can be explained by the assumption that the binding energy between a proton and a neutron is greater than that between two neutrons, i.e., that the free energy of a proton-neutron pair is smaller than that of a pair of neutrons. The discovery of the "fission" of uranium atoms on being bombarded by neutrons is highly significant. From this observation and the existence of only a limited number of isotopes of every element it appears reasonable to assume that when a stellar neutron core reaches a density equal to the critical density of matter aggregated in nuclei it cannot go on existing, as was supposed by Landau, but that approximately one-half of the total number of neutrons would be transformed into protons in order to reach the minimum of free energy. This process would release a huge amount of energy and may lead to catastrophic consequences. Let us make some rough calculations and determine the limiting values of temperature and pressure for a neutron core of the mass of the sun having a uniform density of 10^{14} g/cm^3, this density tentatively being chosen as the critical one. If the neutron gas obeys the laws of perfect gases, the pressure at the center of the neutron sphere will be

$$p_0=\frac{3GM^2r^{-4}}{8\pi}, \tag{11}$$

and the central temperature

$$T_0=\frac{4\pi p_0\mu r^3}{3RM}=\frac{1}{2}\frac{GM\mu}{Rr}, \tag{12}$$

where we have $G=6.67\times10^{-8}$ dyne cm^2/g^2, $R=8.315\times10^7$ ergs/degree and in this case $M=1.98\times10^{33}$ g, $r=10^6$ cm, μ (the molecular weight per free neutron)$=1$ g. After substituting these data in (11) and (12) we obtain

$p_0=10^{28}$ atmospheres and $T_0=1.6\times10^{12}$ degrees.

On our assumption the neutron core would not be stable at temperatures lower than T_0; as we shall presently see, this limiting value is extremely reduced if the interaction between neutrons is taken into account.

The simplest and also the crudest model in dealing with an assembly of particles when there exist attractive forces between the nearest neighbors, consists in taking an average interaction potential per particle proportional to the density of particles and in replacing the total volume by the actual free volume, which is approximately equal to the total volume minus

four times the volume occupied by the particles. A more satisfactory model and a more exact statistical treatment does not modify the qualitative results that one obtains by van der Waals' model and only changes the numerical results by a factor which is of the order of a small integer and, therefore, is of no consequence in our present considerations. In this case the partition function (6) becomes

$$\psi=\left\{\frac{(2\pi mkT)^{\frac{3}{2}}}{h^3}(V-4vN)\exp\left[\frac{N}{V}\frac{\epsilon_1}{kT}\right]\right\}^N, \quad (13)$$

where V is the total volume, v the volume of a neutron, $N=nV$ the total number of neutrons, and ϵ_1 the interaction potential in ergs$\times$cm^3. The free energy is given by

$$F=-kT\log\psi=-kTN\left[\log\frac{(2\pi mkT^{\frac{3}{2}})}{h^3}+\log(V-4vN)+\frac{N}{V}\frac{\epsilon_1}{kT}\right]. \quad (14)$$

From (14) we find for the pressure the following expression:

$$p=-\left(\frac{\partial F}{\partial V}\right)_T=\frac{kTN}{V-4vN}-\frac{N^2}{V^2}\epsilon_1=\frac{nkT}{1-4vn}-n^2\epsilon_1, \quad (14')$$

which can be written in the form given by van der Waals:

$$(p+n^2\epsilon_1)(1-4vn)=nkT. \quad (15)$$

As it is well known, Eq. (15) represents a condensation process for values of T smaller than a certain critical temperature T_c. At temperatures higher than T_c the assembly of neutrons will remain a homogeneous system. At lower temperatures each of the curves of the family (15) has a maximum and a minimum, these curves being bounded by the critical curve having a point of inflection. The value of the critical temperature is defined by

$$\frac{\partial p}{\partial(1/n)}=0=-\frac{kT_c}{[(1/n_c)-4v]^2}+2n_c^3\epsilon_1, \quad (16)$$

and

$$\frac{\partial^2 p}{\partial(1/n)^2}=0=\frac{2kT_c}{[(1/n_c)-4v]^3}-6n_c^4\epsilon_1. \quad (17)$$

On dividing (16) by (17) we obtain

$$1/n_c=12v, \quad (18)$$

where n_c is the critical concentration of the neutron gas. If we take the volume of a neutron to be 10^{-38} cm^3, n_c would be

$$n_c\approx 10^{37}. \quad (19)$$

From the substitution of (18) in (16) there follows

$$T_c=2\epsilon_1/27vk, \quad (20)$$

and from (15) and (20) we obtain

$$p_c=\frac{1}{432}\frac{\epsilon_1}{v^2}. \quad (21)$$

Let us make a rough estimate of the constant ϵ_1 and assume that it is of the order of 1 million electron volt. Thus we may write

$$\epsilon_1=\frac{1\text{ Mev}\times\text{cm}^3}{10^{39}}=1.6\times10^{-45}\text{ erg cm}^3, \quad (22)$$

and finally get numerical values of (20) and (21):

$$T_c\approx 10^8\ ^\circ\text{K}, \quad (23)$$

$$p_c\approx 10^{22}\text{ atmospheres}. \quad (24)$$

This means that only for temperatures of the order of, or higher than, 10^8 °K we may regard a neutron core as homogeneous at all pressures. The internal temperature of normal stars is believed to be much lower than T_c. Therefore, in a star having a neutron core, we may expect the existence of two phases of neutrons: a gaseous one and a condensed one. When the pressure increases beyond a certain limit, which must be smaller than p_c, a sudden condensation of neutrons would start with the corresponding liberation of energy. Let us regard a stellar neutron core which consists entirely of the dilute, or gaseous phase of neutrons, and let the central temperature be lower than T_c. If now in the course of stellar evolution the saturation pressure of the neutron gas pertaining to the central temperature is reached by contraction of the whole configuration, the formation of a con-

densed neutron phase would start at the center. By reason of the greater density of the condensed phase, the star will begin to collapse. The details of this process are difficult to analyze without knowing the change of density and the heat of condensation (latent heat of evaporation). If the latter one can be neglected beside the regular energy liberation in the stellar interior, collapsing can go on until a very thin neutron atmosphere is left around the condensed neutron core. This hypothesis affords a concrete physical basis for Zwicky's[6] suggestion that the supernovae originate from the sudden transition of an ordinary star to a centrally condensed one. It is obvious that a detailed analysis of this problem must await a great deal more experimental data concerning the physical properties of the neutron.

I should like to express my thanks to Dr. Rupert Wildt for helpful discussions on the subject.

[6] F. Zwicky, Astrophys. J. **88**, 522 (1938).

SEPTEMBER 1, 1939 PHYSICAL REVIEW VOLUME 56

On Continued Gravitational Contraction

J. R. OPPENHEIMER AND H. SNYDER
University of California, Berkeley, California

(Received July 10, 1939)

When all thermonuclear sources of energy are exhausted a sufficiently heavy star will collapse. Unless fission due to rotation, the radiation of mass, or the blowing off of mass by radiation, reduce the star's mass to the order of that of the sun, this contraction will continue indefinitely. In the present paper we study the solutions of the gravitational field equations which describe this process. In I, general and qualitative arguments are given on the behavior of the metrical tensor as the contraction progresses: the radius of the star approaches asymptotically its gravitational radius; light from the surface of the star is progressively reddened, and can escape over a progressively narrower range of angles. In II, an analytic solution of the field equations confirming these general arguments is obtained for the case that the pressure within the star can be neglected. The total time of collapse for an observer comoving with the stellar matter is finite, and for this idealized case and typical stellar masses, of the order of a day; an external observer sees the star asymptotically shrinking to its gravitational radius.

I

RECENTLY it has been shown[1] that the general relativistic field equations do not possess any static solutions for a spherical distribution of cold neutrons if the total mass of the neutrons is greater than $\sim 0.7\odot$. It seems of interest to investigate the behavior of nonstatic solutions of the field equations.

In this work we will be concerned with stars which have large masses, $>0.7\odot$, and which have used up their nuclear sources of energy. A star under these circumstances would collapse under the influence of its gravitational field and release energy. This energy could be divided into four parts: (1) kinetic energy of motion of the particles in the star, (2) radiation, (3) potential and kinetic energy of the outer layers of the star which could be blown away by the radiation, (4) rotational energy which could divide the star into two or more parts. If the mass of the original star were sufficiently small, or if enough of the star could be blown from the surface by radiation, or lost directly in radiation, or if the angular momentum of the star were great enough to split it into small fragments, then the remaining matter could form a stable static distribution, a white dwarf star. We consider the case where this cannot happen.

If then, for the late stages of contraction, we can neglect the gravitational effect of any escaping radiation or matter, and may still neglect the deviations from spherical symmetry

[1] J. R. Oppenheimer and G. M. Volkoff, Phys. Rev. **55**, 374 (1939).

produced by rotation, the line element outside the boundary r_b of the stellar matter must take the form

$$ds^2 = e^{\nu}dt^2 - e^{\lambda}dr^2 - r^2(d\theta^2 + \sin^2\theta d\varphi^2) \quad (1)$$

with $$e^{\nu} = (1 - r_0/r)$$

and $$e^{\lambda} = (1 - r_0/r)^{-1}.$$

Here r_0 is the gravitational radius, connected with the gravitational mass m of the star by $r_0 = 2mg/c^2$, and constant. We should now expect that since the pressure of the stellar matter is insufficient to support it against its own gravitational attraction, the star will contract, and its boundary r_b will necessarily approach the gravitational radius r_0. Near the surface of the star, where the pressure must in any case be low, we should expect to have a local observer see matter falling inward with a velocity very close to that of light; to a distant observer this motion will be slowed up by a factor $(1 - r_0/r_b)$. All energy emitted outward from the surface of the star will be reduced very much in escaping, by the Doppler effect from the receding source, by the large gravitational red-shift, $(1 - r_0/r_b)^{\frac{1}{2}}$, and by the gravitational deflection of light which will prevent the escape of radiation except through a cone about the outward normal of progressively shrinking aperture as the star contracts. The star thus tends to close itself off from any communication with a distant observer; only its gravitational field persists. We shall see later that although it takes, from the point of view of a distant observer, an infinite time for this asymptotic isolation to be established, for an observer comoving with the stellar matter this time is finite and may be quite short.

Inside the star we shall still suppose that the matter is spherically distributed. We may then take the line element in the form (1). For this line element the field equations are

$$-8\pi T_1^{\,1} = e^{-\lambda}(\nu'/r + 1/r^2) - 1/r^2, \quad (2)$$

$$8\pi T_4^{\,4} = e^{-\lambda}(\lambda'/r - 1/r^2) + 1/r^2, \quad (3)$$

$$-8\pi T_2^{\,2} = -8\pi T_3^{\,3} = e^{-\lambda}\left(\frac{\nu''}{2} + \frac{\nu'^2}{4} - \frac{\nu'\lambda'}{4} + \frac{\nu' - \lambda'}{2r}\right) - e^{-\nu}(\ddot{\lambda}/2 + \dot{\lambda}^2/4 - \dot{\lambda}\dot{\nu}/4), \quad (4)$$

$$8\pi T_4^{\,1} = -8\pi e^{\nu-\lambda} T_1^{\,4} = -e^{-\lambda}\dot{\lambda}/r; \quad (5)$$

in which primes represent differentiation with respect to r and dots differentiation with respect to t.

The energy-momentum tensor T_{ν}^{μ} is composed of two parts: (1) a material part due to electrons, protons, neutrons and other nuclei, (2) radiation. The material part may be thought of as that of a fluid which is moving in a radial direction, and which in comoving coordinates would have a definite relation between the pressure, density, and temperature. The radiation may be considered to be in equilibrium with the matter at this temperature, except for a flow of radiation due to a temperature gradient.

We have been unable to integrate these equations except when we place the pressure equal to zero. However, one can obtain some information about the solutions from inequalities implied by the differential equations and from conditions for regularity of the solutions. From Eqs. (2) and (3) one can see that unless λ vanishes at least as rapidly as r^2 when $r \to 0$, $T_4^{\,4}$ will become singular and that either or both $T_1^{\,1}$ and ν' will become singular. Physically such a singularity would mean that the expression used for the energy-momentum tensor does not take account of some essential physical fact which would really smooth the singularity out. Further, a star in its early stage of development would not possess a singular density or pressure; it is impossible for a singularity to develop in a finite time.

If, therefore, $\lambda(r=0) = 0$, we can express λ in terms of $T_4^{\,4}$, for, integrating Eq. (3)

$$\lambda = -\ln\left\{1 - \frac{8\pi}{r}\int_0^r T_4^{\,4} r^2 dr\right\}. \quad (6)$$

Therefore $\lambda \geqslant 0$ for all r since $T_4^{\,4} \geqslant 0$.

Now that we know $\lambda \geqslant 0$, it is easy to obtain some information about ν' from Eq. (2);

$$\nu' \geqslant 0, \quad (7)$$

since λ and $-T_1^{\,1}$ are equal to or greater than zero.

If we use clock time at $r = \infty$, we may take $\nu(r = \infty) = 0$. From this boundary condition and Eq. (7) we deduce

$$\nu \leqslant 0. \quad (8)$$

The condition that space be flat for large r is

$\lambda(r=\infty)=0$. Adding Eqs. (2) and (3) we obtain:

$$8\pi(T_4^4-T_1^1)=e^{\lambda}(\lambda'+\nu')/r. \tag{9}$$

Since T_4^4 is greater than zero and T_1^1 is less than zero we conclude

$$\lambda'+\nu'\geqslant 0. \tag{10}$$

Because of the boundary conditions on λ and ν we have

$$\lambda+\nu\leqslant 0. \tag{11}$$

For those parts of the star which are collapsing, i.e., all parts of the star except those being blown away by the radiation, Eq. (5) tells us that $\dot{\lambda}$ is greater than zero. Since λ increases with time, it may (a) approach an asymptotic value uniformly as a function of r; or (b) increase indefinitely, although certainly not uniformly as a function of r, since $\lambda(r=0)=0$. If λ were to approach a limiting value the star would be approaching a stationary state. However, we are supposing that the relationships between the T_ν^μ do not admit any stationary solutions, and therefore exclude this possibility. Under case (b) we might expect that for any value of r greater than zero, λ will become greater than any preassigned value if t is sufficiently large. If this were so the volume of the star

$$V=4\pi\int_0^{r_b} e^{\lambda/2}r^2dr \tag{12}$$

would increase indefinitely with time; since the mass is constant, the mean density in the star would tend to zero. We shall see, however, that for all values of r except r_0, λ approaches a finite limiting value; only for $r=r_0$ does it increase indefinitely.

II

To investigate this question we will solve the field equations with the limiting form of the energy-momentum tensor in which the pressure is zero. When the pressure vanishes there are no static solutions to the field equations except when all components of T_ν^μ vanish. With $p=0$ we have the free gravitational collapse of the matter. We believe that the general features of the solution obtained this way give a valid indication even for the case that the pressure is not zero, provided that the mass is great enough to cause collapse.

For the solution of this problem, we have found it convenient to follow the earlier work of Tolman[2] and use another system of coordinates, which are comoving with the matter. After finding a solution, we will introduce a coordinate transformation to put the line element in form (1).

We take a line element of the form:

$$ds^2=d\tau^2-e^{\bar{\omega}}dR^2-e^{\omega}(d\theta^2+\sin^2\theta d\varphi^2). \tag{13}$$

Because the coordinates are comoving with the matter and the pressure is zero,

$$T_4^4=\rho \tag{14}$$

and all other components of the energy momentum tensor vanish.

The field equations are:

$$8\pi T_1^1=0=e^{-\omega}-e^{-\bar{\omega}}\frac{\omega'^2}{4}+\ddot{\omega}+\tfrac{3}{4}\dot{\omega}^2=0, \tag{15}$$

$$8\pi T_2^2=8\pi T_3^3=0=-e^{-\bar{\omega}}\left(\frac{\omega''}{2}+\frac{\omega'^2}{4}-\frac{\bar{\omega}'\omega'}{4}\right)+\frac{\ddot{\bar{\omega}}}{2}+\frac{\dot{\bar{\omega}}^2}{4}+\frac{\ddot{\omega}}{2}+\frac{\dot{\omega}^2}{4}+\frac{\dot{\bar{\omega}}\dot{\omega}}{4}, \tag{16}$$

$$8\pi T_4^4=8\pi\rho=e^{-\omega}-e^{-\bar{\omega}}\left(\omega''+\tfrac{3}{4}\omega'^2-\frac{\bar{\omega}'\omega'}{2}\right)+\frac{\dot{\omega}^2}{4}+\frac{\dot{\bar{\omega}}\dot{\omega}}{2}, \tag{17}$$

$$8\pi e^{\bar{\omega}}T_4^1=-8\pi T_1^4=0=\frac{\omega'\dot{\omega}}{2}-\frac{\dot{\bar{\omega}}\omega'}{2}+\dot{\omega}' \tag{18}$$

with primes and dots here and in the following representing differentiation with respect to R and τ, respectively. The integral of Eq. (18) is given by Tolman:[3]

$$e^{\bar{\omega}}=e^{\omega}\omega'^2/4f^2(R) \tag{19}$$

with $f^2(R)$ a positive but otherwise arbitrary function of R. We find a sufficiently wide class of solutions if we put $f^2(R)=1$.

Substituting (19) in (15) with $f^2(R)=1$ we obtain

$$\ddot{\omega}+\tfrac{3}{4}\dot{\omega}^2=0. \tag{20}$$

[2] R. C. Tolman, Proc. Nat. Acad. Sci. **20**, 3 (1934).

[3] We wish to thank Professor R. C. Tolman and Mr. G. Omer for making this portion of the development available to us, and for helpful discussions.

The solution of this equation is:

$$e^{\omega}=(F\tau+G)^{4/3}, \tag{21}$$

in which F and G are arbitrary functions of R.

The substitution of (19) in (16) gives a result equivalent to (20). Therefore the solution of the field equations is (21).

For the density we obtain from (17), (19), and (21)

$$8\pi\rho=4/3(\tau+G/F)^{-1}(\tau+G'/F')^{-1}. \tag{22}$$

There is less real freedom in (21) than is apparent from the two arbitrary functions F and G; for taking R a function of a new variable R^* the differential equations (15), (17) and (18) will remain of the same form. We may therefore choose

$$G=R^{\frac{3}{2}}. \tag{23}$$

At a particular time, say τ equal zero, we may assign the density as a function of R. Eq. (22) then becomes a first-order differential equation for F.

$$FF'=9\pi R^2\rho_0(R). \tag{24}$$

The solution of this equation contains only one arbitrary constant. We now see that the effect of setting $f^2(R)$ equal to one allows us to assign only a one-parameter family of functions for the initial values of $\dot{\rho}_0$, whereas in general one should be able to assign the initial values of $\dot{\rho}_0$ arbitrarily.

We now take, as a particular case of (24):

$$FF'=\begin{cases}\text{const.}\times R^2; & \text{const.}>0; \quad R<R_b\\ 0 & ; \quad R>R_b.\end{cases} \tag{25}$$

A particular solution of this equation is:

$$F=\begin{cases}-\frac{3}{2}r_0^{\frac{1}{2}}(R/R_b)^{\frac{3}{2}}; & R<R_b\\ -\frac{3}{2}r_0^{\frac{1}{2}} & ; \quad R>R_b\end{cases} \tag{26}$$

in which the constant r_0 is introduced for convenience, and is the gravitational radius of the star.

We wish to find a coordinate transformation which will change the line element into form (1). It is clear, by comparison of (1) and (13), that we must take

$$e^{\omega/2}=(F\tau+G)^{\frac{1}{2}}=r. \tag{27}$$

A new variable t which is a function of τ and R must be introduced so that the $g_{\mu\nu}$ are of the same form as those in Eq. (1). Using the contravarient form of the metric tensor, we find that:

$$g^{44}=e^{-\nu}=\dot{t}^2-t'^2/r'^2=\dot{t}^2(1-\dot{r}^2), \tag{28}$$

$$g^{11}=-e^{-\lambda}=-(1-\dot{r}^2), \tag{29}$$

$$g^{14}=0=\dot{t}\dot{r}-t'/r'. \tag{30}$$

Here (30) is a first-order partial differential equation for t. Using the values of r given by (27), and the values of F and G given by (26) and (23) we find:

$$t'/\dot{t}=\dot{r}r'=\begin{cases}-(r_0R)^{\frac{1}{2}}[R^{\frac{3}{2}}-\frac{3}{2}r_0^{\frac{1}{2}}\tau]^{-\frac{1}{3}}; & R>R_b\\ -r_0^{\frac{1}{2}}RR_b^{-\frac{3}{2}}[1-\frac{3}{2}r_0^{\frac{1}{2}}\tau R_b^{-\frac{3}{2}}]^{\frac{1}{3}}; & R<R_b.\end{cases} \tag{31}$$

The general solution of (31) is:

$$\begin{aligned}&t=L(x) \text{ for } R>R_b, \text{ with } x=\frac{2}{3r_0^{\frac{1}{2}}}(R^{\frac{3}{2}}-r^{\frac{3}{2}})\\ &\qquad -2(rr_0)^{\frac{1}{2}}+r_0\ln\frac{r^{\frac{1}{2}}+r_0^{\frac{1}{2}}}{r^{\frac{1}{2}}-r_0^{\frac{1}{2}}}\\ &t=M(y) \text{ for } R<R_b, \text{ with } y=\tfrac{1}{2}[(R/R_b)^2-1]\\ &\qquad +R_br/r_0R,\end{aligned} \tag{32}$$

where L and M are completely arbitrary functions of their arguments.

Outside the star, where R is greater than R_b, we wish the line element to be of the Schwartzchild form, since we are again neglecting the gravitational effect of any escaping radiation; thus

$$e^{\lambda}=(1-r_0/r)^{-1} \tag{33}$$

$$e^{\nu}=(1-r_0/r). \tag{34}$$

This requirement fixes the form of L; from (28) we can show that we must take $L(x)=x$, or

$$t=x. \tag{35}$$

At the surface of the star, R equal R_b, we must have L equal to M for all τ. The form of M is determined by this condition to be:

$$\begin{aligned}t=M(y)&=\tfrac{2}{3}r_0^{-\frac{1}{2}}(R_b^{\frac{3}{2}}-r_0^{\frac{3}{2}}y^{\frac{3}{2}})\\ &\qquad -2r_0y^{\frac{1}{2}}+r_0\ln\frac{y^{\frac{1}{2}}+1}{y^{\frac{1}{2}}-1}.\end{aligned} \tag{36}$$

Eq. (36), together with (27), defines the transformation from R, τ to r and t, and implicitly, from (28) and (29), the metrical tensor.

We now wish to find the asymptotic behavior of e^{λ}, e^{ν}, and τ for large values of t. When t is large we obtain the approximate relation from Eqs. (36) and (27):

$$t \sim -r_0 \ln \{\tfrac{1}{2}[(R/R_b)^2-3] + R_b/r_0(1-3r_0^{\frac{1}{2}}\tau/2R_b^2)^{\frac{1}{2}}\}. \quad (37)$$

From this relation we see that for a fixed value of R as t tends toward infinity, τ tends to a finite limit, which increases with R. After this time τ_0 an observer comoving with the matter would not be able to send a light signal from the star; the cone within which a signal can escape has closed entirely. For a star which has an initial density of one gram per cubic centimeter and a mass of 10^{33} grams this time τ_0 is about a day.

Substituting (27) and (37) into (28) and (29) we find

$$e^{-\lambda} \simeq 1-(R/R_b)^2\{e^{-t/r_0}+\tfrac{1}{2}[3-(R/R_b)^2]\}^{-1}, \quad (38)$$

$$e^{\nu} \simeq e^{\lambda-2t/r_0}\{e^{-t/r_0}+\tfrac{1}{2}[3-(R/R_b)^2]\}. \quad (39)$$

For R less than R_b, e^{λ} tends to a finite limit as t tends to infinity. For R equal to R_b, e^{λ} tends to infinity like e^{t/r_0} as t approaches infinity. Where R is less than R_b, e^{ν} tends to zero like e^{-2t/r_0} and where R is equal to R_b, e^{ν} tends to zero like e^{-t/r_0}.

This quantitative account of the behavior of e^{λ} and e^{ν} can supplement the qualitative discussion given in I. For λ tends to a finite limit for $r<r_0$ as t approaches infinity, and for $r=r_0$ tends to infinity. Also for $r \leqslant r_0$, v tends to minus infinity. We expect that this behavior will be realized by all collapsing stars which cannot end in a stable stationary state. Of course, actual stars would collapse more slowly than the example which we studied analytically because of the effect of the pressure of matter, of radiation, and of rotation.

SEPTEMBER 1, 1939 PHYSICAL REVIEW VOLUME 56

Formation of Ions in the Cyclotron

ROBERT R. WILSON
Radiation Laboratory, Department of Physics, University of California, Berkeley, California

(Received July 10, 1939)

Measurements of the initial ionization in a cyclotron, produced by the use of a filament, as a function of the pressure, electron emission, and dee voltage are presented. The amount of ionization is found to be too high to be simply explained by an electron passing between the region between dees only once. A theory is proposed wherein some of the electrons are caught by the changing electric field between the dees and oscillate back and forth many times during a cycle of the dee voltage. Experimental observations which conform to the theory are described.

THE manner of formation of the initial ions in a cyclotron is important as it affects the intensity and homogeneity of the high energy beam. Ideally the ions should be formed in a very small region at the center of cyclotron and at the median plane. Livingston, Holloway and Baker[1] have developed a capillary type of ion source with these characteristics. However, extended filament ion sources are more generally used at present because they give larger circulating currents, and this paper will be concerned only with an analysis of this type of ion source.

The usual arrangement is for the filament to be located under a shield in which a wide slot is cut to permit the electrons to pass up along the lines of magnetic force between the dees and so ionize by collision the gas in the central region of the cyclotron. A potential difference, hereafter referred to as the emission voltage, between the filament and shield accelerates the electrons from the shielded region.

One is first interested in the magnitude of the ionization between the dees caused by the narrow beam of electrons. This was measured directly

[1] M. S. Livingston, M. G. Holloway and C. P. Baker, Rev. Sci. Inst. **10**, 63 (1939).

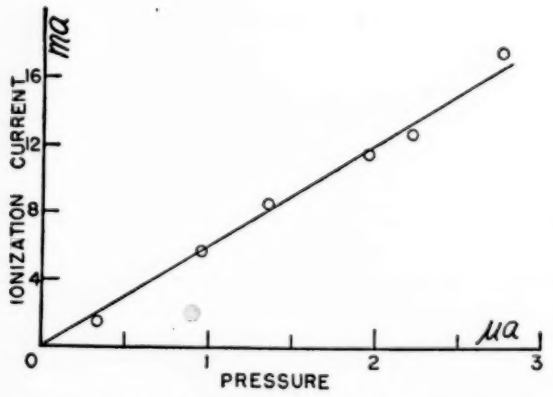

FIG. 1. The total ionization current in milliamperes is plotted as a function of the gas pressure measured in microamperes of positive ion current at an ion gauge. For the data of this curve the emission current was 0.2 of an ampere, and the emission voltage was 600 volts.

by inserting a milliammeter in the ground lead from the center tap of the inductance which was connected between the dees. With the high frequency voltage on, the ions formed are pulled over and caught by one of the dees and give rise to the measured current while the electrons, because of their smaller mass, are constrained to travel along the lines of magnetic forces in tight cycloidal motions and are not caught by the dees. Of course, the large high frequency current must be by-passed by means of a condenser and choke coil. The variation of this ionization current with the pressure of deuterium gas is shown in Fig. 1. The pressure was measured by means of an ion gauge located on the tube leading to the vacuum pumps, and all pressures are given here in units of microamperes of positive ion current in this ion gauge. As determined by a McLeod gauge, one microampere of current at the ion gauge corresponded to a pressure of about $2.7 \cdot 10^{-4}$ mm Hg in the accelerating chamber. This determination depended upon the pumping speed which was kept constant during the measurements. At the optimum operating values of pressure and electron emission, the ionization current was about 15 milliamperes. From Bleakney's[2] measurements of the relative yields of atomic and molecular ions, we would infer that roughly one-tenth of the measured total ionization was comprised of deuterons. Thus, there would be about 1.5 milliamperes of deuterons available for acceleration. It is interesting to note that in the 37-inch cyclotron usually about five percent of this can be accelerated to 8 Mev and deflected to the target chamber, while about half of it can be picked up on a probe. Hydrogen and helium gas yield similar total ionization currents, but, as judged from the relative beams, only about one-half of one percent of the helium ions are doubly charged.

How the ionization current varies with electron emission depends on the position of the filament with respect to the dees, the manner in which the filament is shielded, and whether the emission current is varied by changing the filament temperature or the emission voltage. Fig. 2 indicates a typical variation of ionization current as the emission was increased by changing the filament temperature. While increasing the emission voltage always increases the emission, there is not always a corresponding increase in ionization current, and usually there exists a value of emission voltage corresponding to a maximum amount of ionization and a maximum beam. This optimum voltage is extremely dependent on position of the filament and the shielding. Fig. 3 shows that the ionization current is almost independent of the voltage between the dees—the initial increase of ionization with dee voltage being attributed to the increased ability of the dees to catch the ions.

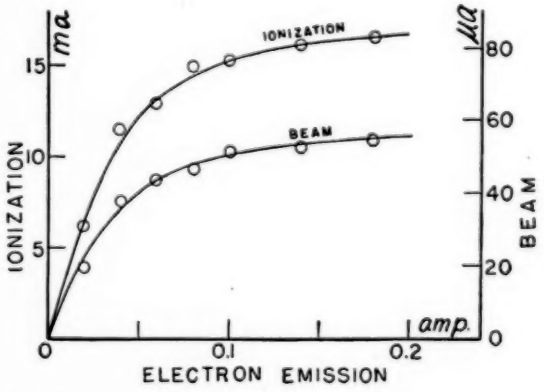

FIG. 2. A typical curve of the total ionization current in milliamperes is plotted as a function of the electron emission current in amperes. The beam current, which is also plotted, is seen to vary proportionally to the total ionization. This is for a single line filament; but if a hair pin or spiral filament is used, the beam does not always vary proportionally to the total ionization. The gas pressure was 3.0 microamperes, and the emission voltage was 600 volts when the above data were taken.

[2] W. Bleakney, Phys. Rev. **35**, 1180 (1930).

If the filament were very narrow and were located electrically midway between the dees, there would be no vertical component of the dee field along the electron's path and its vertical motion would not be affected by the dee voltage. The amount of ionization expected could then be calculated from the data of Bleakney[2] or Compton and Van Voorhis.[3] Thus, for an emission current of 0.3 ampere, emission voltage of 600 volts, and pressure at $6 \cdot 10^{-4}$ mm Hg, only about one milliampere of total ionization would be expected, whereas more than ten times this amount has always been observed. As the electrons are in a crossed electric and magnetic field when traveling between the dees, their horizontal path is cycloidal, and one might expect this to lengthen the path. However, calculations show the cycloids to be extremely small—the diameter of the generating circle is about $2 \cdot 10^{-4}$ cm at most—and the calculated increase in path length is negligible.

To explain the large currents observed, we must remember that the peak voltage between dees is of the order of 100,000 volts and that the chance of the filament being electrically centered between dees is very small. After an electron leaves the shielded region, its subsequent path is conditioned almost entirely by the large dee field. In general the filament will be closer to one dee than the other, and the electrons will only be able to leave the filament region when the voltage on the near dee is positive. When the near dee is negative, the electrons will travel out a short distance until they lose the energy given to them by the emission voltage. If the phase is such that the voltage of the near dee is becoming increasingly negative, the electric field will be greater when an electron is being accelerated back toward the filament so that the electron will return to the filament with a gain in energy and will cause heating of the filament. On the other hand, when the voltage of the near dee is becoming less negative, the electron will return with less energy and cannot repenetrate the emission field to reach the filament as the magnetic field restricts the electrons from moving sideways—they will probably build a space charge which prevents other electrons from leaving the filament during this part of the voltage phase.

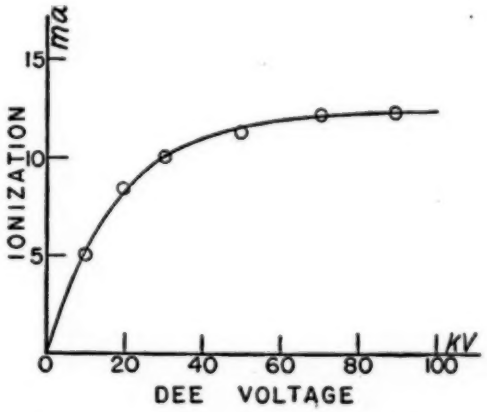

FIG. 3. The total ionization current is plotted as a function of the voltage between the dees. The emission current was 0.2 ampere, the emission voltage was 600 volts, and the pressure was 3.0 microamperes when the data for the above curve were taken.

Now consider when the voltage of the near dee is positive and increasing in magnitude. The electrons are at first strongly accelerated upwards until they pass the level of the bottom edge of the near dee. There the electric field reverses, and the electrons are decelerated until they reach the median plane where the direction of the field again reverses. The electrons are then accelerated upwards until they pass the level of the upper dee edge after which they are strongly decelerated. If the dee voltage had remained constant during the flight of the electron, they would strike the upper cooling plate with a velocity corresponding to the emission voltage. However, during the flight the dee voltage has been increasing and the electrons must do more work against the field in leaving the region between dees than they gained in entering it. Indeed, the difference in energy between entering and leaving the dee region turns out to be greater than the emission voltage so that the electrons cannot strike the cooling plate but must turn back. Nor can the electron, after approximately retraversing its path, return to the filament: rather it is snared and must oscillate up and down until the dee voltage drops to about the value it had when the electron was emitted. Thus, an electron emitted during this phase of the voltage cycle, i.e., near dee becoming increasingly positive, can pass through the region between dees many times and the ionizing power

[3] K. T. Compton and C. C. Van Voorhis, Phys. Rev. 26, 436 (1925); 27, 724 (1926).

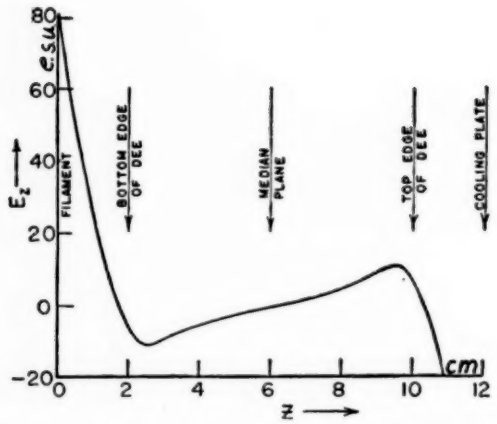

FIG. 4. The vertical component of the electric field along a vertical line situated halfway between the electrical center between dees and one of the dee edges is plotted as a function of Z, the distance above the filament. In the above curve the dimensions are approximately those of the 37-inch Berkeley cyclotron, i.e., distance from filament to cooling plate, 12 cm; dee height, 8 cm; dee separation, 4 cm. The voltage between dees is taken to be 100,000 volts.

thus be increased many fold. Moreover, the electrons are going more slowly and so producing more ions in the neighborhood of the median plane, and they are going faster and producing less ionization in the proximity of the dee edges where ionization might be likely to lead to a voltage breakdown.

In the horizontal plane, the electrons are executing cycloidal motion all the while and walk off in a direction perpendicular to the electric and magnetic field with an average velocity of cE/H. This sidewise motion can amount to about 4 cm for a deuteron magnetic field or about 8 cm for a proton magnetic field in the case of the 37-inch cyclotron. As the length of the filament is from 4 to 6 cm, the region of ionization extends over a distance of about 10 cm. This is disadvantageous as it contributes to the nonhomogeneity of the energy of the beam.

The electrons emitted during the phase when the voltage of the near dee is positive but decreasing in magnitude will gain more energy in entering the region between dees than leaving it and will strike the cooling plate the first time across and with considerable energy. These electrons though will still be speeded up near the dee edges and will go slowest near the median plane so as to tend to give a favorable concentration of ionization. Also during this phase the electrons emitted during the preceding phase can still be oscillating.

More quantitatively, the vertical component of the electric field along a vertical line situated halfway between the electrical center between dees and one of the dees is plotted as a function of the distance from the filament in Fig. 4. This was obtained by an electrolytic tray method. From it were calculated numerically the electron trajectories plotted in Fig. 5, where the height of an electron is shown as a function of the phase for electrons starting at various initial phases. For the calculations standard operating conditions and dimensions of the 37-inch cyclotron were used, i.e., maximum dee voltage, 100,000 volts; frequency, 11 megacycles; emission voltage, 600 volts; dee height, 8 cm. An electron emitted just as the dee voltage has become positive may be slowed up so much on approaching the median plane that it may not be able to cross it. In this case the electron will oscillate about one of the edges of the dee as indicated. Most electrons oscillate past the median plane, however, and some electrons can make about a dozen crossings. Also interesting is the ionizing power of an electron as a function of height as shown in Fig. 6. This was calculated from the data of Fig. 5 and Bleakney's ionization

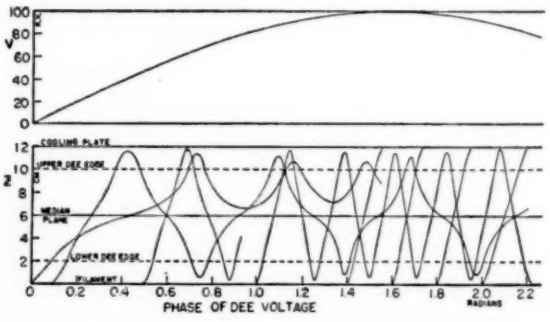

FIG. 5. In the lower curve is plotted the height of an electron above the filament as a function of the phase of the dee voltage when the voltage of the nearest dee to the filament is positive. In the upper curve is plotted the voltage between dees at the phase indicated on the lower graph. An electron starting at zero phase is seen to oscillate about the position of the upper dee edge. An electron which is emitted at an initial phase of 1.0 radian is seen to oscillate back and forth across the median plane and finally return to the filament after the dee voltage has dropped below the value it had when the electron was emitted—in this case after the phase has reached 2.1 radians. Electrons starting after an initial phase of $\pi/2$ radians, i.e., after the near dee voltage starts to become less positive, are seen to cross directly to the cooling plate.

measurements. Curve *a* is for a typical oscillating electron, and curve *b* is for one that just crosses once. It is seen that the ionization will be appreciably greater near the median plane than at the dee edge.

There is considerable experimental evidence that the above actually does occur. Visually, without the dee voltage applied but with the emission voltage on, one sees a sharply defined narrow glow directly above the filament and extending uniformly from the filament to the cooling plate. When the dee voltage is turned on, the glow spreads out and becomes strongest in the vicinity of the median plane and much weaker near the dee edges as Fig. 6 would indicate. When a long probe was put into the 60-inch cyclotron so that it was near the center, a negative current was picked up when the dee voltage was turned on. With an emission of 100 milliamperes and with the probe very near to the filament, a current of about 50 milliamperes was collected which fell off roughly linearly as the probe was moved away from the filament and which reached zero at a distance of about 12 cm from the filament. This was with a proton magnetic field, and considering the dee voltage, etc., the oscillating electrons would be expected to wander out a comparable distance during a half-cycle. Furthermore, as only the electrons emitted during the first half of the positive dee voltage phase will oscillate, one would expect about one-half the emission current to wander off sidewise and be collected by the probe as the above measurement indicates. Also as the magnetic field was increased, the current to the probe fell off more rapidly as the probe was moved away from the filament as would also be expected.

Another phenomenon can be explained by the above theory. When the dee voltage is applied, the emission current is observed to drop to about half-value and then slowly to increase to considerably higher than half-value. When the dee voltage is turned off, the emission current kicks up to a large value and then slowly decreases to the original reading. The size of the kick increases about linearly with the dee voltage and also becomes greater as the filament is moved closer to either dee—being a minimum when the filament is midway between dees. All this is because some

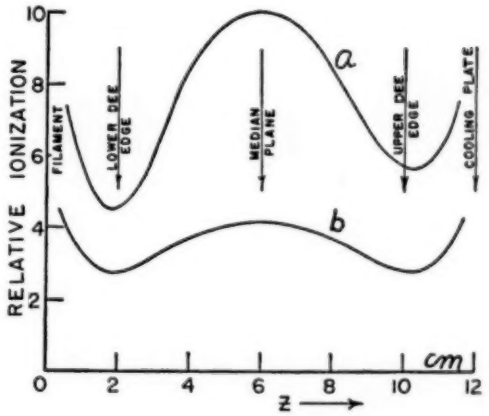

FIG. 6. The relative ionizing power of an electron is plotted as a function of its height above the filament. Curve *a* is for a typical oscillating electron emitted when the phase is about 0.3 radian. Curve *b* is for an electron emitted when the phase is about 2.0 radians, i.e., an electron which crosses directly to the cooling plate. In each case the ionizing power is seen to be increased near the median plane and decreased near the positions of the dee edges.

of the oscillating electrons are about as likely to strike the filament when they stop oscillating as to strike the cooling plate. They will also carry off considerable energy with them which will give rise to a heating of the filament. The electrons emitted when the voltage of the near dee is negative and increasing in magnitude can also cause a considerable heating as explained before. The dee voltage suppresses half of the emission current when it is turned on, but the heating due to the returning electrons increases the temperature of the filament slowly and causes the emission to increase. When the voltage is turned off, the emission should double and then fall off to its original value as the filament cools off. Rough calculations show that the heating by the returning electrons is sufficient to account for the observed increase in temperature.

It is a pleasure to acknowledge the helpful interest taken in this work by Professor Ernest O. Lawrence. I am also especially indebted to Professor Edwin McMillan who took some of the experimental data and to Miss Chien Shiung Wu who made many of the numerical calculations. The support of the National Advisory Cancer Council and the Rockefeller Foundation is also gratefully acknowledged. Acknowledgment is herewith made of services rendered by Works Progress Administration, Project No. 10695.

Relative Intensities of Singlet-Singlet and Singlet-Triplet Transitions

G. W. KING*
Sterling Chemistry Laboratory, Yale University, New Haven, Connecticut

AND

J. H. VAN VLECK
Harvard University, Cambridge, Massachusetts

(Received June 16, 1939)

The ratio of the intensities of singlet-triplet to singlet-singlet transitions can be calculated by means of Houston's formulae in two ways: (a) from the deviations from the interval rule, and (b) from the distance of the singlet level from the center of gravity of the triplet levels. The discrepancy of the two calculations indicates that the integral of the radial functions between the singlet and triplet differs from that for the triplet with triplet, say by a factor λ. The new parameter λ is evaluated (~ 0.75) from the positions of the four levels, and gives intensity ratios in good agreement with the observed.

HOUSTON[1] showed that a forbidden transition such as $^1S_0-{}^3P_1$ is due to spin-orbit interaction,—the mixing of some of the associated singlet ($^1P_1$) with the triplet level ($^3P_1$).

Strangely enough Houston's formulae for the energy levels have never been used to calculate the relative intensity of these particular transitions. The calculations are extremely elementary, and give good agreement with the experimentally determined values.

When spin-orbit interactions are included, the energy matrix between the Russell-Saunders states

$$^3L^0{}_{l+1}\ {}^3L_l{}^0\ {}^1L_l{}^0\ {}^3L^0{}_{l-1} \quad \text{is}^2$$

$$\begin{pmatrix} F-G & & & & \\ & F-G & & & \\ & & F+G & & \\ & & & F-G & \end{pmatrix} + \tfrac{1}{2}\zeta \begin{pmatrix} l & & & \\ & -1 & (l(l+1))^{\frac{1}{2}} & \\ & (l(l+1))^{\frac{1}{2}} & 0 & \\ & & & -(l+1) \end{pmatrix}, \tag{1}$$

where F and G are the electrostatic energies appearing in the Russell-Saunders approximations, and ζ is the integral of the radial functions with the spin-orbit interaction operator, in a central field, *viz.*

$$\zeta = h^2Ze^2(16\pi^2m^2c^2)^{-1}\int r^{-3}R^2r^2dr, \tag{2}$$

where R is the radial wave function. It is to be emphasized that Eq. (2) assumes that the radial wave function is the same for the singlet as the triplet state, an assumption not really warranted, as we shall discuss later.

The energy levels are then, for the case of P states

$$^3P_2 = F-G+\tfrac{1}{2}\zeta, \quad {}^3P_0 = F-G-\zeta$$
$$^{1,\,3}P_1 = F-\tfrac{1}{4}\zeta \pm [(G+\tfrac{1}{4}\zeta)^2+\tfrac{1}{2}\zeta^2]^{\frac{1}{2}}. \tag{3}$$

Equations (3) give the positions of the four levels in terms of three parameters F, G, ζ. Thus the location of three of the states determine the location of the fourth.

The ratio of the f values for the $^1S_0-{}^3P_1$ and $^1S_0-{}^1P_1$ transitions can be determined from the transformation matrix that diagonalizes (1), together with the fact that only $^1S_0-{}^1P_1$ is permitted in the limiting case of pure Russell-Saunders coupling (i.e., between $^1(L-1)^0{}_{l-1}$ and $^1L_l{}^0$). However, as Houston's formula does not fit exactly (does not yield the proper location for the fourth level), the results will be different according as one employs values for the param-

* Part of this work was done as a National Research Fellow, 1937.

[1] W. V. Houston, Phys. Rev. **33**, 297 (1929).

[2] Condon and Shortley, *Theory of Atomic Spectra* (Cambridge University Press, 1935), p. 271.

eters F, G, ζ which yield the correct empirical positions either of (a), $^3P_1$, $^3P_0$, $^3P_2$ or (b), $^1P_1$, $^3P_0$, $^3P_2$ i.e., according as one adjusts the constants so as to give the proper deviations from the interval rule, or the proper singlet-triplet separation, together with, in either case, the correct over-all width for the triplet.

The corresponding formulae for the ratios of the f values are:

$$\text{method (a)}: f_1/f_3=\tfrac{3}{5}(\nu_1/\nu_3)\times(^3P_2-{}^3P_0)^2/(^3P_1-\tfrac{2}{3}{}^3P_0-\tfrac{1}{3}{}^3P_2)^2, \quad (4)$$

$$\text{method (b)}: f_1/f_3=(\nu_1/\nu_3)\cot^2\{\tfrac{1}{2}\sin^{-1}[\tfrac{2}{3}\times 2^{\frac{1}{2}}(^3P_2-{}^3P_0)/(^1P_1-{}^3P_1)]\}. \quad (5)$$

It is seen from Table I that neither method (a) nor (b) gives results agreeing adequately with experiment.

The most natural explanation of the discrepancies is to blame perturbation by other levels, but none seems to be located in a suitable position to account for the anomalies. The real solution of the difficulty appears to be that the radial functions are not quite the same for singlet and triplet states, so that their Hartree, or rather Fock, self-consistent fields are slightly different. It is therefore legitimate to insert an undetermined parameter λ in the off-diagonal matrix element of (1). Then ζ relates to (2) with $R^2=R_3^2$, while $\lambda\zeta$ refers to (2) with R^2 replaced by R_1R_3. Here R_1 and R_3 are, of course, the singlet and triplet radial functions. (Note that the integral with R_1^2 does not occur due to a zero matrix element in (1).) Correspondingly, $\frac{1}{2}\zeta^2$ is replaced by $\frac{1}{2}\lambda^2\zeta^2$ in the radicand of (3). We now have four parameters F, G, ζ, λ, so that (3) will now yield correctly the positions of all four energy levels. The first three can be determined from $^3P_2$, $^3P_0$ and $^1P_1+{}^3P_1$ (the trace of the second order minor between $^3L_i^0$ and $^1L_i^0$ in (1)), and λ from the determinant of this matrix $^1P_1\times{}^3P_1$. Also λ and f_1/f_3 can be evaluated by perturbation formulae accurately enough in the cases of Zn, Sr, Ca. With the parameters thus determined, the computed intensity ratios agree quite well with the experiment,[3] as shown in the last line of the table. Except for Hg, the calculated value is within the experimental error.

TABLE I. *Relative f values of* $^1S_0-{}^1P_1$ *and* $^1S_0-{}^3P_1$ *transitions.*

	Hg	Cd	Zn	Ba	Sr	Ca
$\lambda^1S_0-{}^1P_1$	1,849.57	2,288.02	2,138.61	5,535.53	4,607.34	4,226.73
$\lambda^1S_0-{}^3P_1$	2,536.52	3,261.04	3,075.88	7,911.36	6,892.62	6,572.78
$^3P_2-{}^3P_0$	6,397.9	1,713.0	578.7	1,248.5	581.2	158.1
$^3P_1-{}^3P_2$	1,767.3	541.9	189.8	370.5	186.8	52.3
$^3P_1-\frac{2}{3}{}^3P_0-\frac{1}{3}{}^3P_2$	−365.4	−29.1	−3.1	−45.7	−6.8	−1.5
$^1P_1-{}^3P_1$	14,656.1	13,036.0	14,243.5	5,423.6	7,194.1	8,442.2
F	47,803.95	37,459.7	39,719.8	15,556.5	18,198.3	19,457.667
G_0	5,896.4	6,203.4	7,022.2	2,458.1	3,493.35	4,194.3
$\frac{1}{2}\zeta$	2,132.6	571.0	192.9	416.7	193.7	52.73
λ	0.7578	0.7618	0.7702	0.8414	0.8070	0.8126
f_1/f_3:						
Houston (a)	93	1,097	11,140	237	2,427	54,100
Houston (b)	29	369	3,995	127	1,029	19,500
Improved method	53.4	637	6,757	169	1,582	30,180
Observed	46.8±2	680±100	7,200	146	1,660	33,000

The values of λ are of reasonable order of magnitude, as they are not far different from unity, of about the same size, ~0.75, in all cases.

Further it is probably to be expected that λ is less than unity, since the nodes of the singlet and triplet wave functions will be at different positions. The resulting decrease in the amount of overlapping will thus make the modified integral (2) smaller with a factor R_1R_3 than with R_3^2.

[3] Obtained from dispersion measurements by G. Wolfsohn, Zeits. f. Physik **83**, 234 (1933) (Hg, Cd, Zn) and from anomalous dispersion measurements, W. Prokofiew, Zeits. f. Physik **50**, 701 (1928) (Ba, Sr, Ca).

Elementary Processes in the Sensitized Fluorescence of OH Molecules

ELISABETH REED LYMAN*
Department of Physics, University of Illinois, Urbana, Illinois
(Received July 10, 1939)

The processes involved in the sensitized fluorescence excitation of the OH molecules have been investigated by photometric measurements of the intensities of lines of the (0,0), (1,0) and (1,1) OH bands. Collisions between metastable $^3P_0$ mercury atoms and water molecules produce unexcited OH molecules which are then excited by further collisions with $^3P_0$ mercury atoms to levels whose energies are equal to or less than the energy of the $^3P_0$ mercury atoms. Abnormal rotational energy is produced in the excitation of the OH molecules. Collisions between nitrogen and OH molecules transfer vibrational energy of the OH molecules to rotational energy and also reduce the rotational energy of the OH molecules somewhat toward thermal values. Collisions between helium and OH molecules are very much less effective in transferring energy than nitrogen collisions.

INTRODUCTION

THE effect of elementary processes such as collisions on the rotation of molecules gives information about the transfer of energy between molecules. Some molecules exhibit abnormal rotational energy characteristic of a temperature of several thousand degrees even when the molecules themselves are expected to have kinetic energy corresponding to room temperature. These molecules may lose energy through collisions. Gaviola and Wood[1] first observed an abnormal rotational energy in the fluorescence spectrum of HgH. Rieke[2] has made a study of the molecular processes involved in the production of the excess rotational energy of the HgH molecule and the effects of collisions with foreign gases on the rotation. An example of abnormal rotation reduced by collisions, although less conspicuous than the HgH case, is in the band spectrum of hydrogen excited by electron impact. Addition of a small amount of helium to the hydrogen as discovered by Richardson[3] and further investigated by Roy[4] gives abnormal rotational energy to the hydrogen molecules which disappears with an increase in the helium pressure.

The spectrum of the OH molecule shows abnormal rotational energy when it is excited in discharge tubes.[5] Bonhoeffer and Pearson[6] stated that the source of such energy arises from the process of simultaneous dissociation of H_2O and excitation of OH by electron impact. Oldenberg[7] showed experimentally by a comparison of the absorption spectrum of normal rotation with the abnormal emission spectrum that the abnormally rotating molecules do not originate from the OH molecules normally present in the discharge, but from the simultaneous dissociation and excitation process. After radiation the molecules lose their excess rotational energy through collisions.

Since the process of excitation in electric discharges is complicated, a further key to the explanation of the abnormal rotation of the OH molecules might be found in a study of the spectrum excited under more simple conditions. Flame and arc excitation (thermal types of excitation) show distributions of rotational energy representing thermal equilibrium as expected,[5] but sensitized fluorescence excitation exhibits the characteristic abnormal rotation of the discharge tube spectrum. In fluorescence experiments the elementary processes can be traced in great detail. The following investigation of the rotational energy distribution in the sensitized fluorescence spectrum of OH, therefore, was undertaken in an attempt to explain the source of the excess rotational energy of the OH molecule, and to determine some information about the exchange of energy between OH molecules and foreign gas molecules in collisions.

EXPERIMENTAL

A quartz fluorescence tube was used similar in shape and dimensions to that used by Rieke[2] in

* Experimental work carried out at the Department of Physics, University of California, Berkeley, California.

[1] E. Gaviola and R. W. Wood, Phil. Mag. **6**, 1191 (1928).
[2] F. F. Rieke, J. Chem. Phys. **4**, 513 (1936).
[3] O. W. Richardson, Proc. Roy. Soc. London **111**, 720 (1926).
[4] A. S. Roy, Proc. Nat. Acad. Sci. **19**, 441 (1933).
[5] E. R. Lyman, Phys. Rev. **53**, 379 (1938).
[6] K. F. Bonhoeffer and T. G. Pearson, Zeits. f. physik. Chemie **14**, 1 (1931).
[7] O. Oldenberg, Phys. Rev. **46**, 210 (1934).

his work with HgH. The tube was flattened in the central portion to reduce the absorbing layer of mercury vapor in the fluorescent region. Two vertical quartz mercury arcs were placed one on either side of the flattened portion of the fluorescence tube which was held horizontally. The mercury arcs were watercooled, were each in a magnetic field, and were run at low currents between 1 and 2 amperes. These precautions guarded against self-absorption of the resonance line λ2537. An image of the cross section of the fluorescent region was focused on the slit of the spectrograph by a quartz lens.

The source of mercury vapor was a drop of mercury placed in the tail end of the fluorescence tube. In some experiments water vapor was admitted through a double stopcock arrangement to obtain the desired pressure, and in others continually flowed through the tube. In the nonflowing vapor experiments sufficient hydrogen to quench the fluorescence did not seem to be produced by the dissociation of the water during the time necessary for exposures.

Three groups of photographs were obtained with mixtures of mercury, water vapor and nitrogen; mercury and water vapor; and mercury, water vapor and helium. The spectrograph used was the 21-foot 30,000-line/inch aluminum grating in the Paschen mounting. Photographs of the (0,0), (1,0), and (1,1) bands were taken in the first order. Exposures varying from 1 to 2 hours were necessary with Eastman 40 plates. The plates were developed in Rodinal. The method of calibrating and measuring the intensities of the lines on the plate was described in a previous publication.[5] The lines of the (0,0), and (1,1) bands were identified from data of Heurlinger,[8] and of the (1,0) band from data of Watson.[9]

Results

The relative intensities of the measured lines of the Q_1 branch of the (0,0) band are plotted against the corresponding rotational quantum numbers, J', (Fig. 1). The gas in the fluorescence tube was 3.5 mm of water vapor and 10 cm of nitrogen. The shape of the distribution curve, typical of all OH fluorescence distribution curves

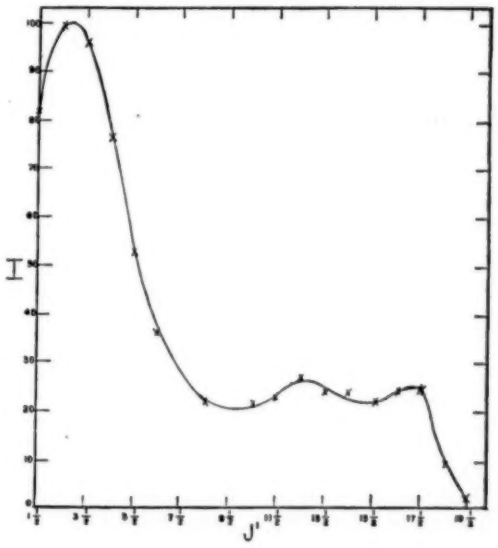

FIG. 1. Intensities of lines of the Q_1 branch of the λ3064 band from the sensitized fluorescence spectrum as a function of the rotational quantum number. 3.5 mm water vapor and 10 cm nitrogen in the fluorescence tube.

obtained, is not thermal since there is an excess of rotational energy among the upper rotational states and a sudden drop-off of intensities starting at $J'=17\frac{1}{2}$. The Q_1 branch is used as an example of all the branches in the (0,0) band because it is the branch least perturbed by overlapping lines. Graphs for the other principal branches in the band showed the same excess rotational energy in the upper rotational levels with sharp decreases in intensities beginning with lines arising from the level $J'=17\frac{1}{2}$. In the (1,0) band a similar drop-off of intensities was found for lines originating above the rotational level $J'=11\frac{1}{2}$. Regardless of the mixtures of gases in the fluorescence tube, the spectrum always showed the sudden decrease of intensity toward zero above the levels $J'=17\frac{1}{2}$ for the (0,0) band and $J'=11\frac{1}{2}$ for the (1,0) band.

Assuming thermal equilibrium among the molecules, there exists a linear relationship according to the Maxwell-Boltzmann theory between the logarithms of I/i and the corresponding rotational term values, $T(K')$, where I is the measured intensity of each line, and i the theoretical intensity factor. The theoretical intensity factors were calculated from Earls'[10]

[8] T. Heurlinger, Dissertation (Lund, 1918).
[9] W. W. Watson, Astrophys. J. **60**, 145 (1924).
[10] L. T. Earls, Phys. Rev. **48**, 423 (1935).

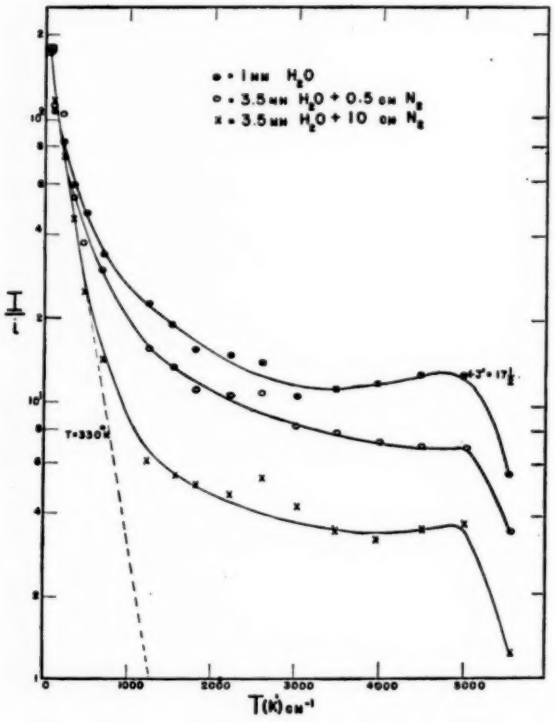

FIG. 2. Rotational term values as a function of log I/i for water vapor-nitrogen mixtures.

adaptations of the Hill and Van Vleck[11] formulas for the $^2\Sigma$, $^2\Pi$ transitions and the term values for the (0,0) band were calculated from data of Heurlinger.[8] Graphs of log I/i *vs.* $T(K')$ for the (0,0) band illustrate clearly the sudden decrease of intensities above $J'=17\frac{1}{2}$. Fig. 2 shows such graphs for three different conditions in the fluorescence tube. The curved line through the points indicates that no thermal equilibrium exists among the molecules. In the case of a small amount of water vapor alone, there is a large amount of excess rotational energy among the high levels. Addition of a small amount of nitrogen reduces the excess rotational energy somewhat, and addition of a greater pressure of nitrogen reduces the excess even more towards thermal values. A straight line drawn through the first few points in the latter case has a slope from which a temperature of 330°K may be calculated. This is of the order of room temperature. Addition of small amounts of helium in the fluorescence tube showed no effect on the reduction of rotational energy comparable to the effect of the addition of nitrogen.

There is a slight enhancement of the lines just before the sharp decrease in intensities. The lines arising from around the level $J'_{(0,0)}=12\frac{1}{2}$ are also enhanced, especially in the case with the greater amount of nitrogen in the fluorescence tube. Both cases of enhancement of intensities are noticeable in other branches besides the Q_1 branch.

If the intensity of the strongest line of the (0,0) band is called 100, and the intensities of corresponding strong lines in the (1,0) and (1,1) bands are compared to this line, an approximate idea of the relative intensities of the bands in relation to one another can be obtained, i.e. a measure of the respective amounts of vibrational energy may be obtained. Table I gives these data. It is noted that the intensities of the (1,1) and the (1,0) bands are weak compared to the (0,0) band when there is an increase in the amount of nitrogen present. There is a large amount of vibrational energy in the (1,0) and the (1,1) bands when a small amount of water alone is in the fluorescence tube. Helium seems to be less effective than nitrogen in reducing vibrational energy.

INTERPRETATION OF RESULTS

In the process of sensitized fluorescence, the $^3P_1$ mercury atoms formed by the absorption of the resonance radiation λ2537 are very effectively transferred to the metastable $^3P_0$ state by collisions with water or nitrogen.[1] According to Beutler and Rabinowitch,[12] the OH molecules are formed in the following manner:

$$Hg(6^3P_0)+H_2O\rightarrow HgH+OH-0.1\text{ v.} \quad (1)$$

TABLE I. *Intensities of strongest lines. Strongest line of (0,0)=100.*

	3.5 MM H_2O +10 CM N_2	3.5 MM H_2O +5 CM N_2	3.5 MM H_2O +1.5 CM N_2	3.5 MM H_2O +0.5 CM N_2	3.5 MM H_2O +1 CM He	1 MM H_2O
(1,0) λ2811	4	4	8	8	19	45
(1,1) λ3122	4	6	8	13	24	50

[11] E. Hill and J. H. Van Vleck, Phys. Rev. **32**, 250 (1928).

[12] H. Beutler and E. Rabinowitch, Zeits. f. physik. Chemie **B8**, 231 (1930).

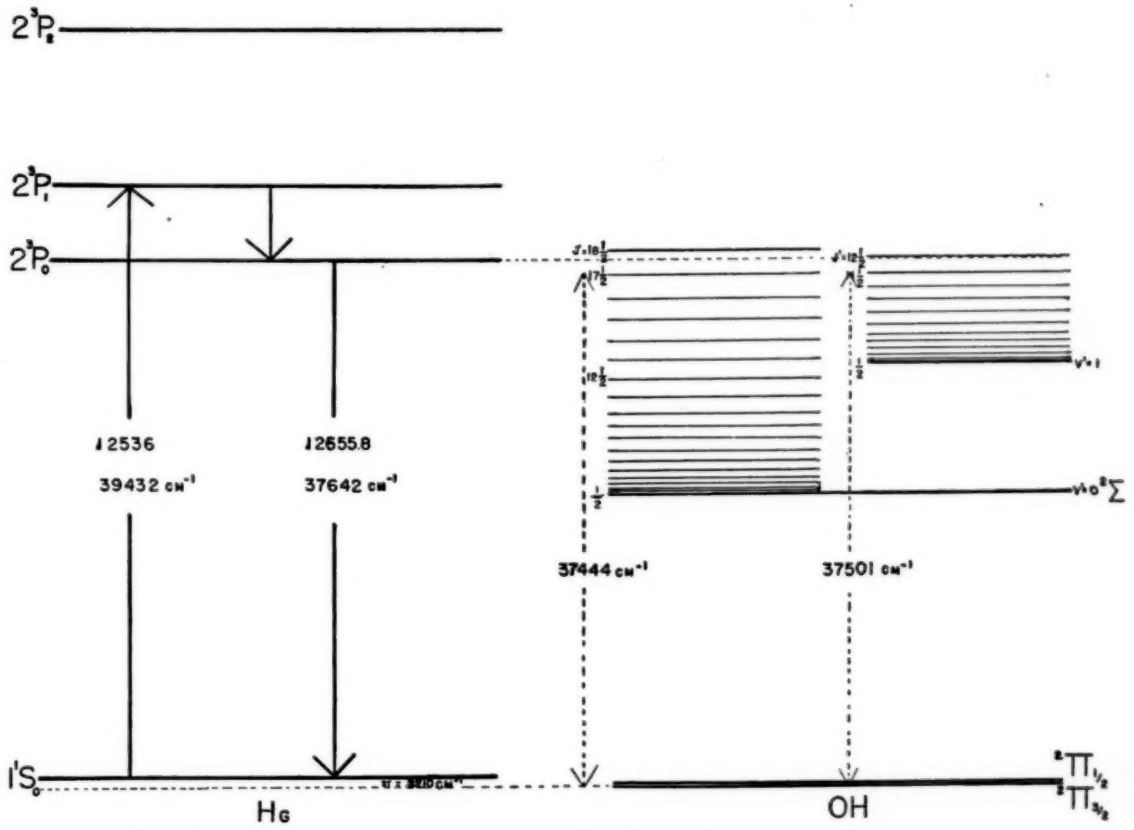

FIG. 3. Vibrational and rotational levels of the OH molecule, and the lower energy levels of the Hg atom.

Since there is a deficiency of energy in (1) and yet OH molecules are known to be formed, the excess energy must be made up from thermal energy of the reacting molecules. The OH molecules, therefore, must be formed in the ground state, $^2\Pi_{3/2,\ 1/2}$, with little if any excess rotation at this point. Since experimental evidence shows that excited OH molecules in sensitized fluorescence do exhibit abnormal rotational energy, the excess rotation must be acquired, as in the case of HgH[2], in the excitation process of the OH molecule:

$$Hg(6^3P_0)+OH \rightarrow Hg(6'S_0)+OH' \qquad (2)$$

or in further collisions during the lifetime of the excited molecule.

The sudden decrease in intensities previously described indicates that few transitions from levels above $J'=17\frac{1}{2}$ for the (0,0) band and $J'=11\frac{1}{2}$ for the (1,0) band are possible, i.e. few molecules can be excited above $J'_{(0,0)}=17\frac{1}{2}$ or $J'_{(1,0)}=11\frac{1}{2}$. The energy corresponding to the level $J'_{(0,0)}=17\frac{1}{2}$ is 37,444 cm^{-1} and to $J'_{(1,0)}=11\frac{1}{2}$, 37,501 cm^{-1}. The energy of the $^3P_0$ mercury atoms is 37,642 cm^{-1}. To the latter value must be added the thermal energy, kT, which is 210 cm^{-1} at 300°K, i.e., Hg($^3P_0$) lies at 37,852 cm^{-1}. Fig. 3 is an energy level diagram for the OH molecule and the mercury atom. The levels $J'_{(0,0)}=17\frac{1}{2}$ and $J'_{(1,0)}=11\frac{1}{2}$ lie below the $^3P_0$ mercury level and $J'_{(0,0)}=18\frac{1}{2}$ and $J'_{(1,0)}=12\frac{1}{2}$ lie above it. The maximum amount of energy that can be given to the OH molecule when it is excited by collisions with $^3P_0$ mercury atoms is, therefore, the energy of the $^3P_0$ mercury atoms. The fact that a few transitions (see Fig. 2) from levels above $J'_{(0,0)}=17\frac{1}{2}$ do occur can be explained by the presence of a few molecules raised to those states by thermal energy alone. The apparent violation of the law of conservation of angular momentum evidenced in the enhancement of the levels $J'_{(0,0)}=16\frac{1}{2}$, $17\frac{1}{2}$ may be explained as due to the large cross section for energy transfer between

molecules in states with nearly the same energy as the $^3P_0$ mercury level.

When nitrogen is present, collisions of the second kind can take place between nitrogen and the excited OH molecules. The energy in excess of electronic energy is redistributed over the degrees of freedom of the OH molecule, and vibrational energy is, therefore, transferred to rotational energy. The reduction of intensity of the (1,0) and (1,1) bands with respect to the intensity of the (0,0) band with increasing pressures of nitrogen (Table I) indicates a reduction of vibrational energy. In Fig. 2 a reduction of rotational energy toward thermal values exists with increasing pressures of nitrogen present in the fluorescence tube. Collisions with nitrogen can remove molecules from higher to lower v' and J' states. The nitrogen molecules can take away rotational energy from the OH molecules. The excess rotational energy in the upper states is not reduced a very great amount, however, by collisions with the nitrogen. There are probably two processes occurring simultaneously during these collisions, a transfer of molecules from high to low rotational states of the $v'=0$ level and at the same time a transfer of molecules from higher vibrational states to high rotational states of the zero vibrational level so that excess rotational energy still exists among the upper states.

A possible explanation of the enhancement of lines arising from the level $J'_{(0,0)}=12\frac{1}{2}$ or from nearby levels of the zero vibrational state arises from the hypothesis of the transfer of molecules in collisions with nitrogen from the higher vibrational states to the high rotational levels of the zero vibrational state. The level $J'_{(0,0)}=12\frac{1}{2}$ lies approximately at the same place in the energy level diagram (Fig. 3) as $v'=1$. From these experiments there is evidence of a loss of excess rotation by collisions during the lifetime of the excited state. Such transfers of energy occur most efficiently for small energy changes. One would expect, therefore, an accumulation of molecules in the low rotational states of the first vibrational level, $v'=1$. Hence transfers of the energy of one vibrational quantum into rotation should be more probable than transfers of nearby amounts. The result of these transfers is the enhancement of the lines originating from the $v'=0$, $J'=12\frac{1}{2}$ level. The more collisions possible during the lifetime of the excited molecules, the greater is the enhancement to be expected. Such an effect is observed as the pressure of nitrogen in the fluorescence tube is increased (Fig. 2).

Conclusions

The correspondence of the energy of the metastable $^3P_0$ mercury atoms and the energies of the rotational states above which the OH molecules are not excited in sensitized fluorescence indicates that the OH molecules obtain their excitation energy from collisions with the $^3P_0$ mercury atoms.

The relatively small effect of collisions with foreign gases, even with nitrogen, on the distribution of energy among the excited OH molecules shows that the abnormal rotational energy of the excited OH molecules is acquired in the excitation process of the OH molecule. There is definite evidence, however, that there is a transfer of vibrational energy into rotational energy as well as some reduction of rotational energy as a result of collisions between nitrogen and excited OH molecules. Collisions between helium and OH molecules are very much less effective than nitrogen collisions.

The present experiments have no bearing on the results of the work on the discharge tube excitation of the OH molecules. The origin of the abnormal rotation in the OH spectrum excited in electric discharges is a different process from that in sensitized fluorescence.[6, 7]

In conclusion the author wishes to express her gratitude to Professor F. A. Jenkins for his interest and suggestions during the experimental part of this research, and to Professor G. M. Almy for many helpful discussions concerning the interpretation of the results.

The Formation of Metallic Bridges Between Separated Contacts*

G. L. PEARSON
Bell Telephone Laboratories, New York, New York

(Received July 12, 1939)

Low resistance bridges were formed between gold, steel and carbon electrodes having separations of $2–70\times10^{-6}$ cm by applying voltages less than the minimum sparking potential. For a given pair of electrodes the field required to form the bridges is a constant and is $5–16\times10^{6}$ volts per centimeter. Measurements of the temperature coefficient of resistance of the bridges identify them as consisting of the material of the electrodes. A study of their resistance as a function of the displacement of one of the electrodes shows that they may be pulled out as well as crushed. At voltages less than those required to form the bridges, field currents exist. These increase rapidly as the field is raised and attain a value around 10^{-10} ampere before the bridges are formed. Calculation of the maximum electrostatic stress on the electrodes at the time of breakdown gives a value 0.05 to 0.0005 times the tensile strength of the electrode material at room temperature. The field is locally higher than that calculated because of surface roughness and the tensile strength is probably lowered by the local heating known to accompany field currents. The data therefore indicate that electrostatic force pulls material from the electrodes to bridge the gap.

THE study of the passage of electric current across small gaps is an old problem, having been investigated by Wood,[1] Earhart,[2] Kinsley,[3] and Hobbs[4] as early as 1900. The results of these early experiments were uncertain, especially those pertaining to the breakdown of the gap at high field strengths. Around 1920 the subject was again investigated by Rother,[5] Hoffman[6] and Rohmann[7] in connection with their study of cold point discharge. These investigators were chiefly interested in the passage of current between separated contacts. The present paper presents data showing that low resistance bridges are formed between separated metallic electrodes at fields of about ten million volts per centimeter and that the material of the bridge is that of the electrodes.

The measurements were made with a displacement device in which the contact could be rigidly fixed and manipulated at will. This apparatus,[8] shown in Fig. 1, consists essentially of a cantilever bar A cut from a solid block of steel and so arranged that motions applied through a calibrated screw B, can be reduced in accordance with the theory of the cantilever bar, by a factor of 300 to 1 when applied to the rod D pivoted near its base. The two contact electrodes C_1 and C_2 are mounted as shown. Rough motions can be obtained by means of the screw F, and stiff springs E and G eliminate any slack motions. With this apparatus contact movements as small as 1×10^{-7} centimeters can be produced and measured.

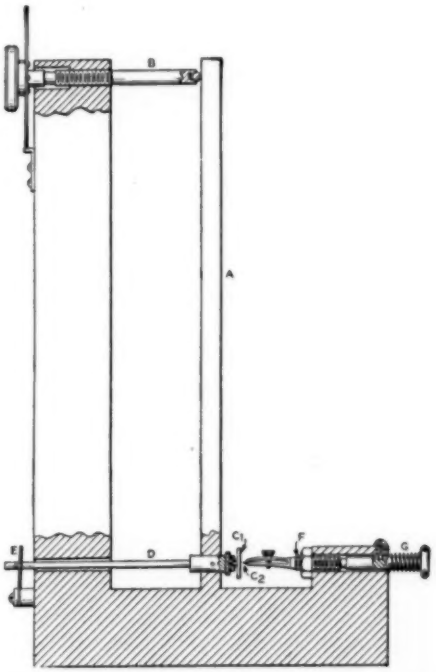

FIG. 1. Cross-section diagram of a cantilever bar device for controlling and measuring small contact displacements.

* Presented orally at the American Physical Society meeting held in Washington, D. C., April 29 to May 1, 1937, G. L. Pearson, Phys. Rev. **51**, 1015(A) (1937).

[1] R. W. Wood, Phys. Rev. (I), **5**, 1 (1897).

[2] R. F. Earhart, Phil. Mag. **1**, 147 (1901); Phil. Mag. **16**, 147 (1908).

[3] C. Kinsley, Phil. Mag. **9**, 692 (1905).

[4] G. M. Hobbs, Phil. Mag. **10**, 617 (1905).

[5] F. Rother, Physik. Zeits. **23**, 423 (1922); Ann. d. Physik **81**, 317 (1926).

[6] G. Hoffman, Zeits. f. Physik **4**, 363 (1921).

[7] H. Rohmann, Zeits. f. Physik **31**, 311 (1925).

[8] Previously described by C. J. Christensen and G. L. Pearson, Bell Sys. Tech. J. **15**, 197 (1936).

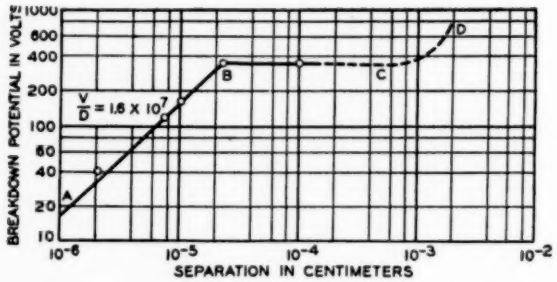

FIG. 2. Breakdown potential as a function of separation for gold electrodes in air at atmospheric pressure.

The contact electrodes used in these measurements were spheres of gold, steel and carbon. The gold electrodes were made by evaporation of the metal on glass spheres having a diameter of three sixteenths inches. This method was used since it gives a smoother surface than that obtained by other methods. The steel electrodes were standard one-quarter inch SKF ball bearings and the carbon electrodes were imported French carbon spheres one-sixteenth inch in diameter. After mounting a pair of spheres in the cantilever bar device (sometimes one sphere and a disk was used as shown in Fig. 1), the following procedure was used for studying the formation and properties of metallic bridges. The point of zero displacement was taken as that at which electrical contact is first established on bringing the electrodes together with a small voltage such as one-tenth volt in the circuit. The electrodes were then separated a known distance and the voltage in the circuit slowly raised until at a definite voltage, depending on the contact separation, a breakdown occurred. When this happened the resistance dropped permanently to a small part of an ohm. Before repeating the experiment the electrodes were rotated so that a clean surface was again obtained. This procedure gave fairly reproducible results as shown by the typical examples discussed below.

Figure 2 shows the results of a series of measurements made with the gold electrodes in air at atmospheric pressure. The abscissae represent separation in centimeters and the ordinates breakdown voltages, both scales being logarithmic. This curve has the same features as those obtained by the early investigators.[2-4] In the region AB breakdown occurs at voltages less than the minimum sparking potential for air, which is about 350 volts at atmospheric pressure. Here the breakdown voltage is directly proportional to the contact separation and the maximum field is 16 million volts per centimeter. In this region a low resistance bridge is always formed between the electrodes at breakdown. In the region to the right of B, a gas discharge occurs at or above the minimum sparking potential in accordance with Paschen's law and no low resistance bridge is ever formed. Over the horizontal portion BC discharge occurs between portions of the spherical electrodes which are at the minimum sparking distance, 6×10^{-4} cm. To the right of C the minimum separation becomes greater than this distance and the discharge voltages therefore increase. Experiments performed on gold spheres in air at pressures less than atmospheric gave low resistance bridges at the same maximum field over the region AB. The discharge voltages in the region BCD, however, depended upon the pressure.

Curves similar to that given in Fig. 2 were obtained for the steel and the carbon electrodes except that breakdown in the region AB occurred at a field of about 5 million volts per centimeter. This lower value is probably due to the fact that these electrodes had surface roughnesses which produced local fields greater than that measured. It should be pointed out that the maximum field strength of 16 million volts per centimeter observed here is greater, by a factor of 8, than those which the best solid dielectrics are known to withstand.

The results of a series of resistance *versus* displacement measurements made on a single contact formed between steel ball bearings are

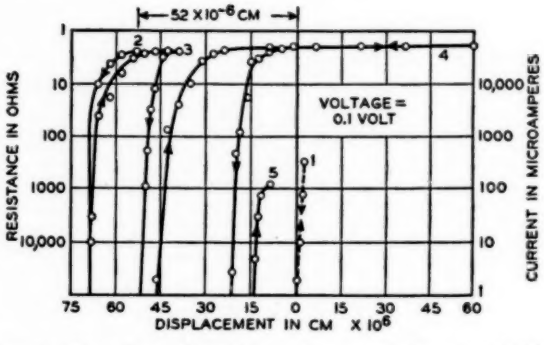

FIG. 3. The effect of tension and compression on a bridge formed between steel electrodes.

[9] A. von Hippel, J. App. Phys. 8, 815 (1937).

shown in Fig. 3. After determining the zero point, as shown by the dotted line, the contacts were separated (to the left in the figure) 52×10^{-6} centimeter and the voltage slowly increased until at 260 volts, which corresponds to a field of 5 million volts per centimeter, a breakdown occurred. The resistance as indicated at (2) was then about 2 ohms when measured with 0.1 volt. (This is mainly circuit resistance as the bridge resistance was approximately 10^{-4} ohm). Further separation pulled out the contact and finally broke it after it was extended about 20×10^{-6} centimeter. The same contact was then remade and under compression returned to its original resistance at (3). Extension broke it again and compression reestablished it and so forth as shown at (4) and (5). This behavior suggests a bridge of metal which extends and breaks in tension and which is crushed in compression.

In order to examine the nature of the material forming these bridges a series of measurements was made to find the effect of temperature on their resistance. By means of a technique developed in the study of the carbon microphone,[10] several different voltages were applied to the electrodes and the resulting bridge resistance measured. From contact theory it is known that the rise in temperature of a short thick bridge is proportional to the square of the applied voltage. When steel electrodes were used the bridge resistance increased with increase in voltage thus indicating a positive temperature coefficient. With carbon electrodes the bridge resistance decreased with increase in voltage. These results indicate that the temperature coefficient of the bridge has the same sign as that of the electrode material.

To confirm this viewpoint Mr. E. J. Ryder of these Laboratories, working with apparatus[11] developed for studying relay contacts, very kindly made a careful quantitative measurement of the temperature coefficient of resistance of a bridge formed between gold electrodes. In this work the temperature was controlled externally by means of a furnace. The measured value of α at room temperatures was 0.0028 in the low resistance bridge while that in a solid gold rod was 0.0034. The small difference between the two

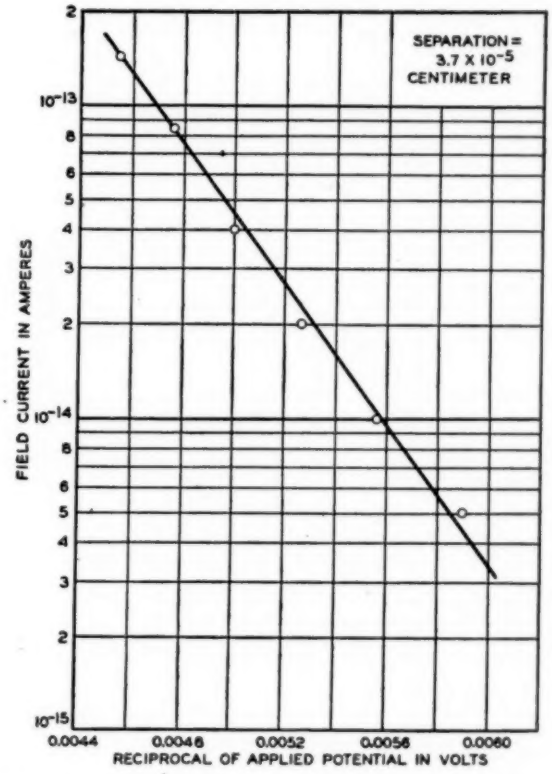

FIG. 4. Field emission current between steel electrodes separated 3.7×10^{-5} centimeter.

values may be attributed to impurities which enter the bridge at breakdown. Furthermore, Ryder measured the breaking strength of the gold bridge and from this calculated the cross-sectional area and the resistance, the latter being in good agreement with the measured resistance. The definite conclusion to be drawn from these experiments is that the bridges are formed from the electrode material.

At fields around a million volts per centimeter field currents are known to exist.[5-7] Accordingly, an electrometer tube circuit was set up to see if such currents could be detected before the bridge was formed. Although this current proved too small to be measured at low voltages, it increased rapidly with increase in the field and attained a value around 1×10^{-10} ampere before the bridge was formed. Fig. 4 shows the current *versus* voltage relationship for steel balls separated 3.7×10^{-5} centimeter. The ordinates represent the current in amperes plotted logarithmically and the abscissae represent the reciprocal of the applied voltage. The straight line relationship

[10] F. S. Goucher, Bell Sys. Tech. J. **13**, 163 (1934).
[11] Bell Lab. Record **16**, 374 (1938).

obtained by this method of plotting identifies the current between the electrodes before breakdown as due to field emission. This curve is reversible if the voltage is not raised so high that a bridge is formed.

Since the radii of curvature of all the electrodes used in these measurements are large in comparison with their separation the electrostatic forces involved can be calculated by means of the following parallel plate equation:

$$F=4.42\times10^{-7}\epsilon(V/d)^2A,$$

where F is the force in dynes, V the voltage, d the separation in centimeters, A the area in square centimeters, and ϵ is the dielectric constant which is 1 for air. For the gold spheres this force is 1.1×10^8 dynes per square centimeter at the time the bridge is formed. The tensile strength of gold is about 2.5×10^9 dynes per square centimeter which is larger by a factor of about 20. For the steel electrodes the calculated electrostatic force and tensile strength are, respectively, 1×10^7 and 2×10^{10} dynes per square centimeter. Differences of this order of magnitude are to be expected since local increases of stress are known to exist because of surface roughness[12] and local heating of the field currents produce softening of the metal electrodes.

It is reasonable to conclude, therefore, that the bridges formed in separated contacts at voltages below the minimum sparking potential are the result of pulling metal from the electrodes by electrostatic force.[13]

In conclusion I wish to thank Dr. J. B. Johnson and Dr. F. S. Goucher for many helpful discussions during the preparation of this paper.

[12] Data of other workers studying field emission from tungsten and molybdenum wires in vacuum indicate that local fields due to roughness may be from 20 to 200 times the average: A. J. Ahearn, Phys. Rev. **44**, 277 (1933).

[13] A somewhat similar type of rupture of the electrodes was observed by A. J. Ahearn (Phys. Rev. **50**, 238 (1936)), while studying field emission from fine wires in a vacuum. In explanation of large increases of current at critical values of applied voltage he suggested a rupturing of the surface where, because of roughnesses the electrostatic force exceeded the tensile strength of the material.

SEPTEMBER 1, 1939 PHYSICAL REVIEW VOLUME 56

Turbulence in Convection in Gases Between Concentric Vertical Cylinders

L. ONSAGER, *Sterling Chemistry Laboratory, Yale University, New Haven, Connecticut*

AND

WILLIAM W. WATSON, *Sloane Physics Laboratory, Yale University, New Haven, Connecticut*

(Received July 6, 1939)

In a thermal diffusion apparatus consisting of two concentric vertical metal cylinders the temperature of the inner hot cylinder is measured for constant power input in the heater as a function of the pressure of the contained gas (N_2 or CO_2). The change from lamellar convection flow to turbulence produces sharply at a certain pressure a cooling which increases with further rise in the gas density. For this critical density the ratio of the remixing by convection to that by diffusion as well as the Reynolds numbers are computed. The latter are around 150; i.e., about $\frac{1}{10}$ the values found for flow through pipes. With increasing temperature difference a minimum value of the pressure for onset of turbulence is found. In order to insure lamellar convection flow in isotope separation by thermal diffusion, conditions should be adjusted so that the ratio of the two remixing effects is not more than $\frac{1}{10}$ these critical values.

IN the discussion of experiments on the separation of isotopes by thermal diffusion, such as those reported by Clusius and Dickel[1] and by Brewer and Bramley,[2] it has been considered that the convection flow in the gas is lamellar.[3] The gas is confined in the gap space a few millimeters in width between two vertical surfaces, one of which is hot. For such a case, as shown in reference 3, the Reynolds number is

[1] K. Clusius and G. Dickel, Naturwiss. **26**, 546 (1938); **27**, 148 (1939).

[2] A. K. Brewer and A. Bramley, Phys. Rev. **55**, 590 (A) (1939).

[3] W. H. Furry, R. C. Jones and L. Onsager, Phys. Rev. **55**, 1083 (1939).

very much smaller than the values at which turbulence occurs in flow through pipes. However, Groth[4] has recently found that with a Clusius hot-wire apparatus having a tube diameter of 12 mm the isotope separation for xenon gas at atmospheric pressure was less when the wire surface was at 1650° than when it was at 1000°. Such a drop in the separation factor would indicate the existence of turbulence in the gas, for the theory indicates that with lamellar convection flow the efficiency of the isotope separation process should always increase with greater temperature difference between the walls. Also Brewer and Bramley have mentioned in a discussion of this method that in their apparatus consisting of concentric glass tubes, the inner one heated, they observed turbulence upon introduction of smoke into the gas.

Since the performance of thermal diffusion apparatus in separation of isotopes should be considerably better with lamellar convection flow existing in the gas, an investigation of the conditions under which the flow becomes turbulent is of value. Now if the convection is lamellar the heat transport of the gas should be independent of the pressure since the mean free path is much smaller than the gap space. But since the Reynolds number increases as the square of the density of the gas,[5] with increasing pressure spontaneous turbulence must always set in at some rather definite pressure even though at low pressures the flow is lamellar. And the heat transport of the turbulent gas should increase with further increase in gas pressure. To observe the onset of turbulence, then, one need simply measure the temperature of the hot wall, with constant power input in the heater, for various gas pressures. At a certain critical pressure the temperature of the wall should begin to drop, and this temperature should fall steadily with further increase in gas pressure.

In the design of thermal diffusion apparatus it is important to know the ratio of the remixing effect due to diffusion to that due to convection. This ratio, K_d/K, is given by Eq. (32) of reference 3:

$$\frac{K_d}{K}=\frac{1890(T_1^2+T_1T_2+T_2^2)}{(T_2-T_1)^2}\times\left(\frac{D\eta}{w^3\rho g}\right)^2, \quad (1)$$

where T_1 and T_2 are the absolute temperatures of the cold and hot walls, respectively, D is the coefficient of self-diffusion of the gas, η its coefficient of viscosity and ρ its density, $2w$ is the distance between the walls and g is the acceleration of gravity. Values of D, η and ρ corresponding to the mean temperature between T_1 and T_2 are to be used. Knowing the density of the gas when turbulence sets in, we may compute the ratio K_d/K for this critical condition. The Reynolds number R should be proportional to $(K/K_d)^{\frac{1}{2}}$. To show this we compute the velocity of flow $v(T)$ from Eqs. (18), (28) and (29) of reference 3, using in the differentiation the fact that $\rho D/\lambda\sim$const. Maximizing this expression for $v(T)$, one gets

$$v_{\max}=\frac{(2w)^2}{18\sqrt{3}}\frac{g\rho}{\eta}\left(\frac{T_2-T_1}{T_2+T_1}\right). \quad (2)$$

Now $v_{\max}=(R\cdot\eta)/(\rho\cdot l)$ so that

$$R=\frac{\rho}{\eta}(2w)v_{\max}=\frac{(2w)^3}{18\sqrt{3}}g\left(\frac{\rho}{\eta}\right)^2\left(\frac{T_2-T_1}{T_2+T_1}\right). \quad (3)$$

Comparison of (1) and (3) shows that $R\leqq(K/K_d)^{\frac{1}{2}}$.

Experimental Procedure

The apparatus consisted of a pair of concentric metal cylinders 82 cm long mounted vertically. The inner copper cylinder was of ½ inch diameter heated indirectly by a G. E. Kalrod heater held coaxially inside it by insulating bushings top and bottom. Thermocouple wires were silver-soldered into this copper tube at the mid-point, and were brought out through the space between the heater and the inner surface of the copper tube in protecting glass sheaths. Surrounding this copper cylinder was one of brass giving in one case an interval between the hot and cold walls of 6 mm, in another case 12.5 mm. The outer brass cylinders were in turn encased with a water condenser through which a good flow of water uniformly at 22°C was constantly maintained. Connecting the inner and outer cylinders at the lower end was a sylphon bellows to take up the differential expansion.

A single small-bore pipe led from the top of the apparatus to the cylinder of gas, either nitrogen

[4] W. Groth, Naturwiss. **27**, 260 (1939).
[5] Cf. Eq. (5), reference 3.

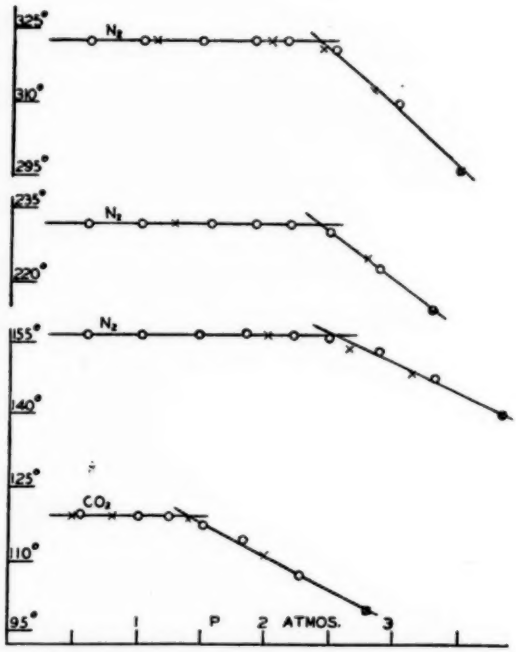

FIG. 1. Plots of the temperature of the hot wall as a function of the gas pressure in each case for constant power input in the heater. 6 mm interval between the hot and the cold surface. Circles indicate observations with pressure increasing, crosses for pressure decreasing. The break in the curves indicates the setting in of turbulence.

or carbon dioxide, with a side connection leading to a pressure gauge reading to 150 lb. and another leading through a valve to a vacuum pump and an open-arm Hg manometer. The heater current was supplied by a large storage battery to insure its constancy. Changes in gas pressure were made slowly and a sufficient time was allowed to elapse after a change for equilibrium to be established before reading the temperature. For each setting of the heater current the temperature of the hot surface was read not only for increasing gas pressure but also as a check for several pressures returning to the initial lowest value.

RESULTS

Typical curves showing the variation of the temperature of the hot cylinder with gas pressure are plotted in Figs. 1 and 2. It is to be noted that the setting in of turbulence indicated by a decreasing wall temperature with increasing gas pressure is abrupt. The critical pressure has been determined for each set of data from the intersection of the two approximately straight lines that may be drawn through the observed points. There is a small but definite variation of this critical pressure with temperature difference between the two walls, other factors remaining constant, and a marked lowering in this pressure for carbon dioxide as compared to nitrogen.

All the data with the resulting values of K/K_d and R computed with the aid of Eqs. (1) and (3) are included in Table I. In place of the unknown coefficients of self-diffusion for N_2 and CO_2 we have had to use the values of D for

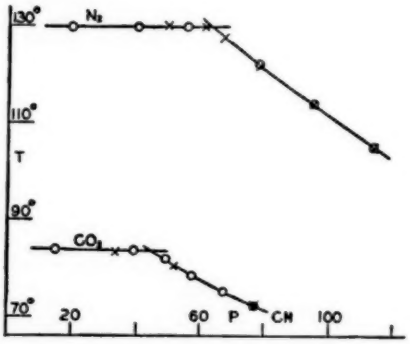

FIG. 2. Same conditions as are listed for Fig. 1 except the space between the hot and the cold surface is 12.5 mm.

O_2-N_2 and for N_2O-CO_2, respectively. The known D, η and ρ for 0°C were in every case extrapolated with the usual formulas to give the values for the mean of the wall temperatures. In agreement with the theory are the large drop in the density at which turbulence begins with increase in the gap space between the cylinders and the indication apparent in the data for CO_2 with the 6-mm gap and for N_2 with the 12.5-mm gap that a minimum value of this density occurs

TABLE I. *Critical pressures at which turbulence sets in, together with values of the ratio K/K_d of remixing by convection to that by diffusion and of the Reynolds number R for these critical densities.*

N_2				CO_2			
t(HOT WALL)	CRIT. P	K/K_d	R	t(HOT WALL)	CRIT. P	K/K_d	R
6 mm between surfaces							
78°C	2.66 atmos.	86.9	138.5	118°C	1.39 atmos.	113.2	160.0
115°	2.57 atmos.	127.2	167.9	214°	1.32 atmos.	100.0	152.7
157°	2.52 atmos.	141.5	177.7	330°	1.46 atmos.	97.7	154.6
232°	2.39 atmos.	131.6	161.1				
322°	2.37 atmos.	86.1	141.4				
12.5 mm between surfaces							
74°C	75 cm	122.9	165	83°	44.5 cm	200.9	211.9
129°	63.5 cm	125.6	167	143°	34 cm	112.0	159.5
177°	57.5 cm	97.0	147.2				
231°	52 cm	62.5	119.0				
282°	55 cm	69.9	126.6				

for a certain temperature difference. According to Eq. (3), with constant Reynolds number the squares of the densities should vary inversely as $(2w)^3$. Such a variation is roughly indicated by our data.

Discussion

The magnitude of these Reynolds numbers is of interest as an experiment in hydrodynamics. They are of the order of one-tenth the values obtained for pure pressure flow through pipes or between plates, and should be around these same values for all gases. This relative ease with which the convection flow changes from the lamellar to the turbulent type is in agreement with the indications of others as mentioned in the introduction above.

These values of the ratio K/K_d should serve as a guide in the determination of operating conditions for the separation of isotopes by thermal diffusion. To insure that the convection flow be lamellar this ratio should be no larger than one-tenth the values we find for the onset of turbulence. In the numerical example for methane gas treated by Furry, Jones and Onsager[3] this condition is strongly satisfied.

SEPTEMBER 1, 1939 PHYSICAL REVIEW VOLUME 56

Wide-Angle Interferences and the Nature of the Elementary Light Sources

P. Selényi
Tungsram Research Laboratory, Ujpest, near Budapest, Hungary
(Received February 24, 1939)

It was proved, in connection with the purely theoretical papers by Halpern and Doermann that a wide-angle optical interference phenomenon can be realized only if the light source is two-dimensional with its third dimension of less than 1/10,000 mm. Observations of the author made in 1911 and 1938 with a simple optical arrangement which fulfills this condition have proved that fluorescence light possesses all the properties of the simple dipole radiation.

In a paper entitled "Theoretical Evaluation of a Wide-Angle Interference Experiment"[1] F. W. Doermann and O. Halpern discuss my recent experimental investigations on wide-angle interferences.[2] They summarize their results in saying "that the source of fluorescence light has been shown to consist of electric dipoles." Stating this they not only omit mentioning that the same conclusion has already been drawn from my observations by myself, but the manner of their discussion gives the impression, that this result can be attained and understood only by a rather complicated theoretical treatment. In reality, the experiment in question is a simple one that can be performed in half a day at the utmost, and it can also be clearly explained in a few lines and without any mathematical formulae.

Figure 1 shows the simple arrangement used by the author. Between the glass prism *Pr* and the thin mica sheet *M* is a film of gelatin, fluorescein, the thickness of which is small in comparison with the wave-length of light. By a concentrated beam of light a small spot of the film is excited to fluorescence and the fringes due to the interference of the rays I and II are observed through a hand-spectroscope, not shown on the figure. Spectroscopic observation is necessary, because the fluorescence light is far from being monochromatic. The experiment was carried out in this form in 1911[3] and it proved the possibility of wide-angle interferences and also the coherence of the emitted light rays within a range of divergence of at least 100°. Repeating this experiment in 1938 under more

[1] F. W. Doermann and O. Halpern, Phys. Rev. **55**, 486 (1939).
[2] P. Selényi, Zeits. f. Physik **108**, 401 (1938); **111**, 791 (1939).
[3] P. Selényi, Ann. d. Physik (4) **35**, 444 (1911). For some similar Röntgen-interferences of W. Kossel and his collaborators see Ergebn. d. exakt. Naturwiss. **16**, 295 (1937).

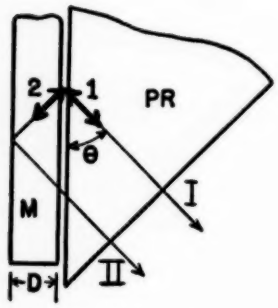

FIG. 1. Prism, *PR*, thin mica sheet *M* and fluorescein film between them.

favorable experimental conditions[2] I obtained the following results: (a) The minima, as observed in the spectroscope at the angle $\theta \approx 45°$, are never completely dark. (b) By inserting in front of the eye an analyzer (e.g. a Nicol prism or a Polaroid filter) in such a position that only the electrical light vector perpendicular to the plan of incidence was transmitted, the fringes became more brilliant and the minima became perfectly dark. Rotating the analyzer by 90° the interference fringes vanish completely.

To explain these observations we suppose for a moment, that fluorescence light is emitted by dipoles and we replace the dipoles distributed at random by three dipoles, oscillating independently and at right angles to each other. The first of these, not shown on Fig. 1, oscillates perpendicularly to the plane of the drawing, emitting, therefore, equal intensities along the rays I and II and producing consequently interference fringes with complete minima, while the two other dipoles (*1* and *2* on Fig. 1) produce no interference at all, because the dipole *1* emits no light in the direction *I* and likewise the dipole *2* emits zero intensity along the direction *II*. These conclusions are, as is to be seen, in best agreement with the above observations. It follows from them, that fluorescence light is in fact emitted by dipoles or, expressed more exactly, our observations are compatible with the assumption that the light is emitted by dipoles, as stated in a similar manner in my paper quoted above, on page 407.

The physical meaning of all of this might perhaps be better elucidated by the remark that this sort of wide-angle interferences (produced by a simple mirror) and the famous experiments of Wiener on stationary light waves are related to each other by the reciprocal theorem of light.[4]

Our observations made with a Nicol prism at the angle of 45° are the counterpart of the special case of Wiener's experiments made at an angle of incidence of 45° by which he demonstrated that two plane waves, crossing each other at the right angle, give rise to perfect interference or no interference at all if the incident rays are polarized in the plane of incidence or at right angles to it, respectively.

Thus the rather complicated theoretical treatment of Doermann and Halpern seems to be almost unnecessary and their formulae, I think, contribute but very little to the understanding of the phenomenon in question. Of course they state that my observations made only at the angle $\theta = 45°$ with a Nicol prism are compatible with a source consisting either of electric dipoles or of magnetic quadrupoles and in order to decide it they refer to my observation made without Nicol prism and at a different angle θ, but in the conclusion they admit, that there is no physical reason for supposing a light source containing magnetic quadrupoles and I myself can assure them that the increase in brilliancy at decreasing θ was in fact due to the finite thickness of the fluorescent layer.

A more detailed discussion of this point seems to be justified by the fact that although in two previous papers[5] the authors had given a very exhaustive theoretical treatment of the wide-angle interferences, and in the second of them (published by Doermann alone) the influence of nonideal reflection has been also considered, they never recognized or at least never mentioned the experimental difficulties existing in this respect. As a matter of fact their treatment is based upon the assumption that the light source is strictly point-like. Therefore the influence of the shape and of the finite dimensions of the light source had not been taken into consideration, though these are the most important experimental factors which generally prohibit the realization of wide-angle interferences.

[4] The reciprocal theorem is not only a useful tool in the theoretical treatment of difficult optical problems, but it is a principle, which can help in finding new optical phenomena. (See my papers quoted above, further Comptes rendus **157**, 1408 (1913) and M. v. Laue, *Die Interferenzen von Röntgen-und Elektronenstrahlen* (Springer, Berlin, 1935), esp. page 31.) Now it is most remarkable that this theorem is based upon the assumption that our light sources are composed exclusively of electric dipoles and therefore would lose its general validity for light sources of different composition.

[5] O. Halpern and F. W. Doermann, Phys. Rev. **52**, 937 (1937); F. W. Doermann, Phys. Rev. **53**, 420 (1938).

We consider the most simple optical arrangement consisting of a plane mirror and of the light source in front of it[6] (see Fig. 1). Let D be the distance of a point O of the light source from the mirror, 2θ the angle of divergence of the rays I and II when emitted; then after reflection of the ray II the path difference d between them becomes

$$d = 2D \sin \theta. \tag{1}$$

Thus if all points of the light source are of the same distance D from the mirror, i.e., if we have a strictly two-dimensional homogeneous light source parallel to the mirror, all is in order; the path difference d depends only on the angle θ and the interference fringes are like the well-known Haidinger-Lummer-rings. In reality we must consider a light source the thickness of which δD is small but not negligible. Then the path difference of the individual partners of rays, emitted from different points of the source, will not be the same, but varies within the limit

$$\delta d = 2\delta D \sin \theta \tag{2}$$

and in consequence of this the sharpness of the fringes diminishes. If δd reaches the value of $\lambda/2$ the fringes disappear almost completely. Therefore δd should be only a fractional part of λ if the fringes are to appear tolerably sharp. Let λ/k be the tolerance of δd then we have

$$\delta d = 2\delta D \sin \theta \leqq \lambda/k \tag{3}$$

or

$$\delta D \leqq \lambda/2k \sin \theta. \tag{3'}$$

Eq. (3) shows that if we have a fixed value of δD and θ is then diminished, δd decreases also, i.e., the fringes become more brilliant. Similarly it follows from Eq. (3') that the greater the divergence of the rays I and II the thinner must be the light source. Even if one is content with rather moderately sharp fringes, k should not be smaller than five. Thus if, for example, θ equals 45°, which is the most interesting case, the dimension of the light source along the normal of the mirror should not exceed $\lambda/7$, i.e., it must be thinner than 1/10,000 mm.

Now it is clear that it is impossible to realize the arrangement we want by placing an ordinary light source L (a flame, a glow discharge tube etc.) behind a fine slit (see Fig. 2). Not only the width of the slit must be smaller than 1/10,000 mm, but the slit-edges S must be also thinner than 1/10,000 mm and they must be in direct contact with the light source, because the light source must have points like O on Fig. 2 lying also at a distance not greater than 1/10,000 mm from the slit to assure a great divergence of the rays I and II. It is quite or almost impossible to fulfill these conditions. Apart from these there arises another difficulty. Besides the coherent rays I and II which are emitted from the same point O of the light source there are other incoherent rays emitted in the same direction, the intensity of which is incomparably greater than that of the coherent rays, in consequence of the extension of the light source.

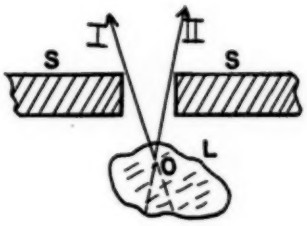

FIG. 2. Extended light source behind a fine slit.

It follows from all these considerations which are also—*mutatis mutandis*—true for the other arrangements proposed by Halpern and Doermann that *the light source* we want for producing the wide-angle interferences *must be originally and essentially a two-dimensional light source*, lying exactly parallel to the surface of the mirror.[7]

So far as I see there is only one way of fulfilling these conditions: A very thin film of a fluorescent substance has to be illuminated by a powerful light source and the light of fluorescence may then be used to produce the interferences as described in my above-mentioned papers. Doubtless the extension of these experiments to other sorts of light sources would be of great interest, but we are, as seen above, prevented from doing so as long as we cannot bring them to a two-dimensional form.

[6] Similar considerations have been given already in my paper quoted above, reference 3, p. 453–454.

[7] *Note added in proof:* That is to say, that *at least* one dimension of the light source, namely that perpendicular to the mirror must be smaller, than 1/10,000 mm. The reduction of two or of all three dimensions under this limit, i.e. the realization of a linear or point-shaped light source of such small extension and of sufficient intensity seems to be almost impossible.

The Angular Distribution of Cosmic-Ray Particles Scattered in 1 Cm of Platinum

J. A. VARGUS, JR.
California Institute of Technology, Pasadena, California
(Received June 22, 1939)

EXPERIMENTS on the scattering of cosmic-ray particles were first reported by Anderson,[1] and recently more extensive measurements were reported by Blackett and Wilson.[2] The results of both of these sets of data are, within experimental uncertainty, in agreement with theoretical expectation.

The two accompanying graphs represent the results of an investigation mentioned briefly in a recent abstract.[3] The theory of multiple scattering is discussed in a recent paper by Williams.[4] Providing $\beta\sim 1$, as is the case with most cosmic-ray particles, the angular distribution of scattered particles, for a particular energy, is given by the Gaussian distribution

$$N(\theta)d\theta=\frac{2N_0}{\pi\theta_m}\exp\left[-\frac{\theta^2}{\pi\theta_m{}^2}\right]d\theta, \qquad (1)$$

where $N(\theta)d\theta$ = number of particles scattered between the angles θ and $\theta+d\theta$, without regard to sign; N_0 = total number of particles scattered; θ_m = mean angle of scattering for the energy under consideration $=(1.37\times 10^3)/E$ deg. (Theoretical; E = energy in Mev.) (1) may be written as

$$N(E\theta)d(E\theta)=\frac{2N_0}{\pi(E\theta)_m}\exp\left[-\frac{(E\theta)^2}{\pi(E\theta)_m{}^2}\right]d(E\theta), \quad (2)$$

where $N(E\theta)d(E\theta)$ = number of particles scattered in such a way that the product of (energy of particle)$\times$(scattering angle) is between $(E\theta)$ and $(E\theta)+d(E\theta)$; N_0 = total number of particles scattered; $(E\theta)_m$ = mean product of energy$\times$ angle of scattering $=1.37\times 10^3$ Mev-deg. (theoretical; E in Mev). (2) represents a universal curve independent of energy.

Only 55 particles among those measured were found to have an energy definitely below 500 Mev.* The observed distribution in $(E\theta)$ is given in Fig. 1, in which the theoretical curve drawn in is given by (2). There is a suggestion that the observed distribution is narrower than that predicted, as found by Fowler and Oppenheimer[5] for electrons of 5–17 Mev, although in view of the small number of particles (55), the discrepancy may well lie within the statistical fluctuations and experimental error. (With the scattering plate in the chamber, only half-lengths of track were available for measurement.) It should be mentioned that, in general, track distortions would cause straight (high energy) tracks to be recorded as curved (low energy). This difficulty would tend to narrow the observed distribution in the same way as recorded in Fig. 1. The experimental value for $(E\theta)_m$ was found to be about 1.4×10^3 Mev-deg., while the value predicted is 1.0×10^3 Mev-deg. The former is critically dependent, for so few particles, upon the few (but relatively heavily weighted) particles which happened to have occurred at large angles of scattering. Particles scattered more than four times the predicted mean angle of scattering were discarded as singly scattered, in accordance with Wentzel's[6] criterion.

Six hundred and seventy particles of energy $\gtrsim$500 Mev were observed. Since the energies involved were beyond the reach of the method of measurement employed here, the method of Eq. (2) could not be used. Consequently, the observed distribution in angle alone was plotted. Now (1) refers to a particular energy, while the

[1] C. D. Anderson, Phys. Rev. **43**, 381 (1933).
[2] P. M. S. Blackett and J. G. Wilson, Proc. Roy. Soc. **A165**, 209 (1938).
[3] J. A. Vargus, Jr., Phys. Rev. **55**, 422 (1939).
[4] E. J. Williams, Proc. Roy. Soc. **A169**, 531 (1939).
* Throughout this communication, the energy values given are on the assumption that the particles are of electronic mass, according to the numerical relationship $E=300H\rho$ where E = energy in Mev; H = magnetic field in gauss; ρ = radius of curvature. The experimental measurement of $H\rho$ is a measurement of momentum. A set of particles with a given distribution in $H\rho$ will undergo multiple scattering in a manner independent of the masses of the particles, providing that β does not vary much from unity, as is the case with most of the particles. In short, under the circumstances, the usual convention, adopted here, of expressing momenta $(H\rho)$ measurements as energies (Mev) does not appreciably affect the comparison of experiment and theory, even though the particles are mostly of the penetrating type, and are presumably mesotrons.
[5] W. A. Fowler and J. Oppenheimer, Phys. Rev. **54**, 320 (1938).
[6] G. Wentzel, Ann. d. Physik **69**, 335 (1922).

higher energy particles observed were of all energies above 500 Mev. To calculate the theoretical angular distribution to be expected, the energy distribution of Anderson and Neddermeyer[7] was used. (These measurements were made with full-length tracks, with no plate in the chamber.) A separate distribution for each 500-Mev range in the energy-distribution curve was plotted according to (1), and the curves added graphically. The resultant angular distribution to be expected is shown by the triangles in Fig. 2. The experimental value of θ_m is about 0.7 deg., while that to be expected from the energy-distribution curve is about 0.8 deg. The observed distribution involves no measurements of energy, except that these nearly straight tracks were above 500 Mev. It again suggests a slightly narrower peak than that predicted. However, in view of the statistical uncertainties of the energy-distribution curve used, the results shown in Fig. 2 may be regarded as indicating rather good agreement with the theory. A similar process applied to Blackett's[8] energy-distribution curve shows an even closer agreement with the scattering data presented, as shown by the circles in Fig. 2. The value of θ_m to be expected from this energy distribution is about 0.7 deg., as measured here. (However, since an energy-distribution curve is partly a function of the geometry of the measuring apparatus, this latter energy-distribution curve is not necessarily applicable to the apparatus at Pasadena, and the improved agreement may or may not be significant.) It is unlikely that such agreement with theory could hold above 500 Mev, together with a breakdown in the range below 500 Mev. Because more accurate energy measurements were involved in the comparison in Fig. 2, and the number of particles is much larger, the agreement found there may be considered as more significant than the discrepancy in the lower range (Fig. 1).

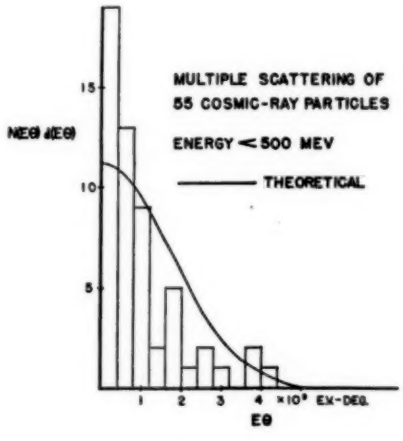

FIG. 1.

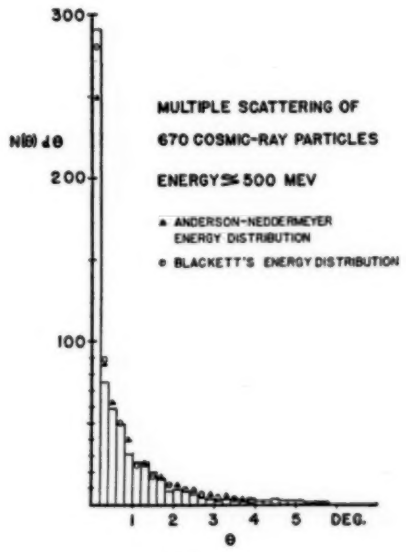

FIG. 2.

Williams[9] has pointed out the importance of scattering in connection with the anomalously low energy losses of cosmic-ray particles traversing metal plates. Since the scattering is independent of the mass of the particles and measurements to date on scattering do not indicate a breakdown of basic theory at high energies, indirect evidence is afforded that the theory of radiation is also valid for high energy particles, and further encouragement is given to the view currently held that the energy-loss anomaly is due to the heavier mass of the particles (mesotrons).

I should like to express my gratitude to Professor C. D. Anderson and to Dr. S. H. Neddermeyer for helpful suggestions, and for providing the cloud-chamber photographs from which these measurements were made.

[7] C. D. Anderson and S. H. Neddermeyer, Int. Conf. Phys. **1**, 173 (1934).
[8] P. M. S. Blackett, Proc. Roy. Soc. **A159**, 1 (1937).
[9] E. J. Williams, Phys. Rev. **53**, 433 (1938).

LETTERS TO THE EDITOR

Prompt publication of brief reports of important discoveries in physics may be secured by addressing them to this department. Closing dates for this department are, for the first issue of the month, the eighteenth of the preceding month, for the second issue, the third of the month. Because of the late closing dates for the section no proof can be shown to authors. The Board of Editors does not hold itself responsible for the opinions expressed by the correspondents.

Communications should not in general exceed 600 words in length.

Multiple Scattering of Fast Electrons

We have made cloud-chamber measurements of the scattering of electrons of 2 to 8 Mev energy in lead and in carbon, under such conditions that the observed deflections are mainly due to multiple scattering. The scattering material was placed across the center of the chamber, and a magnetic field was applied to determine the energy of each electron both upon entering and upon leaving the scatterer. The lead and carbon sheets were made of such a thickness that NtZ^2 was the same for both, to within about three percent. (N = number of nuclei per cc; t = thickness of lamina; Z = atomic number.) Theoretically the scattering should be the same for two laminae, except possibly for a difference of about three percent in the average angle due to a difference in screening.

The results of the measurements are shown in Fig. 1. The projected angle of scattering, for each electron, is multiplied by the mean $H\rho$ value which it had inside the lamina. This allows tracks having a wide range of $H\rho$ values to be plotted together, since in multiple scattering the average deflection is supposed to be proportional to $1/H\rho$. The validity of this was checked by splitting the data into two groups, 2 to 5 Mev and 5 to 8 Mev. The $H\rho\theta$ plots were the same for these two groups, within the statistical fluctuations. The data for lead and carbon give the same value for the average $H\rho\theta$, to well within the accuracy of the experiment. Since all conditions in the experiment remained identical in the measurements with the two laminae, the result gives a clear confirmation of the dependence of scattering upon Z^2, in going from $Z=6$ to $Z=82$. The values for the average (projected) $H\rho\theta$ have been compared with theoretical values computed for our experimental conditions by E. J. Williams.[1] The experimental values are only 58 percent as high as the theoretical values. This discrepancy is in the same direction and of roughly the same amount as that found by Fowler and Oppenheimer[2] and Fowler,[3] for lead at about 10 Mev.

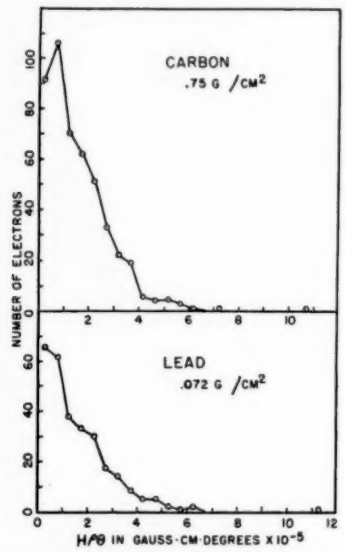

FIG. 1. Scattering of electrons in lead and carbon.

N. L. OLESON
K. T. CHAO
J. HALPERN
H. R. CRANE

University of Michigan,
Ann Arbor, Michigan,
August 15, 1939.

[1] E. J. Williams, Proc. Roy. Soc. **A169**, 531 (1939).
[2] W. A. Fowler and J. Oppenheimer, Phys. Rev. **54**, 320 (1938).
[3] W. A. Fowler, Phys. Rev. **54**, 773 (1938).

Sommerfeld's Fine Structure Constant and Born's Reciprocity

Sommerfeld's fine structure constant $2\pi e^2/hc = 1/137$ appears in the following connection. If a particle is considered as a Gaussian distribution ψ of matter of radial width Δq, then the same particle represents a Gaussian distribution of momenta of width Δp where Δq and Δp are related by the formula

$$\Delta q \Delta p = h.$$

With a certain degree of arbitrariness $\frac{1}{2}\Delta q$ can be identified with the radius and Δq with the diameter D of the particle. Using the customary value for an electric particle we have

$$\Delta q = D = 4e^2/3m_0c^2 \tag{1}$$

and

$$\Delta p = h/\Delta q = m_0c\tfrac{3}{4}(2\pi)137 = 645.6m_0c. \tag{1'}$$

Both Δq and Δp are considered to be measured by an observer at rest outside the particle. We may ask, however, what is the invariant *proper* increase Δp^0 for an observer who himself is accelerated from $p=0$ to a momentum whose value to an observer at rest is Δp? The answer is that Δp^0 is much smaller than the corresponding

Δp, namely [see Eq. (6)]

$$\Delta p^0 = 7.163 m_0 c. \tag{2}$$

Similarly, the *proper* value Δq^0 of the diameter for an inside observer is [see Eq. (8)]

$$\Delta q^0 = 0.881 D. \tag{2'}$$

Whereas (1)(1′) give the product

$$\Delta q \Delta p = 2\pi D m_0 c (\tfrac{3}{4}\,137), \tag{3}$$

(2)(2′) give the product of order

$$\Delta q^0 \Delta p^0 = 2\pi D m_0 c \tag{3'}$$

in which the factor $(\frac{3}{4}\,137)$ has disappeared. *Thus, an electric particle can be characterized as a distribution in space and momentum space such that the product of the widths (uncertainty product) $\Delta q \Delta p = h$ reduces to a proper uncertainty product $\Delta q^0 \Delta p^0 = h_0$ which is of the order of 137 times as small.* The arbitrariness in assuming a certain value for the "diameter" of the particle has been removed by a more consistent calculation to be published later.

We are now going to report the calculations that have led to the proper values Δp^0 and Δq quoted in (2)(2′). In the dimensionless quantities

$$P = p/m_0 c \quad \text{and} \quad E = \epsilon/m_0 c^2, \tag{4}$$

the Einstein energy-momentum equation reads

$$E^2 = 1 + P^2 \quad \text{with} \quad EdE = PdP. \tag{5}$$

A line element dP is the projection of a line element $(dP^2+dE^2)^{\frac{1}{2}}$ on the hyperbola (5). Its proper length is obtained by dividing it by the proper unit of length which is its distance $(P^2+E^2)^{\frac{1}{2}}$ from the zero point. Integrating we obtain the proper increase

$$\Delta P^0 = \int \left(\frac{dP^2+dE^2}{P^2+E^2}\right)^{\frac{1}{2}} = \int_0^{\Delta P} \frac{dP}{(1+P^2)^{\frac{1}{2}}}$$
$$= \ln\{\Delta P + (1+\Delta P^2)^{\frac{1}{2}}\} = \mathrm{Sinh}^{-1}\Delta P. \tag{6}$$

Substituting ΔP from (1) we obtain the result (2). *Born's idea of reciprocity has led us to consider a similar reduction in space.* Starting from the equation

$$(ct)^2 = D^2 + q^2, \quad \text{hence} \quad dq/dt = c\cdot[1+(D/q)^2]^{\frac{1}{2}}, \tag{7}$$

and introducing the dimensionless coordinates

$$Q = q/D \quad \text{and} \quad T = ct/D \tag{7'}$$

we obtain in the same way as in (6)

$$T^2 = 1 + Q^2 \quad \text{and} \quad \Delta Q^0 = \mathrm{Sinh}^{-1}\Delta Q. \tag{8}$$

Then, using $\Delta q = D$ or $\Delta Q = 1$ we obtain the result of (2′). The Eq. (7) is the mathematical formulation of an important result of *Dirac's* that a signal traveling from infinity to the center of the electron saves time as against a signal traveling with velocity c.

ALFRED LANDÉ

Mendenhall Laboratory,
Ohio State University,
Columbus, Ohio,
June 7, 1939.

On the Collimation of Fast Neutrons

Several experiments[1, 2] have been carried out with a beam of neutrons produced by placing a thick wall of water in front of a neutron source and using a hole through the wall as a collimator. It has been observed with cloud chambers[1] that while there are large numbers of hydrogen recoils produced with the chamber in the beam, the number and length are both greatly diminished if the chamber is moved out of the beam. It has also been observed[2] that such a collimating system supplemented by lead shields to cut down γ-radiation from the collimating screen, gives little ionization current when the chamber is taken out past the edge of the beam, compared to that produced in the beam.

The effects of neutron collimation are rather clearly indicated in the accompanying photographs which show the proton recoils produced in a cloud chamber filled to atmospheric pressure with CH_4. The neutrons were produced by the bombardment of lithium or beryllium with 1.2-Mev deuterons accelerated by a cyclotron. A wall of water which was about 75 cm thick in the region of the hole served as the collimator. This hole was about 10 cm in

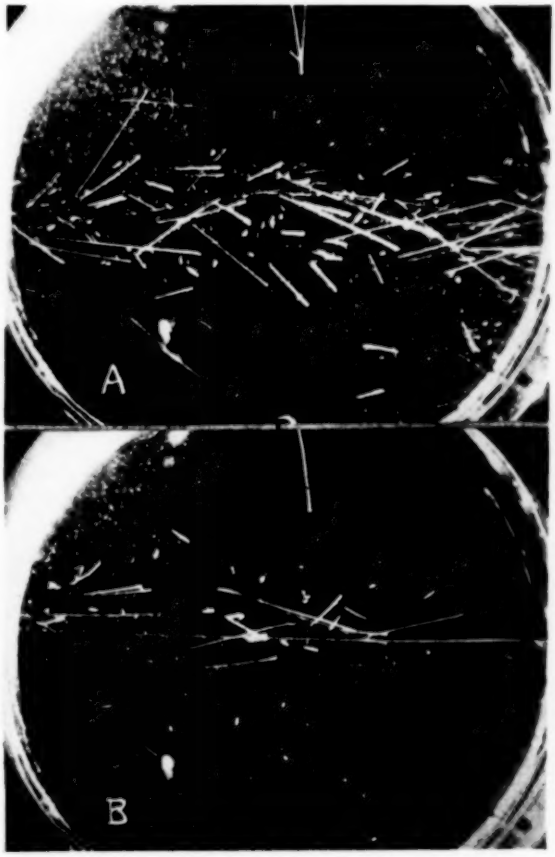

FIG. 1A. Tracks of the recoils in CH_4 produced by a collimated beam of neutrons which passed from left to right through the cloud chamber. Left edge of chamber about 4 cm from collimator. B. Tracks of recoils produced when the nearest edge of chamber was 30 cm from the collimator.

diameter but was stopped down by the insertion of paraffin cylinders with central holes of smaller diameter. These pictures were taken with such a collimator which had a diameter of about 4 cm. In order to avoid unnecessary neutron scattering by the chamber or camera support, they were of light-weight construction throughout. The cloud chamber (diameter 22 cm) was of the rubber diaphragm type with the regulator valve located about 40 cm below the chamber. The light source was a projection lamp with collimating lenses and also located at a distance from the cloud chamber.

Figure 1A shows the recoils produced by the neutrons from a lithium target. The neutron beam entered the chamber on the left side which was about 4 cm from the end of the collimator. Most of the recoils appear to originate in a region which has about the same width as the collimator. At the top of the photograph there appears a wire projecting from the wall of the chamber, on the end of which a weak polonium source had been placed. Fig. 1A shows part of an α-track from this source. Fig. 1B shows the recoils produced by the neutrons from a beryllium target when the nearest edge of the chamber was about 30 cm from the end of the collimating tube indicating that the beam shows no obvious divergence.

R. F. BACHER
D. C. SWANSON*

Cornell University,
Ithaca, New York,
August 4, 1939.

* At present at the University of Florida.

[1] R. F. Bacher and D. C. Swanson, Phys. Rev. **53**, 676 (1938); **53**, 922 (1938).
[2] P. C. Aebersold, Phys. Rev. **55**, 596 (1939); P. C. Aebersold and Gladys A. Anslow, Phys. Rev. **55**, 680 (1939); **55**, 1134 (1939).

A Nuclear Disintegration Induced by the Cosmic Radiation

The presence of heavy ionizing particles in the cosmic radiation has been observed on several occasions and ascribed to nuclear disintegrations taking place under the action of primary cosmic rays. Since the first observation by Anderson[1] different authors have observed cloud tracks attributable to phenomena of this kind.[2] The occurrence of such tracks, very rare at sea level, is much more frequent at high altitudes; the tracks originate either in the metallic parts of the Wilson chamber or in its gaseous atmosphere. The identification of the nature of these particles was generally very uncertain because of the difficulties, often insuperable, of determining the actual direction of their movement and of measuring with any exactitude their range and the curvature of their tracks in a magnetic field.

In most cases however, the properties of protons are in better agreement than those of any other kind of particles with the bulk of recorded observations. A similar conclusion, that is, the occurrence of disintegrations induced by the cosmic rays and resulting in an emission of protons, seems to be suggested by recent experiments with photographic emulsion.[3]

The accompanying photograph (Fig. 1) was taken in a horizontal cloud chamber subjected to a field of 16,400 oersteds. The object of our study was the α-radiation from

FIG. 1. Cloud-chamber photograph showing a polonium α-particle track together with two tracks produced by cosmic rays in the cloud-chamber atmosphere. The long track is due indubitably to a proton of 6.3 Mev. The short one is due either to a proton of 3.7 Mev or a deuteron of 2.0 Mev energy.

Po, canalized into a narrow beam (aperture 10°–15°). The photograph shows one of these α-tracks accompanied by two tracks of another kind which must be ascribed to particles originated in a nuclear reaction induced by the cosmic rays in the chamber atmosphere.* Since the actual direction of these particles is from right to left, they must be positive. We determined the track curvature after the method (described elsewhere)[1] of mean radii of curvature using an enlargement of the negative taken with a single objective. The lighted belt in the chamber being 2.5 cm high, the minimum inclination of the tracks relative to the field direction is 75° for the long track and 55° for the short one. We have determined several $H\rho$ values for different points of the two tracks (see Table I).

The ionization visible on these two tracks is 3 to 4 times less intense than that produced by the Po alphas. The tracks are due, therefore, neither to alphas nor to electrons. Even mesons are excluded, since a meson of a mass $M=200m_0$ and of a $H\rho$ falling between 2.50×10^5 and 3.50×10^5 ought to produce an ionization 10 to 15 times less intense than the ionization observed. The tracks could be, however, ascribed to protons or deuterons. A detailed analysis of the curvature shows indeed that the long track is due indubitably to a proton and that the short one is due either to a proton or to a deuteron; the precision of measurements in this latter case being, however, insufficient to ensure an absolutely univocal identification.

The initial energy of the proton (long track) is equal to 6.3 ± 0.2 Mev. The second particle (short track) possesses an initial energy of 3.7 ± 0.8 Mev if a proton, and of 2.0 ± 0.3 Mev if a deuteron. The total energy of the particles projected in the nuclear reaction we are discussing, must be, therefore, of the magnitude order of 10 Mev.

Assuming that the two tracks are due to two protons or to one proton and one deuteron, we may draw some conclusions as to the energy of the incident rays primarily responsible for the observed nuclear process. Anyone of the reactions which could take place in a cloud-chamber atmosphere consisting of air, water vapor and alcohol

TABLE I. *Values of $H\rho$ at different points along the tracks.*

Long Track			
Distance from origin*	1.28	2.56	3.84 cm
$H\rho(\alpha=90°)$	3.55	3.50	3.46×10^{-5}
$H\rho(\alpha=75°)$	3.65	3.60	3.56×10^{-5}
Short Track			
Distance from origin*	0.77	1.28 cm	
$H\rho(\alpha=90°)$	2.48	2.40×10^{-5}	
$H\rho(\alpha=55°)$	3.15	3.06×10^{-5}	

* Values at NTP.

vapor and which results in an emission of protons or deuterons so highly energetic, demands an initial energy of 35–40 Mev. If we suppose that, simultaneously with observable charged particles the same reactions give birth to one or several neutrons,[5] invisible in a cloud chamber, the incident ray must possess an energy of 60–70 Mev. According to these estimations, the reactions observed must be induced chiefly by the soft component of the cosmic radiation—a conclusion already deduced from the very rapid increase of the discussed phenomena with the altitude.

I. ZLOTOWSKI

Laboratoire de Chimie Nucléaire,
Collège de France, Paris,
July 29, 1939.

* We were able to ascertain the absolute inactivity of the interior of the chamber.

[1] C. D. Anderson, Phys. Rev. **41**, 405 (1932).
[2] P. M. S. Blackett and G. P. S. Occhialini, Proc. Roy. Soc. **A139**, 699 (1933); P. Kunze, Zeits. f. Physik **83**, 1 (1933); C. D. Anderson and S. H. Neddermeyer, Phys. Rev. **50**, 263 (1936); L. Leprince-Ringuet and J. Crussard, J. de phys. et rad. **8**, 213 (1937); R. B. Brode and M. A. Starr, Phys. Rev. **53**, 3 (1938) and many others.
[3] M. Blau and H. Wambacher, Nature **140**, 585 (1937); H. J. Taylor, D. Fraser and V. D. Dathalear, Nature **141**, 472 (1938); M. Blau, Nature **142**, 613 (1938); H. Wambacher, Physik. Zeits. **39**, 883 (1938).
[4] F. Joliot and I. Zlotowski, J. de phys. et rad. **9**, 393 (1938); I. Zlotowski, Comptes rendus **207**, 148 (1938).
[5] See W. Heitler, Phys. Rev. **54**, 873 (1938).

The Beta-Radiation of As^{76} *

The problem of beta-emission is complicated by the possibility that the transition takes place to more than one level in the final nucleus.[1] We have therefore considered it of interest to study rather extensively a spectrum in which other observers have found indications of complexity.

Previous measurements[2, 3] on As^{76} agree that there are two groups of beta-rays, but the estimates of their relative populations are in serious disaccord. No attempt has been made to study the low energy region carefully, although the high energy end of the spectrum seems to have been well analyzed.[3]

The work reported here was done with a hydrogen-filled expansion chamber placed in a magnetic field uniform to ±2.5 percent over the useful volume of the chamber. During a run the field was maintained constant to ±1 percent. Data were obtained for magnetic field strengths of 800 and 342 oersteds. Only those tracks were measured which (1) were not visibly scattered, (2) were at least 10 cm long, (3) initially lay within the same solid angle for each radius of curvature. The radioactive arsenic was chemically separated from cacodylic acid which had been irradiated by slow neutrons from the cyclotron or a $D-D$ source.

Recent experiments[4–6] have shown the distortion of the momentum distribution in a beta-ray spectrum which is caused by "back scattering" due to a finite mass of material behind the source. In our work this effect, which arises essentially from a "forward" and "backward" asymmetry in the scattering of low energy electrons in the source, has been partially compensated for by folding the filter paper on which the active precipitate was deposited so that the source was contained between two equal thicknesses of paper. The total surface density of the source amounted to 29 mg/cm². The maximum thickness of material a beta-particle would have to traverse was 21 mg/cm², corresponding to a momentum loss of about 180 oersted-cm for a beta-particle of $H\rho=2000$. It therefore seems that the finite source thickness could not seriously affect our observations above this value of $H\rho$.

Figure 1 shows the experimental momentum distribution of the beta-particles. The observed upper limit occurs at $H\rho=10{,}600\pm500$ corresponding to 2.71 ± 0.14 Mev. This energy limit agrees closely with that obtained by Harteck, Knauer and Schaeffer.[3] The average energy of the beta-particles is 0.93 Mev.

The decomposition of the experimental curve into components each having a Fermi distribution is only possible by assuming that at least three groups are present, the highest energy group fitting over a region covering 40 percent of the energy spread of the spectrum. The extrapolated end-point of the Fermi plot is 2.78 Mev. If, on the other hand, we assume as the basis for analysis the K-U modification of the Fermi theory, we find that the spectrum may be resolved uniquely into two groups having extrapolated end-points of 0.97 and 3.32 Mev, the low energy group containing 20 percent of the particles. At the high energy end of the spectrum the usual[4–7] divergence from the distribution given by the K-U theory is found. That the number of particles in the low energy group is small was confirmed by an absorption experiment. Gamma-radiation was observed to produce about one percent of the total ionization.

The decay of chemically separated As^{76} was followed for five half-lives and found to have a single period $T=26.75$

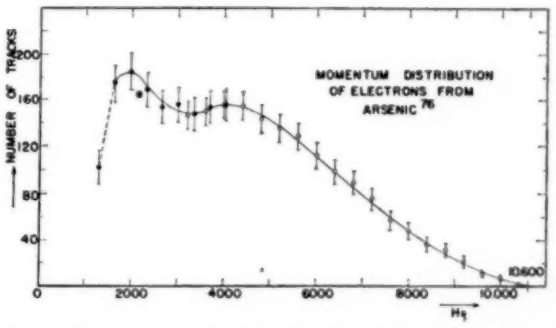

FIG. 1. The momentum distribution of the electrons from As^{76}. The complexity of the spectrum is indicated by the resolution of the two peaks. The observations taken at 342 oersteds are indicated by filled circles, those at 800 oersteds by open circles. The length of the vertical line through a point is the uncertainty estimated by taking the square root of the number of observed tracks corresponding to the point.

± 0.15 hours. Assuming the existence of the two groups suggested by the K-U analysis, the partial disintegration constants may be computed, and these figures taken with the extrapolated energies place the low and high energy groups, respectively, on the second and between the second and third Sargent curves.

The authors are indebted to Professor J. R. Dunning for his continued interest and helpful advice, to Dr. W. H. Zinn for the use of his D−D neutron source, and to Dr. J. Steigman for his aid in performing the chemical separations.

GEORGE L. WEIL
WALTER H. BARKAS†

Pupin Physics Laboratories,
Columbia University,
New York, New York,
August 9, 1939.

* Publication assisted by the Ernest Kempton Adams Fund for Physical Research of Columbia University.
† Now at The Institute for Advanced Study, Princeton, New Jersey.
[1] Bethe, Hoyle and Peierls, Nature **143**, 200 (1939).
[2] M. V. Brown and A. C. G. Mitchell, Phys. Rev. **50**, 593 (1936).
[3] Harteck, Knauer and Schaeffer, Zeits. f. Physik **109**, 153 (1938).
[4] Flammersfeld, Zeits. f. Physik **112**, 741 (1939).
[5] A. W. Tyler, Phys. Rev. **56**, 125 (1939).
[6] J. L. Lawson, Phys. Rev. **56**, 131 (1939).
[7] Martin and Townsend, Proc. Roy. Soc. **A170**, 203 (1939).

The Structure of Electric Particles and the Number 137

In a recent letter to the editor[1] I reported the purely empirical result that the uncertainty product of the ranges in space and in momentum space of an electric particle, $\Delta p \cdot \Delta r = h = 137 \cdot 2\pi e^2/c$, is reduced to a product $\Delta p^0 \cdot \Delta r^0 \approx 2\pi e^2/c$ without the factor 137 if Δp^0 and Δr^0 are the *proper* ranges as measured by an observer on the particle itself. The result was based on Einstein's energy-momentum relation ($E^2 = 1 + P^2$ in reduced units) and on a similar space-time relation ($T^2 = 1 + R^2$ in reduced units). The latter equation (postulate A), established in (I) for the first time, was to characterize the particle in a fashion "reciprocal" to Einstein's relation in the sense of *Born's principle of reciprocity*.[2] The physical meaning of $T^2 = 1 + R^2$ is that a signal sent across the particle travels at a velocity larger than c, in agreement with an earlier result of Dirac's.[3] If, according to Dirac, the time saved by such a signal from infinity to the center of the particle, is $2e^2/3m_0c^3$, then our reduced coordinates are to be

$$R = r \cdot (m_0c^2/e^2\gamma), \qquad T = ct \cdot (m_0c^2/e^2\gamma)$$

with $\gamma = \frac{2}{3}$. However, the question of the magnitude of the factor γ is not quite settled; it is a question of the *classical* theory of the electron.

Starting from the classical equation $T^2 = 1 + R^2$ and from the empirical result of (I) we have tried to work out a more consistent quantum theory of the particle with the aim of having the Sommerfeld fine structure constant $\alpha = 1/137$ appear as the eigenvalue of a linear integral equation whose eigenfunction under an additional condition is the density amplitude $\psi(r)$ of the electric particle (irrespective of its mass). With $\alpha = e^2/\hbar c$ and with $\alpha' = \alpha/\gamma$ the Fourier expansion of quantum theory reads

$$\psi(R) = (\alpha'/2\pi)^4 \int\int\int\int \chi(P) \exp\left[i\alpha'(P \cdot R)\right] dV_P$$

and its inversion. We introduce a similar equation for the *proper* reduced coordinates and momenta (compare with (I)) $P^0 = \sinh^{-1} P$ and $R^0 = \sinh^{-1} R$, namely (Postulate B):

$$\chi^0(P^0) = (\alpha_0'/2\pi)^4 \int\int\int\int \psi^0(R^0) \exp\left[-i\alpha_0'(P^0 \cdot R^0)\right] dV^0$$

and its inversion. Here we have used $\alpha_0' = \alpha_0/\gamma$ where α_0 is a "proper" fine structure constant to be determined later. Identifying $\psi^2 dV$ with $(\psi^0)^2 dV^0$ and $\chi^2 dV_P$ with $(\chi^0)^2 dV_P{}^0$ we obtain a closed chain of equations expressing ψ by χ, χ^0, ψ^0, ψ, and resulting in a *linear integral equation*[4] for $\psi(R)$ whose unsymmetrical kernel K depends on the two parameters α and α_0 since γ is known classically:

$$\psi(R) = \int K(R, R', \alpha_0, \alpha) \cdot \psi(R') \cdot dR'.$$

On the suggestion of L. H. Thomas we add the condition that the electrostatic self-energy equals the rest energy m_0c^2. In our reduced coordinates this condition reads

$$\int\int (1/R_{12}) \cdot \psi^2(R_1) \cdot \psi^2(R_2) \cdot dV dV_2 = \gamma.$$

The integral equation is solved, according to a very rough approximative consideration,[4] by an eigenvalue α_0 of order *unity* if we assume α to be $1/137$, and by an eigenvalue α of order $1/137$ if we assume α_0 to be unity. The latter value would amount to a "proper quantum" $\hbar_0 = e^2/c$ applying to the proper space, as against $\hbar = e^2/\alpha c$.

There is the objection to (B) that *two* quantum theories, one with $\hbar$ and one with $\hbar_0$ cannot hold simultaneously on the ground of the transformation theory. This is true in general. But the point is that if we *require* them to coexist then we are led automatically to special ψ-functions, those representing a *particle*.

ALFRED LANDÉ

Ohio State University,
Columbus, Ohio,
June 28, 1939.

[1] A. Landé, Phys. Rev. **56**, 482 (1939), quoted as (I).
[2] M. Born, Proc. Roy. Soc. **A165**, 291 (1938).
[3] P. A. M. Dirac, Proc. Roy. Soc. **A167**, 148 (1938).
[4] To be published in the J. Frank. Inst. (1939).

THE AMERICAN INSTITUTE OF PHYSICS

INCORPORATED

ADMINISTRATIVE STAFF

HENRY A. BARTON, *Director*

MADELINE M. MITCHELL, *Publications Manager*

Office: 175 Fifth Avenue, New York, New York

JOURNALS

THE PHYSICAL REVIEW

REVIEWS OF MODERN PHYSICS

JOHN T. TATE, *Editor*

J. W. BUCHTA, *Assistant Editor*

JOURNAL OF APPLIED PHYSICS

ELMER HUTCHISSON, *Editor*

THE JOURNAL OF THE OPTICAL SOCIETY OF AMERICA

THE REVIEW OF SCIENTIFIC INSTRUMENTS

F. K. RICHTMYER, *Editor*

JOURNAL OF THE ACOUSTICAL SOCIETY OF AMERICA

FLOYD A. FIRESTONE, *Editor*

THE JOURNAL OF CHEMICAL PHYSICS

HAROLD C. UREY, *Editor*

JOSEPH E. MAYER, *Assistant Editor*

THE AMERICAN PHYSICS TEACHER

DUANE ROLLER, *Editor*

GOVERNING BOARD

For The American Physical Society:

JOHN T. TATE, *Chairman*
University of Minnesota

GEORGE B. PEGRAM, *Secretary*
Columbia University

KARL T. COMPTON
Massachusetts Institute of Technology

For The Optical Society of America:

E. C. CRITTENDEN
National Bureau of Standards

A. C. HARDY
Massachusetts Institute of Technology

W. B. RAYTON
Bausch & Lomb Optical Company

For The Acoustical Society of America:

FLOYD A. FIRESTONE
University of Michigan

HARVEY FLETCHER
Bell Telephone Laboratories

WALLACE WATERFALL
The Celotex Corporation

For The Society of Rheology:

WHEELER P. DAVEY
Pennsylvania State College

MELVIN MOONEY
United States Rubber Products, Inc.

R. L. PEEK, JR.
Bell Telephone Laboratories

For The American Association of Physics Teachers:

PAUL E. KLOPSTEG
Central Scientific Company

FREDERIC PALMER, JR.
Haverford College

F. K. RICHTMYER
Cornell University

The American Institute of Physics is a membership corporation of which five societies are the founding members. These five societies are the principal national societies devoted to pure and applied physics in America. Their names, and those of their representatives who form the Governing Board of the Institute, are given above. The principal work of the Institute is the publication of journals sponsored by the societies or by itself. The names and the editors of the journals are also listed above.

The broad purpose of the Institute is to represent, in all matters of wide or common interest, the five thousand or more members and subscribers associated with the Founder Societies and the journals. It aims to advance the science and profession of physics, and to promote cooperation between pure research, the applied sciences and the industries. To achieve these aims, it is greatly in need of an endowment and is empowered by law to administer grants and funds of any kind.

CONTENTS

PHYS. REV. 56 (1939) SEPTEMBER 1

Intensities of the *K*-Series X-Ray Lines of Tungsten and Platinum . . . W. H. KLEEVER 337

X-Ray *K* Absorption Edges of the Elements Fe (26) to Ge (32) . . . . . W. W. BEEMAN AND H. FRIEDMAN 392

X-Ray Dispersion and Atomic Electron Cloud Distortion in Zinc Crystals . E. M. MCNATT 406

Proton Activation of Indium and Cadmium . . . . . S. W. BARNES 414

Coincidences Between Beta- and Gamma-Rays in Manganese . . . . . LAWRENCE M. LANGER, ALLAN C. G. MITCHELL AND PAUL W. MCDANIEL 422

Mechanism of Nuclear Fission . . . . . NIELS BOHR AND JOHN ARCHIBALD WHEELER 426

On the Behavior of Matter at Extremely High Temperatures and Pressures . FÉLIX CERNUSCHI 450

On Continued Gravitational Contraction . . . . . J. R. OPPENHEIMER AND H. SNYDER 455

Formation of Ions in the Cyclotron . . . . . ROBERT R. WILSON 459

Relative Intensities of Singlet-Singlet and Singlet-Triplet Transitions . . . . . G. W. KING AND J. H. VAN VLECK 464

Elementary Processes in the Sensitized Fluorescence of OH Molecules . . . . . ELIZABETH REED LYMAN 466

Formation of Metallic Bridges Between Separated Contacts . . . . G. L. PEARSON 471

Turbulence in Convection in Gases Between Concentric Vertical Cylinders . . . . . L. ONSAGER AND WILLIAM W. WATSON 474

Wide-Angle Interferences and the Nature of the Elementary Light Sources . . P. SELÉNYI 477

Angular Distribution of Cosmic-Ray Particles Scattered in 1 Cm of Platinum . . . . . J. A. VAN ALLEN, JR. 480

Letters to the Editor:

Multiple Scattering of Fast Electrons . N. L. OLESON, K. T. CHAO, J. HALPERN AND H. R. CRANE 482
Sommerfeld's Fine Structure Constant and Born's Reciprocity . . . . . ALFRED LANDÉ 483
On the Collimation of Fast Neutrons . . . . . R. F. BACHER AND D. C. SWANSON 483
Nuclear Disintegration Induced by the Cosmic Radiation . . . . . I. ZLOTOWSKI 484
Beta-Radiation of As^{76} . . . . . GEORGES L. WEIL AND WALTER H. BARKAS 485
Structure of Elastic Particles and the Number 137 . . . . . ALFRED LANDÉ 486

LANCASTER PRESS, INC., LANCASTER, PA.